UNIFYING WEATHER AND CLIMATE VARIABILITY PREDICTIONS – AN OPERATIONAL SEAMLESS FORECASTING SYSTEM FOR SOUTHERN AFRICA AT TIME SCALES FROM DAYS TO SEASONS

Report to the
Water Research Commission

by

Willem A. Landman[1], Francois Engelbrecht[1], Ruth Park[1], Jacobus van der Merwe[1], Zane Dedekind[1], Asmerom Beraki[2], Johan Malherbe[3], Lerato Mpheshea[1]

[1]Council for Scientific and Industrial Research
[2]South African Weather Service
[3]Agricultural Research Council

WRC Report No. 2050/1/14
ISBN 978-1-4312-0631-5

FEBRUARY 2015

Obtainable from

Water research Commission
Private Bag X03
Gezina, 0031

orders@wrc.org.za or download from www.wrc.org.za

Executive Summary

Southern Africa is associated with a large degree of natural weather and climate variability and is prone to sporadic droughts and floods. Moreover, the southern African region is thought to be particularly vulnerable to anthropogenically induced climate change. In this project we propose the development of a so-called seamless forecasting system, which means that we introduce a common forecast system in order to predict for multiple time scales. The time scales considered include short-range weather prediction through multi-decadal climate projections. The report first addresses various regional climate modelling configurations and describes defensible and actionable multi-decadal regional projections towards the end of this century. During the analysis of the multi-decadal projections evidence is provided that extreme weather and climatic events are likely to increase over southern Africa in a changing climate. The notion of an increase in extremes and their associated societal challenges have subsequently emphasised the importance of the skilful predictions of weather and climate anomalies at lead-times long enough for decision-makers to act upon the forecasts. Weather and seasonal climate model configurations, based on the same atmospheric model used for the multi-decadal projections, the conformal-cubic atmospheric model (CCAM), are subsequently described and verified. Since skilful weather and seasonal climate predictions have been demonstrated here, the confidence in the CCAM's projections of future climate change has subsequently been enhanced. The major findings from this work suggest that the CCAM model code can be used as a seamless forecasting system since it was successfully applied to produce short-range weather forecasts, seasonal climate projections and projections of future climate change. Temperatures are projected to rise over southern Africa and an increase in weather and climate extremes are expected to occur. However, skilful weather and seasonal climate forecasts of the CCAM can predict such extremes. Finally, the notion of developing application forecasts is demonstrated on seasonal streamflows.

The work presented here is testimony of some of the atmospheric modelling work currently being conducted in South Africa. Such modelling endeavours have been made possible through the availability of National computing infrastructure (CHPC), multi-processor machines at a number of institutions involved with weather and

climate modelling, as well as various funding streams including financial support from the South African Government. Future weather and climate modelling work will require sustained support for the use of dedicated state-of-the-art computers in order to enable the running of high to ultra-high simulations and forecasts, large ensemble forecasts, various modelling strategies and Earth System model development and testing. To support these modelling efforts, the analysis in South Africa of model output and in-situ and remotely sensed data should be significantly enhanced in order to improve on our understanding of the coupled ocean-land-atmosphere-ice system. Finally, as has been shown in the project, the development of forecast applications for various sectors may be potentially beneficial and be further developed, tested and may have to be more efficiently linked with strategy development and policymaking.

Acknowledgements

The research team would like to thank the following persons and institutions:

1. Water Research Commission (WRC) for funding and managing the project.
2. Dr David G. Dewitt who produced the SST scenario runs which were analysed in Chapter 4.
3. Mrs Daleen Lötter who made the Kendall's tau maps in Chapter 4.
4. CHPC for providing the computing platform for some of the regional climate change projections.
5. ITC of the CSIR for maintaining the multi-node machine used for the seasonal climate re-forecasts.
6. Mrs Juanette John who organised a workshop with end-users of forecast and projections.

The following members of the reference group are also thanked for their valuable contributions:

1. Mr Chris Moseki Water Research Commission (Chairman)
2. Prof Geoff Pegram University of KwaZulu-Natal
3. Dr Chris Lennard University of Cape Town
4. Dr Liesl Dyson University of Pretoria

Table of Contents

List of Figures

Figure 2.6: Projected change in the total annual rainfall (mm) over Africa, for the periods 2011-2040 (top), 2041-2070 (middle) and 2071-2100 (bottom), relative to 1961-1990. The 90th percentile (right-hand side panel), median (middle panel) and 10th percentile (left-hand side panel) are shown for an ensemble of six downscalings of CGCM projections, for each of the time-slabs. The downscalings were generated using the regional model CCAM. All the CGCM projections contributed to AR4 of the IPCC and are for the A2 SRES scenario.

Figure 2.7: Projected change in the annual frequency of occurrence of extreme rainfall events over Africa, for the periods 2011-2040, 2041-2070 and 2071-2100, relative to 1961-1990. The 90th percentile (right-hand side panel), median (middle panel) and 10th percentile (left-hand side panel) are shown for an ensemble of six downscalings of CGCM projections, for each of the time-slabs. The downscalings were generated using the regional model CCAM. All the CGCM projections contributed to AR4 of the IPCC and are for the A2 SRES scenario. Units are the number of events per grid point per year.

Figure 2.8: Projected change in the annual frequency of occurrence of very hot days over Africa, for the periods 2011-2040, 2041-2070 and 2071-2100, relative to 1961-1990. The 90th percentile (left-hand side panel), median (middle panel) and 10th percentile (right-hand side panel) are shown for an ensemble of six downscalings of CGCM projections, for each of the time-slabs. The downscalings were generated using the regional model CCAM. All the CGCM projections contributed to AR4 of the IPCC and are for the A2 SRES scenario. Units are the number of events per grid point per year.

Figure 2.9: Simulated number of heat-wave events for the present-day period 1961-1990, for the 6 different CCAM A2 SRES scenario projections.

Figure 2.10: Simulated number of heat-wave events for the mid-future period 2041-2070, for the 6 different CCAM A2 SRES scenario projections.

Figure 2.11: Simulated number of heat-wave events for the present-day period 2071-2100, for the 6 different CCAM A2 SRES scenario projections.

Figure 2.12: Regional model simulations of the number of high fire danger days occurring annually over Africa (averaged over the period 1961-1990).

the ECMWF SST ensemble mean, and b) the difference per district between the AGCM forced with statistical SST and the AGCM forced with members of the ECMWF SST forecasts. Negative correlation differences show where the AGCM forced with ECMWF SST is superior.

Figure 4.5: Kendall's tau correlations over 24 years between observed DJF rainfall indices and a) retro-active forecasts of the AGCM forced with the ECMWF SST ensemble mean, and b) retro-active forecasts of the AGCM forced with the ECMWF ensemble members. Correlations significant (1-tailed test) at the 90% level of confidence are marked with an asterisk and correlations significant at 95% with a double asterisk.

Figure 4.6: The number of districts with significant (1-tailed test) correlations. "K" refers to Kendall's tau, "S" to Spearman rank and "P" to Pearson correlation. "90" and "95" respectively refer to the 90% and 95% levels of confidence. "CA SST" refers to the AGCM forced with constructed analogue SST; "ECMWFsc" refers to the AGCM forced with the ECMWF ensemble spread, and "ECMWFem" to the AGCM forced with the ECMWF ensemble mean SST forecasts

.

Figure 4.7: The top three panels show DJF rainfall index differences between cross-validated hindcasts and retro-active forecasts produced by first downscaling the three AGCM systems to rainfall districts. The bottom graphs are area-averaged values of cross-validation (red), retro-active (blue) and observed (grey) values for each of the AGCM systems.

Figure 5.1: C48 quasi-uniform conformal-cubic grid, which provides a horizontal resolution of about 200 km globally.

Figure 5.2: CCAM simulated (top panel) and CRU observed (lower panel) annual rainfall (mm) climatology over southern and tropical Africa (mm), for the period 1979-2004.

Figure 5.3: CCAM simulated seasonal rainfall (mm) climatology over southern and tropical Africa (mm), for the period 1979-2004.

Figure 5.4: CRU observed seasonal rainfall (mm) climatology over southern and tropical Africa (mm), for the period 1979-2004.

Figure 7.5: ECHAM4.5 AGCM operational probabilistic seasonal forecast for surface air temperature for December to February 2010 issued on 4 November 2010.

Figure 7.6: The evolution of ERF from subjective to object probabilistic forecast. The subjective consensus forecast (middle) is the outcome of the AGCM forecasts blended with the conveners' opinion in one of the LRF forum conducted at that time.

Figure 7.7: Operational surface air temperate forecast issued on 6 of December 2000 for the forecast period spanning 17 Dec 2000 to 6 Jan 2001, (a) ECHAM4.5 AGCM and (b) the corresponding observation (obtained from NOAA as indicated in map) but for December. The forecast shows good harmony with observation albeit the slight mismatch in terms of forecast period.

Figure 7.8: The ECHAM4.5 AGCM MSLP forecast (if it were) issued on March 18, 2007. The model indicates the development of trough adjacent south-eastern coast of South Africa on the evening at 18:00 UCT 18 March (c) and it gains its maturity midnight 12hrs later (06:00 UCT 19 March; d). The respective NCEP/R2 field are shown in (a) and (b). The satellite (Meteosat-8) image (RGB Composite (Airmass RGB; 18:00 UCT 18 March) is also shown. The cut-off low incident reportedly caused a massive damage in the coastal infrastructure and tourism industry.

Chapter 1

Introduction

The southern African region exhibits a high degree of natural climate variability, and is prone to the sporadic occurrence of droughts and floods (e.g. Joubert et al., 1996; Mason and Joubert, 1997; Tyson and Preston-Whyte, 2000). Various interannual components of the general circulation together account for this low-frequency variability. A probable cause of low-frequency variability in the atmosphere is the forcing associated with sea-surface temperature (SST) anomalies. These anomalies are themselves a result of coherent atmosphere-ocean interactions. The large thermal inertia of the oceanic surface mixed layer results in these anomalies to have time scales longer than those associated with sub-seasonal variations in the atmosphere (Holton, 2004). In fact, these anomalies are arguably of greatest significance in the forcing of atmospheric circulation at the seasonal to interannual time scales. The scientific basis for doing seasonal forecasting therefore originates from the observation that slowly evolving SST anomalies influence seasonal-mean weather conditions (Palmer and Anderson 1994; Goddard and Mason, 2002). Dry spells, heat waves and prolonged periods of agricultural drought also sporadically occur over the southern African region, often in association with El Niño events. These events have the potential to be predictable on a seasonal time scale and with several months lead-time, and a number of models have been developed for making long-range forecasts of sea-surface temperature (SST) anomalies of the equatorial Pacific Ocean over lead-times of several seasons (e.g. Zebiak and Cane, 1987; Stockdale et al., 1998; Landman and Mason, 2001; Metzger et al., 2004). At the other end of the scale, widespread flooding across the region may result from a number of different weather systems. Tropical cyclones are the most devastating; however, these systems make landfall over the region relatively infrequently (e.g. Reason and Kiebel, 2004). Other types of tropical systems, such as mesoscale convective complexes (MCCs), typically cause flooding over Zambia, Namibia and Botswana. Weather systems from the westerly wind regime, mostly cut-off lows, frequently bring damaging floods to the southern parts of South Africa (e.g. Singleton and Reason, 2007). Seasons of above normal rainfall over the summer rainfall region of South Africa often occurs in association with La Niña events.

Partly because of this high degree of natural climate variability, the southern African region is thought to be particularly vulnerable to anthropogenically induced climate change (e.g. Meadows, 2006; Engelbrecht, 2010). Climate change may indeed manifest itself not only through a change in the long-term mean rainfall, temperature and circulation patterns, but also through a global increase in the frequency of extreme events. Thermodynamic arguments relate global warming to a general increase in intense precipitation and tropical storms at a global scale, rather to a decrease in such events. A greenhouse-warmed climate has more energy (heat) available for the generation and spin-up of tropical cyclones, and potentially also for the generation of more westerly waves, MCCs and thunderstorms. However, anthropogenic forcing may simultaneously alter large-scale circulation patterns (such as shifts in the subtropical high-pressure belt) in such a way that rainfall events, including extremes, are suppressed over certain climate regimes of the Earth (e.g. Seidel et al., 2008). The potential effects of enhanced anthropogenic forcing on the occurrence of extreme weather events over southern Africa therefore require rigorous investigation.

The tools of statistical and dynamical downscaling may be used to obtain high-resolution projections of climate change over southern Africa, from the forcing of courser resolution projections of coupled global climate modes (CGCMs). Only a few such detailed projections have been described over the southern African region (e.g. Hewitson et al., 2006; Tadross et al., 2006; Engelbrecht et al., 2009). These studies have provided some evidence that eastern South Africa may be expected to become wetter, with more extreme rainfall events, in the future climate. Localised, intense convective rainfall events may be expected to increase partially as a result of enhanced surface heating and a more intense heat low over the western interior of South Africa (e.g. Tadross et al., 2006; Engelbrecht et al., 2009). There is also the likelihood for the more frequent formation of the South Indian Convergence Zone (ITCZ) over eastern South Africa under enhanced anthropogenic forcing. This would imply the more frequent formation of tropical temperate cloud bands over the region, and the more frequent occurrence of widespread rainfall from thunderstorms embedded within these cloud bands (e.g. Engelbrecht et al., 2009).

Although the independently performed studies described above provide some evidence that summers over eastern South Africa may become wetter with more intense rainfall events, there is also evidence that the summer rainfall season may be expected to become shorter, with the climate of southern Africa becoming generally drier (e.g. Christensen et al., 2007; Engelbrecht et al., 2009). The ensemble of CGCMs used by the Intergovernmental Panel on Climate Change in Assessment Report 4 (AR4) projected a general strengthening of the subtropical high-pressure belt, leading to a southerly shift in the westerly wind regime. The models conveyed a consistent message of an increase in the frequency of extremely dry winter and spring seasons in southern Africa (Christensen et al., 2007). The regional climate modelling study of Engelbrecht et al. (2010) indicated that the general strengthening of the subtropical high pressure belt over southern Africa, as projected by the CGCMs of AR4, may translate over southern Africa to the more frequent formation of mid-level highs over southern Africa – for all seasons except summer. These highs are known to suppress rainfall over the region through the subsidence they cause (e.g. Tyson and Preston-Whyte, 2000). Consistent with the downscaled scenarios described earlier, the CGCMs of AR4 projected a doubling in the frequency of extremely wet austral summers over southern Africa, despite the region being projected to become generally drier (Christensen et al., 2007).

One of the objectives of this project is to analyse a large and new set of regional projections of climate change over southern Africa. The emphasis would be to analyse the model projected changes in extreme weather events over southern Africa, within the context of anthropogenic forcing. Metrics for which the climate change signal is to be evaluated include extreme rainfall events (localised, intense convective rainfall events that may lead to flash-flooding, as well as widespread rainfall events that may cause flooding at larger scales), dry spell length and duration and the frequency of occurrence of heat-waves. That is, the project also aims to test the hypothesis that extreme weather events over southern Africa may be expected to occur more frequently in the future climate, and to gain more insight into the nature of these changes. Through analysis of the climate change projections mentioned, the project also aims to investigate how some important weather system types, known to cause severe weather over southern Africa, may be expected to change in frequency of occurrence and intensity under enhanced anthropogenic forcing. Of particular

interest would be cut-off lows and tropical cyclones, known to cause large scale flooding, as well as intense thunderstorms, that cause localised flash-flooding.

The observed increase in frequency of hydrometeorological disasters (especially flooding events) since the 1990s has led to the doubling of humanitarian disasters worldwide. Of all the natural disasters, weather and climatic events represent 71% of the large-scale economic disasters and are responsible for 69% of the economic losses (USD1700bn) and 95% of insured losses (USD340bn) globally over the past 6 decades (source: UNDP). Closer to home, severe drought seasons (such as 1982/83) amounted to USD1billion in losses. Moreover, droughts and floods cause damages of at least ZAR174million per year over South Africa (source: OFDA/CRED International Disaster Data Base). However, it has been shown that improvements in early warning systems have contributed to decreases in the numbers of fatalities, injuries and livelihood losses over the last 3 decades (IFRC, 2009). A shortcoming of the early warning systems is that they are based on weather predictions that often provide less than 24 hours' notice of an impending extreme event such as a flood. Therefore, owing to the possible changes in weather and climate extremes as a result of climate change, the development of efficient prediction tools that can effectively provide warnings on floods and storms, droughts and heat waves, with sufficient lead time is a significantly important approach to assist in adaptation to possible increases in hazards associated with such changes. Moreover, there is not much to be gained by preparing to survive the impacts of possible disasters a number of decades from now if one is not equipped to survive more immediate threats. Therefore, developing flexibility and resiliency to weather and climate anomalies necessitates developing flexibility and resiliency to its variability on various time scales not limited only to the multi-decadal, but also inclusive of weather (days 1 to 7) as well as seasonal-to-interannual time scales of weeks to seasons.

The disaster risk management community has up to now largely operated on a reactive mode to disaster that have already happened or disasters predicted with high confidence to occur, for example the prediction of the track and intensity of a probable landfalling tropical cyclone. However, the possibility of using weather and seasonal forecasts beyond just a few days of impending extreme events is still in its infancy. One of the difficulties forecast users face is the drop in forecast performance

(skill) from short-range weather forecasting to seasonal forecasting. In addition, the uncertainties in the seasonal rainfall forecasts are limiting its use, and so does the interpretation of these types of forecasts. For example, although the 2009/10 season was predicted with confidence to be more likely to be dry than wet over the summer rainfall region of South Africa, the larger part of the country received above average summer rainfall totals. Even if the forecast was for wet conditions to occur over that season the wet forecast does not necessarily indicate that there would have been a higher risk of flood events since a wet season could be a result of the frequent occurrence of moderately heavy rainfall. There is therefore a need to develop prediction tools that can more effectively translate their output to information directly relevant to end users, for example the downscaling of seasonal forecasts to catchment level (Landman et al., 2001).

There is a growing trend internationally towards prediction systems that will bridge the gap between weather forecasts and forecasts or projections for much longer time scales (Hudson and Alves, 2009; Vitart et al., 2008). Such a system is called seamless since a common forecast system is used to predict for multiple time scales. There are important alliances between the mathematical models of the atmosphere to predict the weather and those predicting the anomalies associated with climate variability and change. The first one is that many of the important feedbacks that lead to uncertainty in climate predictions are associated with processes such as convection, whose intrinsic time scales lie within the domain of numerical weather prediction (NWP). Moreover, the NWP community has developed code optimization tools and created a supercomputer environment that are also benefitting predictions at longer and much longer time scales, since these developments have, amongst others, lead to increasing the horizontal and vertical resolutions of models configured for climate variability and change projections. However, NWP may also benefit from developments in climate prediction, especially by looking into model errors (ECMWF Newsletter No 115, 2008).

In addition to the planned high-resolution climate change projection work mentioned above, the forecast time-ranges for operational utility to be considered for this project include the World Meteorological Organisation’s defined short- (beyond 12 hours and up to 72 hours), medium- (beyond 72 hours and up to 240 hours) and long-range or

seasonal (from 30 days up to seasons) time scales. Forecasts beyond weather forecasting time scales (i.e. beyond 3 days), are not that common and are generally produced at relatively low resolution (Vitart et al., 2008). In fact, in South Africa it is only the South African Weather Service (SAWS) and recently the Council for Scientific and Industrial Research (CSIR) that produce forecasts operationally at the medium-range time scale. The SAWS's medium-range forecasts are based on the NCEP EFS (http://wwwt.emc.ncep.noaa.gov/gmb/ens/index.html) (Tennant et al. 2007), which is an entirely different system to the one used by the SAWS for forecasts for the first two days. These short-range forecasts are based on the United Kingdom Unified Model. In addition, long-range forecasts are based on a separate system once more. The ECHAM4.5 (Roeckner et al., 1996) has been used at the SAWS for seasonal forecasts. The CCAM model, on the other hand, has been applied at all time-scales and at spatial resolutions varying from high resolution to relatively low resolution for global applications (Engelbrecht et al., 2009, Landman et al., 2009a, Potgieter, 2007), indicating the potential of the model to be used in operational seamless forecasting

Merging forecast models will save resources by not having to run separate systems for weather and longer forecast time ranges. Computing resources can then be used to enlarge the forecast ensemble, and even run an additional seamless forecasts system in order to produce a multi-model ensemble forecast (Krishnamurti et al., 2000, Landman et al., 2009a). A major advantage is also that reforecasts or hindcasts to calibrate a seasonal forecast system will be available to calibrate forecasts for shorter time scales (Vitart et al., 2008). In addition, using different forecasting systems with different physics to produce a forecast spanning over various time ranges may lead to forecasts being inconsistent over these time ranges. Having to run entirely separate systems for various time ranges is therefore suboptimal. Another advantage of the seamless system presented here is that the scheme may allow longer range weather and seasonal climate forecasts to be issued at a much higher frequency than is currently the case. For example, the frequency of issuing a seasonal forecast can be increased from once a month to a few times a month. Such an increased frequency should improve forecasts from the short-range weather to short-lead seasonal forecasts since atmospheric initial conditions will be allowed to influence these forecasts more frequently.

In summary, existing evidence from regional climate modelling studies and the global assessments of the Intergovernmental Panel on Climate Change (IPCC) indicate that the southern African region may be expected to become generally drier, with an increase in the frequency of extreme climatological anomalies. It therefore seems likely that the skilful prediction if such anomalies at the short-, medium- and long-range (seasonal) time-scales will become increasingly important. This project has aimed to gain more insight into the potential effects of enhanced anthropogenic forcing on the occurrence of extreme weather events over southern Africa, through the analysis of a large ensemble of newly derived high-resolution projections of a climate change over southern Africa, and then subsequently aimed to develop operational forecasting systems to skilfully predict such extremes on much shorter time scales.

The analysis of the climate change projections will lead to an improved understanding how some important weather system types, known to cause severe weather over southern Africa, may be expected to change in frequency of occurrence and intensity under enhanced anthropogenic forcing. Of particular interest would be cut-off lows and tropical cyclones, known to cause large scale flooding, as well as intense thunderstorms, that cause localised flash-flooding. The envisaged operational forecasting system can bridge the gap between weather and seasonal forecasts. Skilfully forecast meteograms (the time-evolution of weather parameters, such as rainfall and temperature, and its associated forecast uncertainties as reflected by the forecast ensemble members), will in return provide useful warnings well in advance of an impending high-impact weather or climate event, such as floods or mid-summer drought periods. In South Africa agriculture is heavily dependent on weather and climate. Seamless forecasts may be able to assist in pre-emptive procedures such as switching to drought resistant crops, or give indication of seasonal onset (Tadross et al., 2005). Natural disasters associated with extremely wet spells can lead to the destruction of shelters near rivers – seamless forecasts can also feed into streamflow forecasting systems that can be used for alerts. Tropical cyclones also cause devastation over South Africa. Domoina in 1984 is a good example, and this system produced maximum precipitation exceeded 500 mm over a 5-day period over northern KwaZulu-Natal and southern Mpumalanga. On the other hand, usually to the west of such land-falling systems,

over the central and western plateau, fine and dry conditions prevail, possibly further contributing to periods of droughts there. The system presented in this report will therefore also benefit society if it can successfully produce tropical cyclone tracks and occurrences on various time scales.

Chapter 2

Projections of future climate change over Africa using a seamless modelling system

2.1 Introduction

The southern African region exhibits a high degree of natural climate variability, and is prone to the sporadic occurrence of droughts and floods (e.g. Joubert et al., 1996; Mason and Joubert, 1997; Tyson and Preston-Whyte, 2000). Dry spells, heat waves and prolonged periods of agricultural drought also sporadically occur over the southern African region, often in association with El Niño events. At the other end of the scale, widespread flooding may result from a number of different weather systems. Tropical cyclones are the most devastating, however, these systems make landfall over the region relatively infrequently (e.g. Reason and Kiebel, 2004). Other types of tropical systems, such as mesoscale convective complexes (MCCs), typically cause flooding over Zambia, Namibia and Botswana. Weather systems from the westerly wind regime, mostly cut-off lows, frequently bring damaging floods to the southern parts of South Africa (e.g. Singleton and Reason, 2007). Seasons of above normal rainfall over the summer rainfall region of South Africa often occurs in association with La Niña events.

Partly because of this high degree of natural climate variability, the southern African region is thought to be highly vulnerable to anthropogenically-induced climate change (e.g. Meadows, 2006; Engelbrecht, 2010). Climate change may indeed manifest itself not only through a change in the long-term mean rainfall, temperature and circulation patterns, but also through a global increase in the frequency of extreme events. Thermodynamic arguments relate global warming to a general increase in atmospheric moisture content and intense precipitation events. A greenhouse-warmed climate has more energy (heat) available for the generation and spin-up of intense tropical cyclones, and potentially also for the generation of more westerly waves, MCCs and thunderstorms. However, anthropogenic forcing may simultaneously alter large-scale circulation patterns (for example, through meridional shifts in location of the westerlies and the subtropical high-pressure belt), in such a

way that rainfall events, including extremes, are suppressed over certain climate regimes of the Earth (e.g. Seidel et al., 2008). The potential effects of enhanced anthropogenic forcing on the occurrence of extreme weather events over southern Africa therefore require rigorous investigation.

The tools of statistical and dynamical downscaling may be used to obtain high-resolution projections of climate change over southern Africa, from the forcing of courser resolution projections of coupled global climate modes (CGCMs). Only a few such detailed projections have been described to date for the southern African region (e.g. Hewitson et al., 2006; Tadross et al., 2006; Engelbrecht et al., 2009, 2011; Engelbrecht et al., 2012; Malherbe et al., 2013). These studies have provided some evidence that eastern South Africa may be expected to become wetter during summer, with more extreme rainfall events, in the future climate. Localised, intense convective rainfall events may be expected to increase partially as a result of enhanced surface heating and a more intense heat low over the western interior of South Africa (e.g. Tadross et al., 2006; Engelbrecht et al., 2009; Engelbrecht et al., 2012). There is also the likelihood for the more frequent formation of the South Indian Convergence Zone (ITCZ) over eastern South Africa under enhanced anthropogenic forcing. This would imply the more frequent formation of tropical temperate cloud bands over the region, and the more frequent occurrence of widespread rainfall from thunderstorms embedded within these cloud bands (e.g. Engelbrecht et al., 2009).

Although the studies described above provide some evidence that summers over eastern South Africa may become expected to become wetter with more intense rainfall events, there is also evidence that the summer rainfall season may become shorter, with the climate of southern Africa becoming generally drier (e.g. Christensen et al., 2009; Engelbrecht et al., 2009). The ensemble of CGCMs used by the Intergovernmental Panel on Climate Change (IPCC) in Assessment Report 4 (AR4) projected a general strengthening of the subtropical high-pressure belt over southern Africa, with an associated poleward shift of the westerly wind regime. The models conveyed a consistent message of an increase in the frequency of extremely dry winters and springs in southern Africa (Christensen et al., 2009). The regional climate modelling study of Engelbrecht et al. (2009) indicated that the general strengthening of the subtropical high-pressure belt over southern Africa, as projected

by the CGCMs of AR4, may translate over this region to the more frequent formation of mid-level highs, for all seasons except summer. These highs are known to suppress rainfall over the region through the subsidence they cause (e.g. Tyson and Preston-Whyte, 2000). Consistent with the downscaled scenarios described earlier, the CGCMs of AR4 projected a doubling in the frequency of extremely wet austral summers over southern Africa, despite the region being projected to become generally drier (Christensen et al., 2009). One of the objectives of this project is to analyse a large and new set of regional projections of climate change over southern Africa. These projections were obtained through the application of a high-resolution regional climate model on the computer clusters of the Centre for High Performance Computing (CHPC) in South Africa. The emphasis is on analyzing the model projected changes in extreme weather events over southern Africa, within the context of anthropogenic forcing. Extreme events for which the climate change signal is evaluated include extreme rainfall events, droughts, heat-waves and the number of high fire-danger days. That is, the research tests the hypothesis that extreme weather events over southern Africa may be expected to occur more frequently in the future climate, and aims to gain more insight into the nature of these changes.

In summary, existing evidence from regional climate modelling studies and the global assessments of the Intergovernmental Panel on Climate Change (IPCC) indicate that the southern African region may be expected to become generally drier, with an increase in the frequency of extreme weather events. These aspects are explored in more detail in Chapter 2, through the analysis of a new ensemble of regional projections. It seems likely, however, that the skilful prediction of extreme weather at the short-, medium-, extended- and long-range (seasonal) time-scales will become increasingly important under climate change. The research project therefore also had the aim to develop operational forecasting systems that skilfully predict such extremes on much shorter time scales (as an adaptation tool to climate variability and change). Subsequent chapters report on these developments.

2.2 The conformal-cubic atmospheric model (CCAM)

The dynamic regional climate model applied within the project to project climate change over Africa is a variable-resolution global atmospheric model, the conformal-cubic atmospheric model (CCAM) of the Commonwealth Scientific and Industrial Research Organisation (CSIRO) in Australia (McGregor, 1996, 2005a, 2005b; McGregor and Dix, 2001, 2008). The model uses a semi-implicit semi-Lagrangian method to solve the hydrostatic primitive equations, and employs a fairly comprehensive set of physical parameterizations. The GFDL parameterizations for long-wave and short-wave radiation are used, with interactive cloud distributions determined by the liquid and ice-water scheme of Rotstayn (1997). A stability-dependent boundary layer scheme based on Monin Obukhov similarity theory is employed, together with the non-local treatment of Holtslag and Boville (1993). A canopy scheme is included, as described by Kowalczyk et al. (1994), having six layers for soil temperatures, six layers for soil moisture (solving Richard's equation) and three layers for snow. The cumulus convection scheme uses a mass-flux closure, as described by McGregor (2003), and includes downdrafts, entrainment and detrainment.

CCAM may be applied at quasi-uniform resolution, or alternatively in stretched-grid mode to obtain high resolution over an area of interest. Recent years have seen the advent of variable-resolution atmospheric global circulation models such as CCAM, as an alternative to limited-area models, for the purpose of downscaling the output of CGCMs. An advantage of the variable-resolution approach is that the use of lateral boundary conditions, which are responsible for the artificial reflection of atmospheric waves in limited-area models and the occurrence of spurious vertical velocities near the boundaries, are avoided. Variable-resolution global models may therefore be considered as a specific variety of regional climate models (RCMs). CCAM is a particularly flexible downscaling tool, which through the use of the Schmidt transformation can set of multitudes of grids for multiple-nudging procedures, using either grid-point or spectral approaches (McGregor, 2005b; Thatcher and McGregor, 2009, 2010). The model code has been implemented for parallel processing using Message Passing Interface (MPI) software on the computer clusters of the CHPC.

It has been shown that CCAM may be used to obtain plausible projections of future climate change, as well as skilful simulations of inter-annual and short-range variability (Engelbrecht et al. 2009, Landman et al., 2009; Engelbrecht et al. 2011; Malherbe et al., 2013). It also realistically simulates observed daily climate statistics, such as the number frequency of extreme precipitation events and the tracks of cut-off lows and tropical cyclones over the region (Engelbrecht et al., 2012; Malherbe et al., 2013). The model has been applied across a range of spatial scales, from simulations of global climate at horizontal resolutions of about 200 km, to very fine scale (1 km horizontal resolution) simulations over small areas, such as the Cape Peninsula (Engelbrecht et al., 2011). Application of the shorter time scales has allowed testing of its capability to represent fundamental forcing mechanisms of southern African climate (for example, the El Niño teleconnection to southern African rainfall). The model has also been rigorously tested over other climatological regions, including Australasia (e.g. Nunez and McGregor, 2007; Lal et al., 2008). The adequate performance of this seamless modelling approach across “verifiable” time scales, and across multiple spatial scales, enhances the confidence in its ability to produce credible model projections of future climate change.

2.3 Experimental design of the climate-change projections

The research described in this chapter relies on two regional climate simulation experiments, which have been performed in recent years by the CSIR and CSIRO. In the first experiment the model was forced with the bias-corrected sea-surface temperature (SST) and sea-ice output of six different CGCMs used in AR4 of the IPCC, for the period 1961-2100. The CGCMs downscaled are GFDL-CM2.0, GFDL-CM2.1, ECHAM5/MPI-Ocean Model, UKMO-HadCM3, MIROC3.2-medres and CSIRO Mark3.5. All six of the projections performed are for the A2 emission scenario of the Special Report on Emission Scenarios (SRES). The associated CO_2, sulphate, ozone and aerosol fields were all obtained from the CSIRO. A multiple-nudging strategy was followed, by first integrating

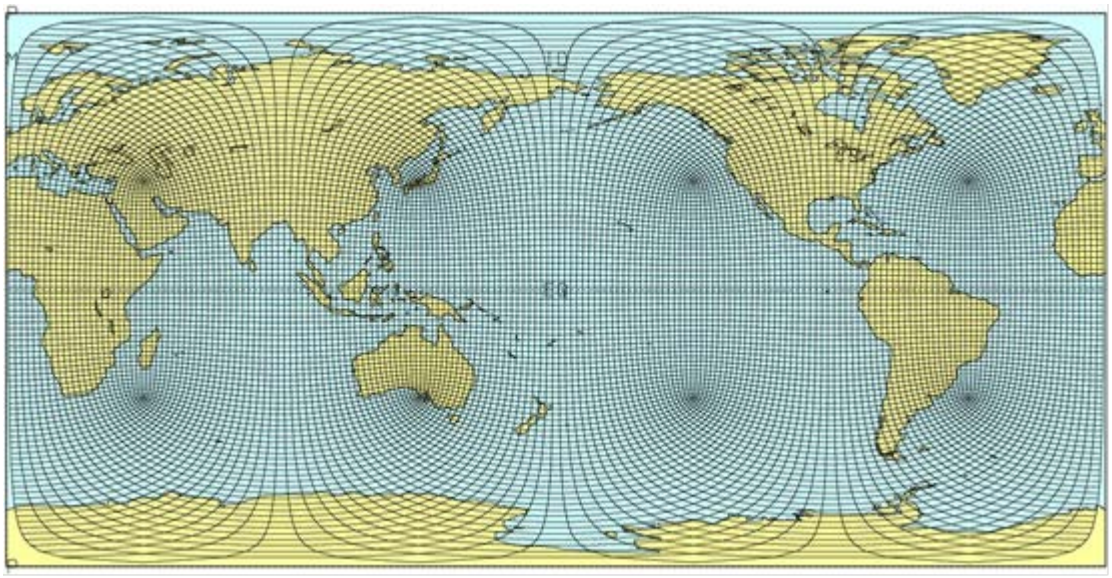

Figure 2.1: Quasi-uniform C48 CCAM grid, having a horizontal resolution of about 2° in latitude and longitude.

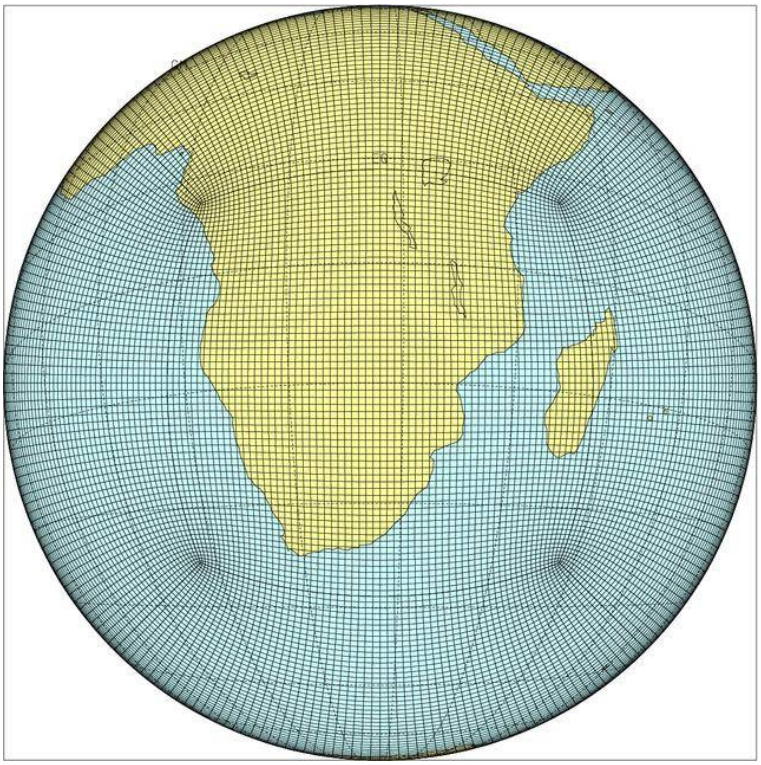

Figure 2.2: Stretched C64 CCAM grid, having a horizontal resolution of about 0.5° over southern Africa and the southwest Indian Ocean.

CCAM globally at quasi-uniform C48 resolution (about 200 km in the horizontal, that is, about 2° in latitude and longitude – Fig. 2.1), forcing the model with the SSTs and sea-ice of each host model, and with CO_2, sulphate and ozone forcing consistent with the A2 scenario. In a second phase of the downscaling, CCAM was integrated in stretched-grid mode over Africa at a resolution of about 0.5° in latitude and longitude (a horizontal resolution of about 50 km – Fig. 2. 2). The higher resolution simulations were nudged within the quasi-uniform simulations, through the application of a digital filter using a 4000 km length scale. The filter was applied at six-hourly intervals and from 900 hPa upwards. An important feature of the simulations is the use of bias-corrected SSTs. A problem common to almost all CGCMs, is the existence of the “cold tongue” bias along the equatorial Pacific. This bias leads to significant distortions of atmospheric flow patterns over the equatorial Pacific in the host CGCMs (e.g. Katzfey et al., 2009; McGregor et al., 2011). The use of bias-corrected SSTs in the simulations described here avoids these distortions in the simulated atmospheric flow, and makes feasible more realistic simulations of the global and also African climate.

The CSIR in CSIRO has since the completion of the climate simulations described above started to collaborate towards downscaling the CGCM projections of the Coupled Model Intercomparison Project Phase 5 (CMIP5) and Assessment Report 5 (AR5) to high spatial resolution globally. The simulations performed are for the Representative Concentration Pathway (RCP) 4.5 and 8.5 Wm^{-2} emissions scenarios. The CGCMs downscaled from CMIP5 include the ACCESS1-0, GFDL-CM3, MPI-ESM-LR, CNRM-CM5, MIROC4h, NorESM1-M, CCSM4, MRI-GCM3 and IPSL-CM5A-MR models. Results from the downscaling of the first three of these CGCMs are presented here. The downscaling involves using the sea-ice concentrations and bias-corrected sea-surface temperatures of the CGCMs, to force very high resolution CCAM simulations performed globally, at a quasi-uniform resolution of approximately 50 km. These simulations will contribute to the Coordinated Regional Downscaling Experiment (CORDEX). In the simulations, CCAM is integrated coupled to the CSIRO Atmosphere Biosphere Land Exchange (CABLE) model, a dynamic land-surface model with the capability to interactively simulate the carbon flux between the land-surface and atmosphere. The downscalings of the CGCM downscalings span the period 1951-2100.

Climate models, including both CGCMs and RCMs, are known to display systematic errors (biases) in their simulations of present-day climate attributes. A simple bias-correction procedure was applied in this research, before the indices relevant to extreme weather events were calculated. First, the CRU TS3.1 data set of the Climatic Research Unit (CRU) was used to calculate the monthly climatologies for the variables of average daily rainfall, minimum temperature, maximum temperature, minimum relative humidity and maximum relative humidity, for the period 1961-1990. For each of the six downscalings performed, the simulated monthly climatologies were calculated for the same period. These were then used to calculate the monthly model biases (separately, for each downscaling). A bias-corrected version of each downscaling was subsequently obtained, by subtracting for each day in the simulation the relevant monthly bias – for each of the variables under consideration. In the case of rainfall, the overestimation/underestimation was expressed as a percentage, and daily rainfall totals were corrected with an appropriate fraction (rather than to subtract the relevant monthly bias). This bias-correction procedure results in the 1961-1990 climatology for each of the six downscalings to be exactly that of CRU TS3.1, however, the inter-annual variability and daily variability remains that of the downscaled simulation. For further discussion and an application of the methodology, see Winsemius et al. (2014).

2.4 Projections of future climate change over Africa – temperature and rainfall

2.4.1 Temperature

Most land areas, including the African continent, are projected to warm faster than the globe on the average – largely due to the heat capacity of the landmasses being significantly lower than that of the oceans (e.g. Christensen et al., 2007). The high-resolution projections presented here describe a consistent pattern of change – the tropics are projected to warm at about 1.5 times the global rate of temperature increase, whilst the subtropics are projected to warm at about twice the global rate of temperature increase (Figs. 2.3 to 2.5). Smaller warming is also projected for the coastal areas in general, in comparison to the interior regions of the continent. These patterns of relative strengths in the warming signal seem to occur independent of the

global mean rate of warming (that is, independent of the specific emission scenario under consideration).

Rapid rises in the annual average near-surface temperature are projected to occur over the African continent during the 21st century under A2 SRES and RCP8.5. The projected changes are shown in Figs. 2.3 (A2 SRES) and 4 (RCP8.5) for the near-future, mid-future and far-future, relative to a present-day baseline period. For each time-slab, the 10th, 50th (median) and 90th percentiles are shown, for the ensemble of projected changes. For the near-future, temperature increases of between 1 and 2°C are projected by most ensemble members. The largest temperature increases are projected for subtropical southern Africa and the northern Sahara. For the period 2040-2060, annual average temperatures are projected to rise by between 3 and 4.5°C (4 and 5°C) for the A2 SRES (RCP8.5) scenario over large parts of the southern African interior, and also over northern Africa. Substantial temperature increases of more than 2°C are also projected for the southern interior and coastal areas. Drastic increases in average annual temperatures are projected for the far-future period. Increases of more than 5°C (4°C) are projected across the southern African interior for RCP8.5 (A2 SRES), with increases of more than 3°C that are projected for the coastal areas. Generally, the pattern and amplitude of projected temperature increases shows close correspondence across the different ensemble members, indicating that the projected signal is robust.

Compared RCP8.5 and A2 SRES, RCP4.5 represents a future where the risks associated with temperature increases over southern Africa are significantly reduced. The projected changes are shown in Fig. 2.5. For the near-future, temperature increases of between 1 and 2°C are projected by most ensemble members (similar to the RCP8.5 downscalings). However, for the period 2040-2060, annual average temperatures are projected to rise by only 2 to 3°C over the southern African interior. Moreover, the projected increases for 2080-2100 are reduced to about 2.5 to 4 °. Although the projected increases of 2.5 to 4°C over the interior regions are still significant, the amplitude of temperature increase is about halved, compared to the RCP8.5 projections for 2080-2100.

There is some seasonal variation in the temperature signal over Africa (not shown), although not nearly as drastic as over mid-latitudinal regions (Christensen et al.,

2007). Over southern Africa the largest temperature increases are projected to occur during the boreal spring. See Engelbrecht et al. (2013a) for a discussion of these aspects.

Keeping the rise in the global average near-surface temperature below 2°C (compared to the global temperature at pre-industrial times) during the 21st century, through a binding international treaty on greenhouse gas emissions, has become a primary objective of the IPCC and the United Nations Framework Climate Change Convention (UNFCC). It is thought keeping the global temperature increase below this threshold that "dangerous climate change" may be prevented. However, the results presented here indicate that even if this target is reached, it would still imply strong warming over large parts subtropical southern and North Africa – in the order of 4°C. The projected rapidly rising temperatures over these regions may be expected to have numerous impacts across many different sectors, for example on agriculture (e.g. Thornton et al., 2011), water resources (through increased evaporation), biodiversity and energy consumption (for example, the household energy demand for cooling in summer may be expected to increase, whilst the demand for warming in winter may be expected to decrease).

2.4.2 Rainfall

Fig. 2.6 shows the projected change in annual rainfall totals (mm) over Africa for the periods 2011-2040, 2041-2070 and 2071-2100 relative to 1961-1990, as obtained from the ensemble of high-resolution CCAM projections under the A2 scenario. The 10th percentile, median and 90th percentile of the ensemble of projected changes are shown. A number of studies have demonstrated the ability of CCAM to realistically simulate the attributes of the present-day rainfall climatology over southern Africa, including annual rainfall totals and the seasonal cycle in rainfall (Engelbrecht et al., 2009), inter-annual rainfall variability (Landman et al., 2009) and the frequency of occurrence of extreme rainfall events (Engelbrecht et al., 2012). The satisfactory simulation of these present-day attributes provides some confidence in the model projections of the future attributes of rainfall over the continent. Moreover, the skill of the CCAM system in deterministic short-range weather prediction (see Chapter 3)

and seasonal prediction (see Chapter 5) further strengthens confidence in the projections of future rainfall patterns.

Consistent with the ensemble of CGCM projections of AR4 of the IPCC, the projected rainfall signal shows great variation across the continent. It seems plausible that the subtropical parts (including southern Africa and the northern Sahara) will become drier in response to enhanced anthropogenic forcing (see also Christensen et al., 2007). Similarly, regions poleward of the subtropics are likely to dry – Mediterranean Africa, north of the Sahara, as well as the winter rainfall region of southwestern South Africa. Conversely, there is evidence that East Africa and tropical Africa are plausible to become wetter. Projections of future changes in rainfall over West Africa (including the Sahel and Guinean coast) and the southern Sahara are more uncertain – there is more variation in the climate change signal across the CCAM ensemble members (see also Christensen et al., 2007). It is interesting to note that the patterns of rainfall change projected by the CCAM ensemble is largely stationary across the different time-slabs, but increases in amplitude as the greenhouse effect strengthens in time (Fig. 2.6). The projected changes in seasonal rainfall totals across the African continent are discussed in some detail by Engelbrecht et al. (2013a).

The ensemble of CCAM projections projects a robust pattern of rainfall increases over East Africa, east of Great Lakes area and extending into the Horn of Africa – consistent with the CGCM projections described in AR4 of the IPCC (Christensen et al., 2007). This signal is robust for annual rainfall totals across the ensemble members (Fig 2.6). Similar patterns of increases in annual rainfall totals over East Africa are described in the projections of Hulme et al. (2001), Ruosteenoja et al. (2003) and in the regional model projection of Engelbrecht et al. (2009). There is evidence that the East African monsoon may be expected to increase in intensity in response to the enhanced anthropogenic forcing and warming of the African continent (e.g. Engelbrecht et al., 2009). This is associated with the increased transport of moisture into East Africa (e.g. northern Mozambique, Tanzania and Kenia) with associated increases in precipitation.

The CCAM projections indicate that it is plausible for large parts of West Africa to become wetter under enhanced anthropogenic forcing. This pattern may be related

to the tropics expanding polewards under climate change (Seidel et al., 2008). However, some of the ensemble members are indicative of a drier future, implicating that greater uncertainty is associated with the projections of climate change over West Africa (compared to the robust pattern of wetting over East Africa). Drying is projected for the North African west coast by most of the CCAM downscalings, a pattern that is consistent with the ensemble of AR4 CGCMs. North of the subtropics this drying occurs in response to the systematic poleward shift of storm tracks (e.g. Christensen et al., 2007). The CCAM ensemble projects wetting over the southern Sahara, in response to the poleward-expanding tropical rainfall region. Off the Guinean coast to the south, and over the Sahel, the projected rainfall changes indicate a wetter future. However, the CGCM projections of AR4 displayed a great deal of variation over this region. A robust pattern of drying is projected across the northern Sahara by the high-resolution CCAM ensemble (Fig. 2.6), consistent with the ensemble of AR4 CGCMs (Christensen et al., 2007). This occurs in association with drying projected over the Mediterranean coast, and the strengthening and northward expansion of the subtropical high-pressure belt. The CCAM ensemble is indicative of quite substantial rainfall increases over the southern Sahara, whilst AR4 of the IPCC concluded that indications of the likely sign of the rainfall signal over this region are inconclusive. The African Mediterranean coast is expected to dry, in response to the large-scale poleward shift of the westerly wind regime and storm tracks, in conjunction with the strengthening and northward expansion of the subtropical high-pressure belt. This signal is robust across the ensemble of CGCM simulations described in AR4, with the rainfall decreases projected to be in the order of 20%. The CCAM ensemble consistently indicates a robust message of drastic decreases in precipitation over the Mediterranean coast and adjacent interior, as large as 40% over some regions.

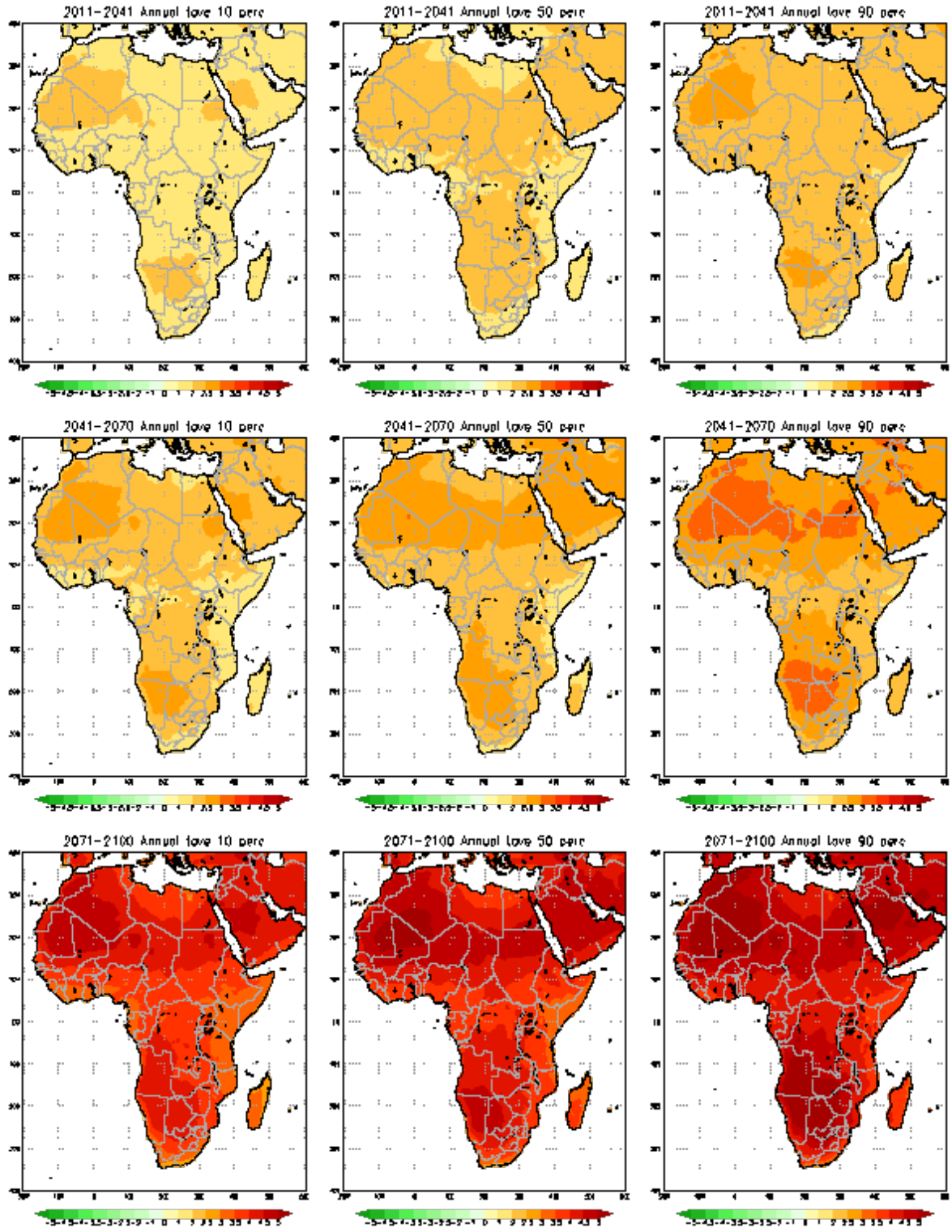

Figure 2.3: Projected change in the annual average temperature (°C) over Africa, for the time-slabs 2011-2040 (top), 2041-2070 (middle) and 2071-2100 (bottom), relative to 1961-1990. The 90th percentile (right-hand side panel), median (middle panel) and 10th percentile (left-hand side panel) are shown for an ensemble of six downscalings of CGCM projections, for each of the time-slabs. The downscalings were generated using the regional model CCAM. All the CGCM projections contributed to AR4 of the IPCC and are for the A2 SRES scenario.

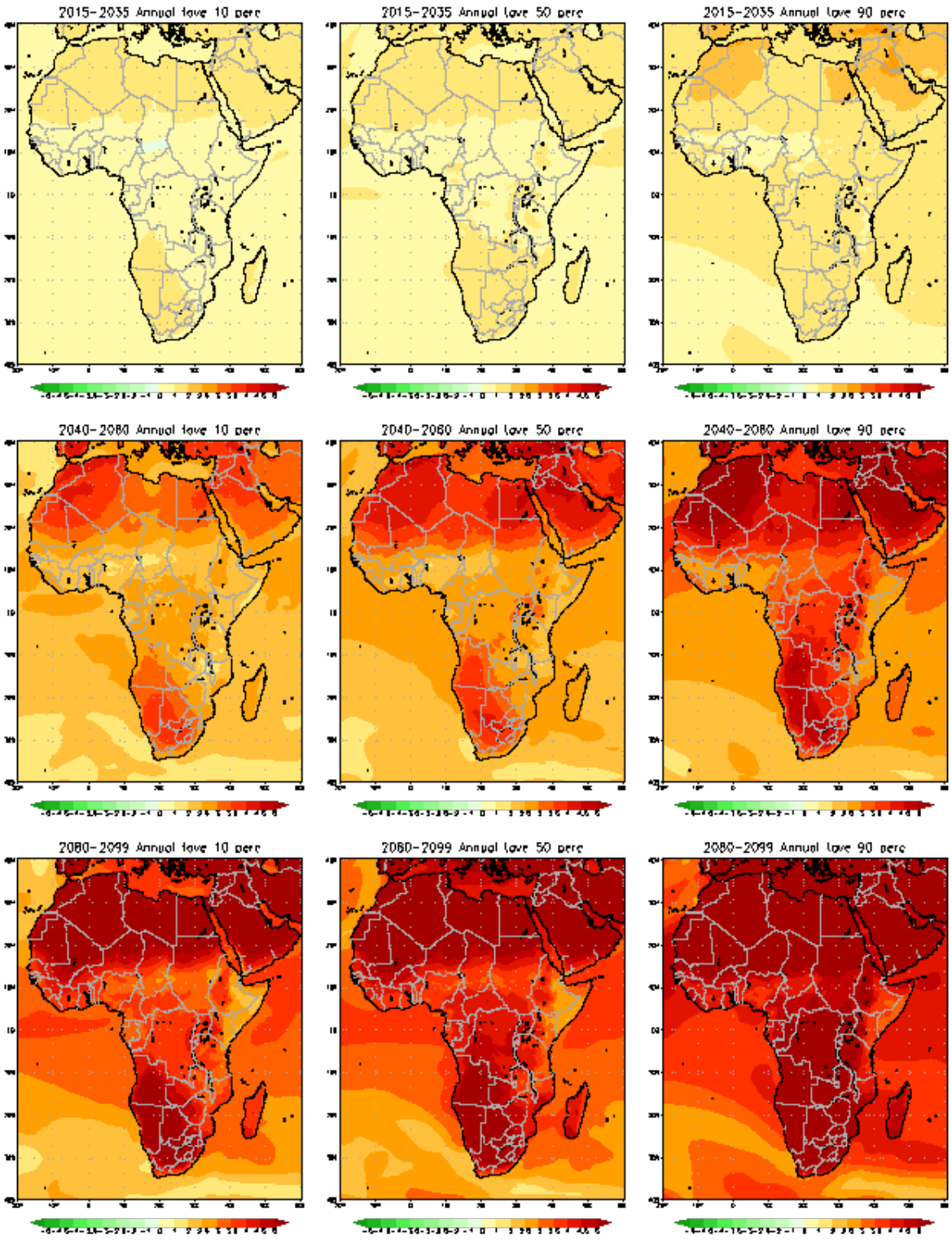

Figure 2.4: Projected change in the annual average temperature (°C) over Africa, for the time-slabs 2015-2035 (top), 2040-2060 (middle) and 2080-2100 (bottom), relative to 1970-2005. The 90th percentile (right-hand side panel), median (middle panel) and 10th percentile (left-hand side panel) are shown for an ensemble of downscalings of three CGCM projections, for each of the time-slabs. The downscalings were performed using the regional model CCAM. All the CGCM projections contributed to CMIP5 and AR5 of the IPCC, and are for RCP8.5.

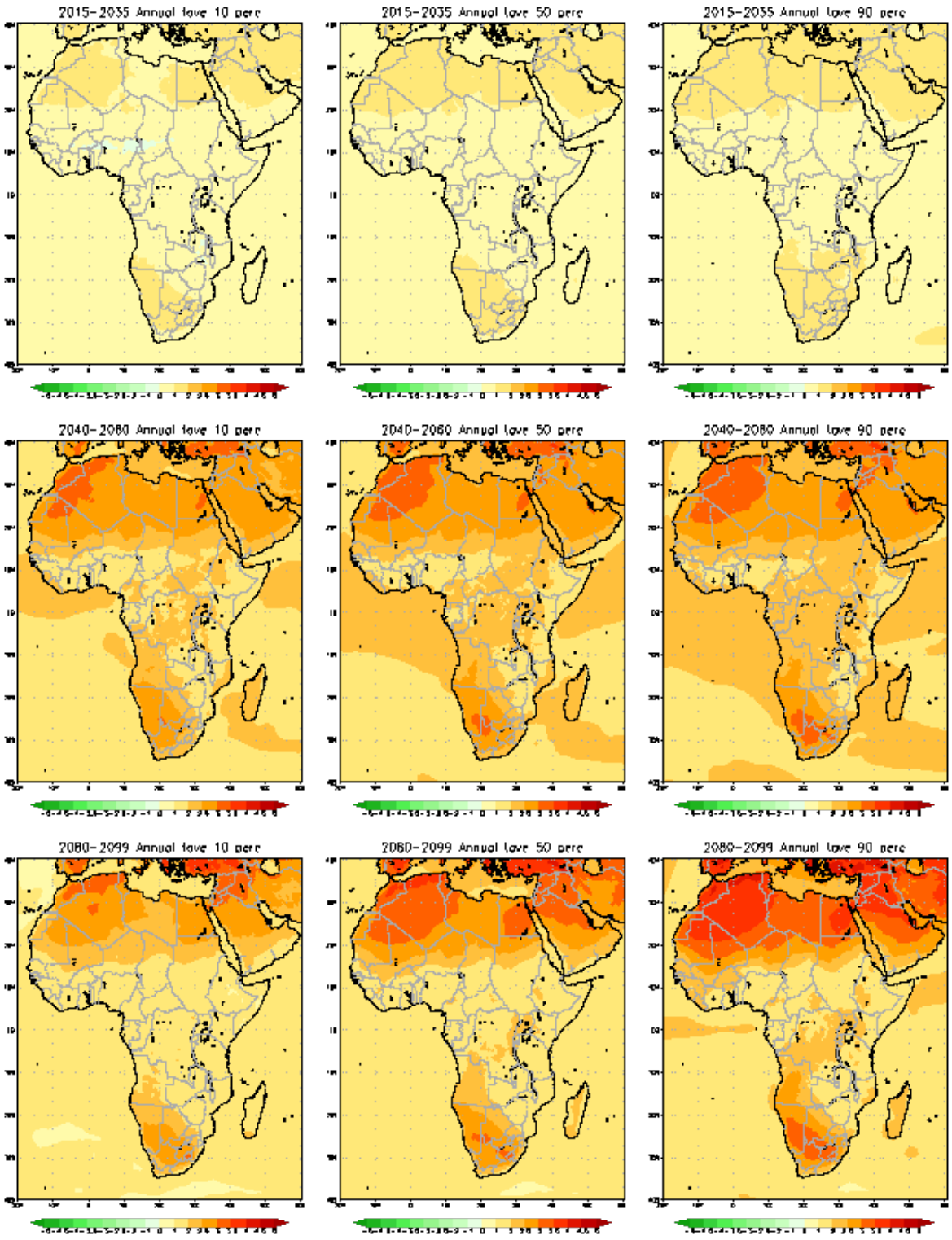

Figure 2.5: Projected change in the annual average temperature (°C) over Africa, for the time-slabs 2015-2035 (top), 2040-2060 (middle) and 2080-2100 (bottom), relative to 1970-2005. The 90th percentile (right-hand side panel), median (middle panel) and 10th percentile (left-hand side panel) are shown for an ensemble of downscalings of three CGCM projections, for each of the time-slabs. The downscalings were performed using the regional model CCAM. All the CGCM projections contributed to CMIP5 and AR5 of the IPCC, and are for RCP4.5.

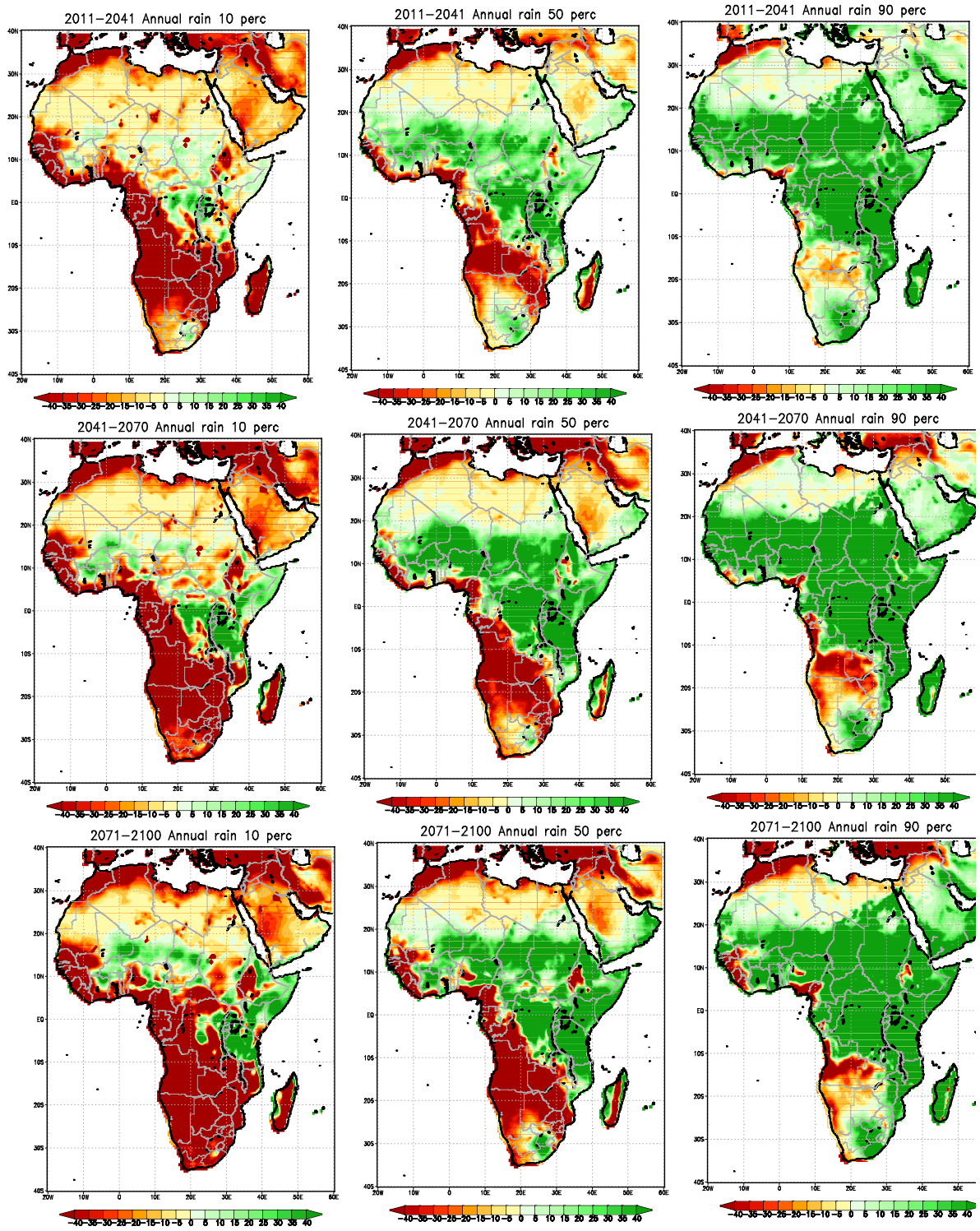

Figure 2.6: Projected change in the total annual rainfall (mm) over Africa, for the periods 2011-2040 (top), 2041-2070 (middle) and 2071-2100 (bottom), relative to 1961-1990. The 90th percentile (right-hand side panel), median (middle panel) and 10th percentile (left-hand side panel) are shown for an ensemble of six downscalings of CGCM projections, for each of the time-slabs. The downscalings were generated using the regional model CCAM. All the CGCM projections contributed to AR4 of the IPCC and are for the A2 SRES scenario.

Most of the CCAM ensemble members project drying for the southern African region (Fig. 2.6) under climate change, in response to the subtropical high-pressure belt strengthening and expanding towards the south (e.g. Engelbrecht et al., 2009). Strong drying is projected for the Limpopo river basin by most ensemble members for all seasons, consistent with the strengthening of the subtropical highs and the northward displacement of the tracks of tropical lows and cyclones (Malherbe et al., 2013). Indeed, a robust pattern of drying over southern Africa is also projected by the CGCMs of AR4 of the IPCC (Christensen et al., 2007). Strengthening of the high-pressure belt in the austral winter is associated with the southward displacement of the westerly wind regime and the cold fronts that bring rainfall to the winter rainfall region of South Africa (the southwestern Cape and the Cape south coast). This is one of the most robust rainfall signals in the CCAM projections (Fig. 2.6), and similarly for the CGCM projections of AR4 (Christensen et al., 2007). The CCAM ensemble provides a robust message of increases in annual rainfall totals across the African tropics (Fig. 2.6). Warming is projected to be associated with an increase or little change in precipitation in the African tropics according to the ensemble of AR4 CGCMs (Christensen et al., 2007). Consistent with the AR4 projections, the CCAM ensemble's projected increases are projected to be rather small (less than 10 %).

2.5 Projected changes in extreme events

The African continent exhibits a high degree of natural climate variability, and is prone to the sporadic occurrence of droughts and floods. Flooding may result from a number of different weather systems. Tropical cyclones are perhaps the most devastating; however, these systems make landfall over Africa rather infrequently, and only over the eastern

coastal areas of Mozambique and South Africa (e.g. Malherbe et al., 2011). Other types of tropical systems, such as mesoscale convective complexes, typically cause flooding over tropical and subtropical Africa. Weather systems from the westerly wind regime, mostly cut-off lows, frequently bring damaging floods to the southern parts of South Africa. At the other end of the scale, dry spells, heat waves and prolonged periods of agricultural drought also occur sporadically as part of the natural climate of the continent, often in association with El Niño Southern Oscillation (ENSO) events. Climate change over Africa may manifest itself not only in a change

in the long-term mean seasonal rainfall, temperature and circulation patterns, but also through an increase in the frequency of occurrence of extreme events. However, the IPCC pointed out in AR4 that research on potential changes in extreme weather events over Africa is limited.

2.5.1 Extreme rainfall events

The projected change in the frequency of occurrence of extreme rainfall events (here defined as 20 mm of rain falling within 24 hours over an area of 0.5° x 0.5°) is shown in Fig. 2.7 (for the 10th percentile, median and 90th percentile of the ensemble of CCAM projections across various time slabs under the A2 SRES scenario). The figure indicates a robust signal of an increase in extreme rainfall events over tropical Africa and to a lesser extent East Africa – consistent with a general (global) increase in such events that is projected to occur in association with an increase in water vapour in a warmer atmosphere. This pattern is robust across the various seasons (see Engelbrecht et al., 2013a). The ensemble of CGCM projections described in AR4 of the IPCC indeed indicates that extremely wet seasons are projected to increase over both East Africa and West Africa (Christensen et al., 2007).

Extreme rainfall events are projected to decrease in frequency over parts of southern Africa (Namibia, Zambia, Botswana and Zimbabwe) and the northern Sahara – consistent with the general patterns of drying projected for these regions (Fig. 2.6). This signal is robust for the southern African region in the ensemble of projections, but is not well-established in the 90th percentile of the ensemble over the northern Sahara and the North African Mediterranean. Over South Africa a projected increase in the frequency of extreme rainfall events is found consistent with earlier studies (e.g. Tadross et al., 2005; Engelbrecht et al., 2011; Engelbrecht et al., 2012) – despite the general decrease in precipitation that is projected for this region. The increase in extreme events may be at least partially be ascribed to the significant increase in surface temperatures over the region (Fig. 2.3). Such an increase in surface temperature would be conducive to a deepening of the continental heat low, and a subsequent increase in the occurrence of heat convection and convective rainfall. In fact, a general decrease in the frequency of cut-off lows over southern Africa has been projected in previously performed simulations (see Engelbrecht et al., 2012). This suggests that the projected increase in extreme precipitation events

over South Africa is the result of an increase in convective rainfall events, rather than in the widespread occurrence of heavy rainfall, as induced by cut-off lows.

The IPCC pointed out in AR4 that potential changes in the frequency of occurrence tropical cyclones over the southwestern Indian Ocean have not been investigated rigorously through modelling studies. Only a single study addressing this topic was available for inclusion in AR4. This found a significant reduction in the frequency of tropical storms in the Indian Ocean under future forcing, using a high-resolution AGCM for its simulations (Oouchi et al., 2006). The ensemble of projections performed at the CSIR has been analysed in detail by Malherbe et al. (2013) to determine whether enhanced anthropogenic forcing may be expected to lead to changes in the frequency of occurrence and tracks of landfalling tropical lows and cyclones over the southern Africa. Most of the downscaled CGCM projections exhibit a pattern of higher rainfall totals and an increase in extreme rainfall events over the Indian Ocean to the north of Madagascar and over northern Mozambique (Figs. 2.6 and 2.7). This is indicative of a northward shift in the preferred location of tropical low and cyclone tracks, as induced by a strengthening of the Indian Ocean High over the southwest Indian Ocean during the late summer – see Malherbe et al. (2013) for a detailed discussion of the underlying circulation dynamics. The general drying that is projected over north-eastern South Africa during the summer and autumn (see Engelbrecht et al., 2013), is partially the result of the northward displacement of tropical low and cyclone tracks over the southwestern Indian Ocean (Malherbe et al., 2013).

2.5.2 Very hot days

Drastic increases in the annual and seasonal frequency of occurrence of very hot days (here defined as days when the maximum temperature exceeds 35°C) are projected (Fig. 2.8, see also Engelbrecht et al., 2013a) across the African continent under the A2 SRES scenario. The figure shows the 10^{th} percentile, median and 90^{th} percentile of the projected change in very hot days across the ensemble. The projected pattern of change is robust. The largest increases in very hot days (increases of more than 100 very hot days per year for 2071-2100 relative to 1961-1990) are projected to occur over southern Africa, the western tropics and southern Sahara and the eastern part of North Africa. The relatively small increases over the

northern Sahara may be attributed to the relatively high occurrence of such days in the present-day climate. Relatively small increases in the number of very hot days are also projected over the eastern escarpment areas of South Africa and the highlands of East Africa.

2.5.3 Heat waves

Over subtropical southern Africa and North Africa, heat waves tend to occur in association with periods of sustained anti-cyclonic circulation and subsidence. That is, heat waves occur when mid-level high-pressure systems dominate the circulation for a sustained period of a few days to weeks. Over southern Africa, dry El Niño summer seasons are also associated with a higher-than-normal frequency in the occurrence of heat waves. That is, heat-waves represent an important mechanism through which seasons of drought impact negatively on agriculture and other sectors at the intra-seasonal time-scale. It is also noteworthy that the maize crop, which is of key importance to subsistence and commercial farming across the African continent, is projected to decrease drastically in yield if continental temperatures are to rise drastically (e.g. Thornton et al., 2011). The maize crop is vulnerable in particular to the occurrence of extreme temperature events. The projected drastic rise in average surface temperature over Africa and in the number of very-hot days (e.g. Figs. 2.3 to 2.5, Fig. 2.8) is therefore a source of particular concern. Moreover, superimposed on these changes, an increase in the frequency of occurrence of heat waves may lead to critical temperature thresholds being exceeded more often. Indeed, there is evidence of the tropical belt widening (Seidel et al., 2007) and the subtropical high-pressure belt strengthening over southern and North Africa under climate change (e.g. Engelbrecht et al., 2009). The latter large-scale change has been shown to occur in association with the more frequent-formation of mid-level highs, and possibly heat-waves, over the subtropics. These aspects are explored in more detail in the current subsection. The World Meteorological Organisation (WMO) definition of a heat-wave is applied in the research: an event where the maximum temperature at a location exceeds the average temperature of the warmest month at that location with 5°C or more, for a period of at least 3 days.

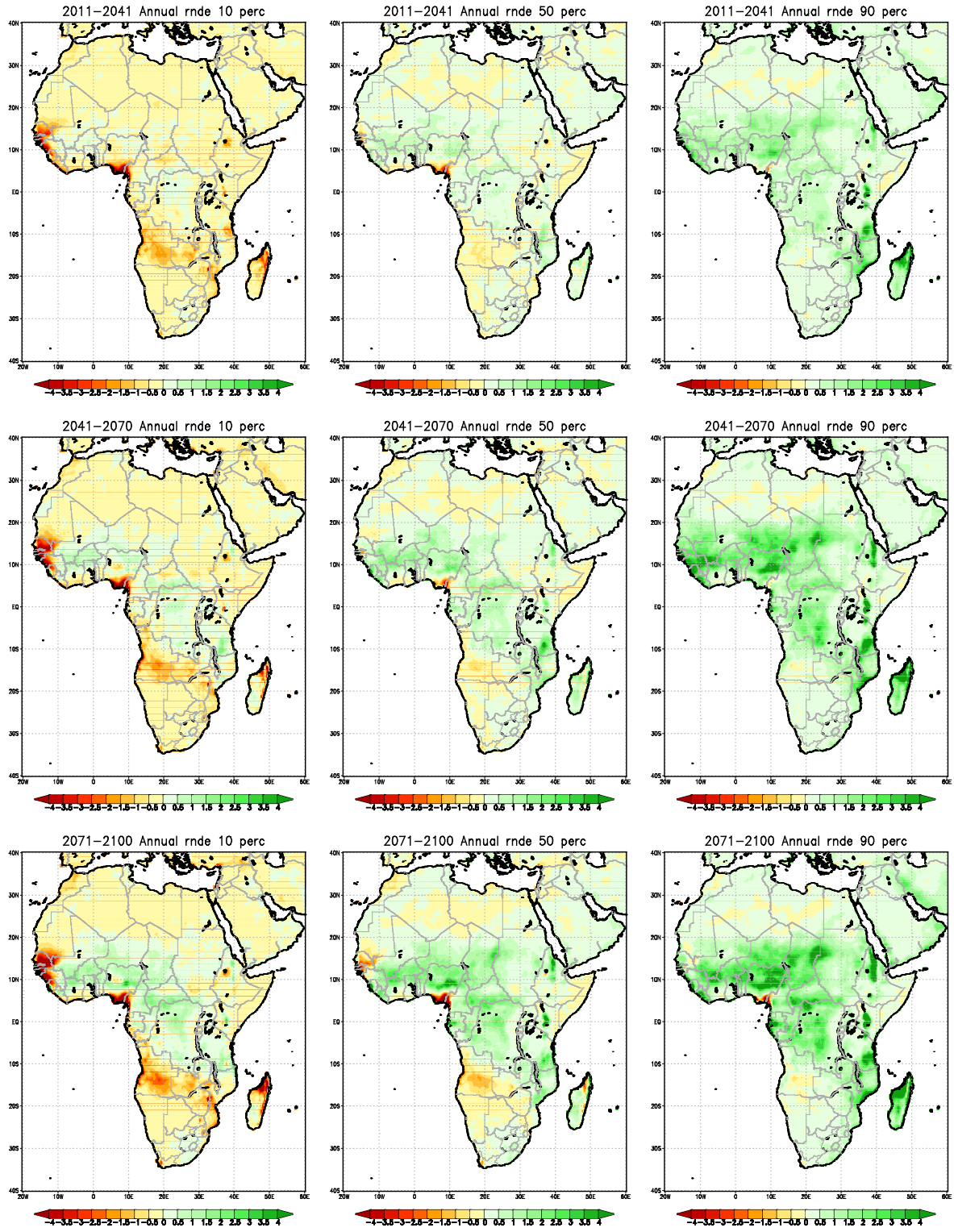

Figure 2.7: Projected change in the annual frequency of occurrence of extreme rainfall events over Africa, for the periods 2011-2040, 2041-2070 and 2071-2100, relative to 1961-1990. The 90th percentile (right-hand side panel), median (middle panel) and 10th percentile (left-hand side panel) are shown for an ensemble of six downscalings of CGCM projections, for each of the time-slabs. The downscalings were generated using the regional model CCAM. All the CGCM projections contributed to AR4 of the IPCC and are for the A2 SRES scenario. Units are the number of events per grid point per year.

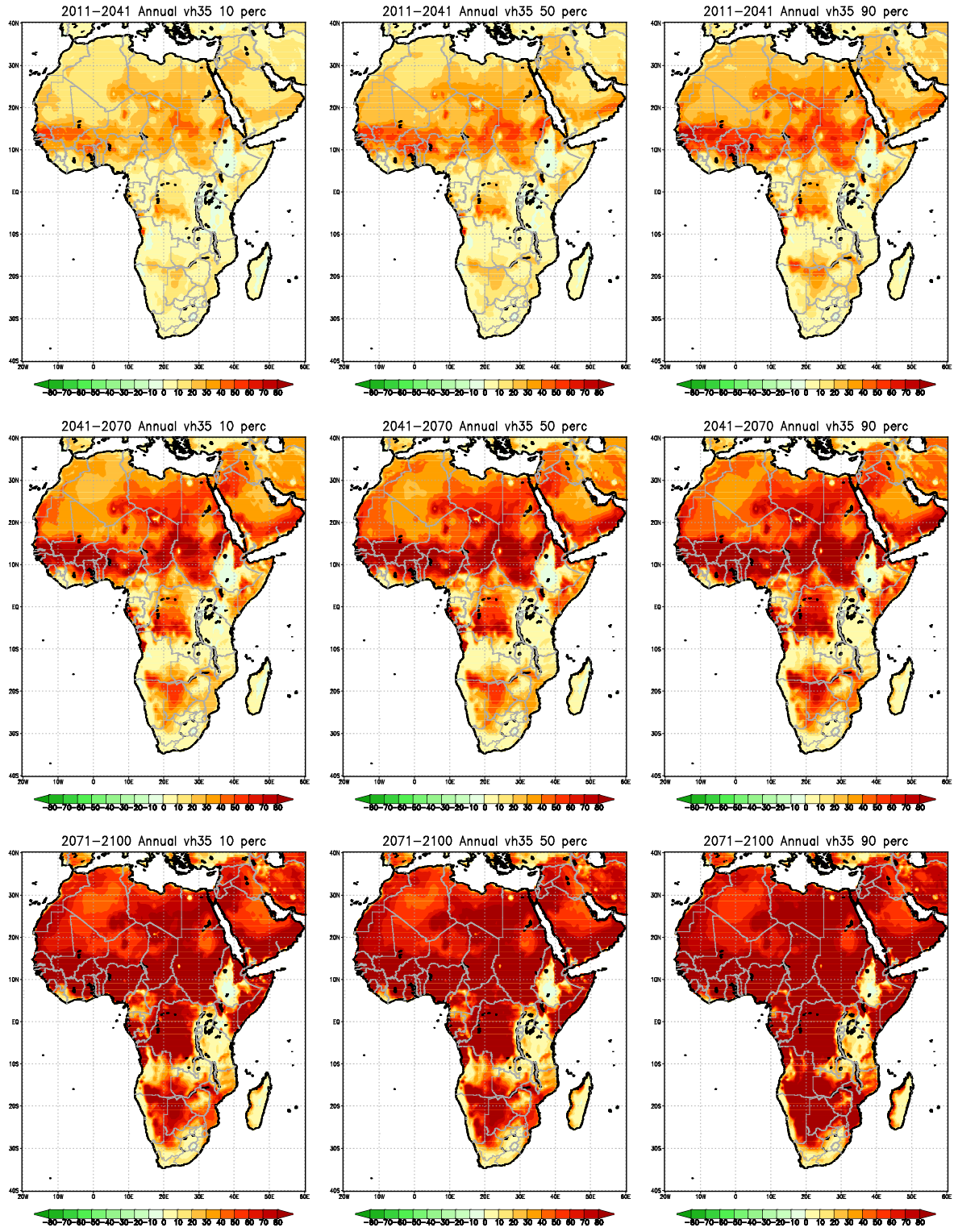

Figure 2.8: Projected change in the annual frequency of occurrence of very hot days over Africa, for the periods 2011-2040, 2041-2070 and 2071-2100, relative to 1961-1990. The 90th percentile (left-hand side panel), median (middle panel) and 10th percentile (right-hand side panel) are shown for an ensemble of six downscalings of CGCM projections, for each of the time-slabs. The downscalings were generated using the regional model CCAM. All the CGCM projections contributed to AR4 of the IPCC and are for the A2 SRES scenario. Units are the number of events per grid point per year.

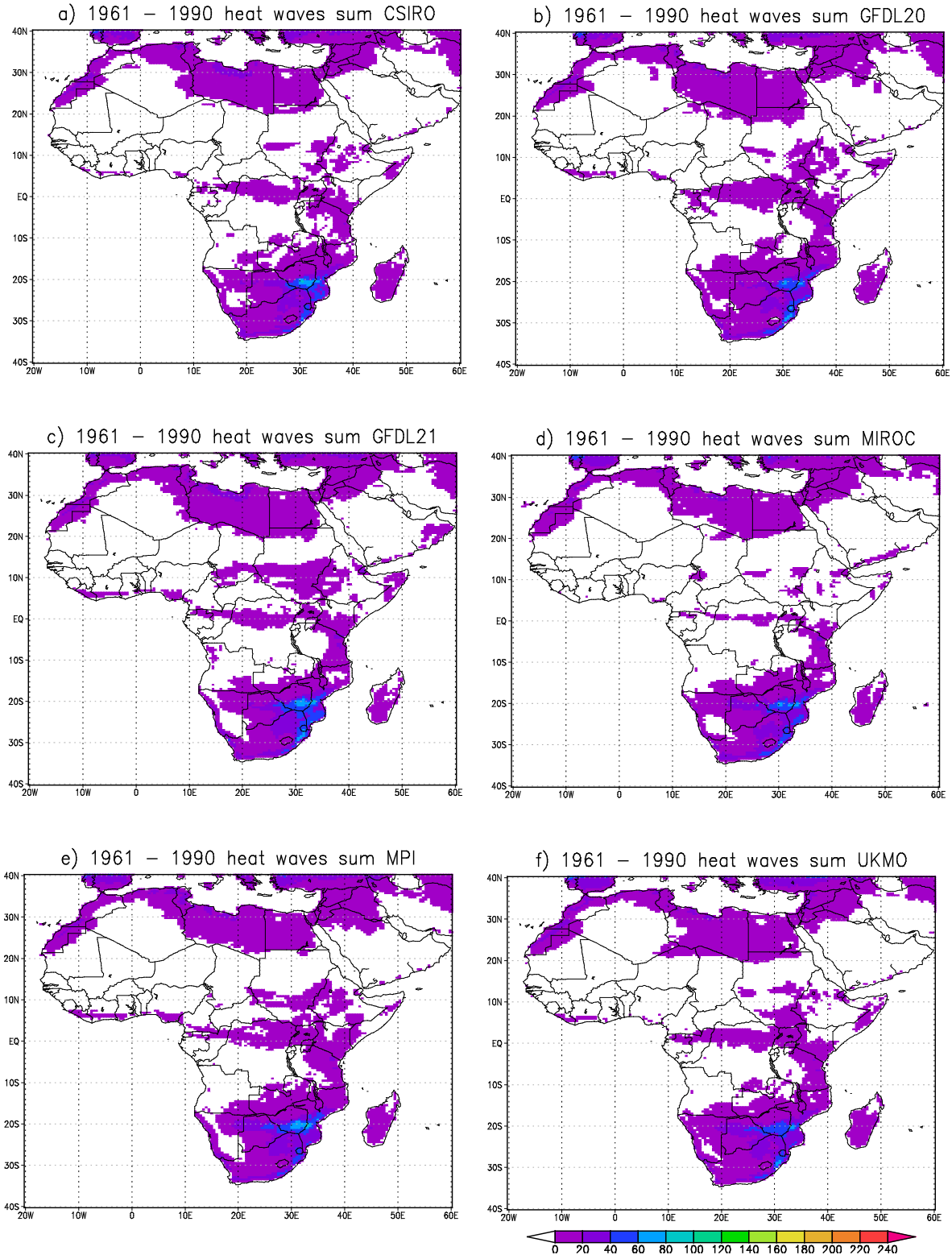

Figure 2.9: Simulated number of heat-wave events for the present-day period 1961-1990, for the 6 different CCAM A2 SRES scenario projections.

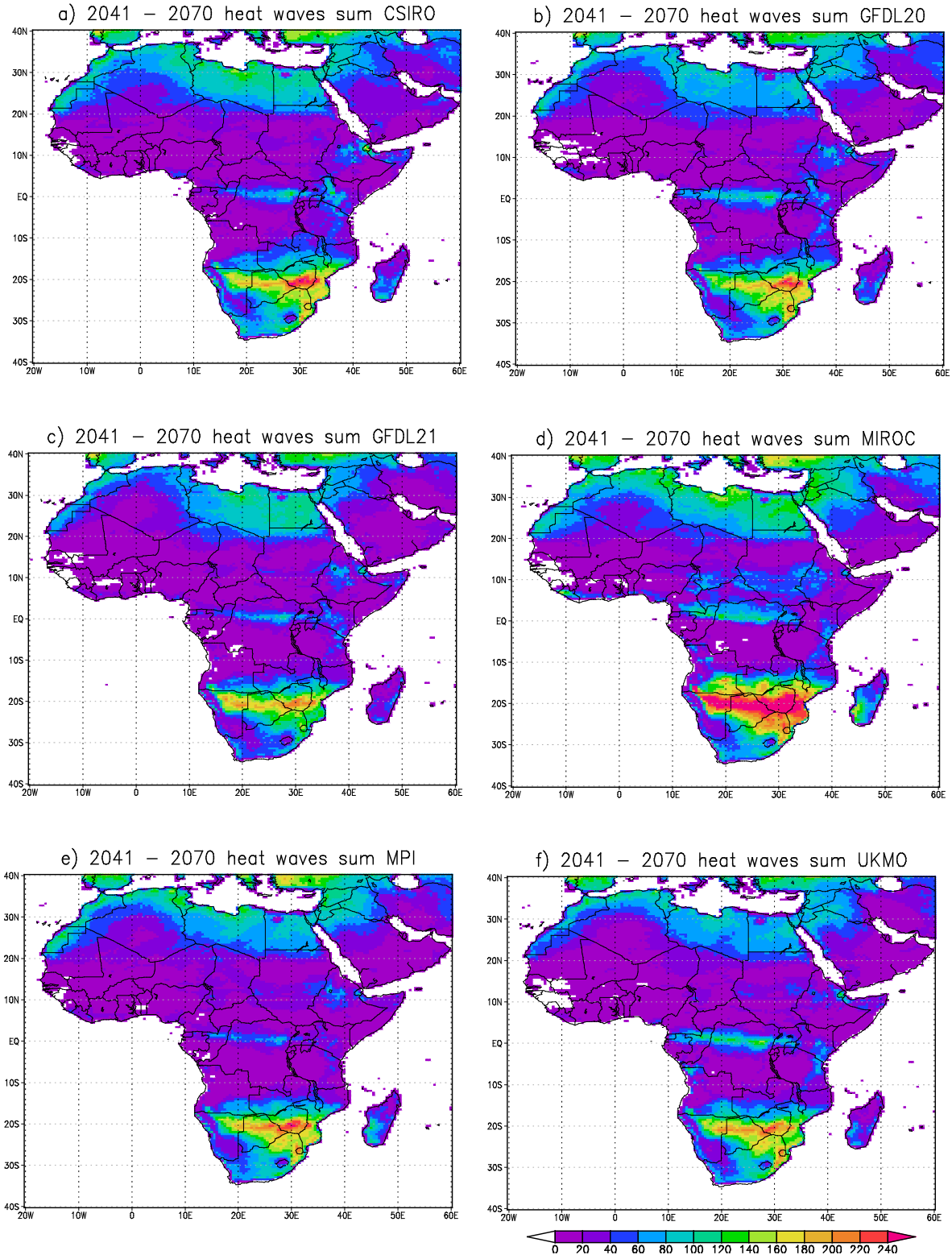

Figure 2.10: Simulated number of heat-wave events for the mid-future period 2041-2070, for the 6 different CCAM A2 SRES scenario projections.

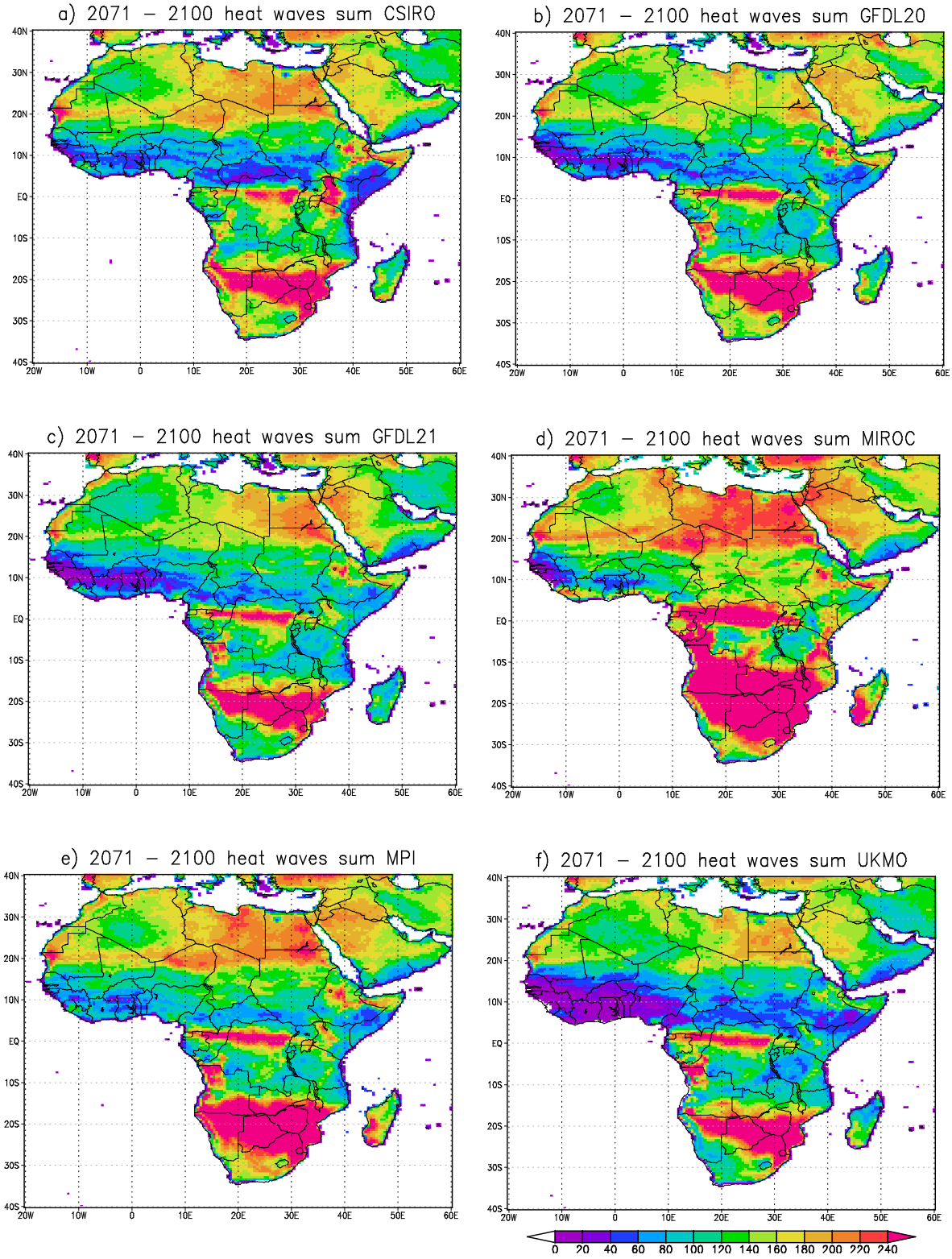

Figure 2.11: Simulated number of heat-wave events for the present-day period 2071-2100, for the 6 different CCAM A2 SRES scenario projections.

The simulated annual average number of heat waves occurring over Africa during the period 1961-1990 is shown in Fig. 2.9, for each of the A2 SRES scenario downscalings described earlier. The highest frequency of heat waves (about 60 over the 30-year period) are simulated to occur in the Limpopo river basin of southern Africa. Generally, southern Africa and North Africa are the regions with the highest frequencies of heat waves. These are regions in the sub-tropical high-pressure belt, prone to the formation of subsidence and mid-level highs. Large parts of tropical Africa and the Sahara are simulated not to experience heat waves in present-day climate. This is due to the high threshold temperatures not being exceeded for sufficiently long periods to satisfy the heat-wave definition. The projected increase in the number of heat-waves across the African domain are shown in Figs. 2.10 and 2.11, for the mid- and far-future, respectively. The highest increases are projected for the regions most prone to heat-waves in present-day climate – the Limpopo river basin and North Africa. Over the Limpopo basin, drastic increases are projected, with some parts of the basin projected to experience more than 200 events during the mid-future period 2041-2070. For the far-future, it is projected that a large part of the southern African region is to experience more than 240 heat wave events. Heat waves are also projected to start occurring over the tropics by the mid-future. This is the result of the critical threshold temperature (defined be the present-day warmest month) being exceeded satisfying the heat-wave definition, due to the systematic increases in the background state temperatures. Heat wave- frequency increases are also projected to be relatively high over North Africa. The projected patterns of changing heat-wave frequencies are robust across the ensemble of regional projections, similar to the projected temperature signal over Africa (Engelbrecht et al., 2013a). With the underlying circulation changes driving the heat-wave signal well understood, it may be regarded as an actionable signal – and probably one of the most important and high-impact aspects of future climate change over Africa. It may be noted that it has recently been shown that the intra-seasonal frequency of occurrence of heat-waves may be predicted skilfully over the northeastern parts of southern Africa, at seasonal time-scales (e.g. Wisemius et al., 2014; Engelbrecht et al., 2013b). Such forecasts may potentially be used as an adaptation tool to the prolonged occurrence of heat waves.

High fire-danger days

Temperatures are projected to rise drastically over Africa during the 21st century under strong emission scenarios such as the SRES A2 scenario (e.g. Engelbrecht and Bopape, 2011; Fig. 2.3). The most drastic temperature increases are projected for the sub-tropical parts of the continent, and are simulated to occur in association with the strengthening of the subtropical high pressure belt over southern Africa and North Africa and the poleward displacement of the westerly wind regime (and cold fronts). These circulation changes imply that it is plausible for large parts of southern Africa and North Africa to become generally drier under future climate change (Fig. 2.6). Generally drier and warmer conditions over the subtropics of Africa are likely to be associated with increased fire risk. Here the McArthur Forest Fire Danger Index (FFDI), through its standard formulation (e.g. Dowdy et al. 2010) is applied to objectively project changes in the number of high fire-danger days over Africa under climate change. The FFDI depends on the calculation of a drought index defined by Keetch and Byram (1968), taking into account the required corrections pointed out by Alexander (1990). The FFDI has been used extensively to study fire risks over South Africa and Australia (e.g. Van Wilgen et al., 2010), and is applied here to the six high-resolution projections of future climate change over Africa under the A2 SRES scenario (described in Section 2.3).

The simulated the annual averages across the continent, of the number of days when the FFDI is rated as high, very high or extreme (FFDI > 12), calculated for the period 1961-1990, are shown in Fig. 2.12 for each of the six ensemble members. The fire danger climatologies of the six downscalings are very similar – this may be attributed to the bias-correction procedure, which has effectively transformed the monthly climatologies of all the downscalings to that of the CRU data (see Section 2.3). The highest values of high fire danger days are simulated to occur over the sub-tropics, including Southern Africa, the Horn of Africa, the Sahel region and the Sahara. Over these regions as many as 90 high fire danger days are simulated to occur annually, with values exceeding 140 days per year over some regions. It may be noted that although the number of high fire danger days are simulated to reach maximum values over regions such as Namibia and the Sahara, the vegetation burning capacity of these regions is low, or insignificant. The lowest numbers of high

fire danger days, less than 20 days per year, are simulated over the tropics with its high frequency of rain days.

Figure 2.13 shows the model projected changes in the number of days per year when the FFDI value is rated as high, very high or extreme (FFDI > 12), for the mid-future period 2041-2070, relative to the baseline period 1961-1990. Figure 2.14 shows the same result, but for the far-future period 2071-2100. The downscaled models project a robust pattern of drastic increases in the FFDI and high fire danger days over Southern Africa, tropical Africa, Madagascar and the Mediterranean coasts of North Africa and South Africa – for the mid- and far-future time-slabs 2071-2100 relative to the baseline period. High fire danger days are projected to increase by 40 days or more per year over large parts of these regions, for the far-future period. These increases are driven by the drastic rises in surface temperature over these regions. However, over the warm deserts of Africa, namely the Sahara and Namib, and also over large portions of the Sahel, the ensemble of downscalings project a robust pattern of decreasing high fire danger days. These are the warmest parts of the African continent, and even in the baseline climate the critical temperature thresholds that trigger high fire danger days are often exceeded. Further temperature increases under the enhanced greenhouse effect therefore have a relatively small effect on increasing the FFDI over these regions. However, with increases in the number of convective rainfall events projected for these regions (Fig. 2.7), the number of high fire danger days is projected to decrease. This may be of little consequence to the desert areas, where the vegetation burning capacity is low – at least for present-day vegetation patterns. It may be an important result for the Sahel region, however, due to the complex interactions between fire and the African savanna.

Below-normal rainfall

It is conventional to issue seasonal forecasts in the form of probabilistic statements of rainfall to be in either of the categories below-normal, near-normal or above-normal. The categories are usually constructed from ranking a specific time-series of (seasonal) rainfall totals in order of magnitude, to find the required set of terciles. Each member of an ensemble of seasonal forecasts is then associated with one of these categories, in order to construct the probabilistic forecast. A similar procedure is followed here, in order to determine whether years of below-normal rainfall, as

defined by present-day time series, may be expected to occur more or less frequently under climate change. More specifically, for each of the six regional model projections for the A2 SRES scenario described in Section 2.3, the period 1961-1990 was used to define the below-normal category of rainfall for each grid-point in the model domain over Africa. Following the procedure described above, ten years in the time-series 1961-1990 are associated with the below-normal category for each grid-point in the model domain (and for each of the ensemble members). It was subsequently determined whether the mid-future (2041-2070) and far-future (2071-2100) periods exhibit increases or decreases in the number of years characterised with below-normal rainfall (in terms of the below-normal category associated with present-day climate). The results obtained using the procedure outlined above are displayed in Figs 2.15 and 2.16, for the mid- and far-futures, respectively. It may be noted that the general patterns of the projected changes are similar for mid-and far-future periods, but with the amplitude of the changes strengthening over time. A number of climate change signals that are robust across the ensemble of downscalings can be discerned from the figures.

The southern African region is projected to experience a general increase in the number of years with below-normal rainfall. However, three of these ensemble members indicate that it is plausible for below-normal rainfall years to occur less frequently over the central interior of the Southern African region. This is consistent with some downscalings indicating increases in rainfall totals over these regions (Fig. 2.6). There is a consistent and robust message across the ensemble members of East and tropical Africa experiencing a decrease in the number of years with below-normal rainfall, which is consistent with most ensemble members projecting increases in rainfall totals over these regions (Fig. 2.6). More uncertainty surrounds the projected futures of the number of years with below-normal rainfall over West Africa. A mixed signal, of both increases and decreases in the number of years with below-normal rainfall, is projected. However, further to north over North Africa and its Mediterranean coast, another robust signal exists in the projections. These regions are projected to see drastic increases in the number of years with below-normal rainfall. The projected changes are consistent with the projected poleward displacement of the westerly winds, and general reductions in rainfall totals projected for these regions (Fig. 2.6).

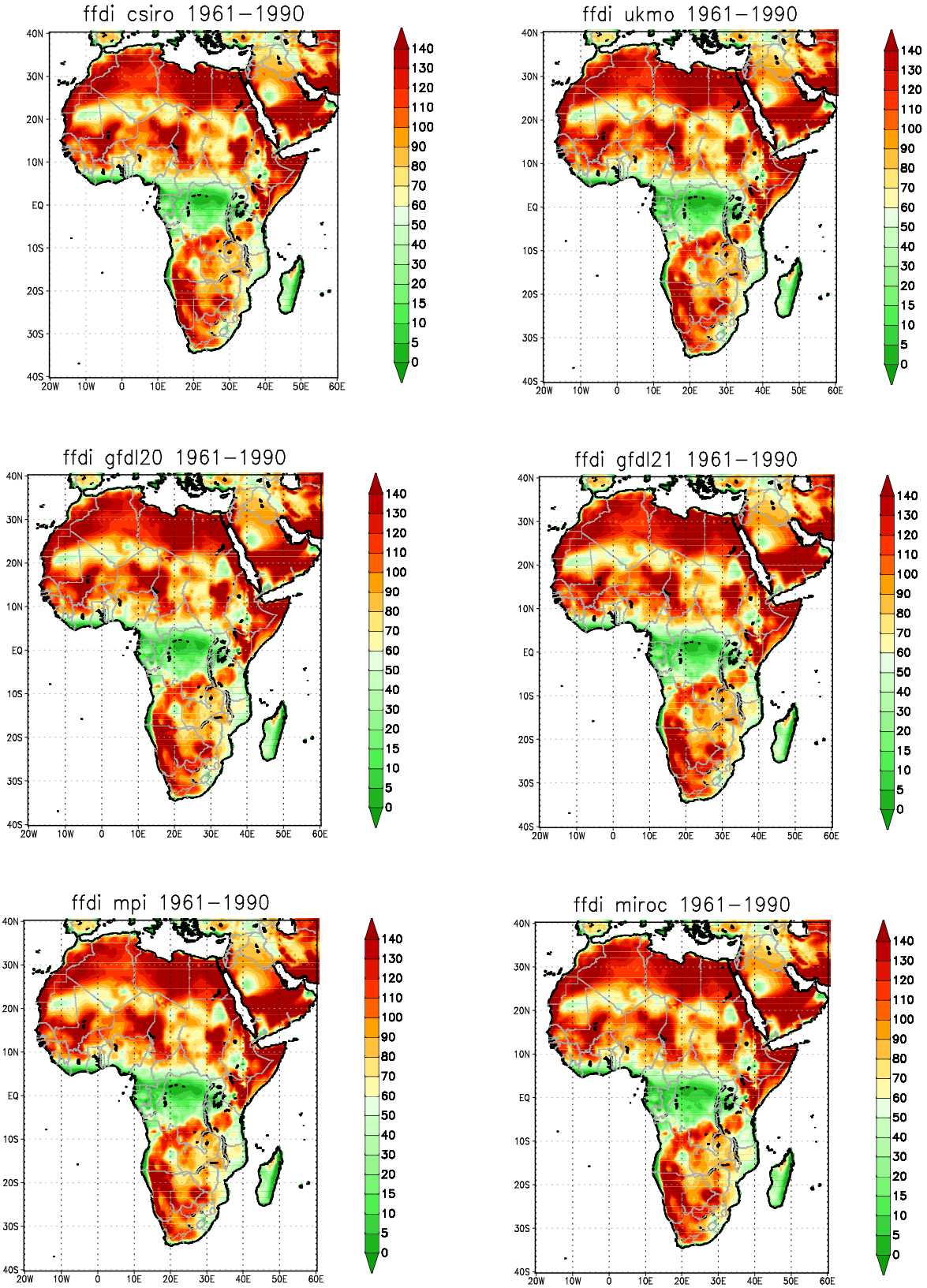

Figure 2.12: Regional model simulations of the number of high fire danger days occurring annually over Africa (averaged over the period 1961-1990).

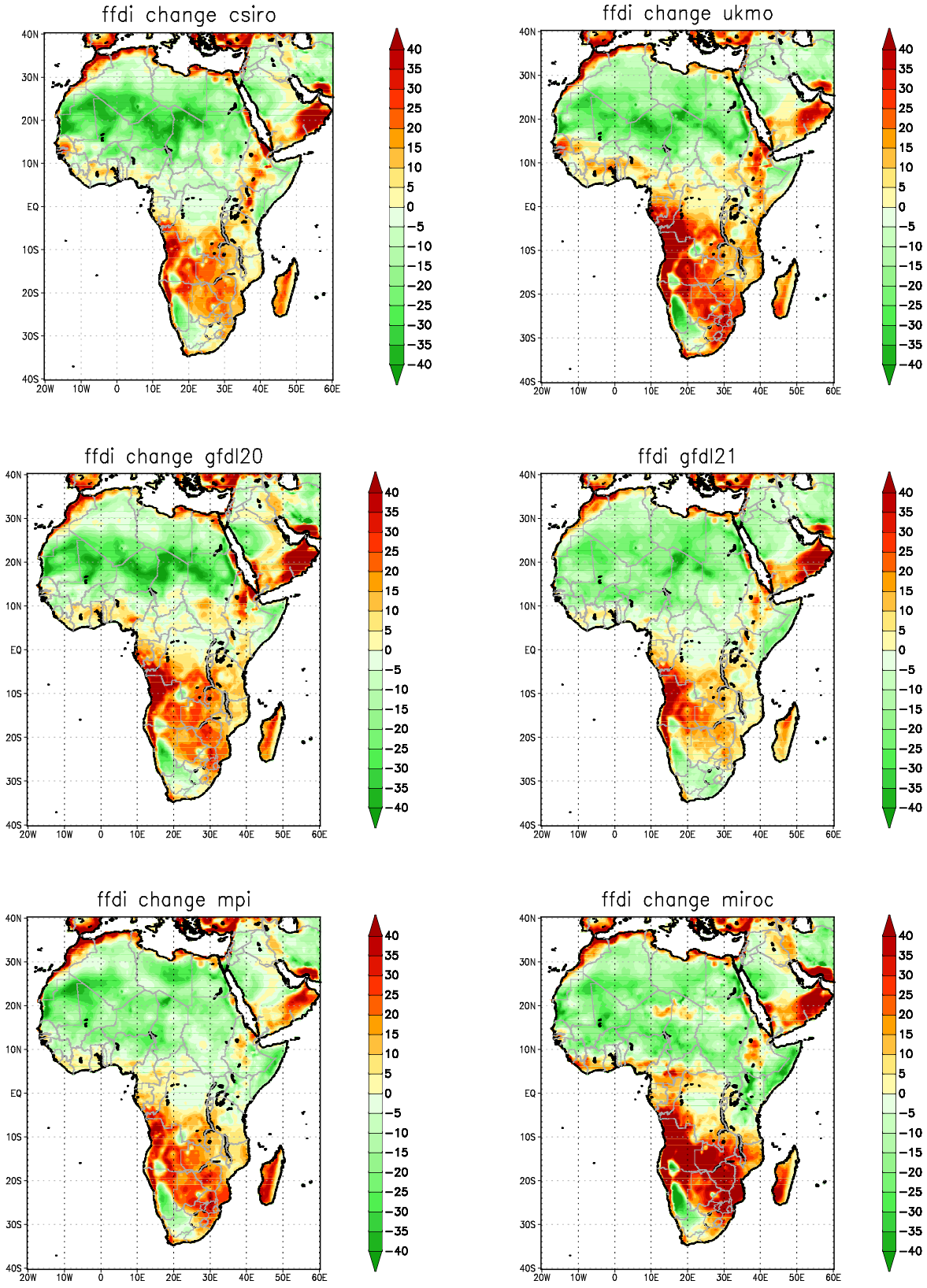

Figure 2.13: Regional model projections of change in the annual number of high fire-danger days over Africa, for the period 2041-2070 relative to 1961-1990.

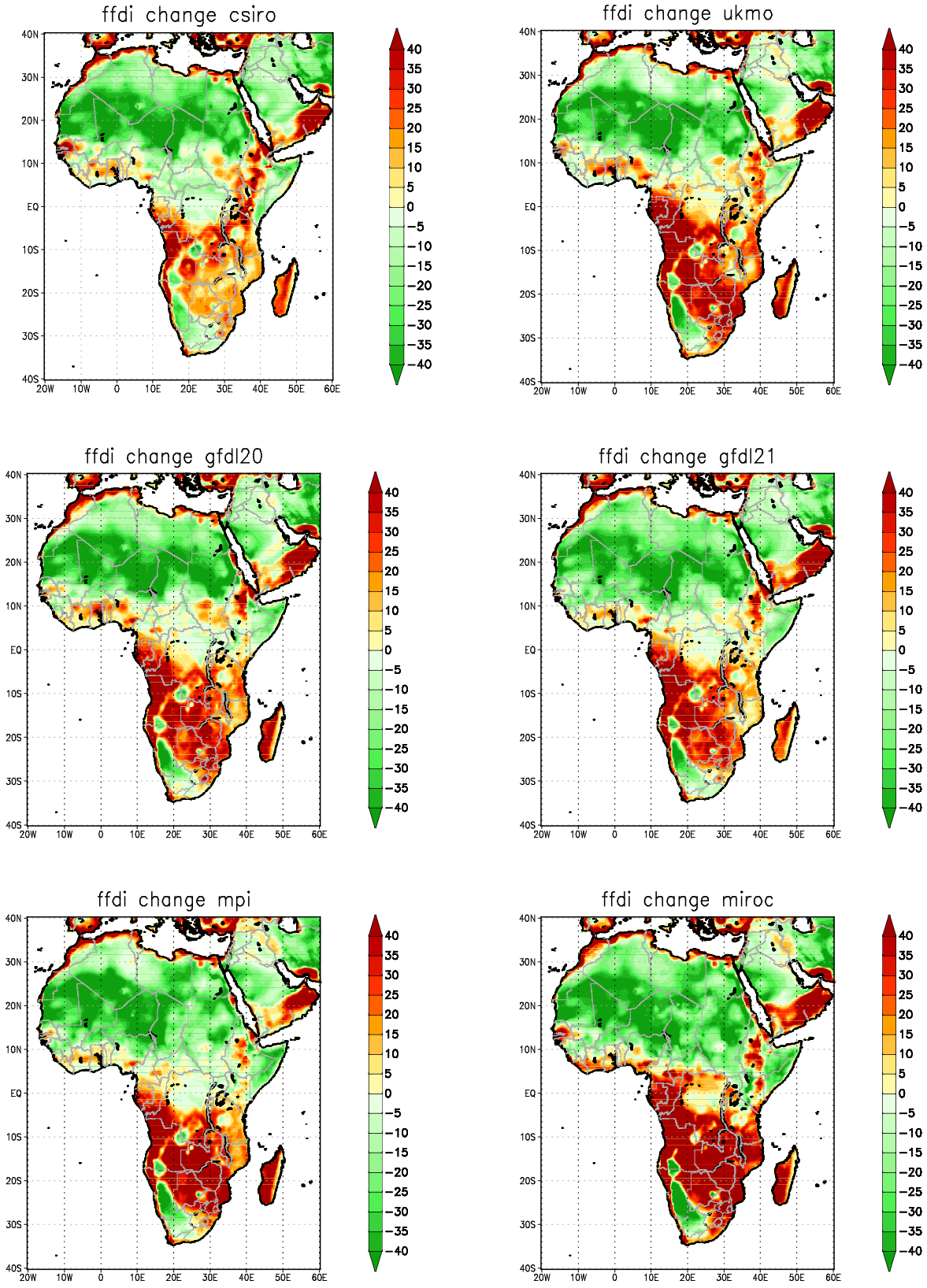

Figure 2.14: Regional model projections of change in the annual number of high fire-danger days over Africa, for the period 2071-2100 relative to 1961-1990.

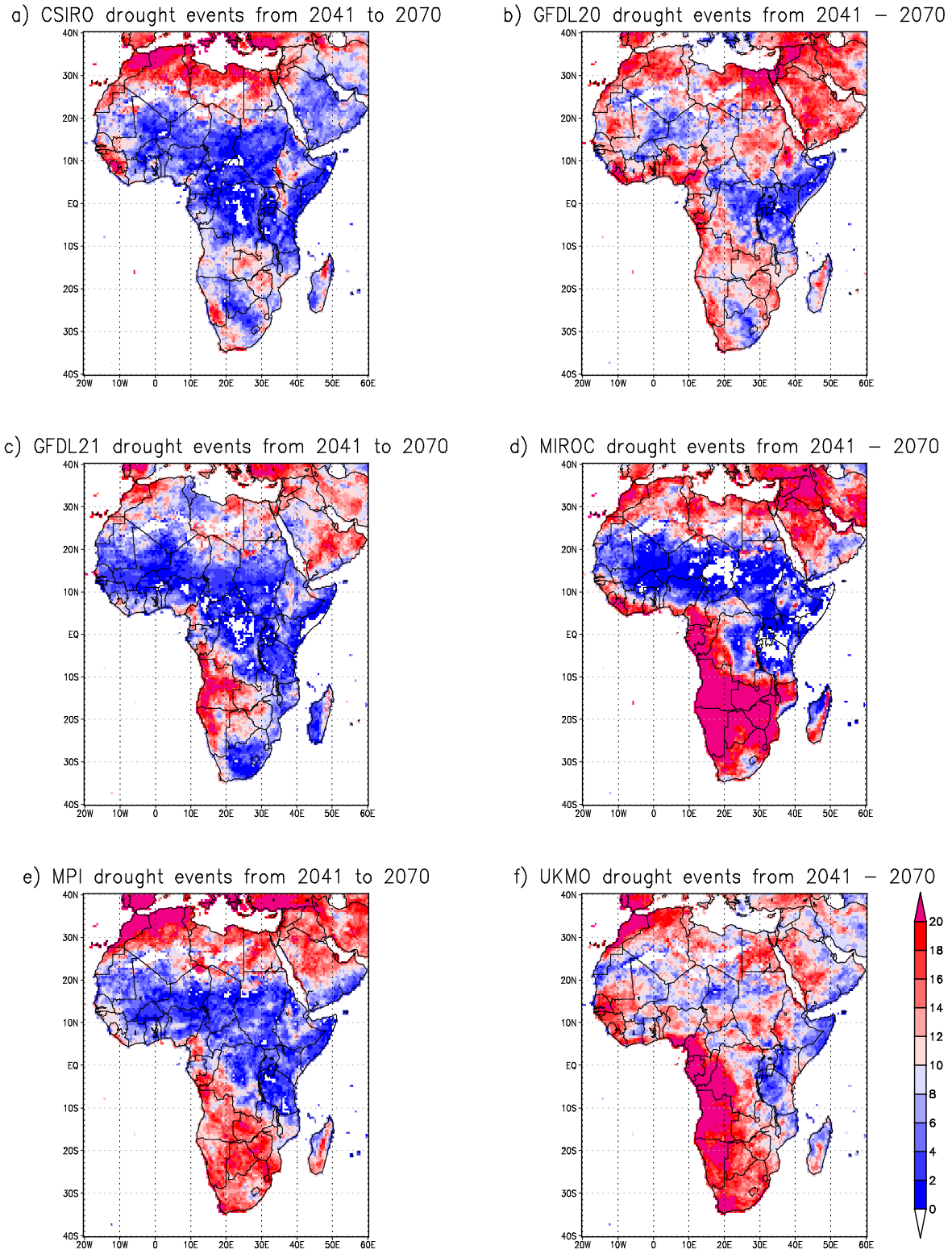

Figure 2.15: Projected number of years with rainfall in the below-normal category, for the period 2041-2071, across the African continent. The period 1961-1990 was used to construct the terciles of below-normal, near-normal and above-normal rainfall.

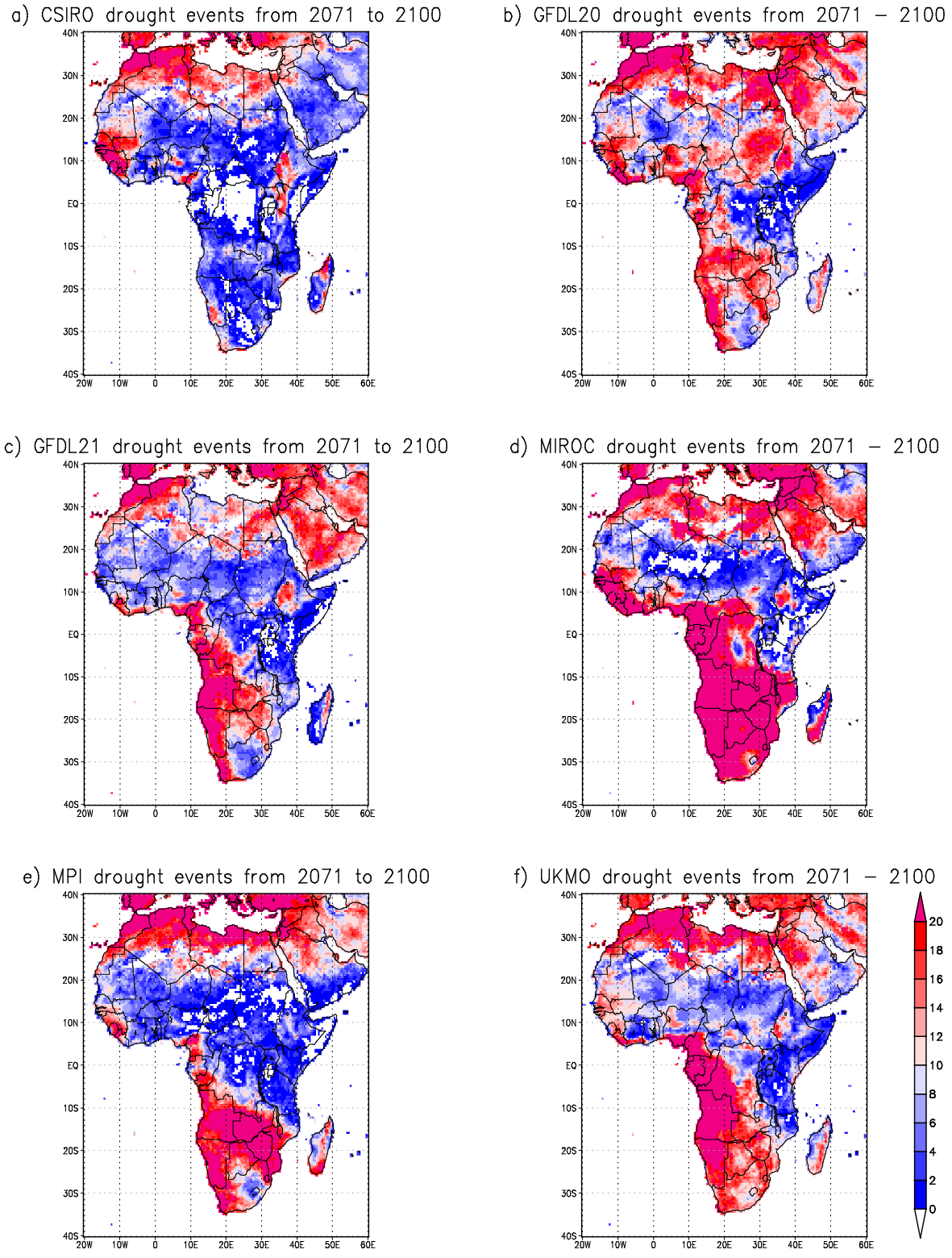

Figure 2.16: Projected number of years with rainfall in the below-normal category, for the period 2071-2100, across the African continent. The period 1961-1990 was used to construct the terciles of below-normal, near-normal and above-normal rainfall.

2.6 Conclusions

An ensemble of high-resolution downscalings of future climate change over Africa has been generated and analysed. The downscaled climates represent multiple CGCMs and three different emission scenarios (SRES A2, RCP4.5, RCP8.5) and span the period 1961-2100. These simulations were subsequently bias-corrected, using the monthly climatologies of rainfall, average temperature and relative humidity of the CRU TS3.1 data set. The projections indicate that drastic climate change, particularly temperature increases, is plausible to occur over Africa during the 21st century under low mitigation scenarios. The median temperature increase for 2071 to 2100, compared to 1961-1990, varies between 3 and 5°C (4 and 7°C) across the continent in the CCAM projections for the A2 (RCP8.5) scenario. The subtropical regions of the continent (southern Africa and the northern Sahara) are projected to warm most, at a rate of about twice the global rate of temperature increase. That is, drastic increases in surface temperature are likely over the subtropical parts of the continent, even if the UNFCCC would be successful in restraining the global increase in temperature to 2°C.

Although the projections of future rainfall changes over the continent show considerable variation across the continent, there are robust signals of some large-scale changes in the CCAM projections. The subtropical parts of the continent (southern Africa and the northern Sahara) are projected to become drier, with even more drastic decreases in rainfall projected for the extra-tropical margins of the continent – the Mediterranean coast of North Africa, and the southwestern Cape and Cape south coast of South Africa. Over these regions, the number of years with below-normal rainfall is also plausible to increase. These changes seem to be driven by the strengthening of the subtropical highs in each of the hemispheres, with an associated poleward displacement of the westerly wind regime. There is also a robust signal of East Africa becoming wetter in response to the strengthening of the East African monsoon. Years with below-normal rainfall are plausible to decrease in number over this part of the continent. More uncertainty surrounds the CCAM projections of future climate change over West Africa and the Sahel, where many CGCMs fail to simulate realistically key aspects of African climate – such as the West African monsoon (e.g. Christensen et al., 2007). It is plausible that extreme

rainfall events will increase in frequency across the tropics, in response to the general increase in moisture in the warmer atmosphere. Over East Africa, where the monsoon is projected to strengthen, robust increases in extreme rainfall events are projected.

The CCAM projections provide evidence that the frequency of occurrence of very hot days is likely to increase across the continent, and in particular over subtropical southern Africa, the western tropics and North Africa. This is to occur in association with the strengthening of the subtropical highs and the poleward displacement of the westerly wind regime, with associated decreases in rainfall over large parts of the continent. Over these regions, drastic increases in the frequency of high fire-danger days and heat-wave events are consistently projected.

Acknowledgements

This research described in this chapter has been co-funded by a CSIR Parliamentary Grant and associated FP7 project DEWFORA. The regional projections are performed though a collaboration between the CSIR and CSIRO in Australia. The CHPC in South Africa is acknowledged for their excellent support in performing the high-resolution simulations.

Chapter 3

Development and Verification of a Short-Range Ensemble Numerical Weather Prediction System for Southern Africa

3.1 Introduction

Southern Africa is positioned in the sub-Saharan region of the African continent and includes several different climatic regions ranging from semi-tropical in the north (Angola, Malawi, Zambia, Mozambique and Madagascar); to semi-arid in South Africa, Botswana and Zimbabwe; to arid in Namibia (Tyson and Preston-Whyte, 2000). This research focuses on southern Africa during the months of January and February, 2009 and 2010, which are austral summer months. Southern African summers have characteristic rainfall patterns. The Cape region of South Africa remains dry and receives very little rain, and the western interior remains arid. The east coast of South Africa as well as the Lowveld receive heavy rain and are very humid as a result of on-shore flow from warm Indian Ocean synoptic weather systems Unstable atmospheric conditions and convective low-pressure cells are prevalent throughout the Highveld interior (Tyson and Preston-Whyte, 2000). In Zimbabwe, northern Botswana, Malawi, Zambia and Angola, the summer rainfall patterns are dominated by the Inter-Tropical Convergence Zone (ITCZ), which moves south of the equator during this time. The ITCZ brings heavy tropical rain to these countries. The ITCZ can also form a Tropical Temperate Trough (TTT), where low pressure troughs that extend across South Africa join the tail end of the ITCZ forming one long, deep trough from the tropics down to the temperate climate of South Africa. TTTs are the most dominant source of convective summer rainfall over southern Africa (Todd, 2004). El Niño Southern Oscillation (ENSO) has a strong influence on the Indian Ocean and southern African climate and its predictability (Cook, 2001; Landman and Beraki, 2012). El Niño episodes frequently result in anomalously dry conditions for the eastern southern African area during the summer season. Alternatively, La Niña is often associated with wetter than normal conditions over the east of southern Africa during the summer months.

Precipitation is a significant weather phenomenon that affects the entire population of southern Africa, especially the poverty-stricken and rural regions, and the largely

agriculture-based economy. The ability to accurately predict rainfall events in the summer season over southern Africa is paramount. In areas adjacent to the Indian Ocean and Mozambican Channel there is strong onshore flow of warm, moist air that causes considerable rainfall and floods over these regions. From a social aspect, these coastal regions are often found to be impoverished (Mozambique, South Africa, Madagascar and even as far inland as Zimbabwe), and do not have the resources or capacity to be able to manage destructive rainfall events. Accurate summer rainfall forecasts are able to help impoverished regions avoid destruction of property, death and crop failure. More knowledge regarding summer rainfall events can capacitate vulnerable areas to become aware of and be able to put in place protective measures for future destructive weather. In order to improve the quality of precipitation forecasts made for southern Africa, innovative short-range weather forecasting techniques must be explored.

Numerical Weather Prediction (NWP) models are used to predict short-range future weather phenomena by having reliable initial conditions to run the model, as well as an accurate representation of the atmosphere (Kalnay, 2003). Ensemble prediction systems (EPS) are considered to be an effective way to probabilistically forecast a range of possible future states of the atmosphere, given its current state; while also addressing the problems of uncertainties in the initial conditions, and inaccuracies in the model approximations (Tennant and Toth, 2006). EPSs were introduced in order to allow forecasters to produce reliable forecasts with lead times of greater than a few days. As opposed to deterministic forecasting, which is a process of predicting a single output, probabilistic predictions present a range of possible future outcomes (Du et al., 1997). Therefore, probabilistic forecasts are more likely to capture specific events than deterministic forecasts, since they are more accommodating of possible outcomes. This is especially important when it comes to predicting rainfall. Deterministic rainfall forecasts are reliable with a one – maximum two – day lead time. Forecasts made for more than two days ahead in time will begin to be influenced by the uncertainty inherent in the atmosphere, and this uncertainty is not captured in deterministic forecasting. Probabilistic rainfall predictions represent the likelihood of a rainfall event and therefore even when forecasts are being made for more than two days ahead, probabilistic rainfall forecasts can still be considered reliable.

The number of members that make up an EPS contributes greatly to the performance of the system (Buizza and Palmer, 1997; Buizza, 2008). Multiple ensemble members can be created through perturbation methods or lagged-average forecasting. Probabilistically, an increase in ensemble size provides a larger spread, a larger distribution of forecast outcomes that all contribute to the final probabilistic EPS forecast. The average forecast of an EPS has been verified to be more skilful than any one of the individual members (Grimitt and Mass, 2001; Hamill and Collucci, 1997). A wider spread of forecasts makes it more likely that the final EPS forecast will include more extreme forecast values that will result in the model being able to predict extreme weather. However, computational capacity imposes a limit on the number of members that can be combined in the EPS since calculating an endless number of members is simply impractical (Kalnay, 2003).

The objective of this research is to verify and conclude which of four differently configured EPSs produce the most skilful precipitation forecasts over southern Africa, and whether a high spatial resolution results in more skilful precipitation forecasts than a coarse resolution. The four ensemble systems will differ in size, and the simulations will be executed at both a low and a high spatial resolution over southern Africa.

3.2 Methodology

This research will focus on daily rainfall during January and February 2009 and 2010. The CCAM will be used to produce rainfall forecasts at low (50 km) and high (15 km) resolution, at four initialisation times, with two cumulus parameterisation schemes. Four different ensembles will be configured using these 8 possible members, and rainfall forecasts will be produced at both resolutions. Verification will be performed to analyse the skill and accuracy of these ensembles in relation to the observational rainfall data. The verification methods that will be used are: the Root Mean Square Error, Brier Skill Score, Relative Operating Characteristic and Reliability Diagrams. The high resolution ensembles will be individually assessed and then compared to each other in order to establish which ensemble configuration is the most skilful overall; the same will be done for the low resolution forecasts. The high and low resolution ensemble pairs will also be compared to each other so as to

establish whether the high or low resolution forecasts are most skilful. It will finally be concluded which ensemble prediction system is the most skilful system.

3.2.1 The conformal-cubic atmospheric model

The conformal-cubic atmospheric model (CCAM) was devised by Rancic et al., 1996, and has since been developed at the Commonwealth Scientific and Industrial Research Organisation (CSIRO) (McGregor, 2005). It is a variable-resolution cube projected onto the globe at a resolution of 200 km. Because the CCAM is described as a cube, it is orthogonal and isotropic (McGregor et al., 2008; 2011). Orthogonality results in the grid lines being perpendicular, therefore allowing vectors (e.g. wind) to be decomposed into their orthogonal parts. Since CCAM is isotropic, the coordinates are non-polar (Euclidean), and hence the three dimensions can be treated equally.

The CCAM is configured such that it is a variable resolution model, and therefore can function both as a global climate model (GCM) and be downscaled to a regional climate model (RCM). The variability ensures that the boundary conditions from the GCM into the RCM are continuous, thus preserving the integrity of the atmospheric characteristics over the boundaries (McGregor et al., 2009). Because the CCAM can be used as a GCM and a RCM, the CCAM can model global low resolution as well as extremely high spatial resolution over a small area (Engelbrecht et al., 2011). In addition to this range of functions, the CCAM can also produce predictions from short-range weather to multi-decadal climate change projections (Engelbrecht et al., 2011). Figure 3.1 is an example of CCAM scaled over the southern African domain.

The CCAM uses a dynamical spectral downscaling technique in order to scale from low to medium to high resolution, and stretch the grid to focus on a specific domain (stretch-grid mode). This technique is known at the Schmidt Transformation (McGregor et al., 2011), proposed by Schmidt in his 1977 paper “Variable Fine Mesh in a Spectral Global Model” (Fox-Rabinovitz et al., 2008). The Schmidt transformation is a conformal process of both stretching and rotation (Hardiker, 1997). The stretching transformation is an iteration process of the linear equations that dictate the GCM, in order to transform to a higher resolution. The rotation

transformation is to move the area of high resolution to be over the domain of interest.

In previous studies of precipitation over southern Africa the CCAM was able to produce satisfactory simulations of annual rainfall, as well as intra-annual and realistic daily rainfall patterns (Engelbrecht et al., 2005). These forecasts were all made on a climate change time scale. In the 2011 study, climate and seasonal time scales were verified to be reliable, but high resolution simulations were largely unverifiable due to the lack of observational data. In the SADC domain, the most accurate forecasts were recorded over Zambia and Zimbabwe. (Engelbrecht et al., 2011).

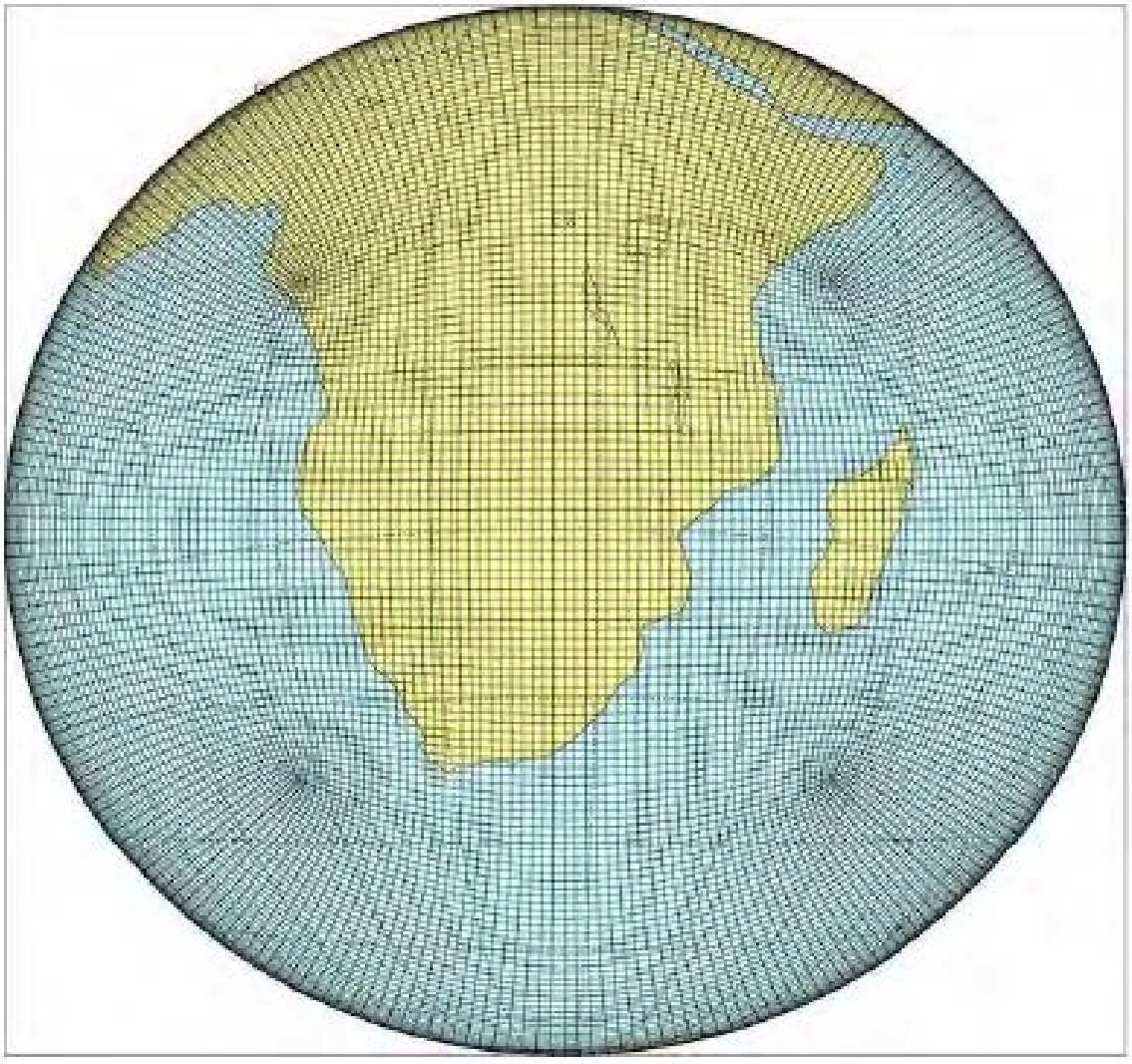

Figure 3.1: CCAM scaled from 200 km to 60 km resolution (Engelbrecht et al., 2011)

3.2.2 Data

The CCAM configuration used here does not have its own data assimilation system. However, the model is initialised with initial conditions obtained from the National Oceanic and Atmospheric Administration (NOAA) Global Forecast System (GFS) database (http://nomads.ncdc.noaa.gov/data.php). The observation data at 50 km and 15 km resolution for the southern African domain used for this research is from the Tropical Rainfall Measuring Mission (TRMM) data archive (http://www.trmm.gsfc.nasa.gov/) and The initial data is assimilated and issued four times a day, at 00h00, 06h00, 12h00 and 18h00 GMT, and so the CCAM can be initialised four times a day, producing four forecasts a day. TRMM is an initiative run by NASA to monitor tropical rainfall, and is a part of the Global Precipitation Analysis which produces real-time three-hourly global precipitation data from analysed TRMM data.

3.2.3 Creating the ensembles

The domain of the CCAM was reduced to the SADC region through spectral nudging techniques (Thatcher and McGregor, 2009). The digital filter is applied at a length scale of 4000 km in order to force the large-scale synoptic features (Thatcher and McGregor, 2010). Model dynamics simulate the small-scale events, such as thunderstorm systems. For this study, the model will be spectrally nudged from the Schmidt Factor 1 resolution of 200 km, to a resolution of 50 km which will be considered in this study to be coarse resolution; and further nudged to a high resolution of 15 km. In this stretch-grid mode, the CCAM can function as a limited area model over southern Africa.

The model has two different cumulus convection parameterisation schemes which can be used to initialise the model. There is a cloud microphysics scheme that has been developed by Rotstayn (1997), and a cumulus convection scheme that has been created by McGregor (2003). These schemes describe the complicated and detailed cloud microphysics and dynamical processes (Engelbrecht et al., 2007; Thatcher and McGregor, 2010). The ensembles will be constructed using these time-lagged members – what is known as the ‘lagged average forecasting’ technique. Time-lagged ensemble forecasting has been used successfully for short- and

medium-ranged forecasting (Hoffman & Kalnay, 1983; Lu, 2007). The lagged average forecast method is used in this research because multiple sets of real initial data are available, which makes time-lagged forecasting possible. However, this does place a limit on the number of ensemble members that can be created.

Configured thusly, the CCAM can be run a maximum of eight times a day: four times for each cumulus parameterisation scheme. This means there is a maximum of eight different ensemble members. Usually ensemble members obtained through lagged average forecasting are all given equal weight, since estimating the relative weights according to how recent the initial conditions are has proven very difficult and impractical (Kalnay, 2003). Therefore, the members in all of these ensemble systems are to be given equal weighting. Four ensembles are going to be analysed in this paper, and they are to be constructed as follows:

Ensemble 1: The two most recent members – 18h00 from both parameterisation schemes
Ensemble 2: The four most recent members – 12h00 and 18h00 from both parameterisation schemes.
Ensemble 3: The six most recent members – 06h00, 12h00 and 18h00 from both parameterisation schemes.
Ensemble 4: All eight members.

These four different configurations were chosen in order to see the effect of ensemble size on forecast skill, and also to see whether including older members in an ensemble affects the forecast skill. It is possible that the more members an ensemble includes, the more skilful the system becomes, since it is more likely to capture outlying events. It is also possible that ensembles which include older members (initialised at times 00h00 and 06h00) could be less skilful than ensembles made up of only recent members, because the older members may amplify inaccuracies that have been minimised in the more recent members.

3.2.4 Verification

The verification of the four ensembles will be evaluated by studying four skill measurements. Multiple assessments must be calculated, since no single measurement can completely describe the attributes of the forecast (Stanski et al., 1989). The four methods that will be used here are: The Root Mean Square Error, Brier Skill Score, Relative Operating Characteristics, and Reliability Diagrams. These verification measures can be split in to two categories: deterministic and probabilistic verification measures. The root mean square error is a deterministic verification score, whereas the Brier skill score, the relative operating characteristics and the reliability diagrams are probabilistic verification methods. The results of these assessments will determine the quality of the forecasts made by each ensemble system.

3.2.4.1 Root mean square error (RMSE)

The RMSE is a measure of accuracy, and is represented by the average magnitude of error in the forecast. This is calculated by taking the difference between the forecast and observed values, squared; these values for each point are then summed and averaged to produce the Mean Square Error. The square root of this is taken to produce the RMSE. The RMSE values are plotted against the time intervals of the forecast. The more accurate the forecast, the closer to zero the RMSE values should be. The closer the forecast is to the observations, the smaller the RMSE. As the time steps increase the error becomes larger in value, and the less skilful the forecast will be. Uncertainties inherent in the model (and in the weather) make forecasting future time-steps progressively more difficult. This makes the RMSE of each prediction system increase with time.

$$RMSE = \sqrt{\frac{\sum_{i=1}^{n}(\bar{y}_i - y_i)^2}{n}}$$

Equation 3.1: Formula of the Root Mean Square Error

3.2.4.2 Brier skill score (BSS)

The Brier Score (BS) is calculated by averaging the square differences between forecast probability,p_i, and observation,o_i, pairs. The observation value is measured as either 1 if the event occurred or 0 if the event did not occur. (Stanski et al., 1989). Therefore, the BS is negatively-oriented and a perfect forecast has BS = 0. When evaluating the skill of an ensemble, the smaller the value of BS, the more accurate the forecast. The value of the BS increases with an increase in time-step because the further the forecast in from the initialisation time, the more difficult it is to simulate the atmosphere and produce forecasts close to the observations.

$$BS = \frac{1}{n}\sum(\bar{p}_i - \bar{o}_i)^2$$

Equation 3.2: Formula of the Brier Score

The BS can be decomposed into three terms describing reliability, resolution and uncertainty:

$$BS = \frac{1}{n}\sum_{i=1}^{I} N_i(\bar{p}_i - \bar{o}_i)^2 - \frac{1}{n}\sum_{i=1}^{I} N_i(\bar{o}_i - o_i)^2 + \bar{o}(1 - \bar{o})$$

Equation 3.3: Decomposition of the Brier Score, where I indicates the number of forecast categories, and N the number of times said forecast category is used in the collection of forecasts.

The first term is the reliability term, which is the weighted average of the difference between the forecast probabilities and the observed frequencies. This term measures the calibration of the system: how accurately the system forecasts probabilities. The more reliable a system is, the closer the reliability term is to zero. The second term is the resolution term, which is the average square difference between the observed frequencies in each category, and the mean observed frequency of the entire sample. This term measures how well the system is able to tell the different categories apart, irrespective of the forecast probabilities (Atger, 1999). The last term is the uncertainty term which is independent of the forecast system and measures the variance of the observations.

The BSS is calculated by comparing the BS of the forecast to the BS of a reference forecast (e.g. persistence or climatology); and therefore BSS is a measure of the skill of the forecast with reference to the accuracy of the forecast determined by the BS. The BSS is the conventional way of measuring the forecast skill (Wilks, 2006, Buizza and Palmer, 1998).

$$BSS = 1 - \frac{BS_{forecast}}{BS_{reference}}$$

Equation 3.4: The BSS in terms of the reference and forecast BS. Since a perfect BS = 0, perfect BSS is equal to 1, with no skill equal to or less than 0.

3.2.4.3 Relative operating characteristics (ROC)

The ROC is a measure of how well a forecast system is able to distinguish between events and non-events. The ROC diagram illustrates the false alarm rate versus the hit rate within a range of probability thresholds. The contingency table pictured in Figure 3.2 shows how the attributes of the forecasts can be calculated. False alarm: event is forecast but not observed. Hit rate: event is forecast and observed. Forecast systems that exhibit good discrimination have ROC curves that approach the upper-left corner of the diagram closely – approach a perfect forecast, and area of 1. Forecast systems have very little skill if the curve falls below the (0, 0) to (1, 1) diagonal – the lower threshold for a useful forecast is the diagonal, and these curves have an area of <0.5.

		Observed		
		Yes	**No**	
Forecast	**Yes**	Hit	False Alarm	Total Yes-Forecast
	No	Miss	Correct Negative	Total No-Forecast
		Occurrences	Non-Occurrences	**TOTAL**

Figure 3.2: Contingency Table.

The False Alarm Rate is defined as the ratio of the false alarms to the total non-occurrences:

$$False\ Alarm\ Rate = \frac{False\ Alarms}{False\ Alarms + Correct\ Negatives}$$

The Hit Rate is defined as the ratio of the hits to the total occurrences:

$$Hit\ Rate = \frac{Hits}{Hits + Misses}$$

3.2.4.4 Reliability diagram

A Reliability diagram illustrates how well-calibrated a forecast system is. The diagram is a plot of conditional event relative frequencies:

$$p(o_i|y_i)$$

A perfect or well-calibrated forecast has a function which lies along the 1:1 diagonal of the diagram. In this case, the conditional event relative frequency is almost equal to the forecast probability:

$$p(o_i|y_i) \approx y_i$$

A forecast is unconditionally biased if the function lies entirely to the left, or to the right of the 1:1 diagonal line. If the function is entirely to the right of the diagonal, the forecasts are considered to be constantly too large when compared to the conditional event relative frequencies, and hence the average forecast is greater than the average observation – this signifies overforecasting. If the function is entirely to the left of the diagonal, the forecasts are considered to be constantly too small when compared to the conditional event relative frequencies, and hence the average forecast is smaller than the average observation – this signifies underforecasting. A forecast is conditionally biased when the slope of the function is either shallower or steeper than the 1:1 diagonal line. In these cases, the magnitudes of the forecast biases depend on the forecasts themselves. A function that has a slope shallower than the diagonal indicates an overconfident forecast. This implies poor resolution, since the conditional event relative frequencies are all near the climatological probability (they depend only weakly on the forecasts). A function that has a slope steeper than the 1:1 diagonal is an underconfident forecast.

This implies good resolution, since the average square differences are large and therefore the system is able to distinguish different outcomes clearly.

3.3 Results

Although this study was done for both January and February 2009 and 2010, the results for each year were very similar. Therefore the explicit results for only 2010 are included, with the results for the same months in 2009 being almost identical.

3.3.1 RMSE

Weather forecast error increases with increasing lead-time (Kalnay, 2003), a notion that is also shown in the verification of the ensemble mean hindcasts of January and February 2010 (Figure 3.3). However, the forecast error initially increases at a higher rate for the low resolution case as opposed to the high resolution case. Notwithstanding the smaller errors associated with forecasts for the first few days, forecast errors made towards the longest lead-time forecasts (i.e. forecast errors for days 5 to 7) are about equally large for both resolutions, thus suggesting that the high-resolution forecasts are mainly advantageous for forecasts up to about day 4. This is consistent with research where it is concluded that forecast error becomes so large at long lead-times that it essentially renders the forecast as inaccurate (Lu et al., 2007; Bowler et al., 2008).

The graphs of Figure 3.3 which show average RMSE for the ensembles show that the high resolution forecast consistently has lower error than the low resolution forecasts. Up to the three-day lead time the high resolution forecasts have error of less than 1 mm for all ensembles which is a very small margin of error, indicating good accuracy. The graphs showing the RMSE curves show that the low resolution forecasts have a constant increase in error for forecasts made for after day 1, showing an immediate drop-off in accuracy for all four ensembles with an increase in lead-time. The high resolution forecasts made up to day 4 have little error, followed by a sharp increase in error from day 4 to day 7 indication a drop-off in accuracy for forecasts made by all four ensembles after a four-day lead time.

Figure 3.4 of the spatial representations of the RMSE difference maps shows the difference in error between the high resolution forecasts made by Ensemble 4 and 1, and Ensemble 4 and 3. It is seen in all four cases that although there is little difference in error between the four ensembles, the error difference between the ensembles decreases as the size of the ensemble increases.

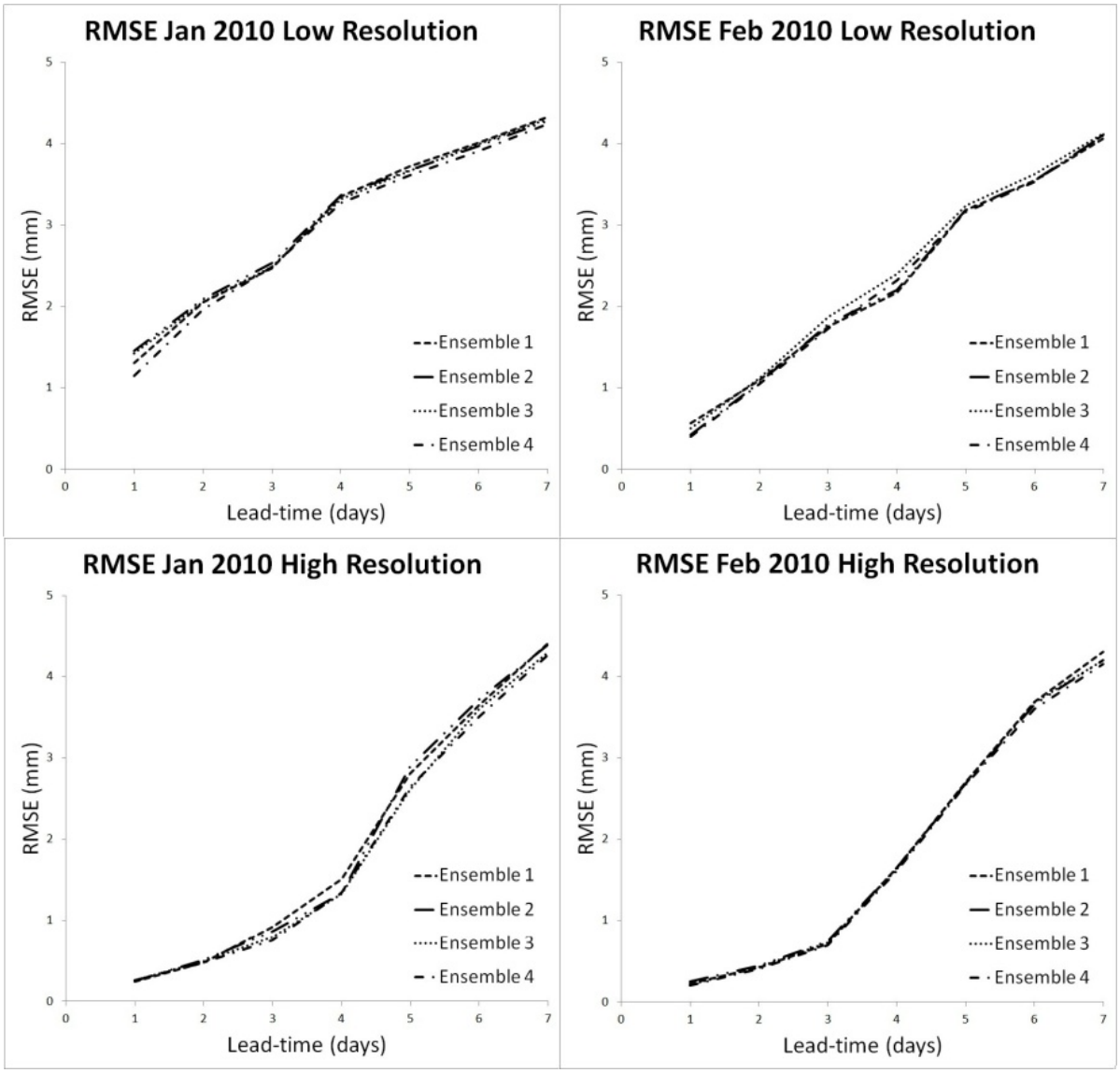

Figure 3.3: RMSE graphs for January and February 2010. Left top: January 2010 low resolution. Left bottom: January 2010 high resolution. Right top: February 2010 low resolution. Right bottom: February 2010 high resolution.

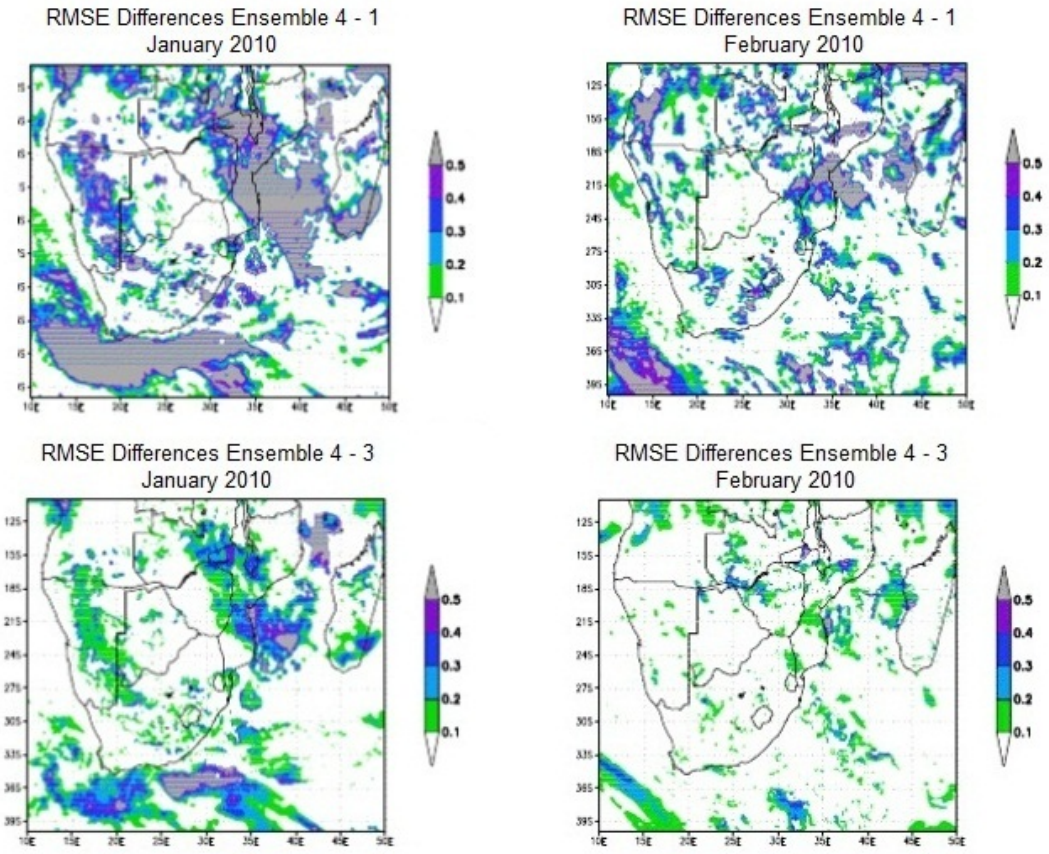

Figure 3.4: Difference in error at high resolution between Ensemble 4 and Ensemble 1, and Ensemble 4 and Ensemble 3. Left: January 2010. Right: February 2010.

3.3.2 Brier score

The Brier Skill Score is a measurement of the accuracy of the model forecast relative to that of a reference forecast, in this case chosen as the persistence forecast. This skill indicates how much better the forecasts made by the model are in comparison to the method of persistence, and is therefore also an indication of how useful the model forecasts are. A perfect BSS is equal to 1, with no skill equal to 0. Short-range weather prediction models have a natural decrease in skill with an increase in lead-time. This is expected since forecasts made for long-lead times are more affected by the chaotic nature of the atmosphere and the uncertainties in the model than short lead-times because the model cannot perfectly predict future changes in atmospheric conditions.

For this study, the BSS has been calculated for all four ensemble systems, at high and low spatial resolution, for the months of January and February 2010. The results are presented here graphically in Figure 3.5, showing the measure of skill for each case. For each of the two spatial resolutions, the BSS curves of the four ensembles are superimposed onto the graphs in order to easily interpret the effect of ensemble size on forecast skill. It can be seen from Figure 3.6 that for all four months, and at both resolutions, all four ensembles demonstrate similar skill. Figure 3.6 also illustrates the drop-off in skill as the lead-time increases which is expected due to the difficulty in predicting an inherently chaotic atmosphere.

This analysis of the BSS shows how altering ensemble size and spatial resolution affects the skill of the model systems. The ensemble size can be concluded to have little effect on the skill of the forecast, with the largest EPS having slightly improved skill over the others in some cases. In order to further increase the skill of the EPS, more ensemble members need to be introduced to contribute to the system. The high spatial resolution forecasts display better skill than the low resolution forecasts in some cases, but they are generally seen to be similarly skilful. The interpretation thereof is that the resolution of the model must be increased further in order to increase the skill of the forecasts.

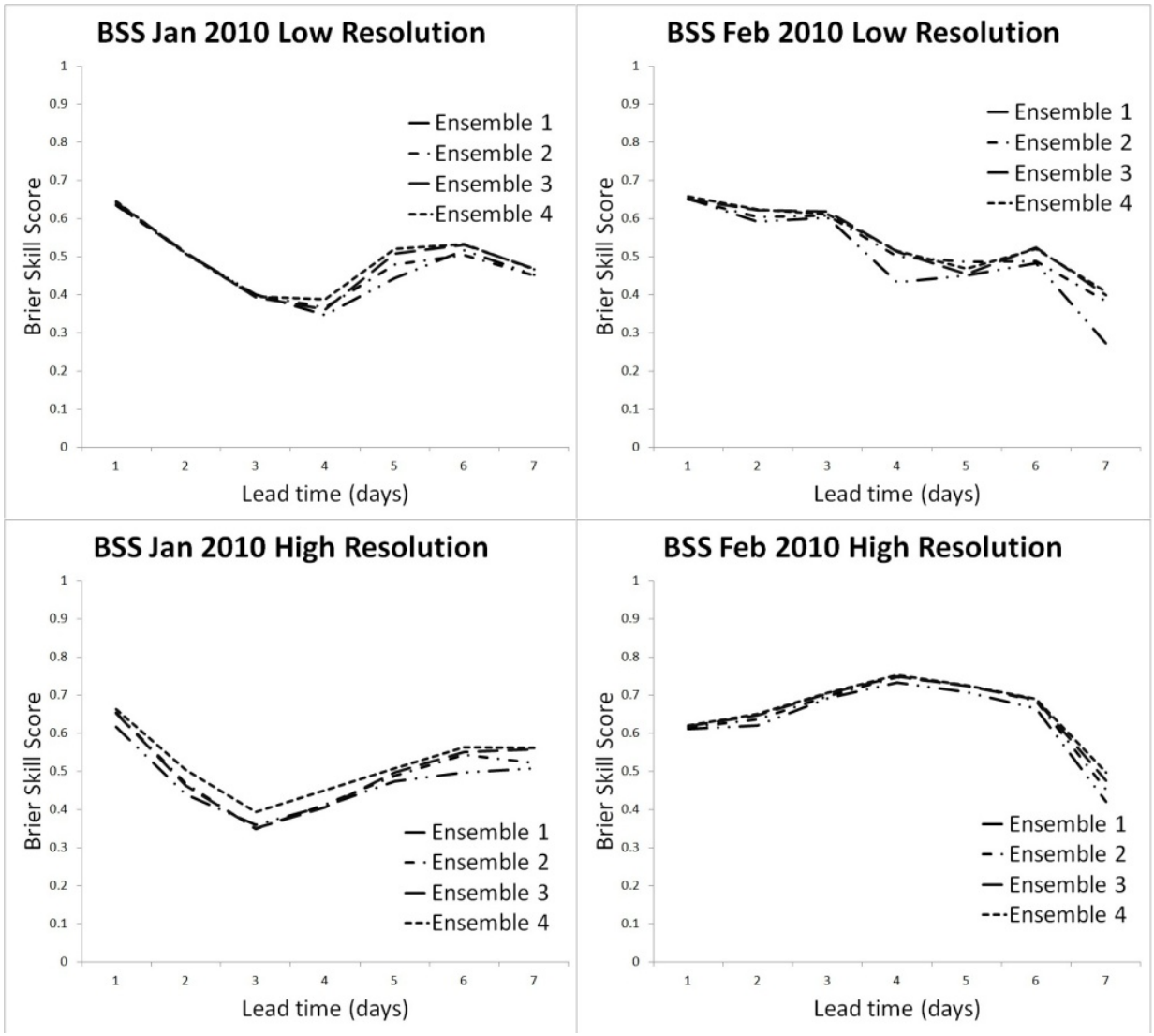

Figure 3.5: BSS curves for January and February 2010, low and high resolution.

3.3.3 ROC

In this section the ROC is used to measure the ability of the EPSs to discriminate two thresholds. The first threshold of 1 mm was chosen since in this study, any recorded precipitation of less than 1 mm was considered to be no rainfall. Therefore a threshold of 1 mm assesses how well the EPSs discriminate between rainfall and no rainfall. The second threshold of 5 mm was chosen as the threshold of heavier rainfall. This limit assesses the ability of the EPSs to discriminate between light -, and more heavy rainfall events.

3.3.3.1 Threshold of 1 mm

This section discusses the ability of the EPSs to discriminate precipitation events: rainfall or no rainfall. The areas under the ROC curves were calculated and the results are shown on the graphs in Figure 3.6 and Figure 3.7. From these figures it can be seen that the high resolution forecasts far out-performed the low resolution forecasts in every case.

Figures 3.5 and 3.6 show the ROC graphs of each EPS for January and February 2010 respectively, with the high and low resolution forecasts superimposed. These figures show a large difference between the high and low resolution systems. The high resolution curves are more rounded and approaching the top left corner, whereas the low resolution curves are close to the diagonal line of no skill. The conclusion that can be drawn from this is that an increase in spatial resolution will most likely result in an increase in ROC score, irrespective of ensemble size.

3.3.3.2 Threshold of 5 mm

This section analyses how well the EPSs perform in discriminating precipitation events: rainfall above 5 mm or rainfall below 5 mm. The areas under the ROC curves were calculated and the results shown on the figures Figure 3.8 and 3.8. It can be seen that there is a large discrepancy between the high and low resolution forecasts, and the high resolution forecasts out-perform the low resolution forecasts in every case. Also evident from the figures is a trend of increase in ROC area with increase in ensemble size. The increase is not large, but even so, this indicates that an increase in ensemble size results in an improvement in the discrimination ability of the ensemble systems.

Figures 3.7 and 3.8 show the ROC graphs of each EPS at high and low resolution for January and February 2010 respectively. Figure 3.8 and 3.9 illustrate a significantly large difference between the high and low resolution systems, where the high resolution curves capture far more area than the low resolution. This difference in area indicates that there is a considerable increase in skill with an increase in spatial resolution.

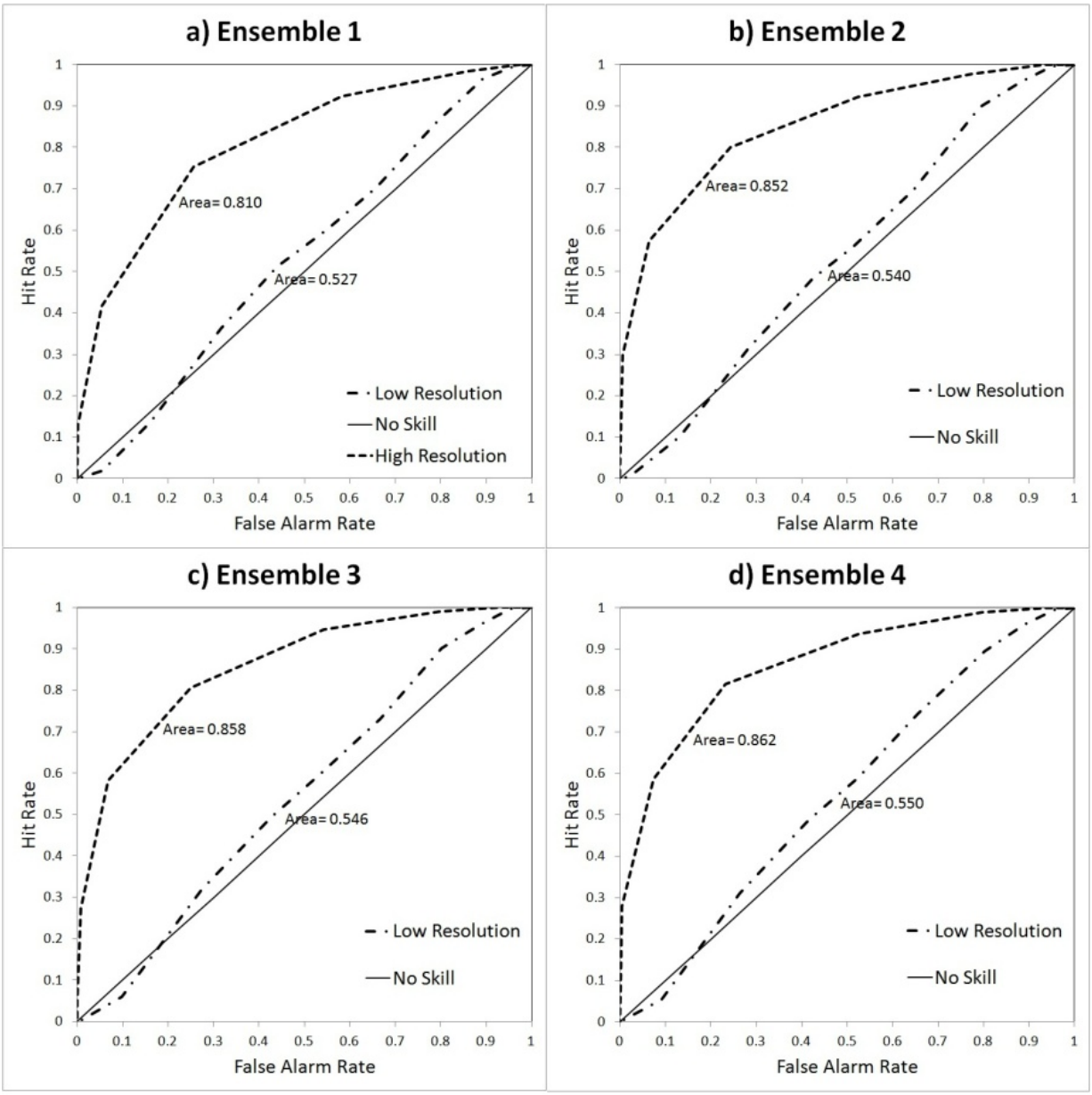

Figure 3.6: 1 mm threshold ROC diagrams for January 2010 at high and low resolution. **a)** Ensemble 1, **b)** Ensemble 2, **c)** Ensemble 3, **d)** Ensemble 4.

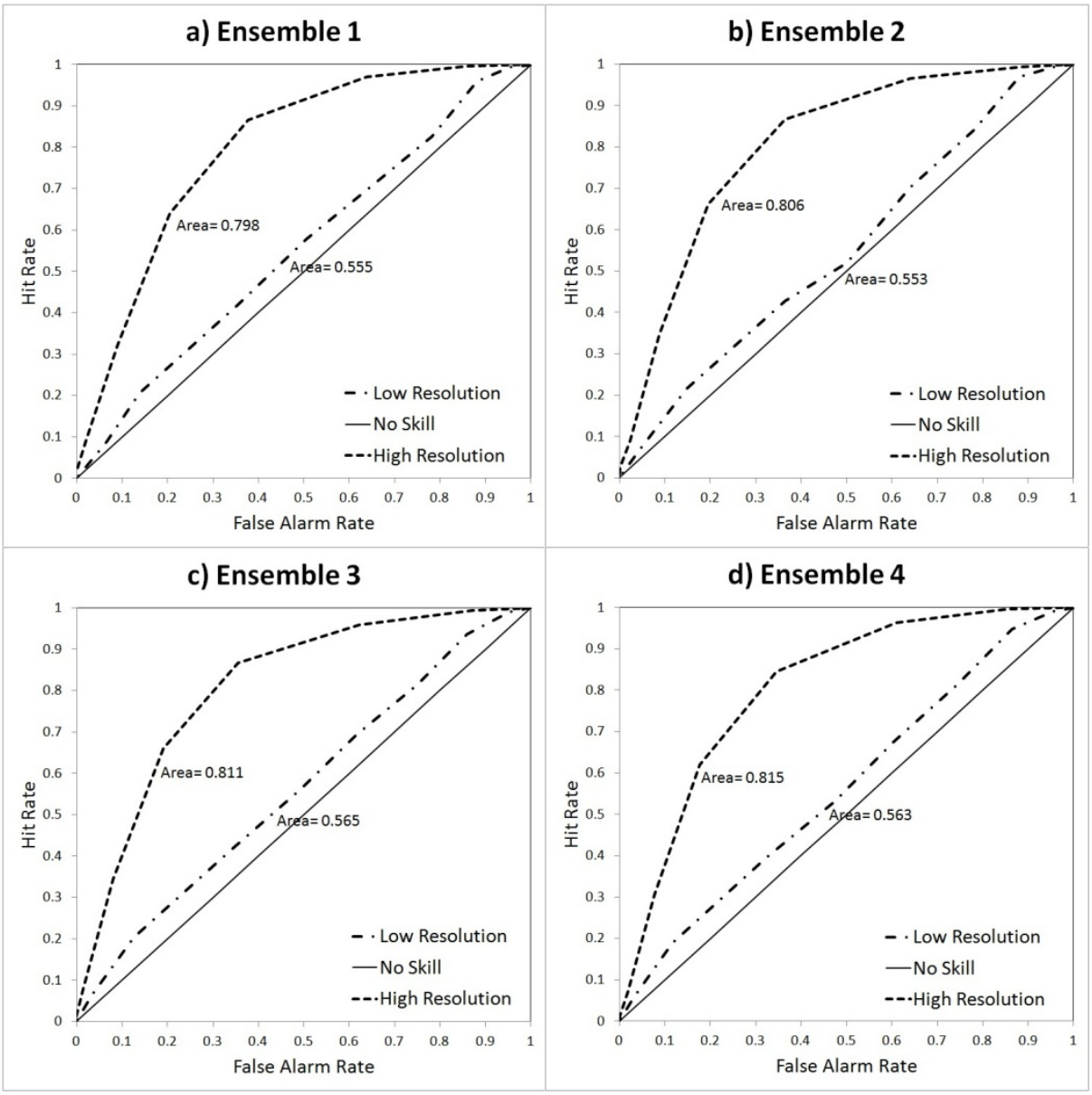

Figure 3.7: 1 mm threshold ROC diagrams for February 2010 at high and low resolution. **a)** Ensemble 1, **b)** Ensemble 2, **c)** Ensemble 3, **d)** Ensemble 4.

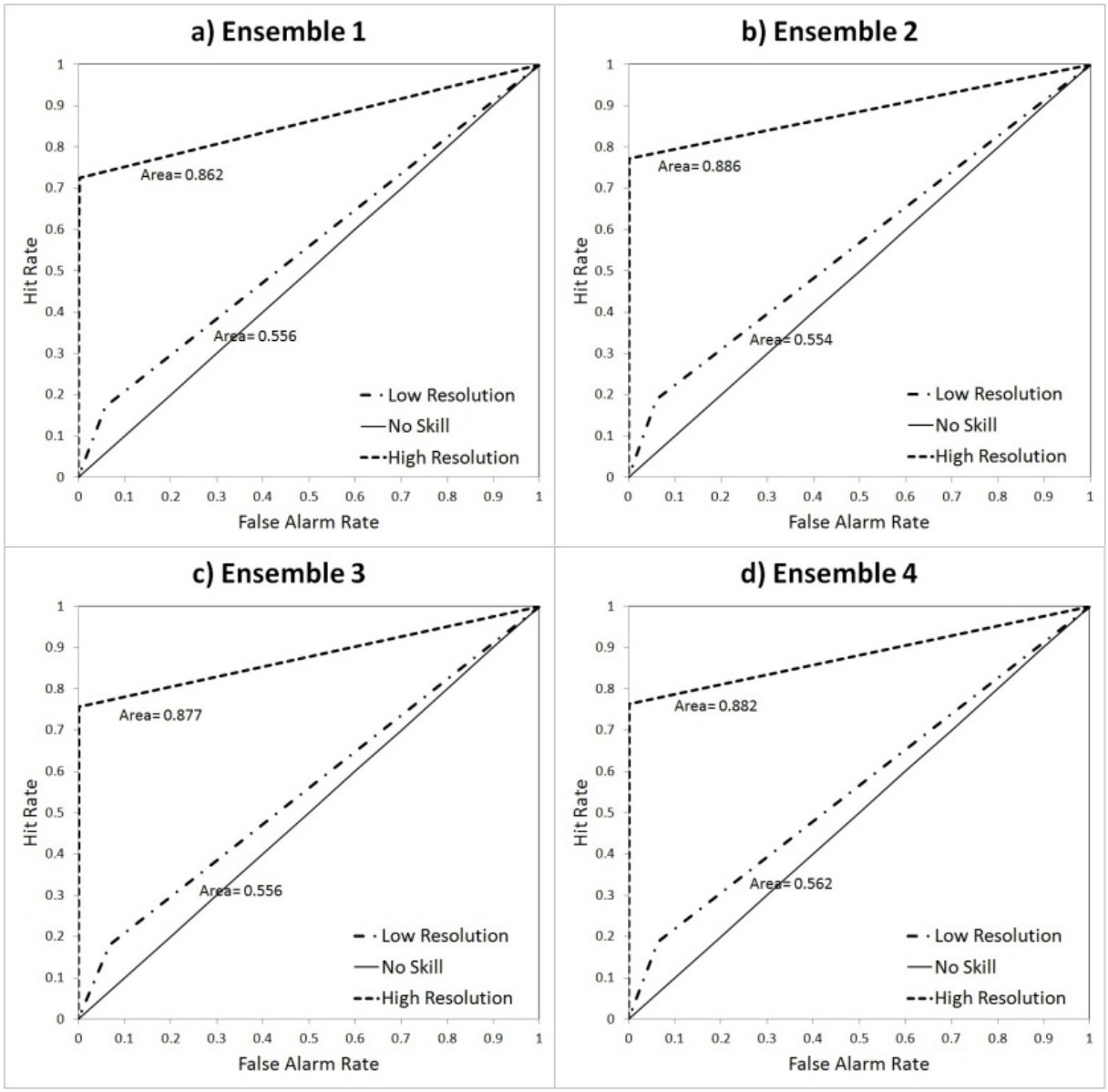

Figure 3.8: 5 mm threshold ROC diagrams for January 2010 at high and low resolution. **a)** Ensemble 1, **b)** Ensemble 2, **c)** Ensemble 3, **d)** Ensemble 4.

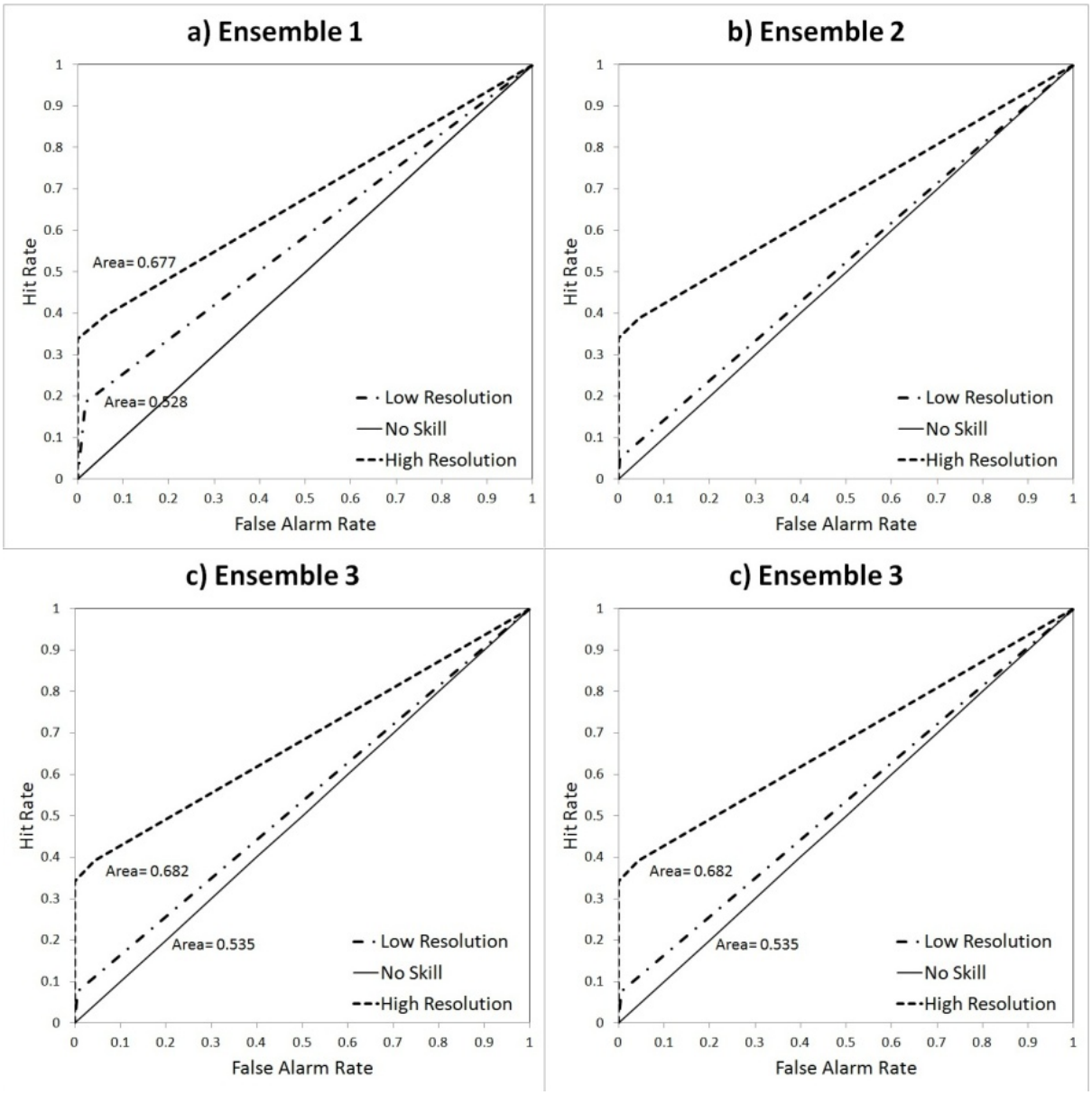

Figure 3.9 1 mm threshold ROC diagrams for February 2010 at high and low resolution. **a)** Ensemble 1, **b)** Ensemble 2, **c)** Ensemble 3, **d)** Ensemble 4.

3.3.4 Reliability diagrams

This analysis explores the reliability of each of the four ensemble systems, for each month, for low and high resolution. The individual reliability points are averaged into a straight line: the closer the gradient of this straight line is to 1 (perfect reliability), the better the reliability. The gradients of each reliability line are compiled into Table 3.3 below.

Figure 3.10 shows that for January 2010, in most cases the high resolution forecasts have a gradient closer to the line of perfect reliability than the low resolution forecasts. Figure 3.11 shows that during February 2010 the four ensembles display a huge improvement from the low to the high resolution. This indicates that, generally, there is an improvement of reliability with an increase in spatial resolution. There is also a general trend of improvement of reliability with an increase in ensemble size: in almost every case for both the low and high resolution systems the gradients of the reliability lines approach 1 as the ensembles become bigger.

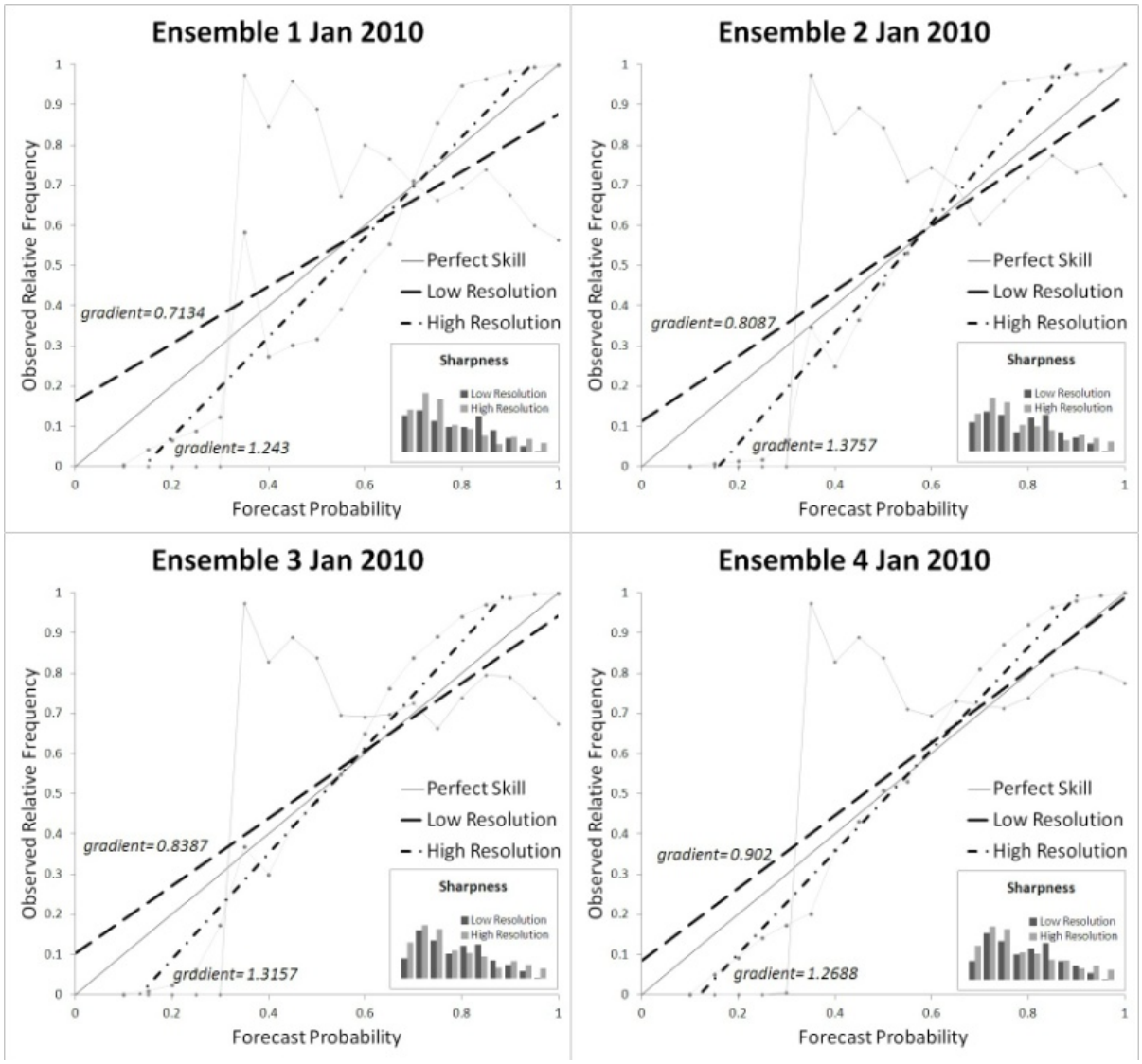

Figure 3.10: Reliability diagrams for January 2010 at high and low resolution. **a)** Ensemble 1, **b)** Ensemble 2, **c)** Ensemble 3, **d)** Ensemble 4.

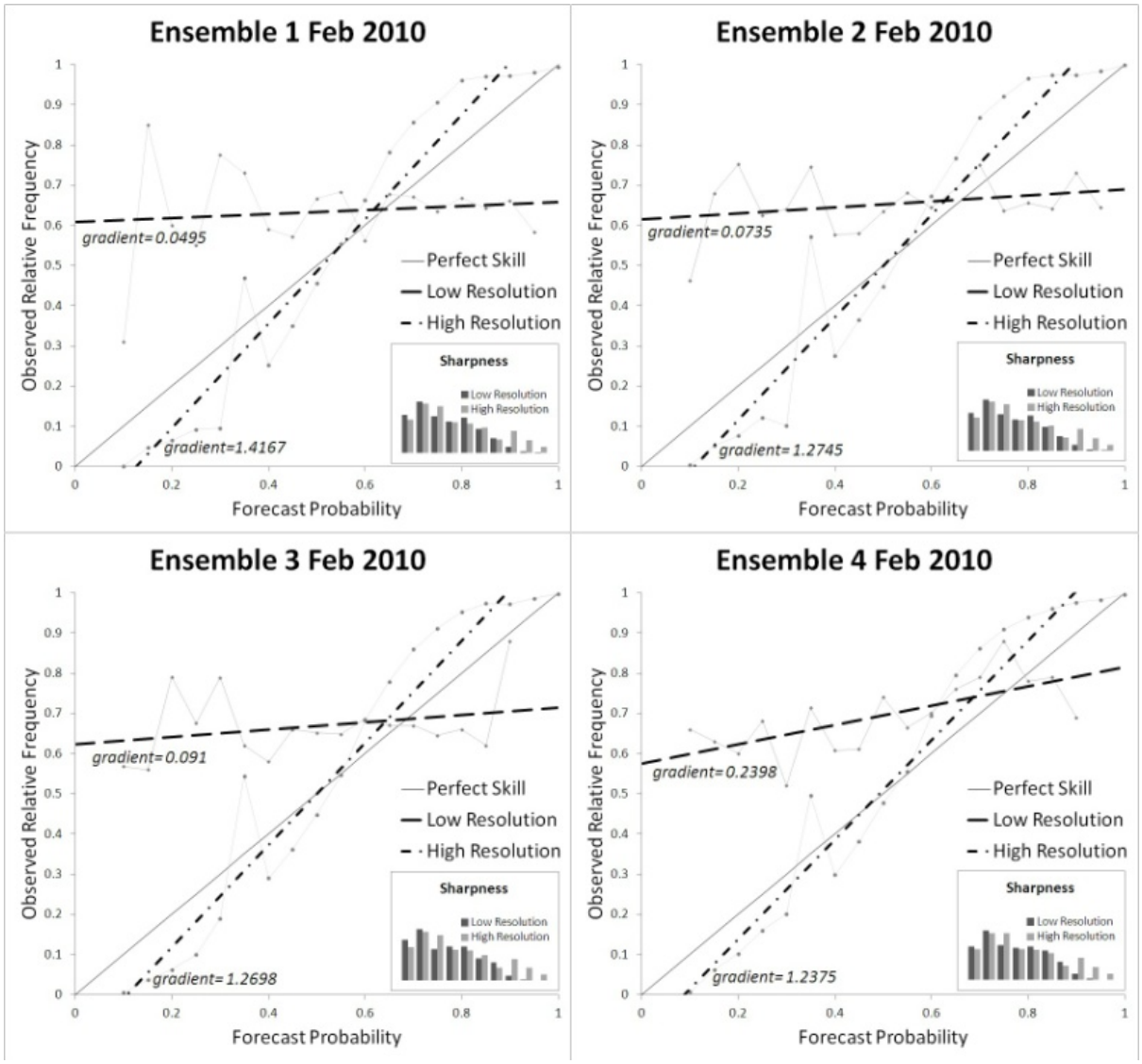

Figure 3.11: Reliability diagrams for February 2010 at high and low resolution. **a)** Ensemble 1**, b)** Ensemble 2, **c)** Ensemble 3, **d)** Ensemble 4.

3.4 Conclusion

The largest ensemble system (8 members) run at the high spatial resolution (15 km) outscores in discrimination and reliability, and is more skilful than, all the other systems. Although the skill scores for each month are similar for all eight EPSs, the largest ensembles at each resolution display greater skill than the others; and Ensemble 4 (8 members) at high resolution is the most skilful in all but one case. The ROC diagrams show that all of the EPSs at high resolution far outscore those at the low resolution, and that the Ensemble 4 run at high resolution performs the best of all systems when discriminating both 1 mm and 5 mm of rainfall. Finally, the

reliability was generally the best for the high resolution Ensemble 4 system, although the sharpness of all the EPSs was seen to be low.

For the first hypothesis, the RMSE results show a very similar error curve for all four EPSs. However, the difference in error spatial maps display areas of error difference that illustrate the error decreasing with an increase in ensemble size. The skills of all four EPSs are very similar, however, the BSS curves show an improvement, albeit small, in skill with an increase in ensemble size. It can therefore be concluded that in order for an EPS to begin demonstrating an improvement in skill, the EPS needs to be of a size much larger than the eight members considered here. The ROC graphs for the 1 mm discrimination of rainfall show the area under the curve increasing slightly as the ensemble size increases, establishing that the largest ensemble has a greater ability to discriminate 1 mm of rainfall. The ROC graphs for discriminating 5 mm of rainfall display a small increase in area with an increase in ensemble size, suggesting that a further increase in ensemble size would increase the ability of the model to discriminate 5 mm of rainfall. The reliability of the EPSs was tested with Reliability Diagrams, and these showed that in most cases there was a trend of increasing reliability with an increase in EPS size. Notwithstanding the small difference in skill, the general conclusion that can be drawn from the testing of this hypothesis is that the largest EPS performed best in all verification scores.

The effect of spatial resolution on the performance of the EPSs was tested for the second hypothesis. The RMSE graphs show that the errors in the high resolution forecasts are less than in the low resolution forecasts. This result is particularly pronounced up to the four-day lead time, where the high resolution EPSs have error far smaller than the EPSs at low resolution. The ROC curves for 1 mm exhibit a considerable improvement from the low and high resolution forecasts, with the high resolution forecasts showing an excellent ability to discriminate 1 mm of rainfall. The 5 mm threshold ROC curves show this same result, with the high resolution EPSs far out-performing the low resolution EPSs. The Reliability Diagrams display a general trend of increase in reliability with increase in spatial resolution, especially in the months of February 2009 and 2010, when the high resolution EPSs have substantially better reliability than the low resolution EPSs. The final result from this hypothesis is that the EPSs at high resolution outscored the low resolution EPSs in every case.

The two hypotheses above provide the results that the largest sized EPS performs the best when being assessed with the four chosen verification scores, and that the EPSs perform best at high resolution. It can therefore be concluded that the most successful EPS was found to be the largest ensemble: Ensemble 4, at a high spatial resolution. In almost all cases, the largest ensemble at the highest resolution was found to outscore all the others.

The results from this work provide a great practical improvement in short-range numerical weather prediction. Implementing large ensemble and high resolution EPSs will result in a reduction in error, an increase in the ability to discriminate rainfall thresholds, and an increase in reliability. In order to improve these scores even further, future research should concentrate on creating very large ensemble using perturbation techniques, and increasing the spatial resolution to a very fine grid. Other verification scores could also be studied, such as bias, in order see where the EPS could be further improved. A way to try to improve the configuration of the CCAM in the future would be to introduce different cumulus parameterisation schemes into the model and test whether they are more skilful at resolving small-scale cloud systems. A different way to proceed would be to include the EPSs into a multi-model ensemble and contribute to a larger system of weather models.

Chapter 4

SST prediction methodologies and verification considerations for dynamical mid-summer rainfall forecasts for South Africa

4.1 Introduction

South Africa's seasonal rainfall variability is associated with different levels of predictability and is dependent on the time of the year: Spring (September-October-November) season rainfall totals are for the most part not predicted with high confidence owing to the fact that this season is mostly influenced by transient weather systems, while the best forecast skill has been demonstrated during mid-summer (Landman et al., 2005; Landman et al., 2012) when the tropical atmosphere starts to dominate the atmospheric circulation over South Africa (e.g. Mason et al., 1996, Landman and Mason, 1999). Some useful prediction skill is also found during austral autumn (Landman et al., 2005). However, the modelling work presented here only focuses on mid-summer (December to February – DJF) owing to the relatively high skill found for this season (Landman et al., 2005, Landman et al., 2009, Landman et al., 2012) and because the larger part of South Africa's austral summer rainfall areas receive most of their rainfall during this season.

The use of dynamically based atmospheric models as *real-time operational* seasonal forecasting tool has been used in South Africa since the turn of the century (e.g. Landman et al., 2001). Major advances in the use of atmospheric general circulation models (AGCMs) for operational seasonal forecasting in South Africa continued to occur also at the Universities of Cape Town and of Pretoria, and at the Council for Scientific and Industrial Research. A notable recent advancement is the development of a fully coupled ocean-atmosphere model at the South African Weather Service (SAWS; Beraki et al., 2014). In addition a notable acquisition by SAWS is the World Meteorological Organizations Global Producing Centre for Long-Range Forecasts (GPCLRF) status. As part fulfilment of this obligation, SAWS runs the ECHAM4.5 AGCM (Roeckner et al., 1996) operationally, and so this model is the focus of this chapter. However, the ECHAM4.5 forecast ensembles used in this study are obtained from the Data Library of the International Research Institute for Climate and Society (IRI) and not from the archives of SAWS since the IRI archived

data set of this AGCM is more comprehensive. For example, the IRI has available a variety of ECHAM4.5 hindcast sets and for various forecast lead-times. These archived sets can be used to help determine some of the modelling strategies SAWS, and possibly other institutions in South Africa involved with AGCM operations, can follow in order to optimize their own operational seasonal forecasting systems.

Employing predicted or persisted SST anomalies in AGCMs provides means of generating forecasts of seasonal-average weather (Graham et al. 2000, Goddard and Mason, 2002) since the evolution of global sea-surface temperature (SST) anomalies over several months ahead is predictable especially over the tropics, even with statistical models (Landman and Mason, 2001). Coupled ocean-atmosphere general circulation models (CGCMs) have also been increasingly used worldwide for operational seasonal forecast production (e.g. DeWitt 2005, Graham et al., 2011). Furthermore, it has been shown through the DEMETER (Development of a European Multimodel Ensemble system for seasonal to inTERannual prediction) project that fully coupled systems can predict both the evolution of SSTs and atmospheric conditions at elevated levels of skill (Palmer et al., 2004) relative to AGCM skill (Graham et al., 2005). The foundations laid by the DEMETER and other projects contributed towards the development of a coordinated system for seasonal to decadal prediction, assessed via a comprehensive set of 46 years of hindcasts produced by state-of-the-art climate models (van der Linden and Mitchell, 2009). Notwithstanding these modelling developments, when skilful SST forecasts are used AGCMs may perform equally well as the current CGCMs (Troccoli et al., 2008) and so CGCMs can benefit AGCMs by applying their predictions of SST evolution to force AGCMs with (Li et al., 2008). Here we want to investigate to what extent an AGCM's mid-summer seasonal forecasts for South Africa is sensitive to the SST forecasting strategy selected to force the atmospheric model. Mid-summer rainfall is the season often associated with the highest level of skill (Landman et al., 2012) and so the effect various modelled options of the forcing SST fields may have on the AGCM's forecast skill for specifically mid-summer rainfall totals over South Africa is therefore the main focus of the chapter.

4.2 Data and methods

The district rainfall data set of the South African Weather Service (Van Rooy, 1972) is used to calculate 3-month DJF seasonal rainfall totals for 93 evenly distributed locations across South Africa (see Figures 4.4 and 4.5 for the locations of the centroids of the districts). This data set is available from 1921 and is updated every month. Here we consider only the rainfall data from 1968 through 2002 in order to match the available AGCM hindcasts used in this chapter.

The ECHAM4.5 AGCM hindcast data used here are obtained from the Data Library of the IRI (http://iridl.ldeo.columbia.edu/) and consists of three sets. Each of the three AGCM experiments was composed of an ensemble of 24 integrations. The atmospheric initial conditions for all three experiments are described in Li et al. (2008). In summary the atmospheric initial conditions for each of the three sets of experiments at any given start time are identical and were generated by adding random machine precision level perturbations to the wind field during the model spin-up period, thus no observed initial conditions were used for any of the experiments. The first AGCM set (available from 1957 to July 2008) consists of 24 ensemble members and was produced by forcing each of the 24 runs with identical SST anomalies that were predicted using constructed analogues (Van den Dool, 1994). The two additional AGCMs sets, also consisting of 24 ensemble members each and available from 1958 to 2001, were a result of forcing the atmospheric model with two separate configurations of dynamically predicted SST. The first of these sets was a result of forcing each of the 24 AGCM runs with the identical ensemble mean of ECMWF SST forecasts (9 members) created during the DEMETER project. The second set of AGCM forecasts forced with dynamically predicted SST was created by considering each of the nine ECMWF SST ensemble members – a scenario of SST forecasts are therefore considered by using some SST ensemble members 3 times and some only 2 times in order to produce a set of 24 AGCM ensemble members. The least number of times an SST ensemble member is used is two and no ensemble members are identical. The three experiments only differ in their prescribed SST forcing. Owing to the availability of archived DEMETER hindcasts, only a 1-month lead-time is considered here which implies that DJF hindcasts are produced near the beginning of November.

Empirical downscaling or recalibration of GCM fields to regional rainfall has already been successfully employed for southern Africa (e.g. Landman and Goddard, 2002, Landman and Beraki, 2012) and it has been shown conclusively that by empirically post-processing GCM large-scale fields is a necessary requirement for optimal seasonal rainfall forecast performance for South Africa, especially for mid-summer predictions (e.g. Landman and Goddard, 2002, Shongwe et al. 2006). Model output statistics (MOS; Glahn and Lowry, 1972) equations are developed here because they can compensate for systematic deficiencies in the global models directly in the regression equations (Wilks, 2011). Variables such as large-scale atmospheric circulation are better simulated by most models than rainfall and should probably be used instead in a MOS system to predict seasonal rainfall totals. In fact, the model's 850 hPa geopotential heights have been found to be a proven southern African seasonal rainfall predictor using MOS (Landman and Goddard, 2002, Landman et al., 2005, Landman et al., 2009, 2012, Landman and Beraki, 2012) and this field is again used here as predictor. The predictor sets are respectively the ensemble means for each of the three 24-member AGCM experiments and the predictand the 93 South African districts which remain the same for each experiment. The predictor fields used in the MOS are restricted over a domain that covers an area between the Equator and 45°S, and 15°W to 60°E. This domain is large enough to compensate for the model's biases of the large-scale circulation. The MOS equations are developed by using the canonical correlation analysis (CCA) approached described in Barnett and Preisendorfer (1987) and the downscaling procedure is reported on in detail in earlier work as applied to southern African seasonal rainfall prediction (Landman et al., 2001, Landman and Beraki, 2012, Landman et al., 2012).

In order to minimize artificial inflation of forecast skill, the downscaled forecast performance should mimic a true *operational* forecasting environment where no prior knowledge of the coming season is available. The MOS models are first trained with information from 1968/69 and leading up to and including 1977/78. The first MOS training period is therefore 10 years. The seasonal rainfall of the next year, 1978/79, is then predicted using the trained MOS model. The MOS model is subsequently retrained using information leading up to and including 1978/79 (11 years) to predict for 1979/80 conditions. This procedure is continued until the 2001/02 DJF rainfall is

predicted using a MOS system trained with data from 1968/69 to 2000/01, resulting in 24 years (1978/79 to 2001/02) of independent downscaled forecast data. Such a procedure is referred to as retro-active forecasting (e.g. Landman et al. 2001). Cross-validation (Michaelsen, 1987) is performed over the entire 34-year period from 1968/69 to 2001/02. In order to minimize the chance of obtaining biased results a large 5-year-out window is used. The first 10 years are subsequently discarded resulting in 24 years of cross-validated downscaled hindcast (deterministic) over the same period as the retro-active downscaled forecasts, i.e. 1978/79 to 2001/02.

The skill of the three AGCM-MOS systems (the AGCM forced with statistically predicted SST and the same AGCM forced with two different configurations of ECMWF SST forecasts) is determined both probabilistically and deterministically. Probabilistic verification is conducted on the 24 years of retro-active DJF rainfall forecasts, while deterministic verification is performed on the 24 years of cross-validated hindcasts. For the former the observed and predicted fields are separated into three categories defining above-normal, near-normal and below-normal DJF rainfall totals. Two approaches are adopted here: The first is the familiar equi-probable 3-category description (the thresholds are respectively the 33rd and 67th percentile of the climatological record) and the second approach defines the below- and above-normal threshold values respectively by the 15th and 85th percentile values of the climatological record, i.e. seasonal extremes. Probabilistic MOS forecasts for each of the 24 retro-active years are obtained from the error variance of the cross-validated predictions using the ensemble mean (Troccoli et al., 2008) for each of the various training periods required for generating the retro-active forecasts. Verification results of only the above-normal and below-normal categories are presented owing to the low skill found for the near-normal category.

Two of the main attributes of interest for probabilistic forecasts are discrimination (are the forecasts discernibly different given different outcomes?), and reliability (is the confidence communicated in the forecast appropriate?). The forecast verification measures presented here for testing of the aforementioned attributes are the relative operating characteristic (ROC) (e.g. Mason and Graham, 2002), and the reliability diagram (Hamill, 1997). A ROC graph can be constructed by plotting the forecast hit

rates against the false-alarm rates. For good forecasts the hit rate will accumulate faster than the false-alarm rate resulting in a ROC graph that curves towards the upper left. For perfect discrimination the area beneath the curve would be 1.0, and for no skill the area beneath the curve would 0.5 (the ROC curve will coincide with the diagonal) or lower. ROC applied to probabilistic forecasts indicates whether the forecast probability was consistently higher when a flood or drought season occurred compared to when it did not occur. Although the ROC is a verification procedure recommended by the World Meteorological Organization, it has been criticized because the reliability of the forecast probabilities is ignored (Troccoli et al., 2008).

Forecasts are considered reliable if there is consistency between the predicted probabilities of the defined rainfall categories and the observed relative frequencies of the observed rainfall being assigned to these categories. The reliability diagrams presented below are used to assess if the downscaled models are able to produce well-calibrated probability forecasts and include reliability curves for the above- and below-normal categories along with their respective least-squares regression lines. The regression lines are calculated with weighting relative to how frequently forecasts are issued at a given confidence. Forecasts are considered perfectly reliable when these weighted regression lines lie perfectly along the diagonal of the reliability diagram, but when the regression lines lie above (below) the diagonal observed above- or below-normal values tends to occur more (less) frequently and then the forecasts are considered under-confident (over-confident). Frequency histograms are also included and show the frequencies with which forecasts occur in probability intervals of 10%, starting at 5%. The ROC graph has an advantage over the reliability diagram in being less sensitive to sampling errors, and so can be more meaningfully constructed given the small sample sizes typical of seasonal forecasting (Troccoli et al., 2008). The interpretation of ROC scores and reliability diagrams in general can be found in Troccoli et al., (2008), Barnston et al., (2010), Wilks (2011) and Jolliffe and Stephenson (2012), among others.

For the deterministic verification work three correlation values are calculated: Pearson or “ordinary” correlation to measure the association between the deterministic cross-validated hindcasts and the DJF rainfall at each district over the 24 years, and the robust and resistant alternatives to the Pearson correlations, namely the Spearman rank correlation and Kendall’s tau. The Spearman correlation

is simply the Pearson correlation, but using the ranks of the hindcasts and of the observations. Kendall's tau is calculated by considering the relationships among all possible matchings of the hindcast and observation pairs (Wilks, 2011). Spearman and Kendall's tau (both are non-parametric tests) are better suited than Pearson for verification of precipitation since rainfall has a non-Gaussian distribution. What additionally makes the Kendall's tau attractive is that it has close affinities to the area beneath the ROC curve (Jolliffe and Stephenson, 2012) used here for verification of the probabilistic retro-active forecasts.

4.3 Model performance

The deterministic retro-active DJF rainfall forecasts across the 93 districts and over the 24-year test period (1978/79 to 2001/02) from each of the three AGCM-MOS models along with the observed are shown in Figure 4.1. Both predicted and observed values are normalised since the rainfall distribution over South Africa varies from wet over the eastern parts to semi-arid to arid over the western parts. El Niño (marked "El") and La Niña (marked "La") seasons are also shown on the figure. El Niño and La Niña seasons are identified according to the so-called Oceanic Niño Index. The top panel of Figure 4.1 shows each district's DJF rainfall index as predicted by the AGCM forced with statistical SST. Below that are the rainfall index forecasts produced by the AGCM forced with the two SSTs configurations of the ECMWF coupled model. From the figure one notices the similarities between the middle two panels (AGCM forced with ECMWF SST) and that these two forecasts are somewhat different to the forecasts shown in the top panel (forcing the AGCM with statistical SST), especially during the late 1980s and the first half of the 1990s. Take note that the three forecast systems tend to predict dry (wet) conditions during El Niño (La Niña) seasons, although it may not always turn out to be dry (wet) during El Niño (La Niña) seasons as can be seen when the forecasts are compared to the observed (bottom panel). Next we will do proper verification over the 24-year test period in order to determine how the various forecast systems compare with the observed and subsequently with each other.

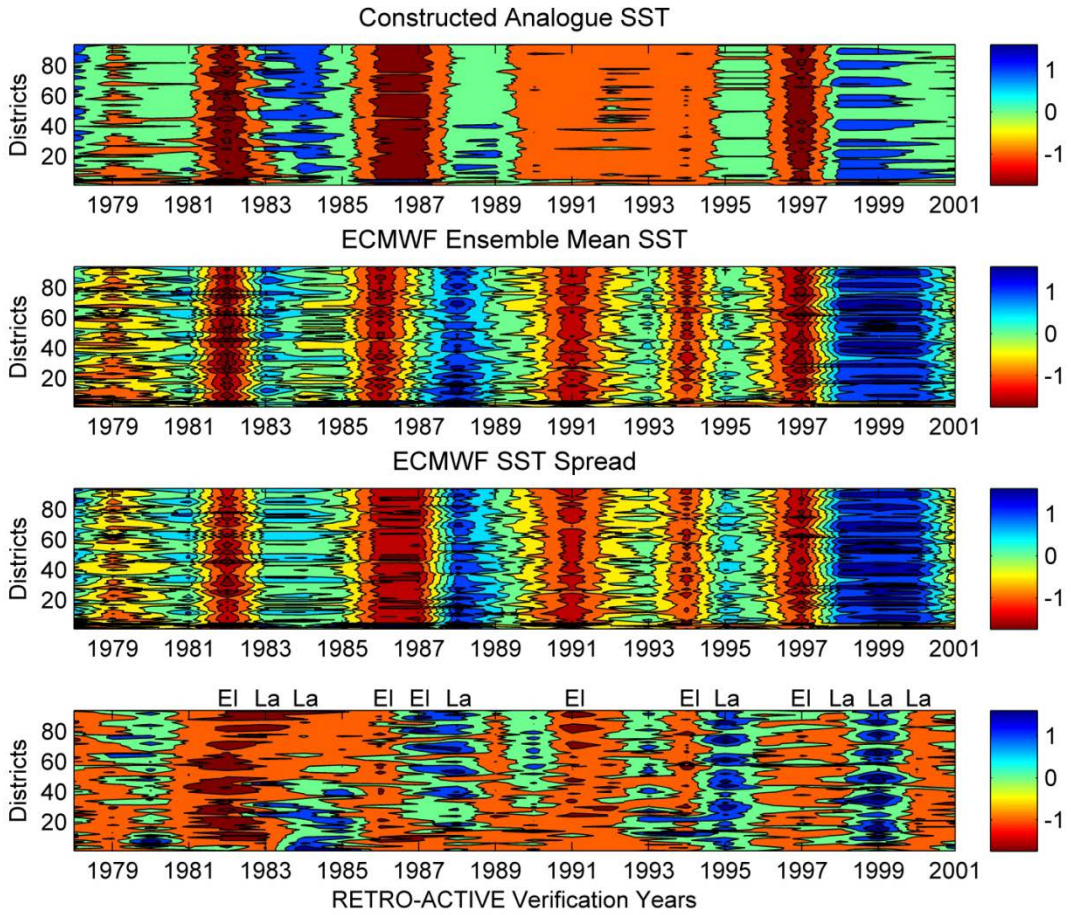

Figure 4.1: Statistically downscaled DJF rainfall indices across 93 South African rainfall districts over 24 years produced by using a retro-active prediction procedure. The top panel shows the forecasts produced when the AGCM is forced with statistical SST, the second from top panel when the AGCM is forced with the ensemble mean SST of a coupled model, the third panel when forced with a spread of SST ensemble members of a coupled model and the bottom panel is the observed DJF rainfall indices. DJF forecasts are produced in early November.

Skill levels of the retro-active downscaled probabilistic forecasts of the three AGCM-MOS models are shown in Figures 4.2 and 4.3 (ROC scores and reliability diagrams, respectively). Figure 4.2 shows that the highest ROC scores are found when forcing the AGCM with the SST forecasts from the coupled ECMWF model. Moreover, the forecasts associated with the ECMWF SST ensemble mean are also somewhat superior to the forecasts associated with the ECMWF SST ensemble spread. Furthermore, the higher ROC scores are found for the extreme cases (respectively lower and higher than the 15th and 85th percentile values), especially when predicting for extremely *wet* seasons. The reliability plots of Figure 4.3 are for the extreme cases only and show very similar results for both cases of ECMWF SST predictions, but show lower reliability when using this statistical SST forecast model: The regression lines on Figure 4.3 (weighted least-squares regression of the respective

reliability curves) are close to the diagonal for the ECMWF SST forced extreme forecasts, but show over-confidence (regression lines are shallower than the diagonal) for the statistical SST forced forecasts, especially for predicting extremely dry years. None of the three forecast systems show strong sharpness (the level of confidence that is communicated in the forecasts) since the most frequent forecast category is near 15%, the climatological probability for the extreme cases. The verification results presented thus far agree with what has been suggested by the forecasts shown in Figure 4.1: The AGCMs forced with SSTs predicted by the coupled model are superior to the AGCM forced with statistical SST and that the two SST scenarios resulted in similar levels of skill although the AGCM forced with an ensemble mean SST seems superior.

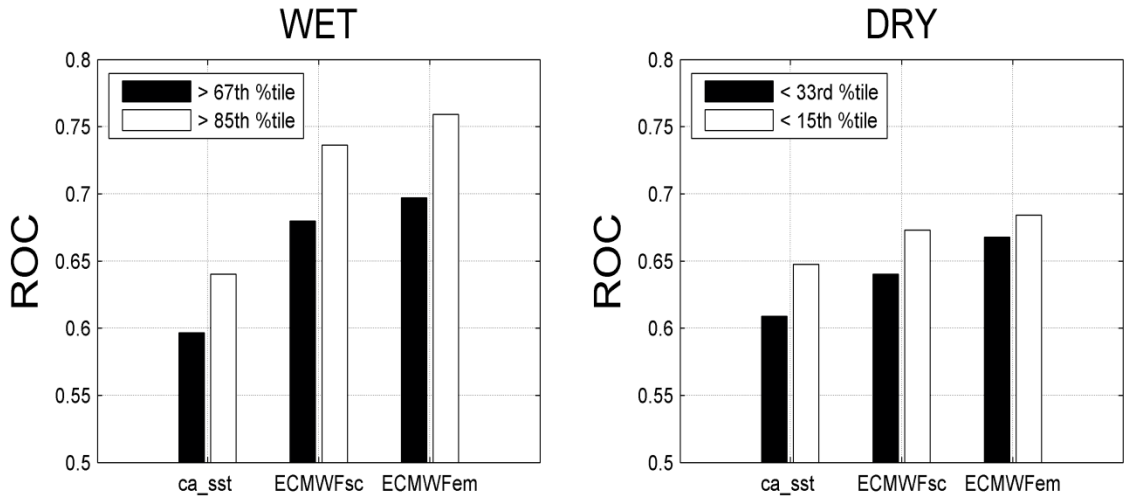

Figure 4.2: Relative operation characteristic (ROC) scores for wet (left panel; upper terciles and 85th percentile threshold) and for dry (right panel; lower terciles and 15th percentile thresholds) conditions during DJF over South Africa. The ROC scores are calculated over a 24-year test period for predictions made early November by an AGCM forced with constructed analogue (ca_sst), ECMWF ensemble spread (ECMWFsc) and ECMWF ensemble mean (ECMWFem) SST forecasts, and then statistically downscaled to district level.

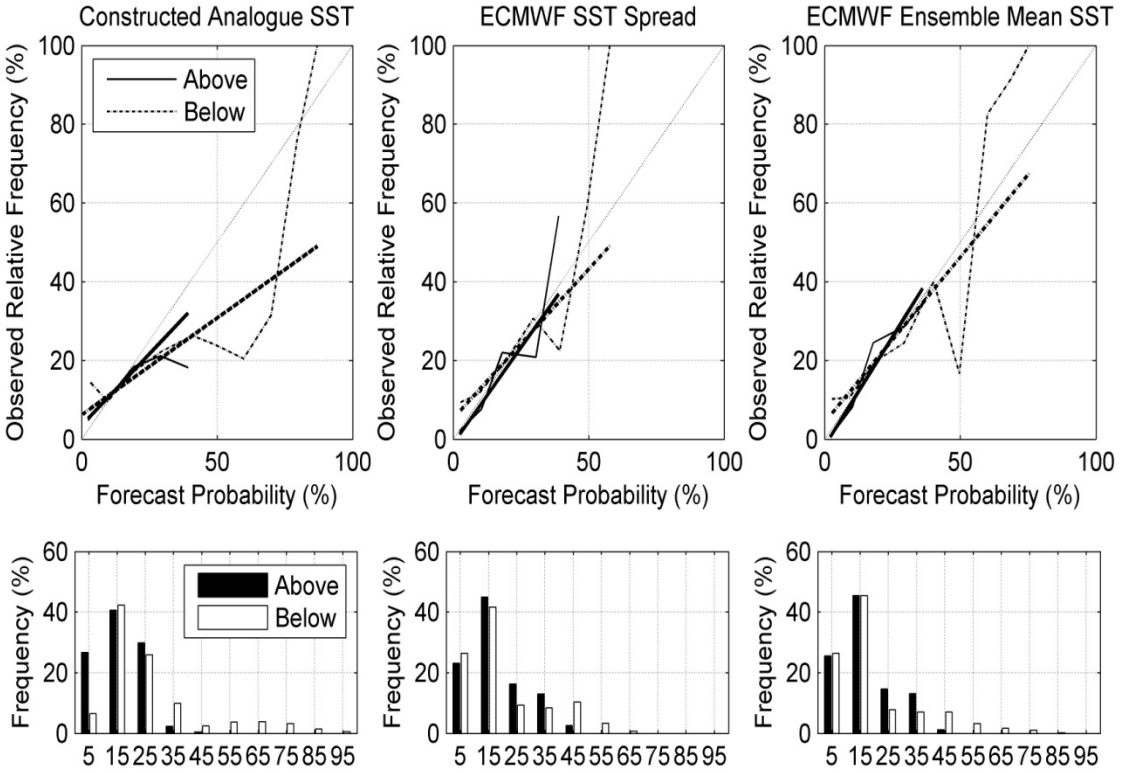

Figure 4.3: Reliability (top row) and frequency (bottom row) diagrams for the downscaled DJF extreme rainfall forecasts. The reliability diagrams show both the reliability curves for very wet and for very dry seasons, and their associated weighted least-squares regression lines. The histograms indicate the frequencies for forecasts of probabilities of < 5%, 5-15%, etc.

The AGCM forced with statistical SST is thus considered to be the weakest of the three systems and so we will subsequently find out the locations in South Africa where the AGCMs forced with ECMWF SST are superior. For this analysis we use Kendall's tau owing to its close affinities to ROC scores (Jolliffe and Stephenson, 2012). Kendall's tau correlations between retro-active forecasts of the three AGCM-MOS models and observed DJF rainfall indices are subsequently calculated. Figure 4.4 a) and b) show respectively the Kendall's tau difference per district between the AGCM forced with statistical SST and the AGCM forced with the ECMWF SST ensemble mean, and the difference per district between the AGCM forced with statistical SST and the AGCM forced with members of the ECMWF SST forecasts. Negative correlation differences show where the AGCM forced with ECMWF SST is superior. Most of the improvement is found over the central parts of South Africa and the AGCM forced with the ECMWF SST ensemble mean shows the largest improvement over the AGCM forced with statistical SST. Figure 4.5 a) and b) show the Kendall's tau correlations between the retro-active forecasts of the AGCM forced

with the ECMWF SST ensemble mean, and the correlations between the retro-active forecasts of the AGCM forced with the ECMWF ensemble members, respectively. Correlations significant at the 90% level of confidence are marked with an asterisk and correlations significant at 95% with a double asterisk. This figure confirms the verification results above that the AGCM forced with the ensemble mean SST to be superior. Moreover, this conclusion is further manifested by using the Spearman rank as well as the (ordinary) Pearson correlation. Figure 4.6 represents the number of districts (out of 93) with local significance at respectively the 90% and 95% level of confidence for all three correlation parameters calculated from the retro-active forecasts. A larger number of districts found to be significant implies that a larger area of South Africa is associated with significant correlations. For both levels of confidence and all three correlations, the AGCM forced with the ensemble mean SST of the ECMWF coupled model is found to be the best configuration for DJF rainfall predictions over South Africa. Also take note that the non-parametric rank correlations are generally more conservative (fewer districts with local significance) than the Pearson correlation that requires that the predicted and observed values are normally distributed.

Two approaches for creating model forecasts for testing have been presented here: Cross-validation and retro-active forecasting. For the MOS downscaling, the Climate Predictability Tool is used, and this software uses cross-validation to generate the required error variances for the subsequent creation of retro-active probability forecasts (Troccoli et al., 2008). This configuration may pose problems with short data sets owing to the even shorter initial training period. In fact, the initial training period used in this chapter for predicting the first retro-active year (1978/79) is only 10 years (1968/69 to 1977/78) and so the question arises if such an initial small sample, albeit incrementally increased by one year during the retro-active forecast procedure, does not impact negatively on the forecast skill of the systems being tested. Figure 4.7 shows for each AGCM system the differences of the predicted DJF rainfall indices between the cross-validation hindcasts and the retro-active forecasts. Shadings of blue (red) show where and when the retro-active process has predicted anomalies larger (smaller) than those of the cross-validation hindcasts. At the bottom of the figure an area-averaged time series over the verification period for each AGCM configuration is also presented. The time series represent the observed

(grey), cross-validated (red) and retro-active (blue) area-averaged values. With the exception of a small number of cases (e.g. 1987/88 of the ECMWF SST spread) the cross-validated and retro-active forecasts are in strong agreement. This result has provided evidence that the retro-active procedure followed in this chapter may not have been negatively impacted by the initial small samples used to predict over the 24-year test period since it produced similar results to the cross-validation procedure.

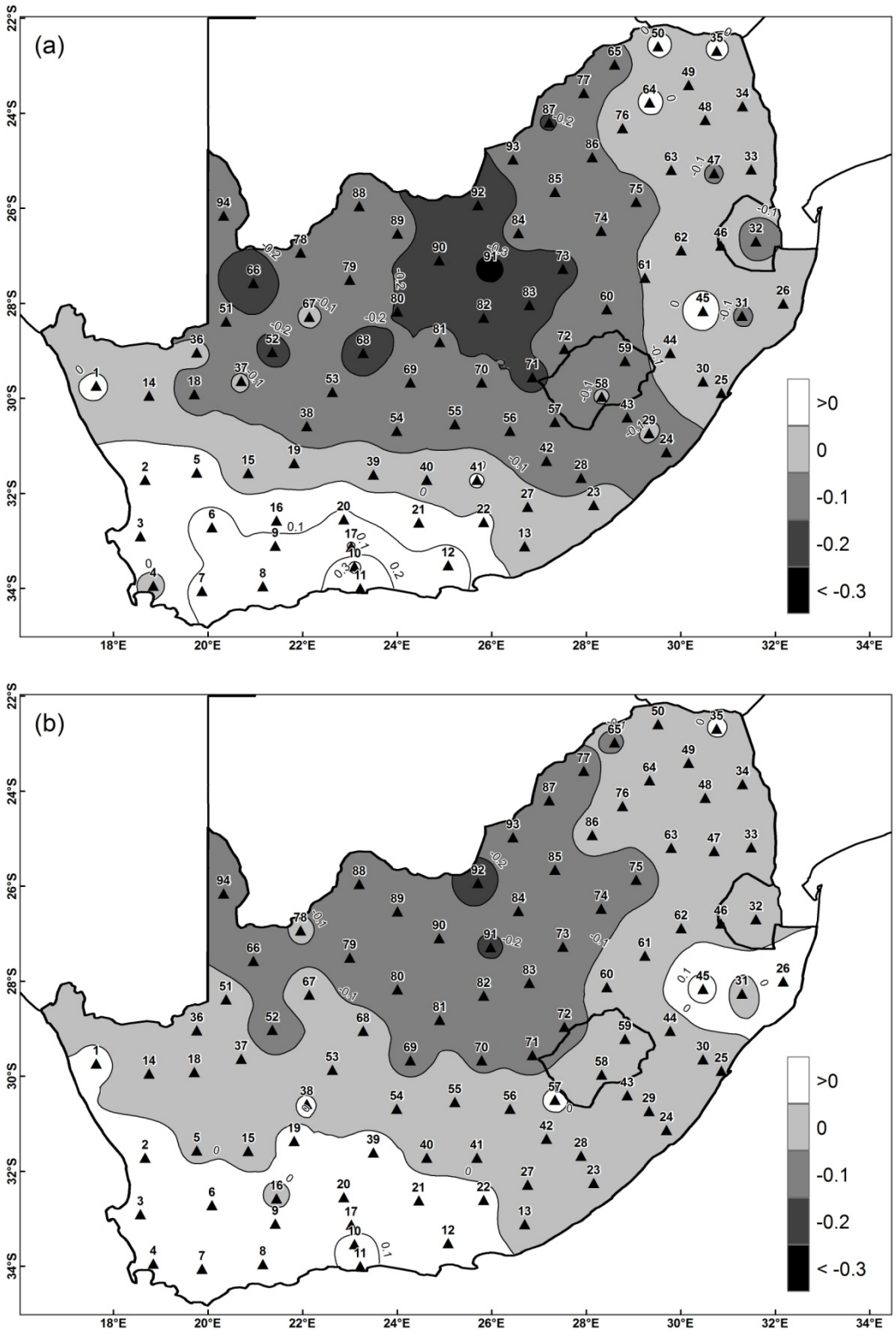

Figure 4.4: Kendall's tau correlation differences. Correlations are first calculated over 24-years between retro-active forecasts produced respectively by each of the AGCM forecast systems and the observed. Kendall's tau differences are shown per district between the a) AGCM forced with statistical SST and the AGCM forced with the ECMWF SST ensemble mean, and b) the difference per district between the AGCM forced with statistical SST and the AGCM forced with members of the ECMWF SST forecasts. Negative correlation differences show where the AGCM forced with ECMWF SST is superior.

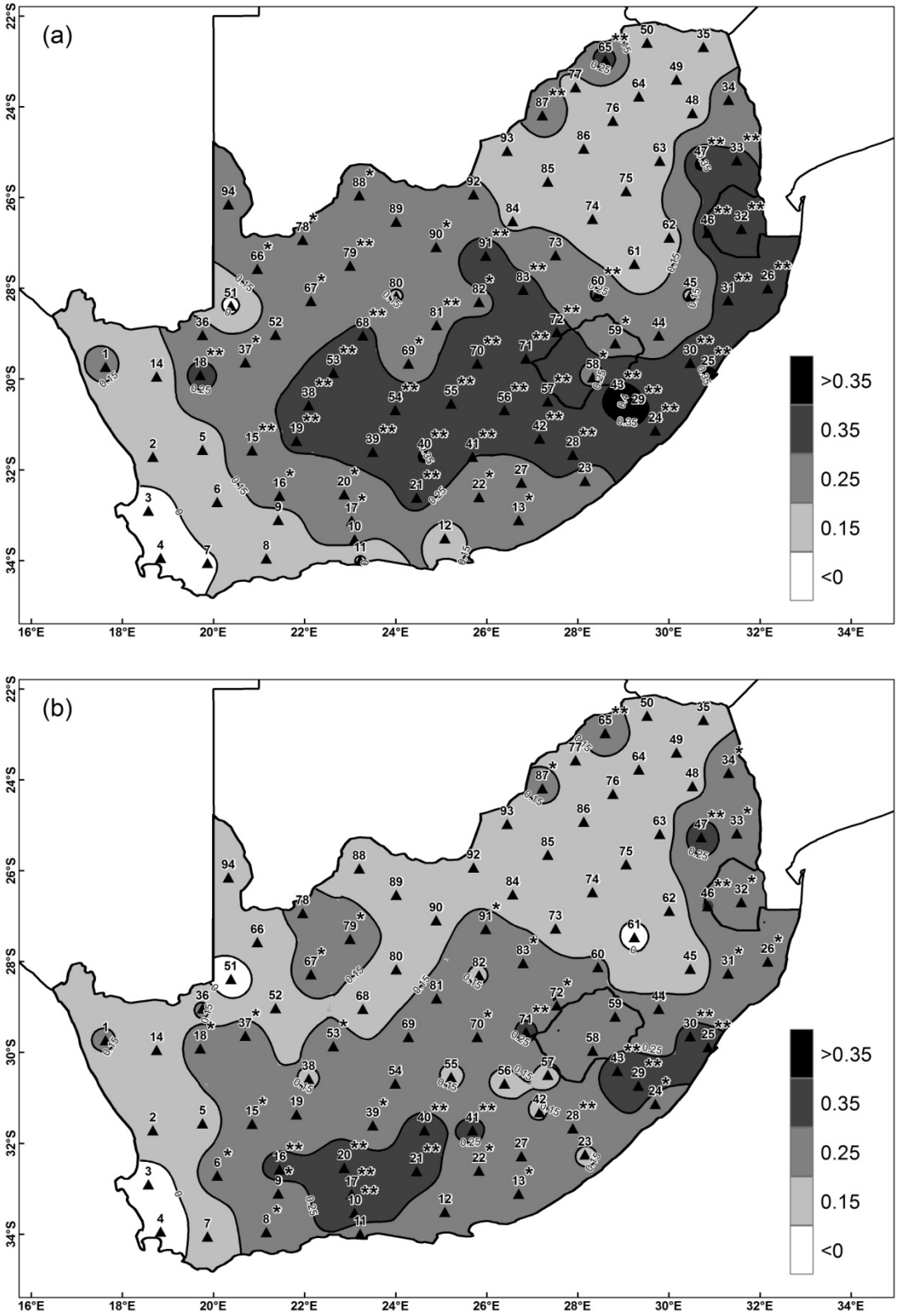

Figure 4.5: Kendall's tau correlations over 24 years between observed DJF rainfall indices and a) retro-active forecasts of the AGCM forced with the ECMWF SST ensemble mean, and b) retro-active forecasts of the AGCM forced with the ECMWF ensemble members. Correlations significant (1-tailed test) at the 90% level of confidence are marked with an asterisk and correlations significant at 95% with a double asterisk.

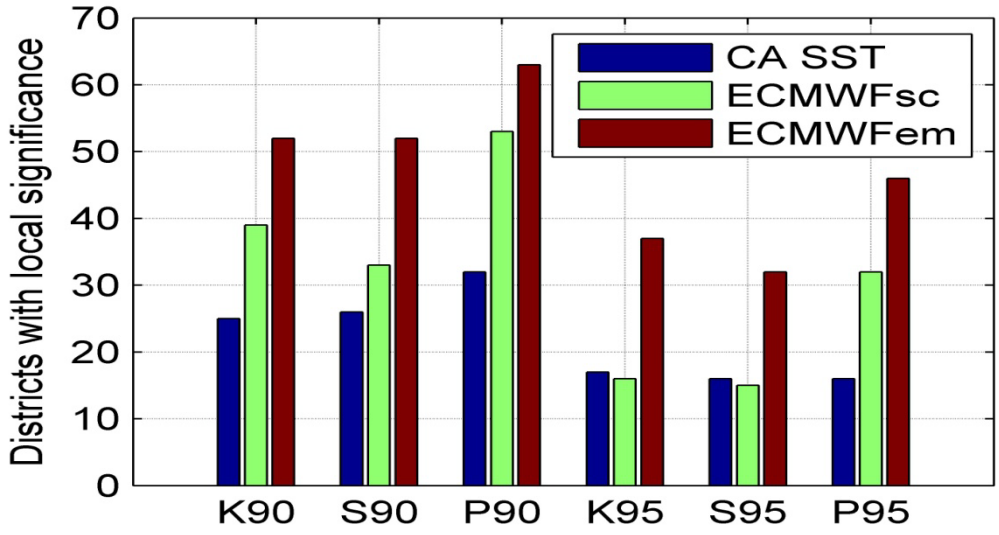

Figure 4.6: The number of districts with significant (1-tailed test) correlations. “K” refers to Kendall’s tau, “S” to Spearman rank and “P” to Pearson correlation. “90” and “95” respectively refer to the 90% and 95% levels of confidence. “CA SST” refers to the AGCM forced with constructed analogue SST; “ECMWFsc” refers to the AGCM forced with the ECMWF ensemble spread, and “ECMWFem” to the AGCM forced with the ECMWF ensemble mean SST forecasts.

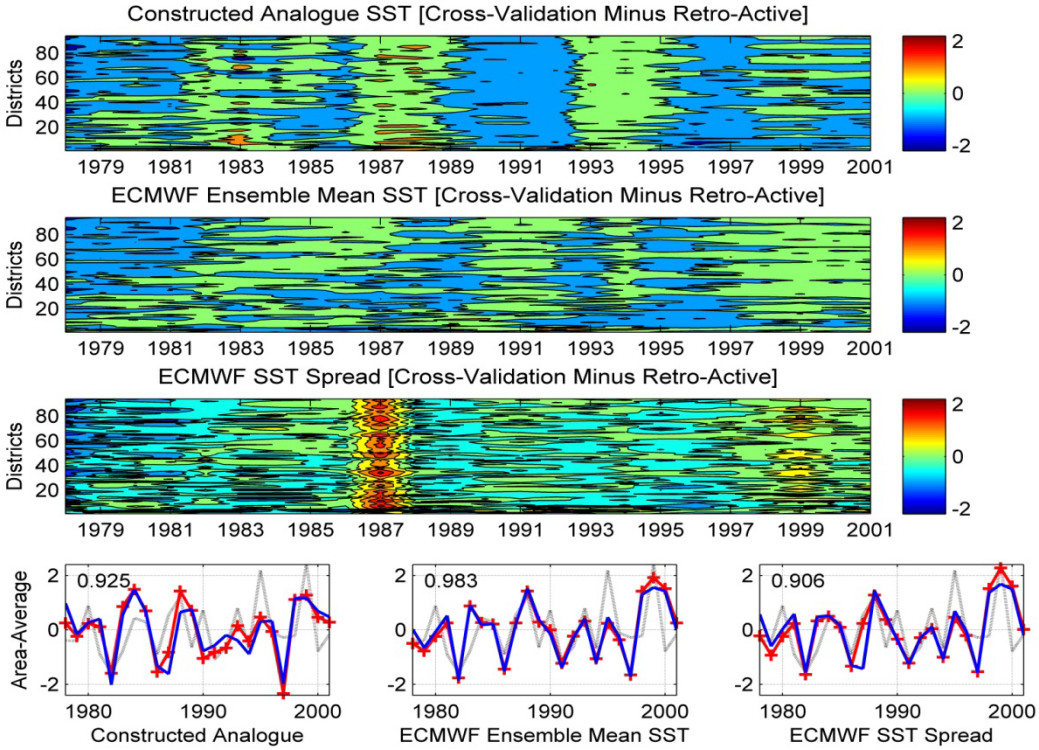

Figure 4.7: The top three panels show DJF rainfall index differences between cross-validated hindcasts and retro-active forecasts produced by first downscaling the three AGCM systems to rainfall

districts. The bottom graphs are area-averaged values of cross-validation (red), retro-active (blue) and observed (grey) values for each of the AGCM systems.

4.4 Discussion and conclusions

Coupled models represent the state-of-the-art in seasonal climate forecasting. However, given perfect SST to force an AGCM, i.e. in an AMIP-like integration (Gates, 1992), AMIP runs have been shown to perform as well as a coupled model that uses the same AGCM when simulating South African seasonal rainfall totals (Landman et al., 2012). Thus, AGCMs may perform at least as well as fully coupled models over South Africa when skilful SST forecasts are used to force the AGCM. Since AGCMs do not require the same amount of computing resources required by coupled models, higher resolution, larger ensembles and longer lead-time forecasts can be produced by an AGCM. Moreover, the generation of hindcasts (re-forecasts) to assess model performance and to calibrate model output are more easily achieved with an AGCM (Troccoli et al., 2008). Although coupled modelling on seasonal time scales has recently been launched in South Africa (Beraki et al., 2014) the use of AGCMs in this country may thus continue for quite a few years to come.

Modellers need to consider options on how to describe the lower boundary forcing, and in this case SST, in an effort to optimise AGCM-based systems for operational forecast production. In this chapter three different strategies to predict the forcing SST were investigated and the results have shown that AGCMs skill is strongly influenced by the choice of SST prediction strategy. Although it has been suggested that the best practice may be to utilize different sources of SST predictions which may be weighted according to region and season in a multi-model ensemble approach (Li et al., 2008), the results presented here show that the best AGCM forecast for South African mid-summer rainfall is from a single best SST forecast field (the ensemble mean is a more skilful representation than each of the individual members).

The verification results of the three downscaled 24-year probabilistic forecast sets show that none of the three SST forecast methodologies lead to AGCM skill levels over South Africa that are so low for a particular forecast system to be completely discarded. In fact, ROC scores for all three cases are above 0.5 for both the usual 3-

category terciles case as well as for seasonal extremes (15th and 85th percentile thresholds of the climatological rainfall record, respectively). Moreover, all three AGCM modelling strategies are associated with reliable above-normal forecasts. However, the best modelling strategy (improved discrimination as well as reliability) is found when using SST forecasts from a coupled model to force the AGCM, and in particular when using the ensemble mean SST forecasts as opposed to using the ensemble spread, i.e. the uncertainties involved with the predicted SST fields. Regarding the SST statistical forecast model, it should be noted that the lower rainfall forecast skill associated with the statistically predicted SSTs could be a result of the SST forecast method used and choice of testing region (South Africa) and not that statistical SST forecasts are of poor quality. In fact, there has been a number of studies presented on successful statistical prediction models for ENSO (e.g. Barnston and Ropelewski, 1992, Tangang et al., 1998) and for the larger part of the tropics and mid-latitude oceans (Landman and Mason, 2001). An appropriate selection of an SST prediction methodology has been shown to be important in order to ensure that seasonal rainfall predictions from AGCMs provide the best forecast guidance. Such a selection could include statistical model forecasts, coupled model forecasts as well as combining these forecasts through multi-model ensemble methodologies.

Only verification results for the outer two categories were presented since there is usually little skill to be derived from predicting the near-normal category (Van den Dool and Toth, 1991). The same has been found here even with a near-normal category that comprises of more than half of the climatological data. The notion of low predictability of the middle category is also being supported by earlier verification work on South African seasonal rainfall predictions (Landman and Beraki, 2012, Landman et al., 2012). Owing to this low predictability of forecasts for “average rainfall conditions” for a coming season to occur, forecast producers in South Africa may want to reconsider issuing such forecasts to forecast users. This notion of excluding forecasts for the near-normal category is already being practiced by SAWS who acts as the official disseminator of seasonal forecasts in South Africa.

The results presented here may be case specific, and so this modelling study may need to be expanded to other rainfall seasons such as the austral autumn season that is also associated with useful forecast skill over South Africa (Landman et al., 2005) and for longer lead-times that will additionally add greater uncertainty in predicted SST anomalies. To this end seasonal forecast modellers in South Africa have started to produce multi-decadal hindcast sets as well as real-time operational forecasts of global SSTs, based on a statistical model that uses antecedent SST as predictors (Landman and Mason, 2001) and on recalibrated CGCM forecasts by following the methodology presented by Tippet et al., (2005) but for the global oceans. These SST forecast sets are available on the same 1°x1° resolution as the Optimum Interpolation v2 data (Reynolds and Smith, 1994) and are available from the Council for Scientific and Industrial Research. The hindcast set can be used to develop a set of retro-active AGCM hindcasts and for operational AGCM forecast production. Optimizing SST forecasts with sufficient lead-times is a very important endeavour in a country such as South Africa where computing infrastructure is sufficient to run AGCMs with fairly high-resolution, and also to produce multi-ensemble forecasts operationally in real-time, but where it still remains challenging to run coupled ocean-atmosphere models operationally and in real-time with the same resolution and ensemble size as the current AGCMs. Moreover, optimized AGCM configurations are important for the establishment of baseline skill levels against which current and future coupled models can be compared against.

Chapter 5

Simulating and predicting seasonal climate

5.1 Introduction

This Chapter deals with two aspects of seasonal forecast modelling when using an atmospheric general circulation model (AGCM). The first is to analyse simulations of the AGCM when forced at its lower boundary, through the specification of observed monthly sea-surface temperature (SST) and sea-ice fields. That is, the model's ability to simulate realistic atmospheric responses, to key modes of variability such as El Niño and La Niña events, may be investigated through such simulations. These simulations typically span over multi-decadal periods, and involve providing the atmospheric model with the observed state of the atmosphere only once, at the beginning of the simulation. Since the model is forced with observed (rather than predicted) SSTs, the skill of an atmospheric model in simulating inter-annual climate variability in AMIP runs is thought to provide an upper boundary of the model's seasonal forecasting skill. The second approach involves testing the AGCM when provided with predicted SST in order to determine how the model can be expected to perform under operational forecast conditions. Here we will focus on forecast skill of the AGCM to produce both deterministic and probabilistic forecast information for southern Africa.

5.2 The conformal-cubic atmospheric model (CCAM)

CCAM is a variable-resolution global atmospheric model, developed by the Commonwealth Scientific and Industrial Research Organisation (CSIRO) (McGregor, 1996, 2005a, 2005b; McGregor and Dix, 2001, 2008). It employs a semi-implicit semi-Lagrangian method to solve the hydrostatic primitive equations. The model includes a fairly comprehensive set of physical parameterizations. The GFDL parameterizations for long-wave and short-wave radiation are employed, with interactive cloud distributions determined by the liquid and ice-water scheme of Rotstayn (1997). A stability-dependent boundary layer scheme based on Monin Obukhov similarity theory is employed (McGregor et al., 1993), together with the

non-local treatment of Holtslag and Boville (1993). A canopy scheme is included, as described by Kowalczyk et al. (1994), having six layers for soil temperatures, six layers for soil moisture (solving Richard's equation) and three layers for snow. The cumulus convection scheme uses a mass-flux closure, as described by McGregor (2003), and includes downdrafts, entrainment and detrainment. CCAM may be applied at quasi-uniform resolution, or alternatively in stretched-grid mode to obtain high resolution over an area of interest. Figure 5.1 shows the quasi-uniform conformal-cubic grid, of C48 (about 200 km) resolution in the horizontal, which was employed to obtain the course-resolution simulations performed as part of this deliverable. In order to obtain the simulations (Gates, 1992), CCAM was forced at its lower boundary with observed monthly SST and sea-ice fields. The simulations span the period February 1979 to November 2005. An ensemble of simulations was obtained, using a lagged-average forecasting approach, with each ensemble member initialised during a different day of February 1978. The model was forced with the climatological average concentrations of CO_2, ozone and aerosols during the integrations – which is the conventional set-up when performing AMIP simulations.

5.3 Simulations using CCAM

The simulated (top panel) and observed (lower panel) average annual rainfall over southern and tropical Africa, for the period 1979-2004, are displayed in Figure 5.2. The observations were obtained from the Climatic Research Unit (CRU), in the form of the 0.5° resolution CRU TS3.1 data set. The figure indicates that many of the key synoptic-scale features of African rainfall are well represented in the CCAM simulations. These include the west-east gradient in rainfall over South Africa, the west-east slot of relatively dry conditions that extend from Botswana into Zimbabwe, and the relatively high rainfall totals of tropical Africa and northern Mozambique. The model overestimates rainfall totals to some extent, most noticeably over the eastern escarpment areas of South Africa.

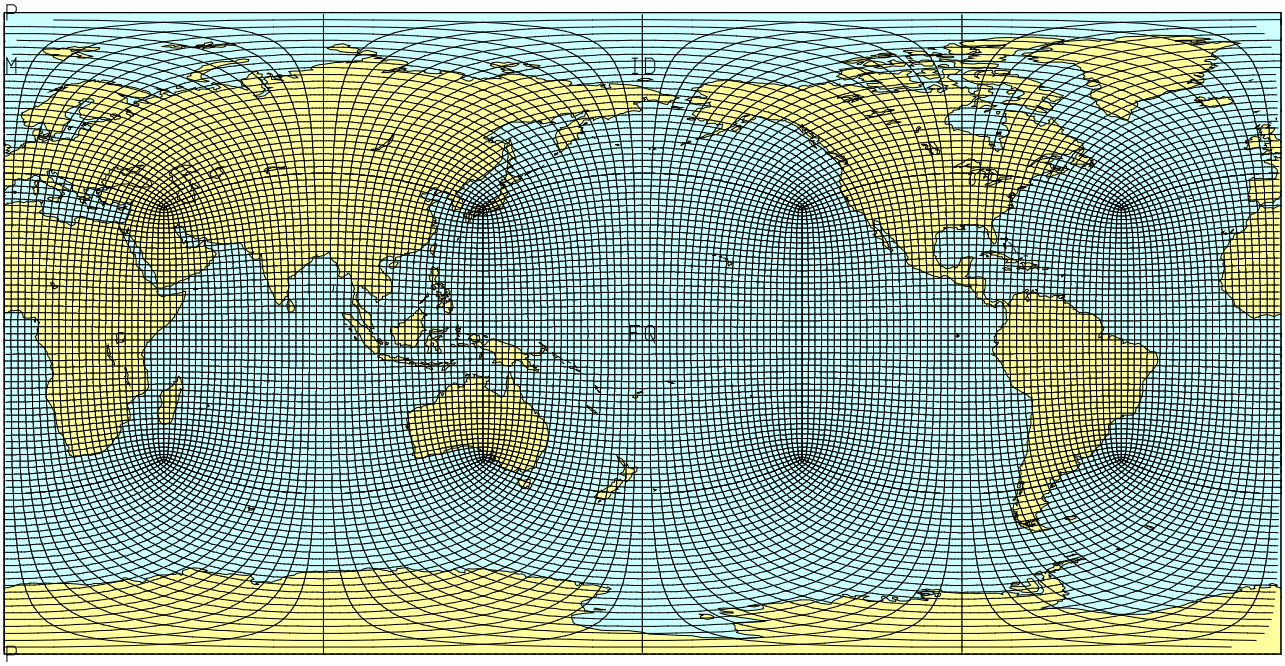

Figure 5.1: C48 quasi-uniform conformal-cubic grid, which provides a horizontal resolution of about 200 km globally.

The CCAM simulated seasonal rainfall totals, averaged over the period 1979-2004, are displayed in Figure 5.3, for winter (June-August, JJA – upper left panel), spring (September-October, SON – upper right panel), summer (December to February, DJF, lower left panel) and autumn (March-May, MAM, lower right panel). The corresponding observed fields, from the CRU climatology, are displayed in Figure 5.4. The seasonal cycle in rainfall over the African continent is well captured in the simulations. Winter is simulated to be dry over subtropical Africa, with the onset in rainfall simulated to occur in spring over the eastern parts of South Africa, in correspondence with observations. The southern displacement of the high rainfall band associated with the Inter-Tropical Convergence Zone (ITCZ), from winter to spring to summer, is clearly visible in the simulations, as well as the northward shift in the location of the ITCZ, from summer to autumn to winter. Despite the course resolution of the simulations, the model is capable of simulating the winter rainfall maximum over the southwestern Cape, although rainfall totals are drastically underestimated. Figure 5.5 provides an additional illustration of the simulations that have been obtained – the top panel shows the intra-annual cycle in rainfall as simulated over the east coast of South Africa (30 °E 30 °S), as well as the inter-annual rainfall variability .

An ensemble of 12 simulation coarse-resolution simulations have been obtained, using the variable-resolution atmospheric model CCAM at quasi-uniform resolution. The simulations have been shown to verify well against the observed synoptic-scale rainfall patterns, for both annual and seasonal rainfall totals. Of particular importance is the ability of the model to realistically simulate the west-east gradient in rainfall over South Africa, the dry slot extending from Botswana to Zimbabwe, and the relatively high rainfall totals over tropical Africa and northern Mozambique. The model also simulates the seasonal cycle of rainfall over tropical and southern Africa, including the meridional displacement of the ITCZ, and the onset of rainfall over eastern South Africa in spring, realistically. The model overestimates rainfall in general, and in particular over the eastern escarpment of South Africa. However, rainfall totals are drastically underestimated over the southwestern Cape, probably due to the southern Cape mountain ranges not being sufficiently resolved at the model's horizontal resolution of about 200 km.

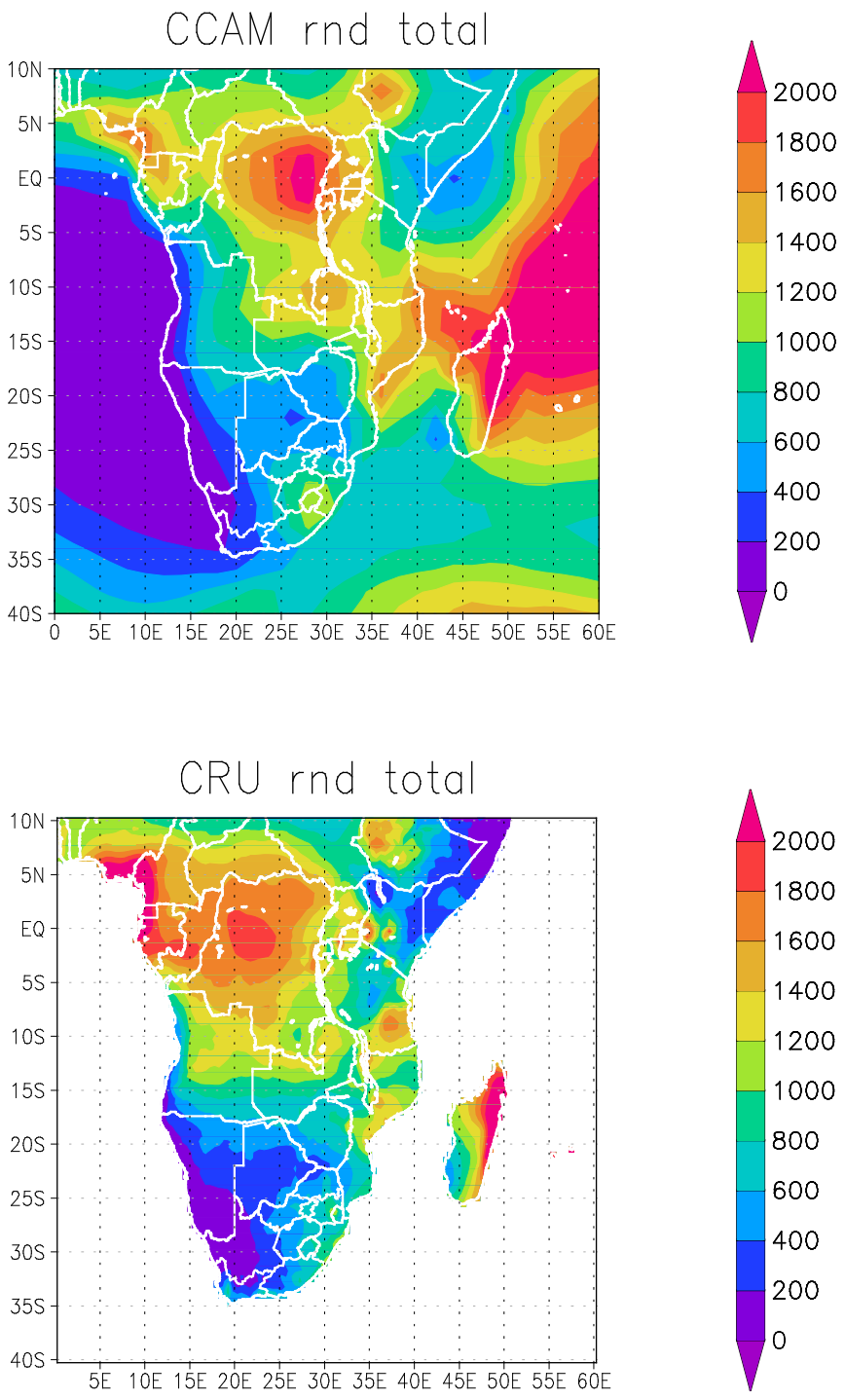

Figure 5.2: CCAM simulated (top panel) and CRU observed (lower panel) annual rainfall (mm) climatology over southern and tropical Africa (mm), for the period 1979-2004.

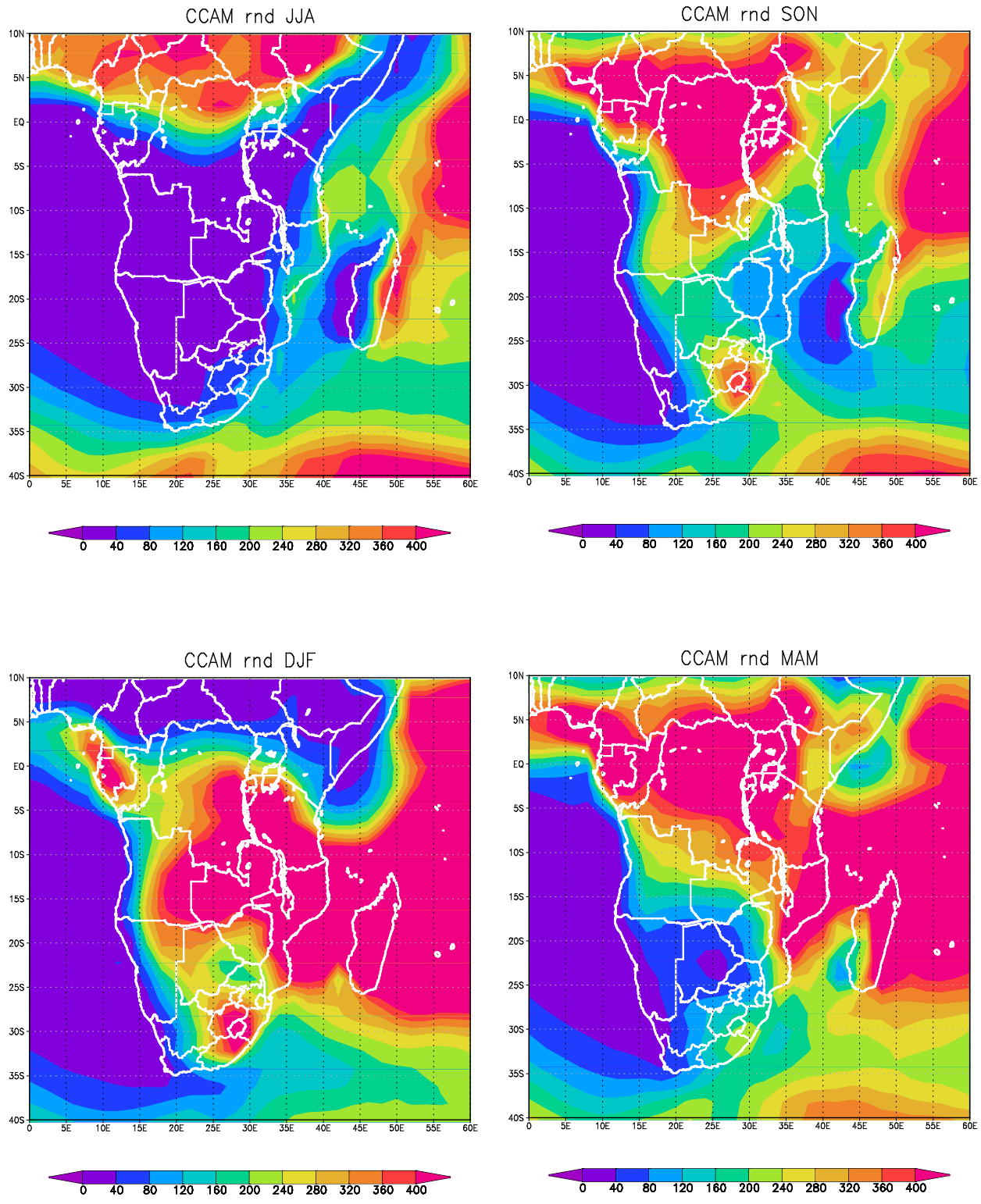

Figure 5.3: CCAM simulated seasonal rainfall (mm) climatology over southern and tropical Africa (mm), for the period 1979-2004.

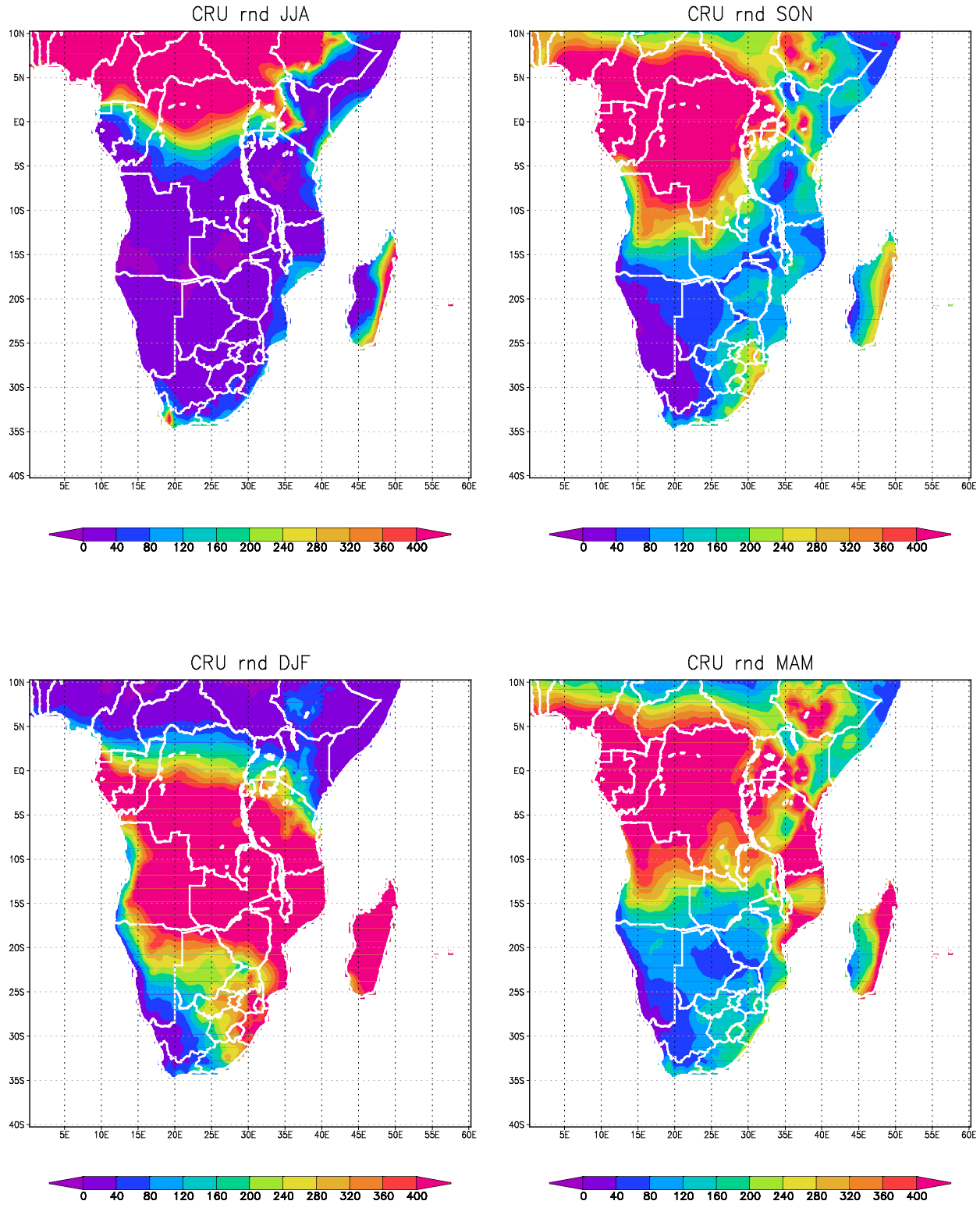

Figure 5.4: CRU observed seasonal rainfall (mm) climatology over southern and tropical Africa (mm), for the period 1979-2004.

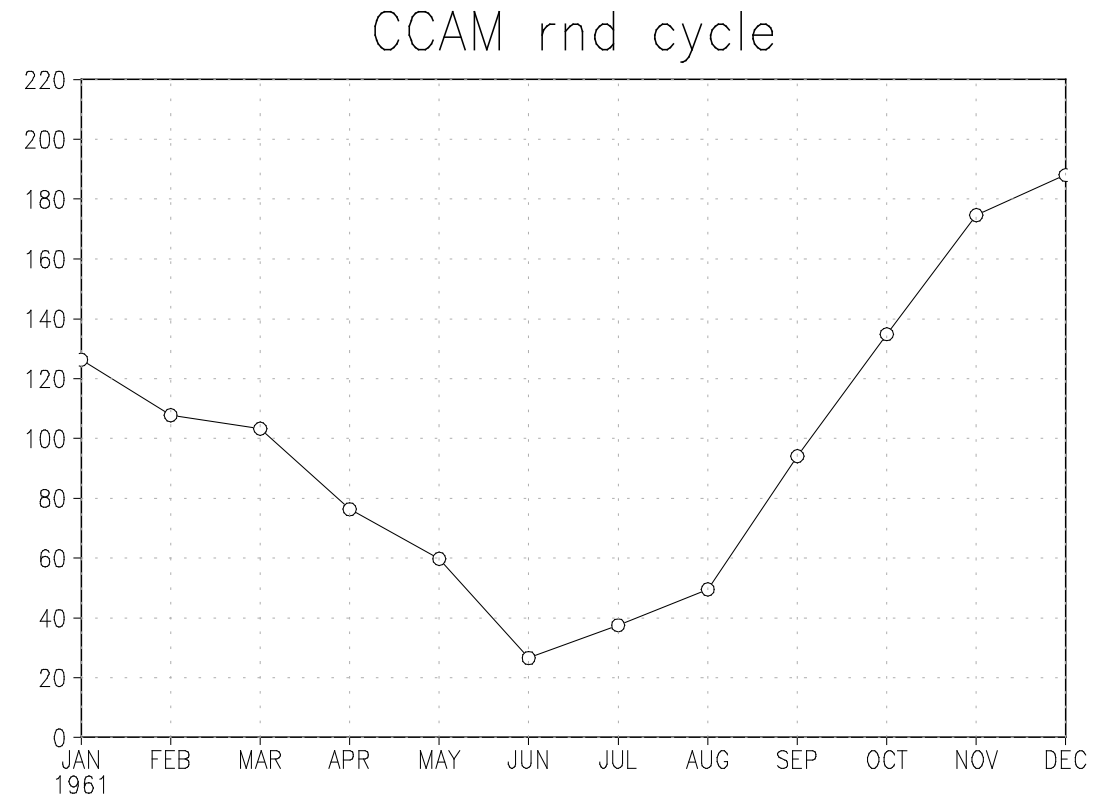

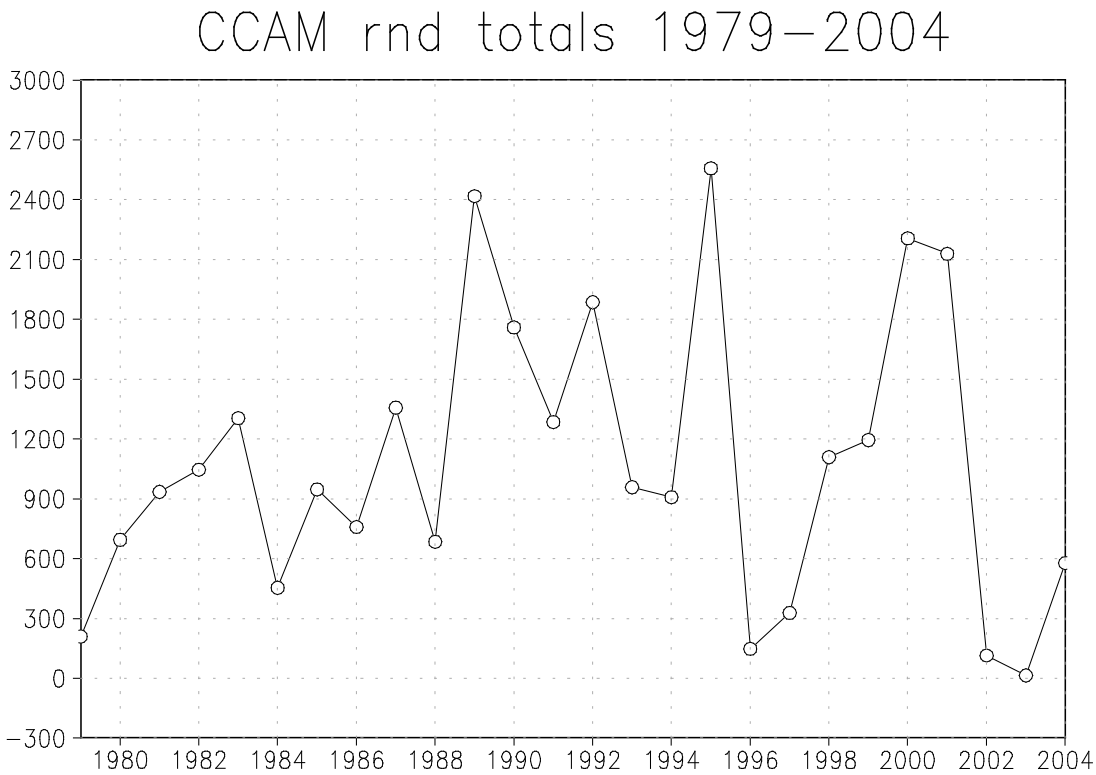

Figure 5.5: CCAM simulated annual cycle and inter-annual variability in rainfall (mm) over the east Coast of South Africa (30° E 30° S), for the period 1979-2004.

5.4 Verification of downscaled seasonal simulations

Next, the downscaling of these simulations from 200 km to the CRU resolution of 0.5°x0.5° resolution is performed, followed by the description of the verification of the downscaled simulations. The procedure to do the downscaling has been described in Chapter 4 and in the literature (Landman and Beraki, 2012; Landman et al., 2012). The verification data sets consist of 1) the CCAM large-scale fields simulated by providing the atmospheric model with perfect sea-surface temperatures as the boundary forcing and then linearly projecting the CCAM output to the respective variables of seasonal total rainfall and maximum temperatures and 2) the CRU data set (Mitchell and Jones, 2005).

Two of the main attributes of interest for probabilistic forecasts are discrimination (are the forecasts discernibly different given different outcomes?) and reliability (is the confidence communicated in the forecast appropriate?). The forecast verification measures presented here for testing of the aforementioned attributes are the relative operating characteristic (ROC) (e.g. Mason and Graham, 2002), and the reliability diagram (Hamill, 1997). A ROC graph can be constructed by plotting the forecast hit rates against the false-alarm rates. For good forecasts the hit rate will accumulate faster than the false-alarm rate resulting in a ROC graph that curves towards the upper left. For perfect discrimination the area beneath the curve would be 1.0, and for no skill the area beneath the curve would 0.5 (the ROC curve will coincide with the diagonal) or lower. ROC applied to probabilistic forecasts indicates whether the forecast probability was consistently higher, for example, when a flood or drought season occurred compared to when it did not occur. Although the ROC is a verification procedure recommended by the World Meteorological Organization, it has been criticized because the reliability of the forecast probabilities is ignored (Troccoli et al., 2008).

Forecasts are considered reliable if there is consistency between the predicted probabilities of the defined rainfall (or temperature) categories and the observed relative frequencies of the observed rainfall (or temperature) being assigned to these categories. The reliability diagrams presented below are used to assess if the CCAM

is able to produce well-calibrated probability forecasts and include reliability curves for the above- and below-normal categories along with their respective least-squares regression lines. The regression lines are calculated with weighting relative to how frequently forecasts are issued at a given confidence. Forecasts are considered perfectly reliable when these weighted regression lines lie perfectly along the diagonal of the reliability diagram, but when the regression lines lie above (below) the diagonal observed above- or below-normal values tends to occur more (less) frequently and then the forecasts are considered under-confident (over-confident). Frequency histograms are also included and show the frequencies with which forecasts occur in probability intervals of 10%. The ROC graph has an advantage over the reliability diagram in being less sensitive to sampling errors, and so can be more meaningfully constructed given the small sample sizes typical of seasonal forecasting (Troccoli et al., 2008). For the deterministic verification work a robust and resistant alternatives to the Pearson correlations, namely the Spearman rank correlation, is used. The Spearman correlation is simply the Pearson correlation, but using the ranks of the hindcasts and of the observations. Spearman (a non-parametric test) is better suited than Pearson for verification since the predictand most often has a non-Gaussian distribution. Here we have done the verification over a 16-year period from 1989 to 2004.

Figures 5.6 to 5.15 show the rainfall and maximum temperature verification results for the five run-on seasons of October-November-December (OND), November-December-January (NDJ), December-January-February (DJF), January-February-March (JFM) and February-March-April (FMA). The rainfall verification results are presented first.

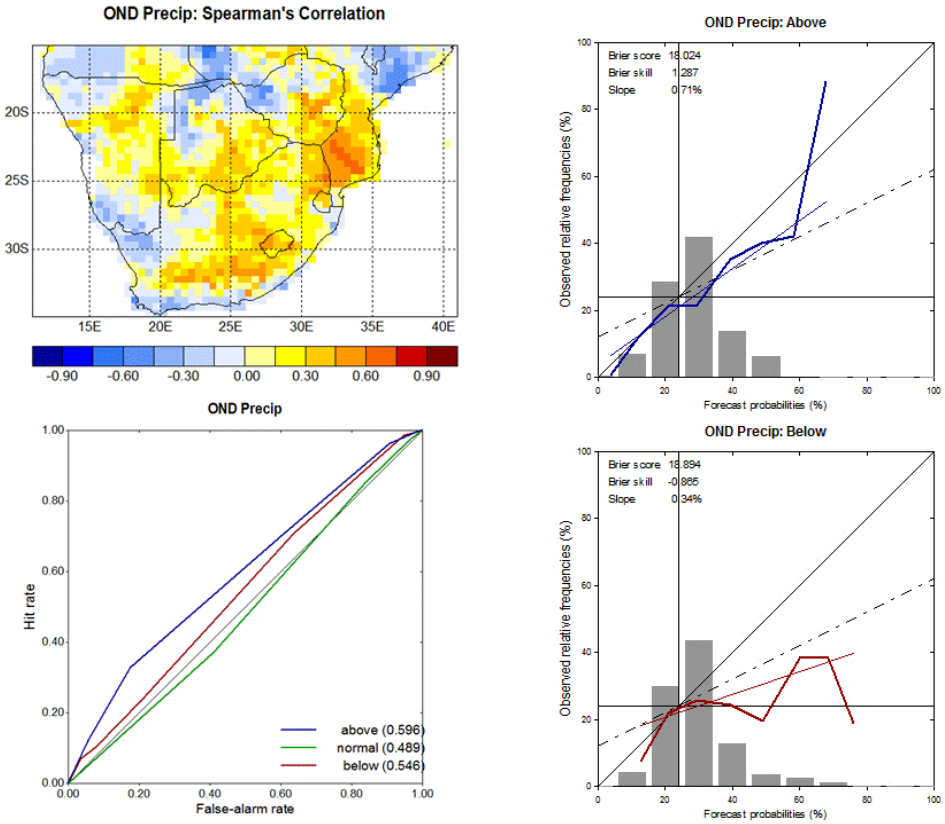

Figure 5.6: Verification results for OND rainfall. Top left is the Spearman's correlations, bottom left is the ROC graph, and on the right the reliability diagrams for respectively the above-normal and for below-normal categories (75th and 25th percentile thresholds).

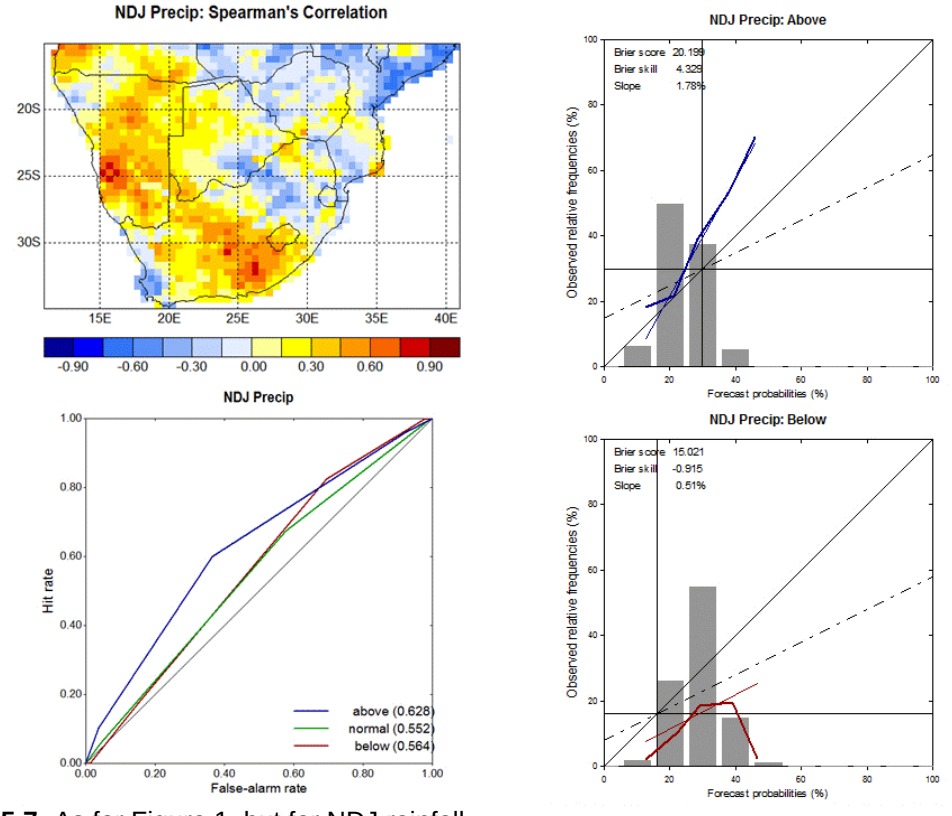

Figure 5.7: As for Figure 1, but for NDJ rainfall.

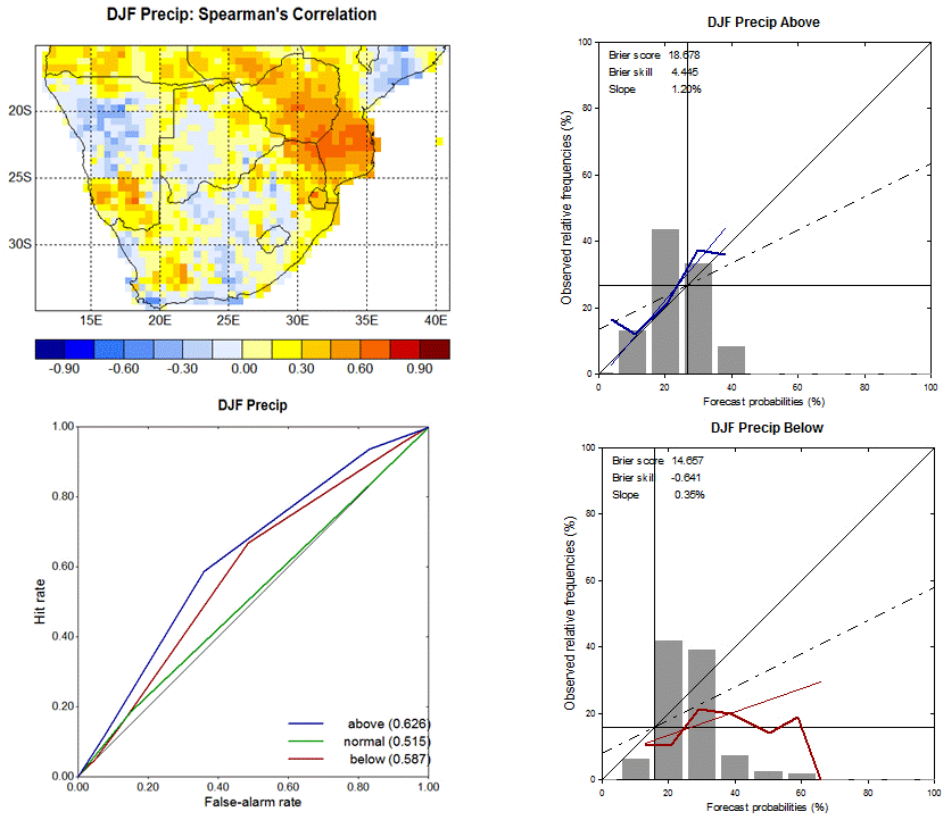

Figure 5.8: As for Figure 1, but for DJF rainfall.

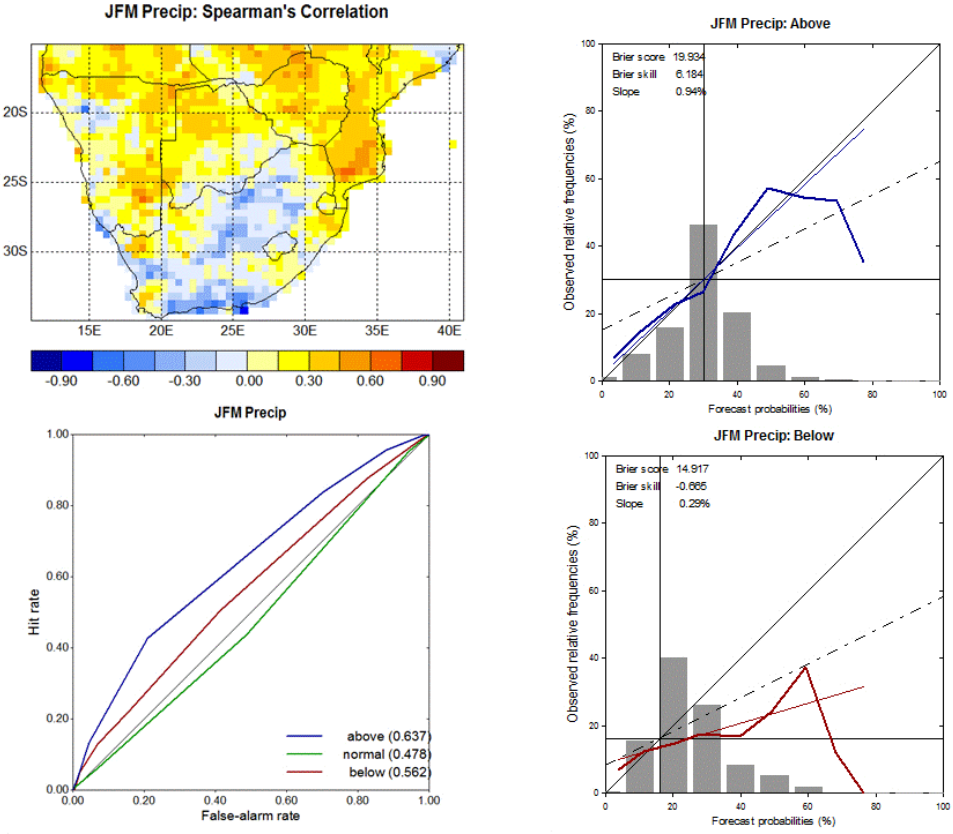

Figure 5.9: As for Figure 1, but for JFM rainfall.

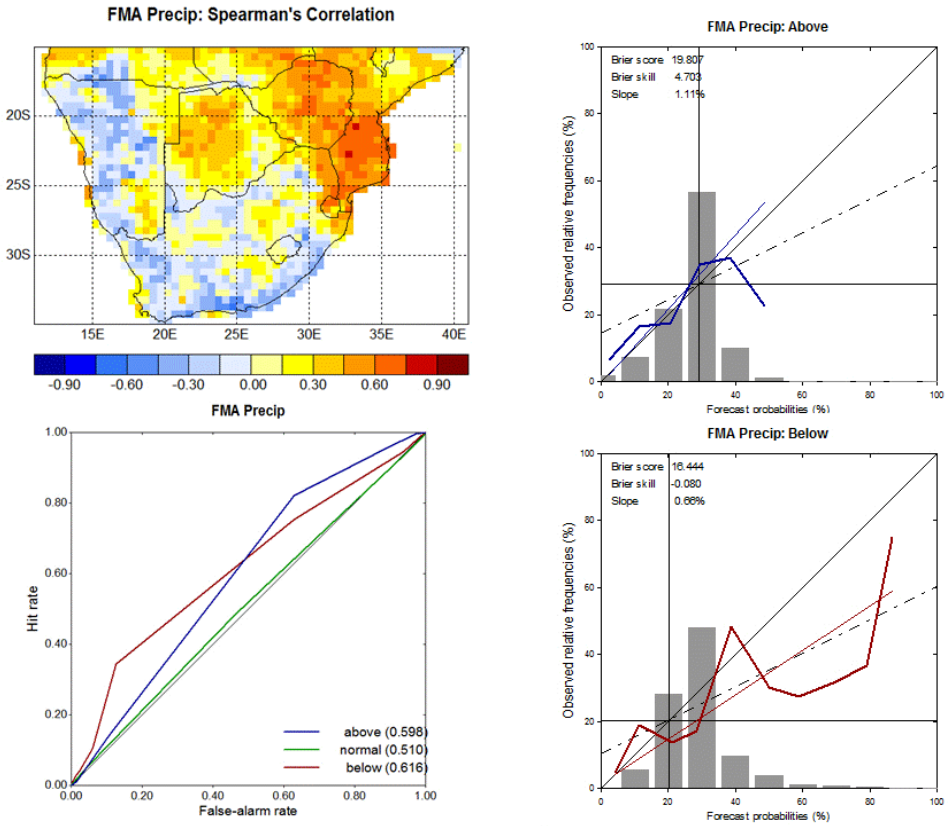

Figure 5.10: As for Figure 1, but for FMA rainfall.

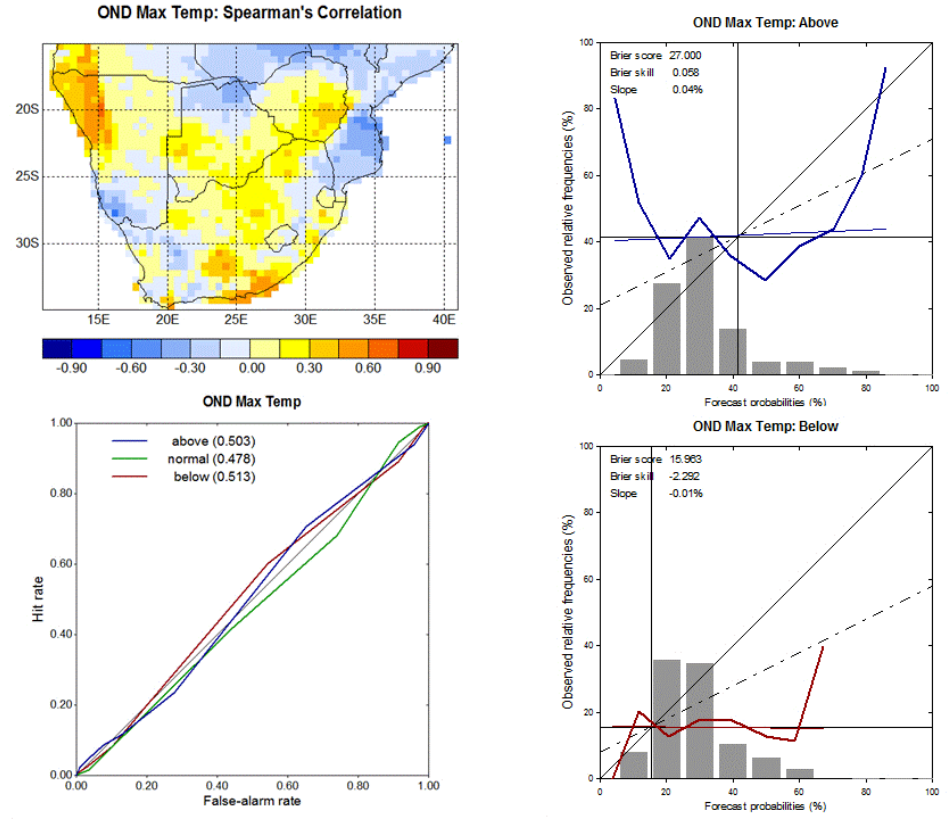

Figure 5.11: As for Figure 1, but for OND maximum temperatures.

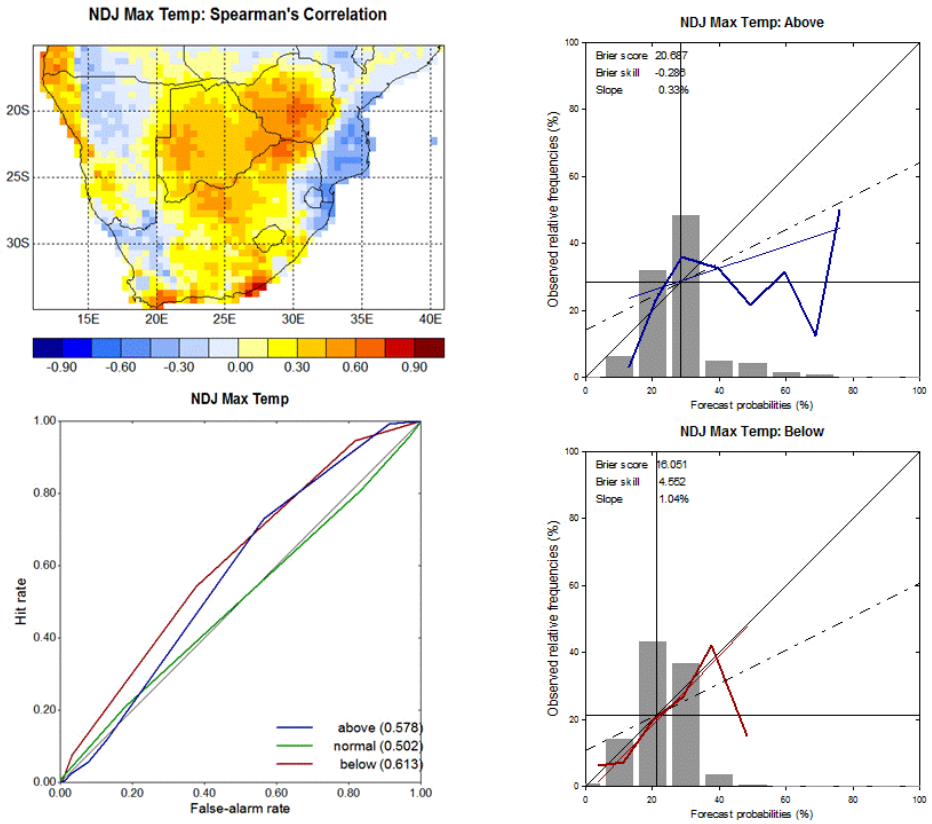

Figure 5.12: As for Figure 1, but for NDJ maximum temperatures.

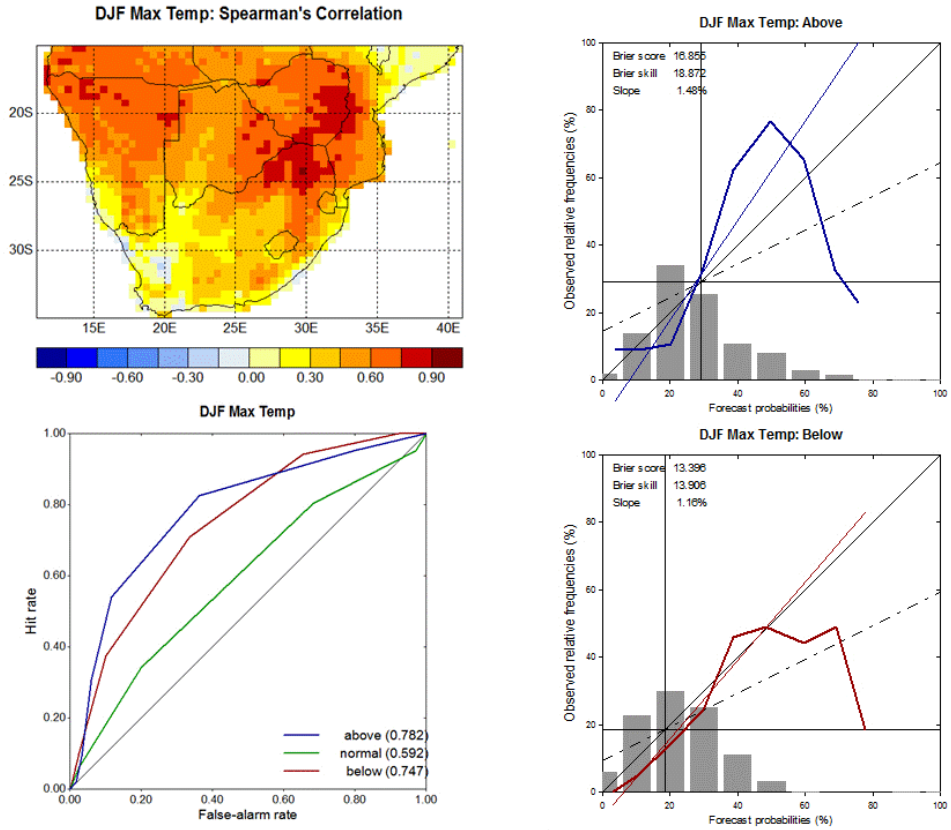

Figure 5.13: As for Figure 1, but for DJF maximum temperatures.

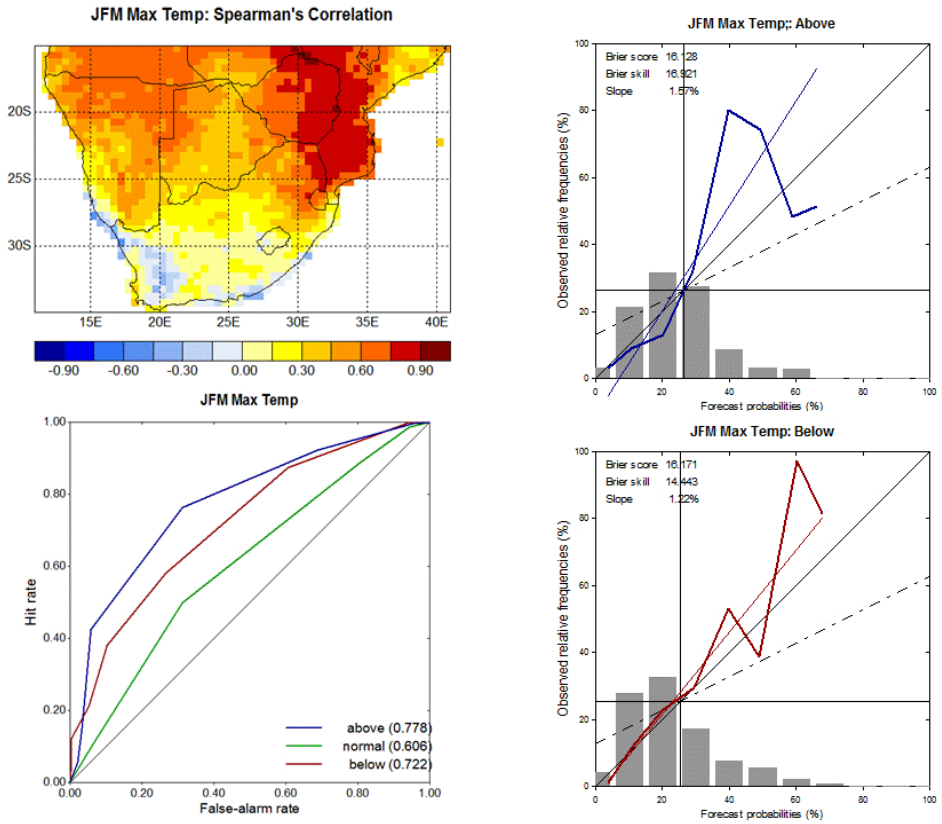

Figure 5.14: As for Figure 1, but for JFM maximum temperatures.

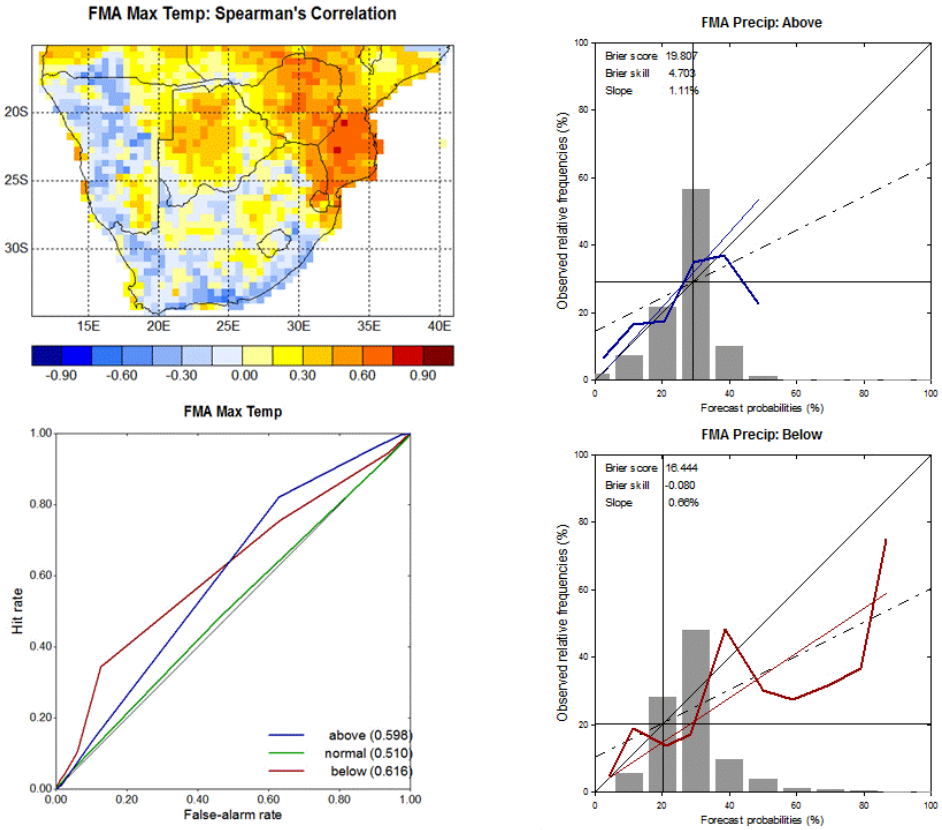

Figure 5.15: As for Figure 1, but for FMA maximum temperatures.

Further explanation and interpretation of the verification calculations can be found in the literature (Wilks, 2011; Jolliffe and Stephenson, 2012) and in Chapter 4. As a general conclusion, the CCAM has the ability to skilfully simulate seasonal rainfall and maximum temperatures, both deterministically (see Spearman's maps) and probabilistically (see ROC graphs and reliability plots). The following conclusions can be drawn from the verification statistics of the CCAM simulations presented above:

1. Seasonal forecast skill is a function of both location and time of the year – the north-eastern parts of South Africa and adjacent regions are often associated with the highest levels of skill for both rainfall and maximum temperatures.
2. Skill is generally the lowest during Spring, improves towards mid-summer and then declines towards Autumn.
3. Maximum temperatures are associated with higher levels of skill than rainfall totals.
4. Droughts are often simulated with over-confidence, while wet seasons are more likely to be simulated with high levels of reliability.
5. The near-normal category consistently has the lowest skill (van den Dool and Toth, 1991).

5.5 The operational CCAM forecast system

One of the main reasons why seasonal forecast modelling is being conducted is to test the CCAM's ability to simulate the dynamics and evolution of the ocean-atmosphere-land system. For this purpose the CCAM is forced with predicted global sea-surface temperature anomalies and started from a set of atmospheric initial conditions in order to provide an ensemble of operational forecasts up to 6 months ahead. CCAM seasonal forecasts are produced each month from an ensemble of 12 members, generated by using a 24-hour lagged average forecast method. The model is initialized from the 0Z analysis fields obtained from the Global Forecasting System (GFS) and is forced with SST anomalies predicted by the CSIR's multi-model system. Figure 5.16 shows a scheme that describes the model configuration.
The sea-surface temperature (SST) anomalies are predicted first up to 7 months ahead in order to enable the CCAM to predict the evolution of atmospheric states up

to 6 months ahead. The predicted SST anomalies are then given to the CCAM and together with the ensemble of atmospheric initial conditions, produce global forecasts of a range of meteorological variables such as rainfall, temperature and atmospheric circulation. The latter variable is used in the final stage of the configuration (Figure 5.16) to recalibrate or downscale to rainfall and temperatures over southern Africa. The SSTs have been re-forecast over a 28 year period as shown in Figure 5.17. A detailed description of the SST re-forecasts can be found in Beraki et al (2013). Global SST re-forecasts and operational forecasts are provided to the CCAM so that re-forecasts and real-time forecasts of the atmospheric model can respectively be produced.

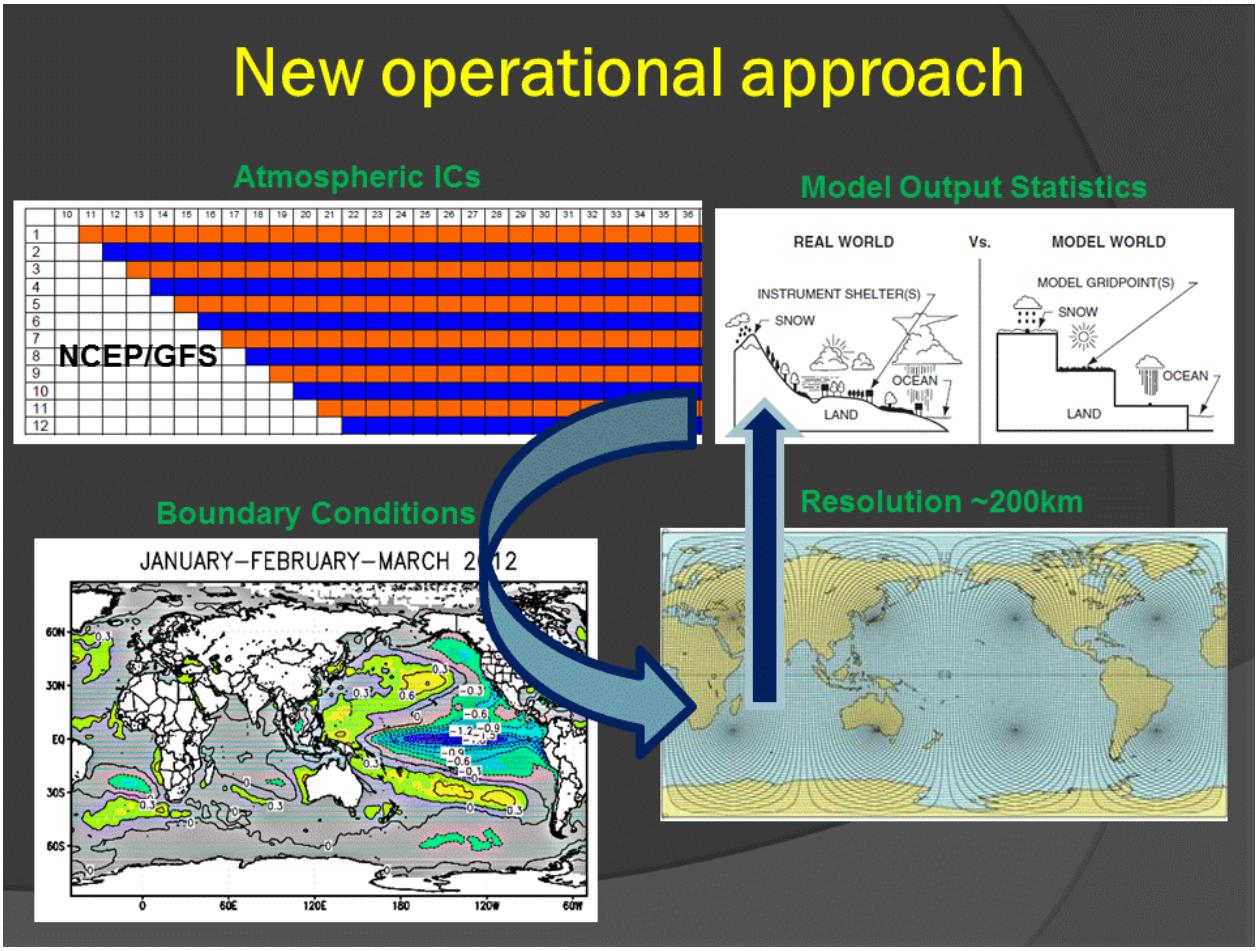

Figure 5.16: Schematic of the CCAM configuration for producing seasonal forecasts.

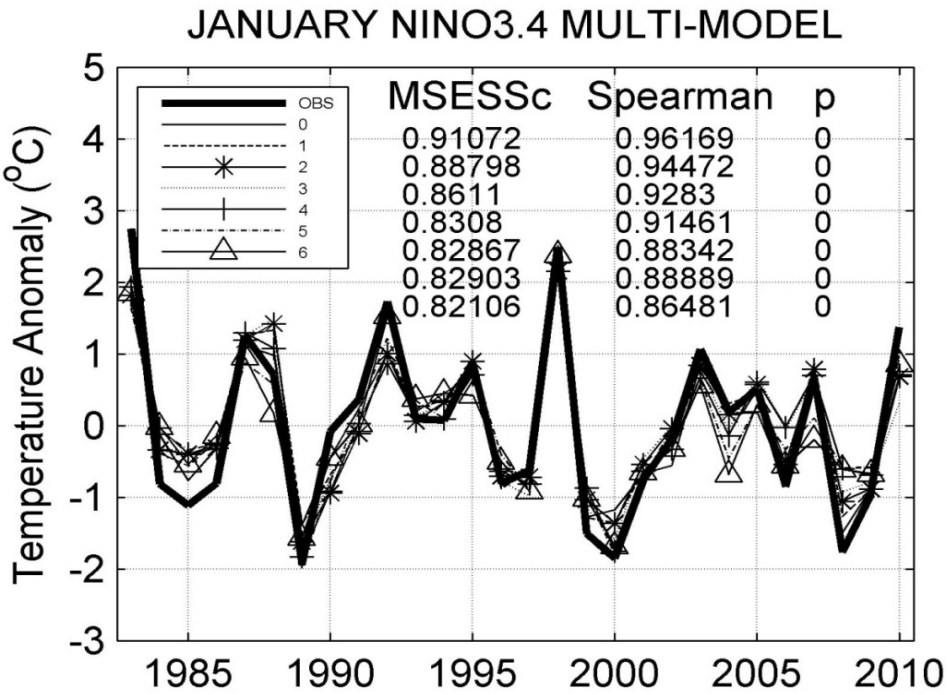

Figure 5.17: Observed (thick black line) and re-forecast (thin lines with various markings) January Niño3.4 SST. MSESSc is the mean squared error skill score for the various lead-times (0 to 6 months), with climatology the reference forecast. Spearman rank correlations and associated p-values are also shown.

Global forecasts are produced once a month by about the 13th. These forecasts are displayed on the website of the South African Risk and Vulnerability Atlas (SARVA). Raw forecast output is made available to the South African Weather Service for consideration and subsequent inclusion in their multi-model forecast system (Landman et al., 2009). Forecasts distributed each month include the anomaly fields for minimum and maximum temperatures, rainfall and 850 hPa geopotential heights. Figure 5.18 (a-d) shows forecast maps issued in February 2014.

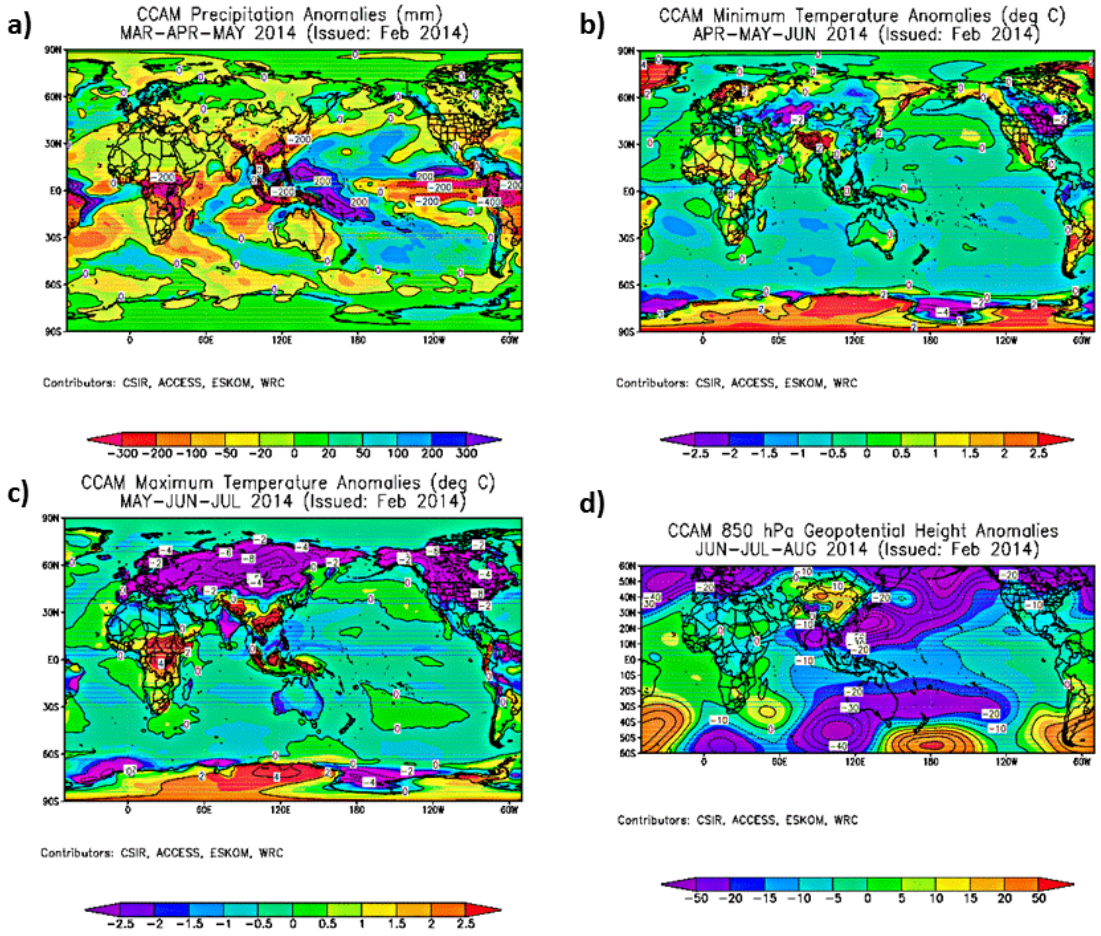

Figure 5.18: Examples of CCAM seasonal anomaly forecasts (ensemble mean) produced in February 2014**. a)** Rainfall forecast issued at a 1-month lead time **b)** minimum temperature forecast issued at a 2-month lead time**; c)** maximum temperature forecast issued at a 3-month lead time; **d)** 850 hPa geopotential height forecast issued at a 4-month lead time.

5.6 Verification of downscaled seasonal re-forecasts

The 3-month season on which the atmospheric forecast verification is focussed is from December to February (DJF) and re-forecasts are presented at a 1-month lead-time for 26 seasons from 1983/84 to 2008/09. From Figure 5.6 to 5.15 one can see that the season of highest predictability using this CCAM configuration is DJF. DJF as the most predictable season has also been found with other modelling studies (e.g. Landman et al., 2012). This notion was subsequently further explored in order to test the CCAM's operational forecast skill in producing 26-years of re-forecasts (1983/84 to 2008/09) through mimicking a real-time operational forecast set-up for seasonal climate. The same downscaling procedure described above for the CCAM simulations are followed here, but this time by training the downscaling model on CCAM re-forecasts and testing it over the 16-year period from 1993/94 to 2008/09.

Figure 5.19 show the verification results of downscaling the 850 hPa geopotential re-forecasts for DJF over 26 years. Here the CCAM was initialised in November in order to produce a 1-month forecast. By comparing this verification result with Figure 5.8, similar levels of skill are obtained by the re-forecasts, albeit lower: lower ROC scores and enhanced over-confidence with the prediction of anomalously wet DJF seasons. For both simulation and re-forecast skill the CCAM is over-confident in the prediction of anomalously dry seasons, a result also found with other studies (e.g. Landman et al., 2012).

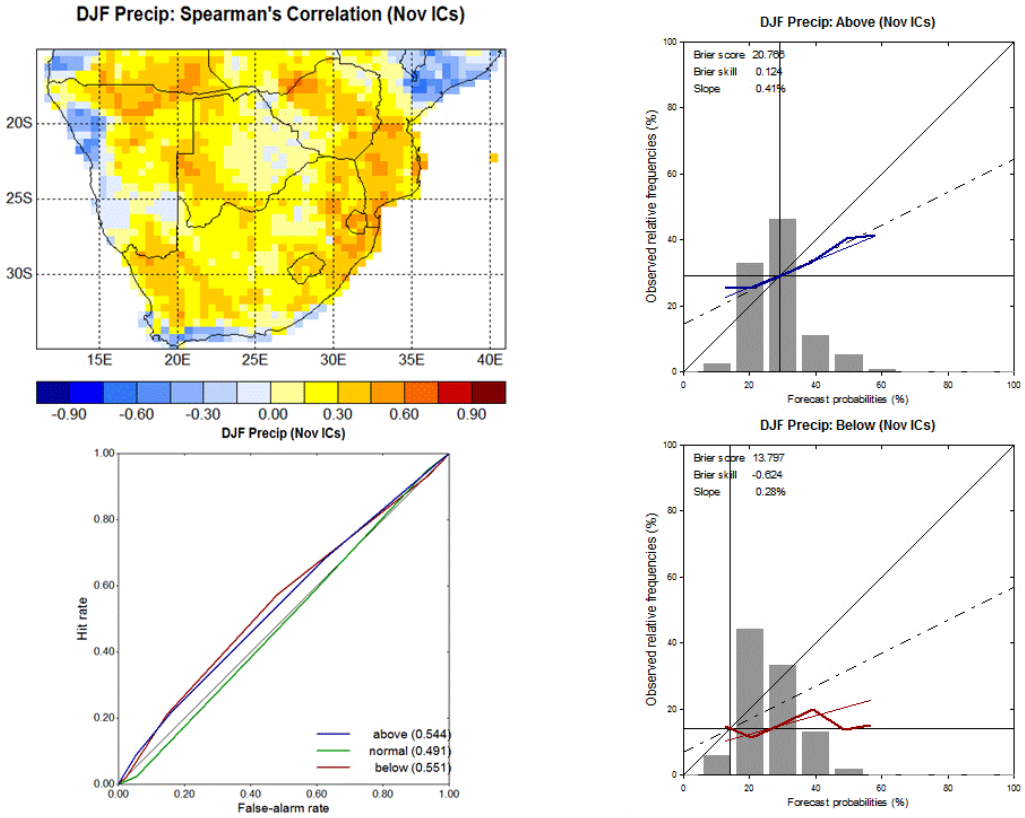

Figure 5.19: Verification results for DJF rainfall, retro-actively predicted at a 1-month lead-time. Top left is the Spearman's correlations, bottom left is the ROC graph, and on the right the reliability diagrams for respectively the above-normal and for below-normal categories (75th and 25th percentile thresholds).

The 1-month lead-time re-forecast skill estimates for maximum temperature during DJF are presented in Figure 5.20. Comparing maximum temperature re-forecast skill with simulation skill (Figure 5.13) show similar deterioration in skill as was found with DJF rainfall. In addition, the forecast and simulation performance of the CCAM system is higher for temperatures as compared to rainfall. The following conclusions can be drawn from the verification statistics of the CCAM re-forecasts presented above:

1. Similar skill levels between the simulations and the re-forecasts are found at the short lead-time of one month presented here – not much skill is lost as a result of forcing the CCAM with SSTs predicted over the model's integration period.

2. Higher skill levels are also found for maximum temperature predictions as opposed to those for rainfall predictions.

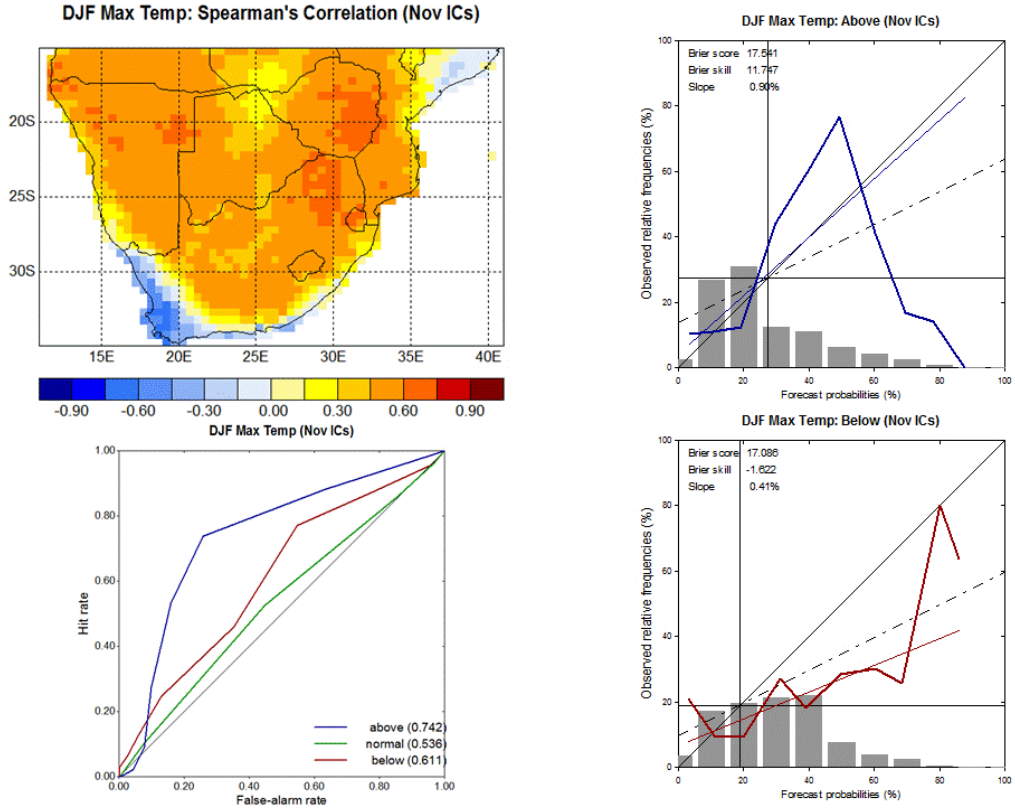

Figure 5.20: As for Figure 5.19, but for maximum temperatures.

5.7 Conclusions

The CCAM has already been used for a number of configurations and tested over southern Africa (Engelbrecht et al., 2011). In this Chapter the CCAM's configuration as operational seasonal forecasting system was described in some detail, including examples of operational forecasts and of verification statistics. This forecast system is being run operationally at the Council for Scientific and Industrial Research (CSIR) and the operational forecasts are provided each month to a select group of forecast users. Among these users are the South African Weather Service and ESKOM.

CCAM's configuration presented here for operational forecast production is designed in such a way that it captures the uncertainties in the atmospheric initial conditions through lagged average forecasting, and is forced with skilful predictions of SST seven months into the future. Such a forecast system is similar to what is in use at some international centres and therefore is a good representation of state-of-the-art seasonal forecast modelling when using atmospheric general circulation models.

Verification statistics show that the CCAM as seasonal forecast model has skill, but that the skill is restricted to certain areas and to certain times of the year. For example, the area inclusive of the north-eastern parts of South Africa, southern Mozambique, the larger part of Zimbabwe and southern Zambia seem to be associated with the highest skill for both rainfall and maximum temperatures, and that the best skill may also be largely restricted to the mid-summer season of DJF. These findings are similar to what has been with other modelling systems (e.g. Landman et al., 2012).

Chapter 6

Products: Displays and tailor-made output

6.1 Display systems for weather and seasonal forecasts

Various forecast products have been developed during this project. The products are representing the modelling performed over a range of forecast time scales associated with weather prediction through seasonal climate forecasts. All of the products are based on the output of the conformal-cubic atmospheric model (CCAM) which is the atmospheric model being used through the project.

Figures 6.1 and 6.2 show examples of the weather forecasts produced by the CCAM at about a 15 km resolution. Figure 6.1 shows the total rainfall forecast (accumulated over 24 hours from 2 am) for the next four days and the predicted maximum temperatures in degrees Celsius. In Figure 6.2 the predicted sea-level pressure together with the 500 hPa geopotential height fields show the positioning and intensity of tropical cyclones that may enter or develop in the Mozambique Channel. The figure also shows 7-day forecasts for selected cities – it shows minimum and maximum temperatures, accumulated rainfall and wind speeds in knots.

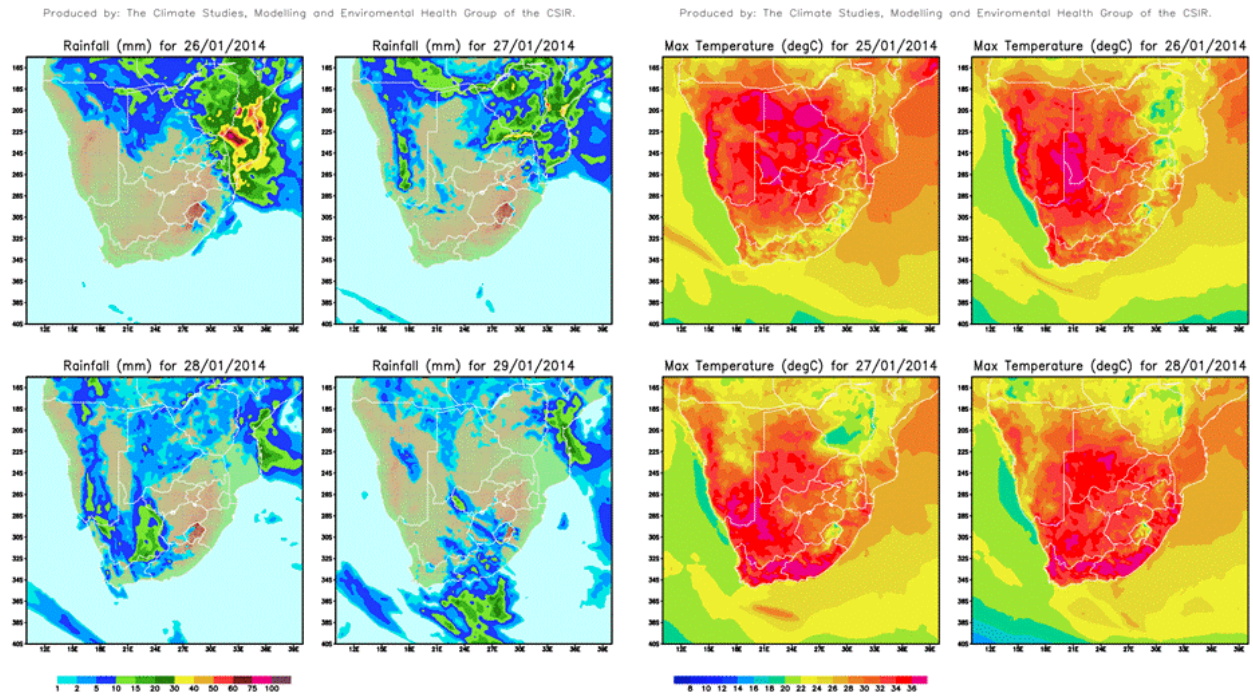

Figure 6.1: CCAM rainfall (accumulated over 24 hours; left panel) and maximum temperatures (°Celcius; right panel) 4-day forecasts. The rainfall forecasts are from initializing the CCAM on the

morning of the 26th of January 2014, while the maximum temperatures are from the 25th of January initialisation.

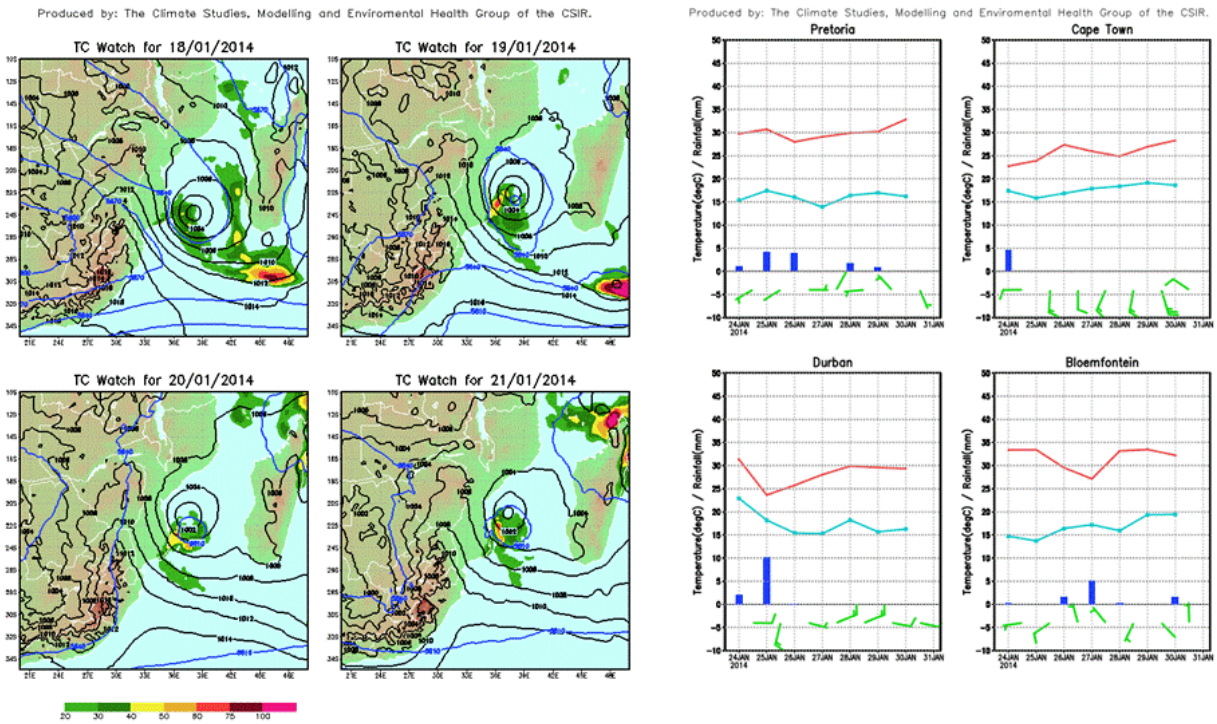

Figure 6.2: Sea-level pressure and 500 hPa geopotential heights predicted 4 days ahead in order to show where and when tropical cyclones may develop in the Mozambique Channel (left panel) and city-specific forecasts 7 days ahead. The latter show minimum and maximum temperatures, accumulated rainfall and surface winds in knots.

For the seasonal forecast part global forecasts are produced at a resolution of about 200 km. Figures 6.3 to 6.6 show predicted anomaly maps of the newly configured CCAM seasonal forecast system. The seasonal forecasts, presented as anomalies in the figures, are produced from an ensemble of 12 members, generated by using a 24-hour lagged average forecast method. The model is initialized from the 0Z analysis fields obtained from the Global Forecasting System (GFS) and is forced with SST anomalies predicted by the CSIR's multi-model system. Ensemble mean fields are shown here.

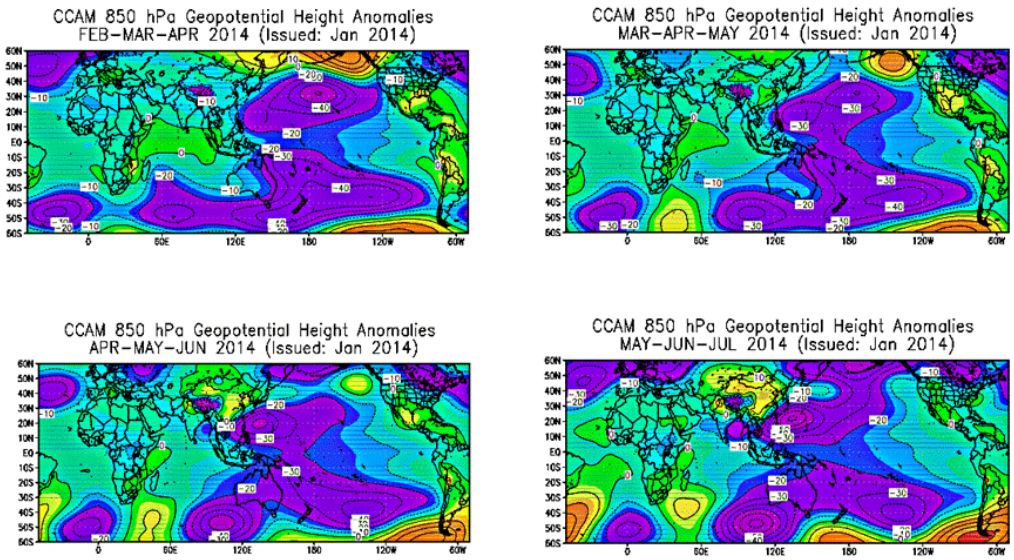

Figure 6.3: Seasonal forecast produced in January 2014 for the 850 hPa geopotential height field. Ensemble mean anomalies are presented.

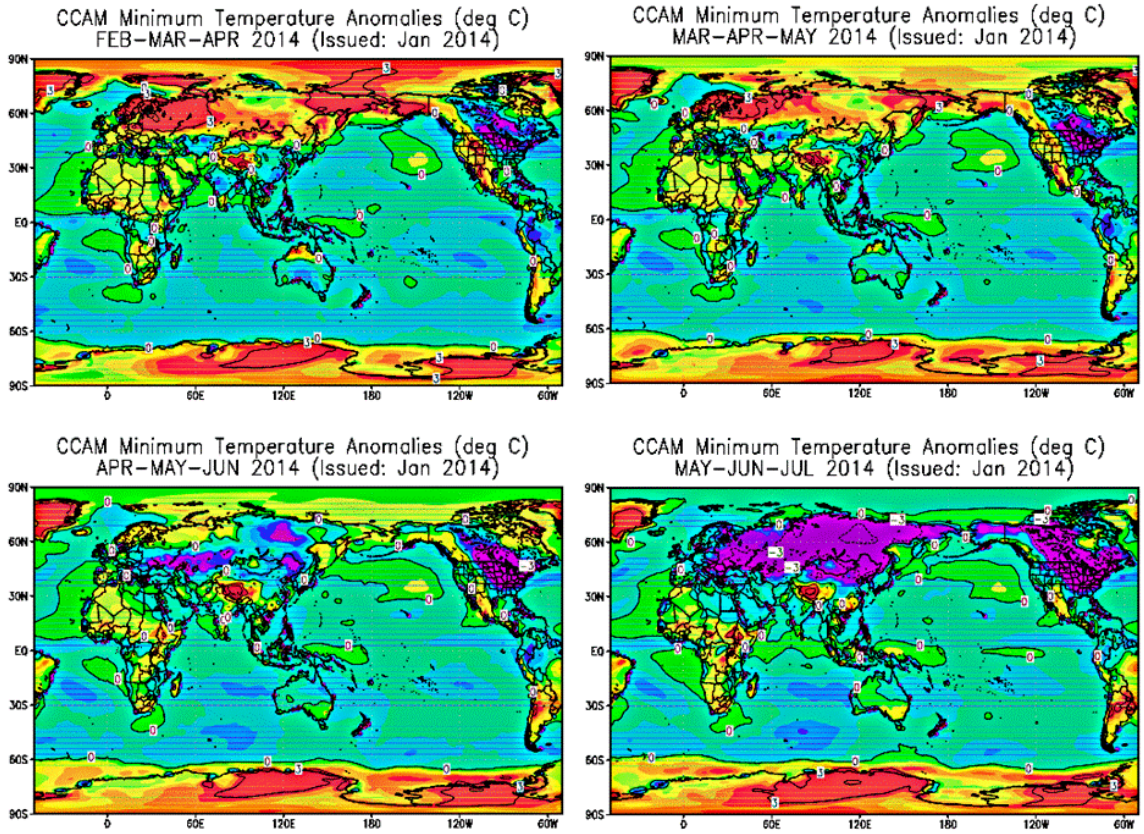

Figure 6.4: As in Figure 6.3, but for minimum temperatures.

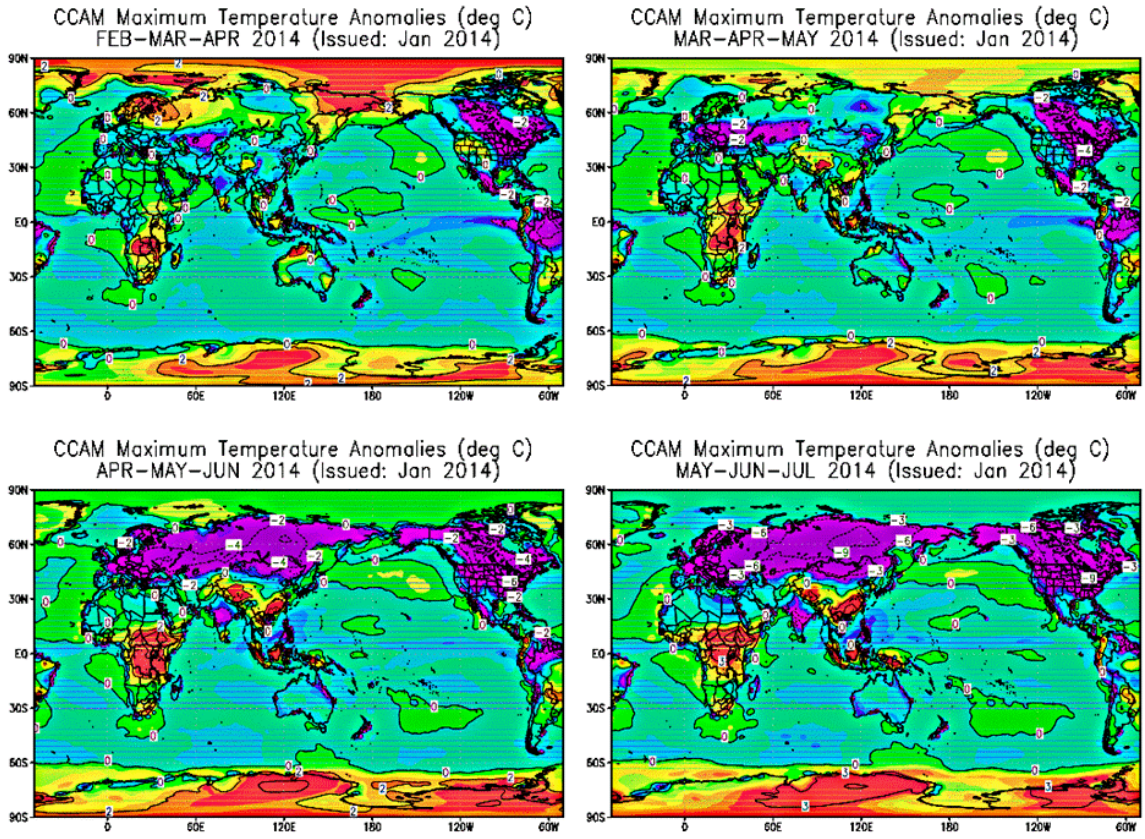

Figure 6.5: As in Figure 6.3, but for maximum temperatures.

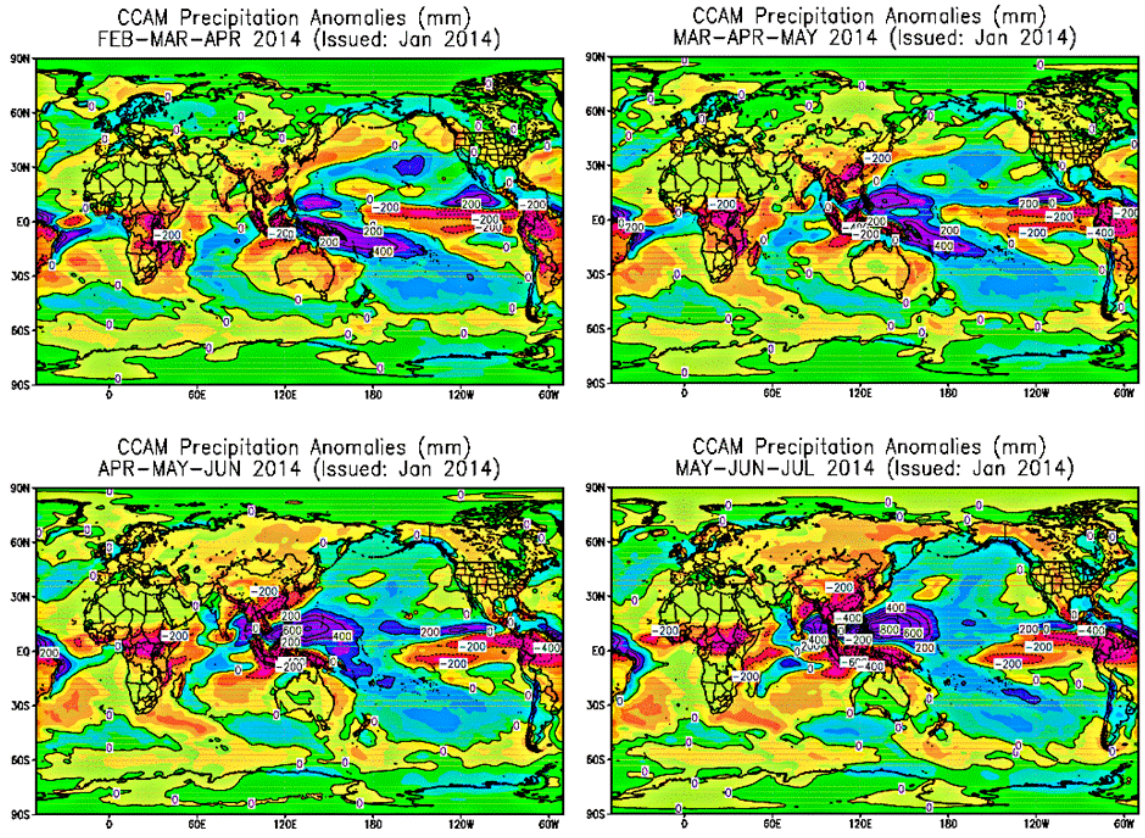

Figure 6.6: As in Figure 6.3, but for rainfall totals.

Seasonal forecasts may best be presented as probabilistic statements. Figure 6.7 shows a probabilistic rainfall forecast issued in November 2011 for the 2011/12 December to February season. The forecast is a result of statistically downscaling 850 hPa geopotential height fields of the CCAM at ~200 km resolution to CRU rainfall at ~50 km resolution. The downscaling is performed by developing linear equations between AMIP-style CCAM simulations, and then using the operational forecast of the CCAM as predictor for the coming season's rainfall (Landman and Goddard, 2005). Two sets of forecasts are presented in Figure 6.7. The top row shows the above- and below-normal rainfall forecasts when the percentiles of the climatological record were used to determine the category thresholds, while the bottom row shows forecasts when the 15th and 85th percentiles of the climatological record were used to calculate the thresholds. The forecasts of the bottom row thus represent forecasts for the likelihood of an extreme season to occur. Forecasts for the near-normal category are not presented owing to the low skill usually found for this category (van den Dool and Toth, 1991; Landman et al., 2012).

Ensemble forecasts of a single variable, e.g. rainfall rate or maximum temperatures, at a single location (or an average over an area) can be displayed using a so-called meteogram where the value of the variable is presented as a function of time instead of on a map (e.g. Figure 6.7). This type of forecast display of a particular variable and at a specific location (e.g. a watershed) may make more sense to a forecast user than a mapping of a large area. Figures 6.8 and 6.9 are examples of meteograms for respectively rainfall rate (mm/day) and for maximum temperatures. In Figure 6.8 the observed monthly climate is represented by the red line and the 1- and 2-standard deviations, based on the 12-member ensemble forecast, by the blue and green shadings respectively. The same type of meteogram is presented in Figure 6.9, but for maximum temperatures. Along with the maximum temperature meteogram, the number of days within the 12-member ensemble exceeding predetermined temperature thresholds and their observed equivalent are also presented. This representation of predicted and observed temperatures can give the user an indication of whether or not there will be a lower or higher number of days associated with temperature extremes.

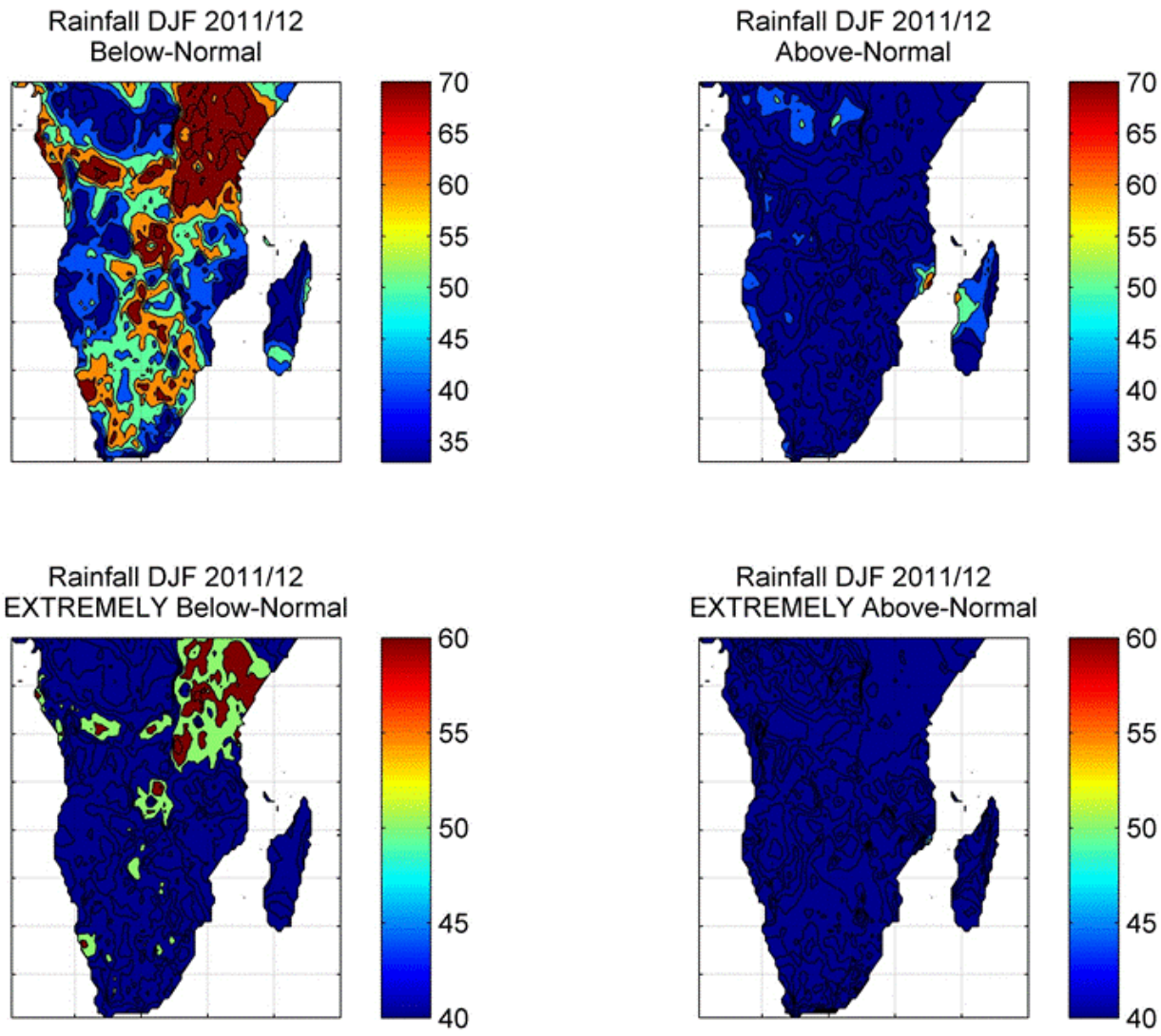

Figure 6.7: Probabilistic rainfall forecast issued in November 2011 for the 2011/12 DJF season. The colour bars represent forecast probabilities.

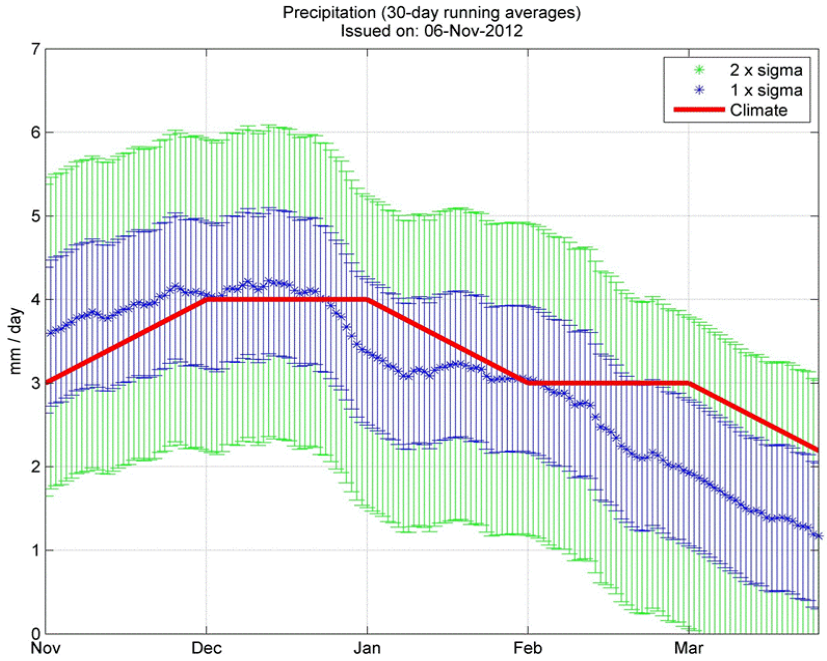

Figure 6.8: Seasonal forecast meteogram for the Pretoria area issued in November 2012 for the next 5 months. The red line is the observed climatology. The 1- and 2-standard deviations are calculated from the 12-member ensemble.

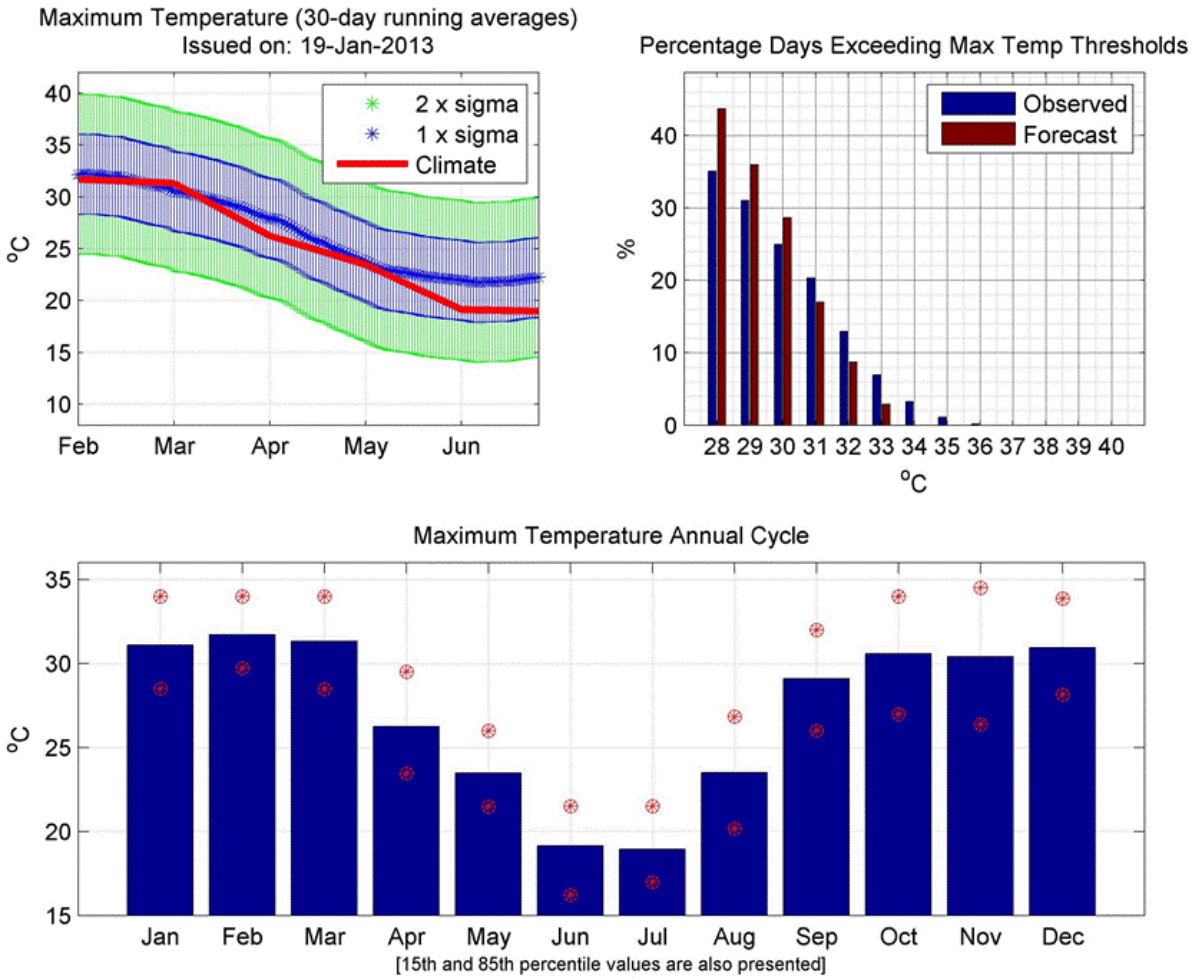

Figure 6.9: Maximum temperature meteogram, exceedances and annual cycle for the Pretoria area. This forecast was issued in January 2013 for the next 5 months.

6.2 Seasonal streamflow forecast system

The project aims, in addition to the prediction of atmospheric variables such as rainfall, to predict derivatives of rainfall, and for this particular deliverable, streamflow. The CCAM output has also been configured to produce forecasts for streamflows. The streamflow data used here are the Quaternary catchment data for 1946 catchments across South Africa produced by the University of KwaZulu-Natal (Schulze et al., 2005). Model output statistics (MOS; Wilks, 2006) is applied to the 850 hPa height fields of the CCAM's DJF simulations for the period 1979/80 to 1998/99, in order to produce downscaled DJF simulations for both the 1946 catchments (accumulated streamflows) and for 963 South African Weather Service rainfall stations (seasonal rainfall). Figure 6.10 shows the cross-validated (3-year-out approach) streamflows (left) and rainfall (right) over the eastern part of South Africa. Skill over the western part is limited, except for the Orange River basin. Take note of the similarities in skill when simulating rainfall and streamflows.

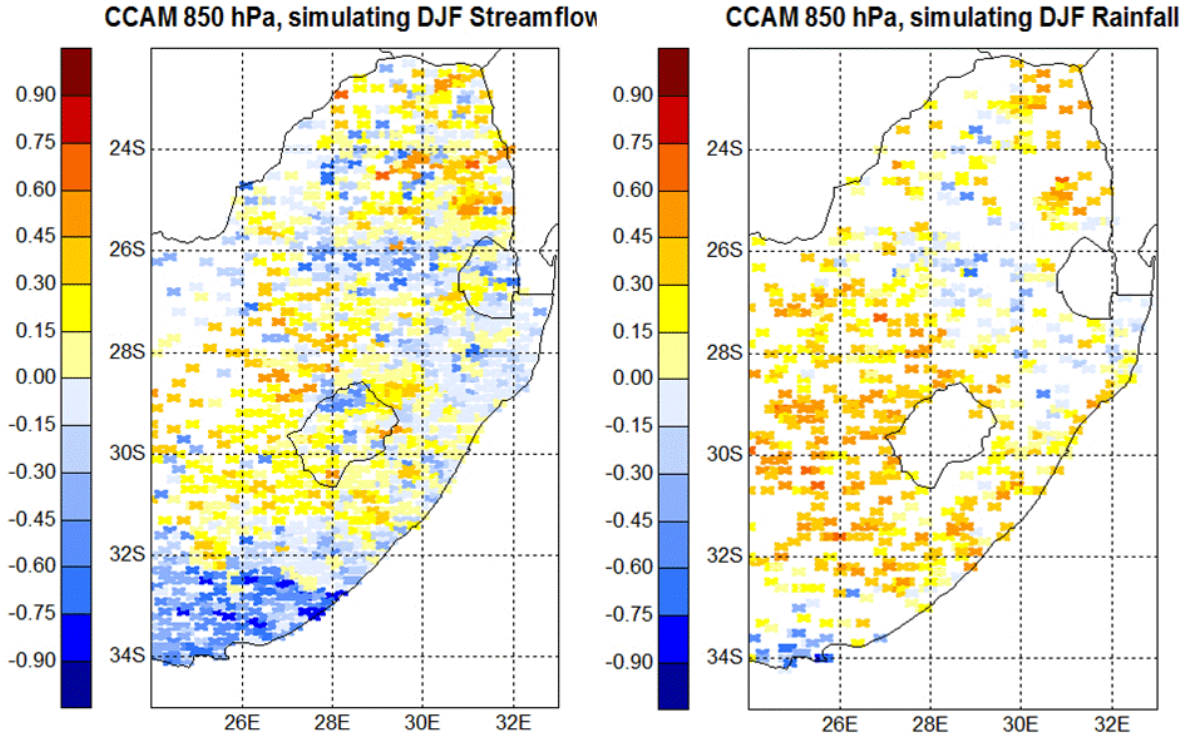

Figure 6.10: Spearman rank correlation values between observed and cross-validated downscaled DJF streamflow (left) and rainfall (right). The downscaling was done by using the CCAM's 850 hPa geopotential heights as predictors in a MOS approach.

Next we will show the CCAM-MOS system's ability to simulate past severe flooding season (1999/2000) as well as a drought season (2000/2001) over this area. Figure 6.12 shows the probabilistic streamflow forecasts over the eastern half of South Africa during the 1999/2000 DJF season. This season was associated with tropical cyclone landfall and was one of the wettest seasons in the recent past. The simulated probabilities are calculated for three equi-probable categories of above- (high flows), near- (about average flows), and below-normal (low flows). Here we only present the above- and below-normal categories since the prediction skill of the middle category is usually very low. The probabilities are obtained by considering the ensemble mean of the CCAM simulations, and then calculating the error variance of the cross-validated downscaled hindcasts (Troccoli et al., 2008). Figure 6.11 shows enhanced probabilities for above-normal flows to occur, and much reduced probabilities for low streamflows to occur.

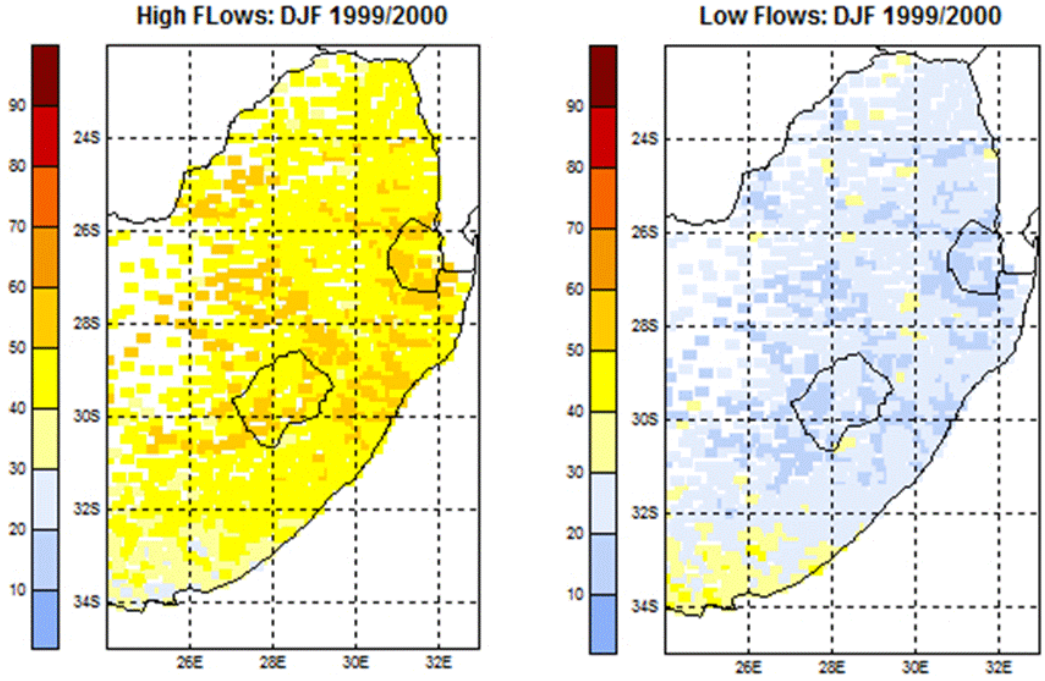

Figure 6.11: Probabilistic simulations of DJF 1999/2000 streamflows, obtained by using the CCAM's 850 hPa geopotential height fields as predictors in a MOS system.

Figure 6.12 shows the probabilistic simulations of streamflow for the dry DJF season of 2000/2001. For this season the downscaled simulations show enhanced probabilities for below-normal streamflow to occur. The two examples of Figures 6.11

and 6.12 therefore show how the MOS system is able to skilfully simulate streamflows for two seasons beyond the model training period. Another example of the CCAM-MOS system's ability to skilfully simulate streamflows is shown in Figure 6.13. Here we used different thresholds to the ones shown in Figures 6.11 and 6.12 – the threshold of Figure 6.13 are for the 85th- and 15th- percentile values of the climatological records, therefore representing seasonal extremes. Take note of the probabilistic simulation for extremely high flows to occur during FMA 2011 along the Orange River catchment shown in Figure 6.13. Also shown on the figure are the Spearman rank correlations over the catchment and a picture taken of the Augrabies waterfall during the simulation period.

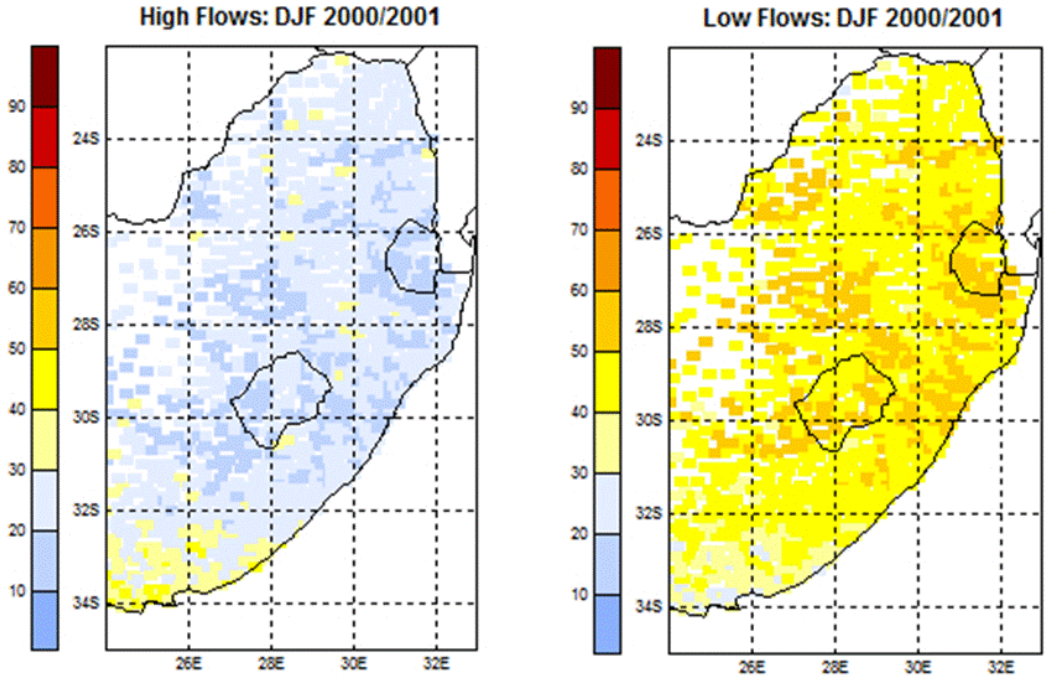

Figure 6.12: As for Figure 6.11, but for DJF 2000/2001.

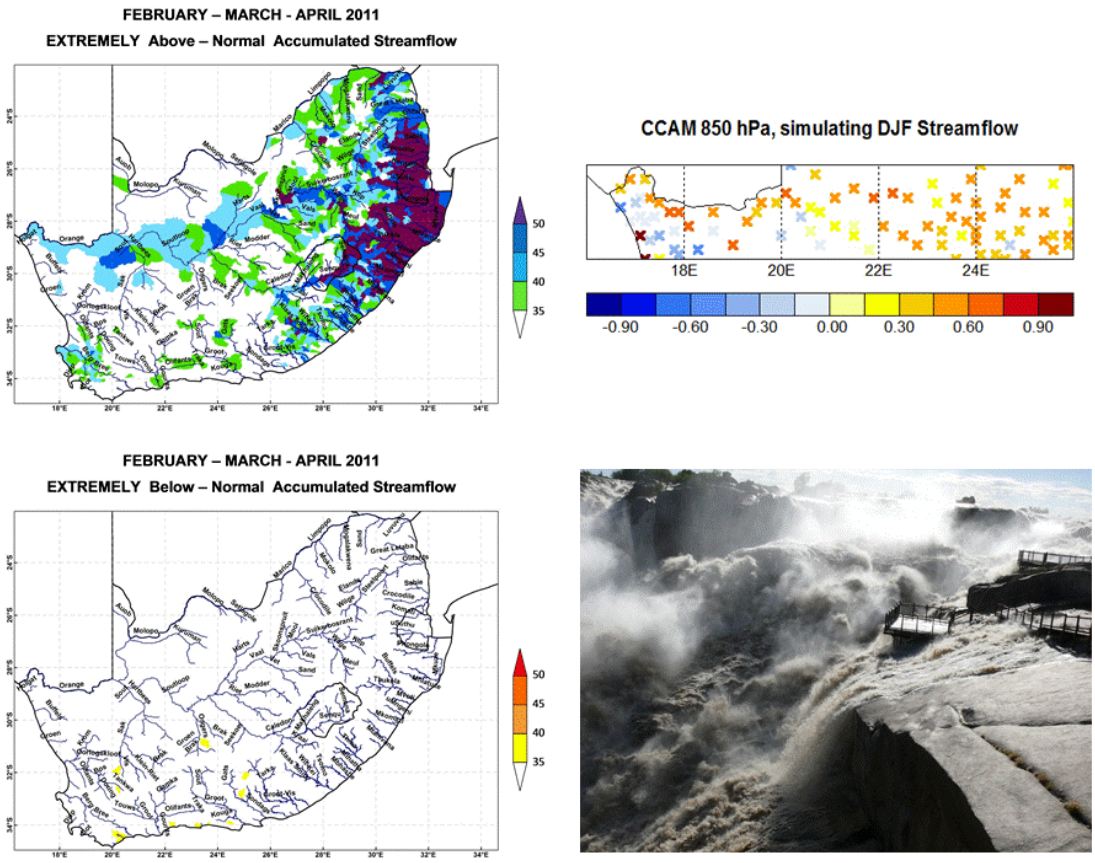

Figure 6.13: Simulations of extreme flows for the FMA 2011 season, Spearman rank correlations over the Orange River catchment, and a picture taken of the Augrabies waterfall during the simulation season of FMA 2011.

6.3 Tropical cyclone track forecasting system

Tropical cyclone track forecasts can be used for advanced warning to Meteorological Services and disaster managers of countries affected by possible tropical cyclone land-falling. Tropical cyclone landfall within the south-west Indian Ocean (SWIO) basin occurs on average about 3 times per year over Mozambique and Madagascar (Mavume et al., 2009). Moreover, tropical cyclones and less intense tropical systems from the SWIO are responsible for a large contribution towards widespread heavy rainfall events over the eastern parts of southern Africa (Malherbe et al., 2012). This section describes the operationalization of a seasonal tropical cyclone track forecasting system applied during the late summer of 2014.

6.3.1 Data and methodology

The CCAM was used to perform simulations at a 2° resolution. The forecast data used here were generated by the CCAM forecast system in February 2014. The

primary focus here is the tracking of tropical systems from the SWIO and into Madagascar or into the eastern parts of southern Africa. For this reason the area of interest (Figure 6.14) includes Madagascar and allows for the tracking of tropical systems from 80° E. Of relevance also is the tendency for tropical cyclones to develop/track across the Mozambique Channel or to locate to the east of Madagascar (areas indicated by the coloured blocks).

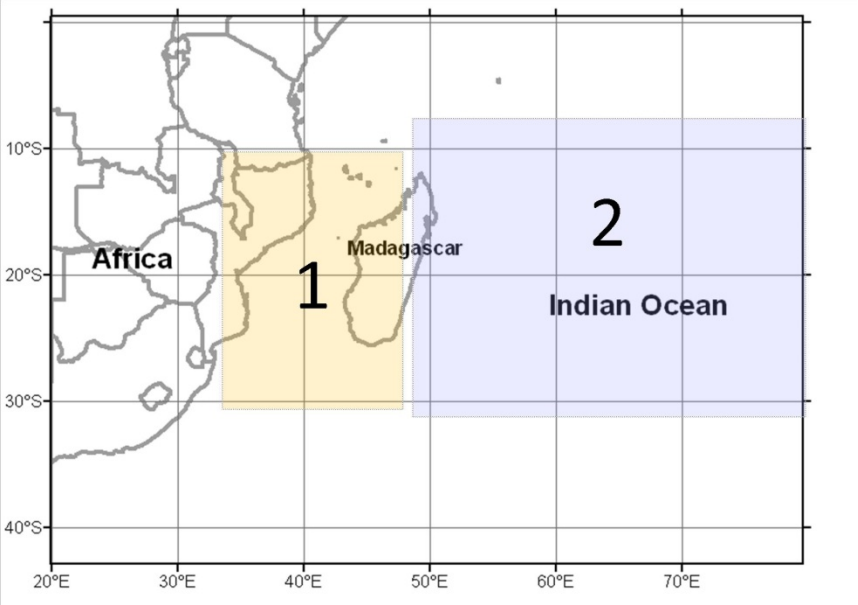

Figure 6.14: Area of interest, with the Mozambique Channel **(1)** and the area to the east of Madagascar **(2)** as main focus areas indicated.

A tropical cyclone tracking algorithm, modified for tropical systems specifically as described in Malherbe et al., 2012, was available for application, to be tested with operational data as it becomes available. The following is the list of operational simulated fields considered in the tracking algorithm:

1. Geopotential height of the 700 hPa pressure level
2. Geopotential height of the 500 hPa pressure level3
3. Temperature at the 250 hPa pressure level
4. 10 m wind strength
5. Zonal and meridional wind vectors at the 700 hPa pressure level

Relative vorticity was calculated from the wind vectors at the 700 hPa level, and plays an important role in the identification of lows in the tracking algorithm. In the tracking algorithm, vorticity minima were identified through the application of a multi-

grid point stencil. To identify the existence of a warm core low, a pressure minimum in the region of the vorticity minimum must be found within a specified radius from the vorticity minimum. The pressure minimum needed to be reflected also at the 500 hPa level, in close proximity of the 700 hPa low, or in other words, the system had to be vertical through much of the troposphere. At 250 hPa, there needed to be a temperature maximum within a specified radius from the vorticity minimum at 700 hPa. To identify a tropical cyclone, a cut-off minimum value for the maximum wind strength within a specified minimum distance from the vorticity minimum is 13 ms^{-1} (Walsh et al., 2007). The tracking algorithm considered all identified tropical cyclones, and tracks the vorticity minima at 700 hPa associated with warm lows emanating from the original identified tropical cyclone in time.

Data management included production of monthly datasets of daily values for the above mentioned variables. The data were interpolated to a geographic Lat/Lon projection from the CCAM projection. The tracking algorithm was adjusted in order to be operational with daily data instead of 6-hourly data as used previously, implying testing and changing of certain thresholds. The algorithm has been made available to the CSIR for further operational tracking of tropical cyclones simulated by CCAM. The International Best Track Archive for Climate Stewardship (IBTrACS – Knapp et al., 2010) is updated until the end of 2013, and will only later be updated to include data for 2014. Because the operational simulated fields for the period February to June 2014 were considered, another source of observed tropical cyclone tracks was used. The observed tracks as reported by the Australian Bureau of Meteorology (http://www.australiasevereweather.com/cyclones) for the South Indian Ocean provided the information for actual tropical cyclone occurrence. Data in this online database with current observations also include input from Meteo-France at La Reunion, ensuring good representation of conditions over the SWIO.

6.3.2 Results and discussion

Figure 6.15 shows the forecast tracks of tropical cyclones by CCAM for the forecast period from 1 February through 15 March. For comparison the observed tracks are also indicated as obtained from the database hosted by the Australian Bureau of Meteorology for comparison. The period 1 February 2014 to 15 March 2014 is too

short to draw unequivocal conclusions regarding the accuracy of tropical cyclone track forecasts. Nevertheless, observations over especially the Mozambique Channel seem to support the CCAM forecast. The total number of systems simulated over the Mozambique Channel (2) and also over the area to the east of Madagascar (2) compare favourably with the observed (1 and 2 respectively). The genesis area near the northern coast of Mozambique also shows good correspondence between the simulated and observed datasets. More importantly, the tracking algorithm is being used in operational mode. Figure 6.16 shows the forecast tracks for the period 1 February to 30 June 2014 over the area of interest. The methodology is also available to consider in future not only tropical cyclones (as shown here), but all warm-core lows in the region. While it was applied here operationally only on a single ensemble member, it can also be applied to multiple ensemble members, allowing for the identification of potential high-risk areas at the beginning of a tropical cyclone season.

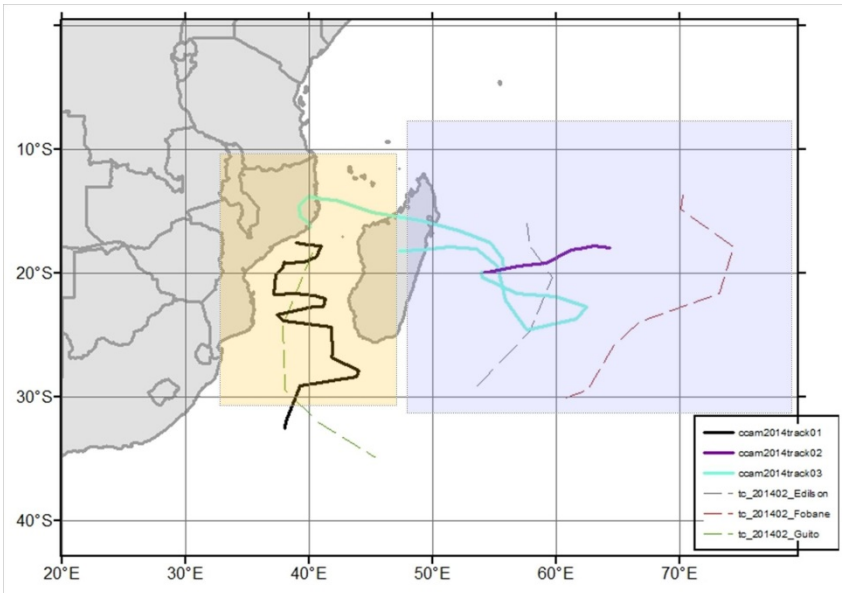

Figure 6.15: Tropical Cyclone tracks simulated by CCAM in the seasonal climate simulation for February 2014 (solid lines) and observed tracks (broken lines) since 1 February 2014 according to the dataset hosted by the Australian Bureau of Meteorology.

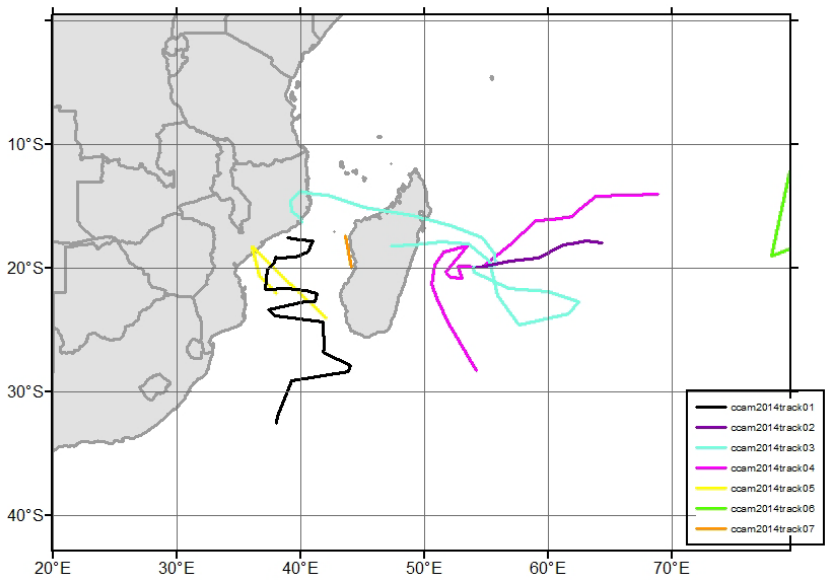

Figure 6.16: Tropical Cyclone tracks simulated by CCAM in the seasonal climate simulation for 1 February to 30 June 2014.

Chapter 7

Introduction to the seamless forecast system of the South African Weather Service

7.1 Introduction

The concept of seamless prediction is the notion of a single dynamical core that supports all time-scales ranging from short-range weather forecasts to centennial climate change. This idea was originally articulated in the Development of a European Multi-model Ensemble system for seasonal-to-interannual Prediction project (DEMETER; Palmer et al., 2004) that suggested the Multi-Model Ensemble Prediction System (MMEP) that supports the seasonal forecast to be also used for the climate change realizations. The articulation stirs a proliferation of international curiosity towards the development of prediction systems that bridge the gap between weather forecasts and forecasts or projections for much longer time scales (Vitart et al., 2008). Improving on the low forecast skill presently found for the second week leading up to the first month of the forecast holds great societal and economical value, since success in the development of such systems should improve on the prediction of wet and dry spells and its duration, extremes and high-impact weather events, seasonal onset and cessation, and also the general improvement in forecasts or projections on all time scales.

One of the problem areas identified at the start of this project was that different forecasting systems were engaged to address weather and climate information needs across a wide-range of timescales. Currently the South African Weather Service (SAWS) employs different methods to compile the weather and climate information. In this context, the medium-range (days 3 to 10) timescale forecasts, for instance, are still based on the National Centers for Environmental Prediction (NCEP) Ensample Prediction System (EPS; Tennant et al., 2007), the short-range forecasts are based on the United Kingdom Unified Model and the extended-range (beyond 10 days and up to 30 days) and seasonal forecasts, are based on the

Atmospheric General Circulation Model (AGCM) ECHAM4.5 (Roeckner et al., 1996). With this in mind we attempted to reconfigure the ECHAM4.5 AGCM in a manner that can support a seamless forecasting system that may provide a unified weather and climate advisory or warning.

7.2 Methodology

7.2.1 Model description

The global climate model ECHAM4.5 (Roeckner et al., 1996) was originally evolved from the spectral weather forecast model of the European Centre for Medium Range Weather Forecasts (ECMWF; Simmons *et al.,* 1989). Numerous modifications (in dynamics and physics) have been applied to this model at the Max Planck Institute for Meteorology (MPI) in order to make it suitable for climate predictions and it is the fourth generation in a series. The model is one of the best available forecasting tools and holds promising predictive capability in the southern Africa region (Landman et al., 2008). With the introduction of a state-of-the-art data-assimilation interface at the South African Weather Service (SAWS) as we explain hereafter, it becomes technically possible to use the model in operational seamless forecasts. It is also planned to modify the system for timescales beyond seasonal forecasts such as decadal and multi-decadal climate projections.

Currently, the model can be configured for different vertical and horizontal resolutions as a function of adjustable model time steps. In addition, a message passing interface (MPI) integration in the model code renders the model to run efficiently using parallel processing capabilities on high performance computing systems (HPCS). However, the standard model configuration is adopted to minimize computational strain. The prognostic variables are represented by truncated series of spherical harmonics with triangular truncation at wave number 42 (T42) except for the moisture and trace substances. Vertically 19 unevenly spaced hybrid sigma layers are allowed. The model uses the vertical coordinate system of Simmons and Burridge (1981). The model employs a semi-Lagrangian transport scheme of Williamson and Rasch, (1994) for water vapour, cloud water and trace substances. It uses the Longwave radiation of Fouquart and Bonnel (1980) and shortwave radiation of Morcrette et al. (1986). Cumulus convection is parameterized using the mass flux

scheme of Tiedtke (1989), but incorporates the modifications introduced by Nordeng (1996). The turbulent surface fluxes are calculated from Monin-Obukhov similarity theory (Louis, 1979), but different from its predecessors. A higher-order closure scheme (Brinkop and Roeckner, 1995) is used to simulate the vertical diffusion of heat, momentum, moisture and cloud water. Horizontal diffusion is computed using Laursen and Eliasen (1989) scheme. The orographic gravity waves are represented by the wave drag parameterization due to Miller et al. (1989).

7.2.2 Data assimilation and model initialisation strategy

The atmospheric initial conditions are emanated from the National Centers for Environmental Prediction, Department of Energy (NCEP/DOE) Atmospheric Model Intercomparison Project (AMIP) II Reanalysis (R2) dataset. To use the NCEP/DOE product, however, it has to be reconciled with the model resolution and format. Hence, the NCEP atmospheric states are consistently transformed to horizontal and vertical resolution (T42L19) of the ECHAM4.5 AGCM. In general, the data assimilation process involves: 1) the transformation of pressure to hybrid-sigma coordinate system (Simmons and Burridge, 1981) and 2) grid to spectral space transformation. The latter is applied on prognostic variables (such as temperature (T), vorticity (ξ) and divergence (D)) albeit the specific humidity remains in the corresponding Gaussian grid resolution.

The vertical coordinate system transformation requires the application of interpolation or curve fitting techniques that demands cautious treatment. The ECHAM4.5 AGCM is found to be sensitive to a vertical interpolation that hardly maintains the balance of vertical profile of time dependent variables. The initialization strategy we adopt in this study capitalizes the best available information. In addition, we are able to constrain the AGCM with a balanced and suitably transformed realistic atmospheric state. Currently the ensemble system is constructed using a time-lagged average forecasting techniques first suggested by Hoffman and Kalnay (1983). Similarly, the soil moisture initial state is updated at the time of each model initialization time; this information is obtained from the Climate Prediction Center (CPC) monthly mean dataset. The AGCM uses the simple biosphere model (Sellers

et al., 1986) and soil hydrology parameterization scheme suggested by Dümenil and Todini (1992).

The AGCM was subsequently forced with three SST scenarios reproduced from a multi-model system. The SST scenarios presumably account the mean and spread of the ensembles. The procedure we followed to incorporate the uncertainties was that once the ensemble mean was computed, the model error history which accounts the different lead-times was identified from the dominant mode (first mode) of the principal component analysis (PCA). Generally speaking the AGCM is driven in a manner that collectively explores uncertainties that presumably arise from imperfections in the atmosphere, land surface and ocean states.

7.3 ECHAM4.5 AGCM seamless integrations

The focus in this section is the evaluation of the forecasting system and thus the skill of the model is assessed for different timescales ranging from weather to seasonal forecasts based on 9-month integrations. For the medium-, extended-range and seasonal timescales the retroactive runs are used which consist of 30 ensemble members for 28 years (1982-2009). For the weather forecast, however, the model runs 4 times a day and the forecast is issued daily using 4 ensemble members.

An instance of a seamless forecast of the ECHAM4.5 AGCM which covers from weather to seasonal time-scale is shown in Figure 7.1. It is a plume of daily rainfall forecasts plotted using one of the 9 months integrations of the model that would have been issued on the 4th of November 2009. This unified weather and climate forecast composite seemingly captures the observed annual cycle during the austral summer season of 2009/2010 averaged over the Southern African Development Community (SADC) region. The ensemble average (green line) lies in the middle of the enable amplitude (blue region). It is a more smoothed line and did not really capture the observed weather fluctuations. Notwithstanding, the observed diurnal cycle is well represented by the ensemble spread and the general trend of the annual cycle is well captured.

Figure 7.2 (a) and (b) show the Pearson correlation coefficients of surface air temperature for medium- and extended-range timescales respectively. The skill scores are computed based on the ensemble mean of the 40 day integrations of the model which constitutes in total 1344 hindcast cases against the blended station and NCEP reanalysis (Kalney *et al*., 1996) dataset. The shaded regions show statistical significance at the 95% confidence level using a t-test procedure. The result suggests that the model is more skillful on the medium-range timescale albeit the two timescales share coherent spatial skill patterns. The forecast system, however, has marginal skill over the most part of the southern Africa region except over the southern edge of the SADC region suggesting that there is still room for further improvements and fine-tuning of the forecasting system. In addition, a statistically recalibration procedure applied to the operational extended-range forecasts of the SAWS yields promising results (maps not shown).

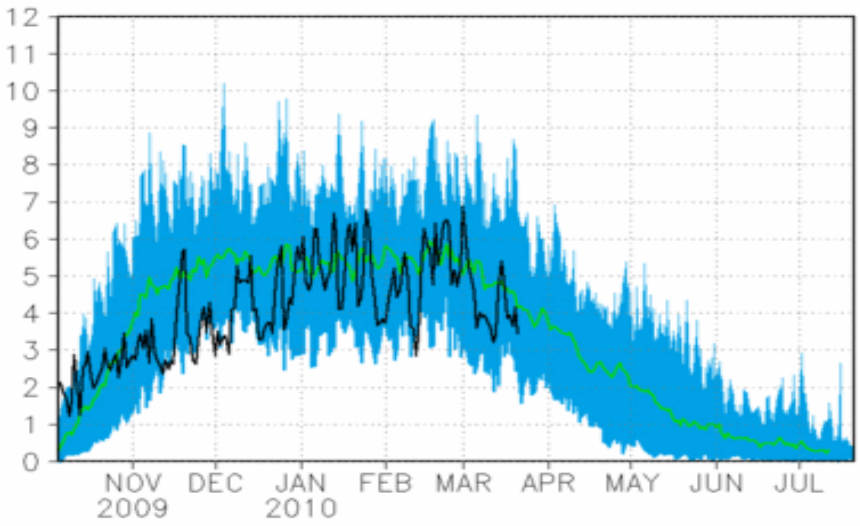

Figure 7.1: An example of a seamless forecast issued on the 4th of November 2009. It is plume of daily rainfall forecasts for consecutive 9 months starting from October 2009 averaged over the SADC region; where green is the ensemble mean, light blue is ensemble spread and black is observation (station data over South Africa blended with NCEP elsewhere).

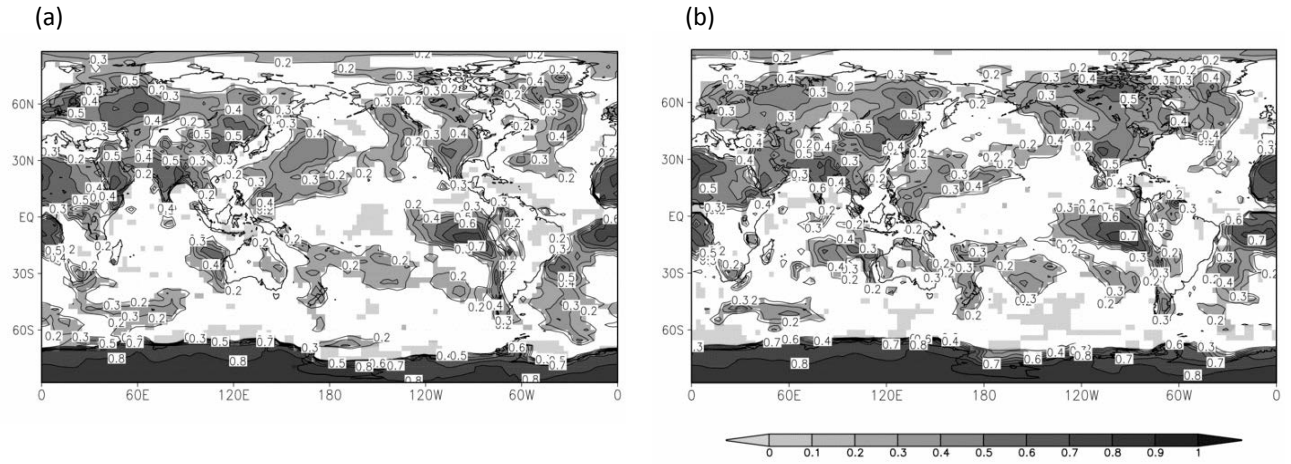

Figure 7.2: Skill of the ECHAM4.5 AGCM in predicting surface air temperature as measured using a correlation coefficient **(a)** medium-range and **(b)** extended-range forecasts based on the ensemble mean of all hindcast cases computed against NCEP reanalysis. Shaded areas are statistically significant at the 95% level.

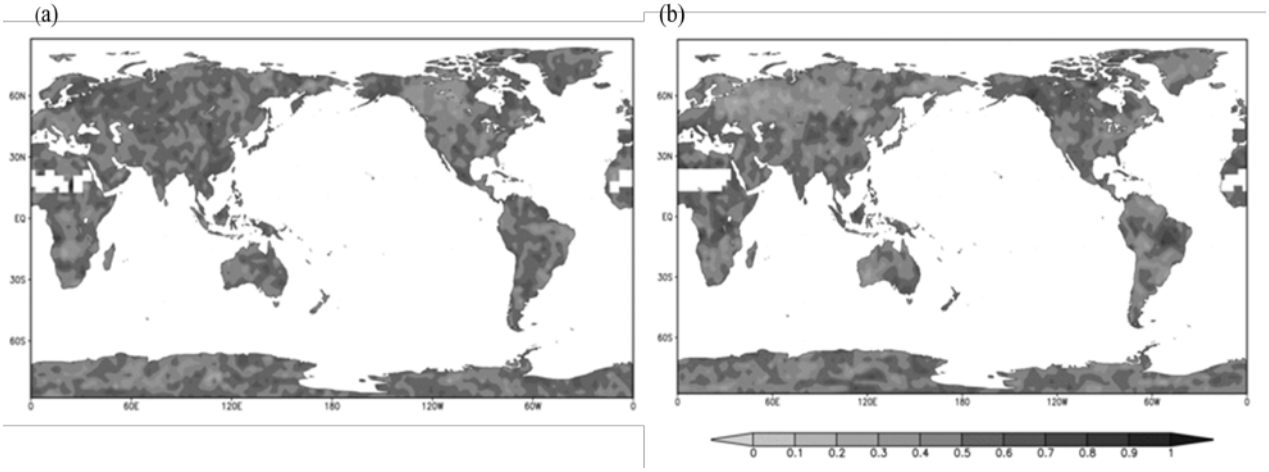

Figure 7.3: Skill of the ECHAM4.5 AGCM in predicting total precipitation probabilistically in the extended-range timescale (day 11 to day 30); ROC area **(a)** below-normal and **(b)** above-normal computed using model hindcasts against station data over South Africa and NCEP reanalysis elsewhere. Each forecast case were to be issued on the 4th of January each year (1981- 2009).

The ECHAM4.5 AGCM's probabilistic forecast performance is also explored for the extended-range (Figure 7.3) and seasonal (Figure 7.4) timescales probabilistically. The former is more consistent with the deterministic assessment particularly for the below-normal category which implies that it has also marginal skill over most of part of the SADC region (dark grey).

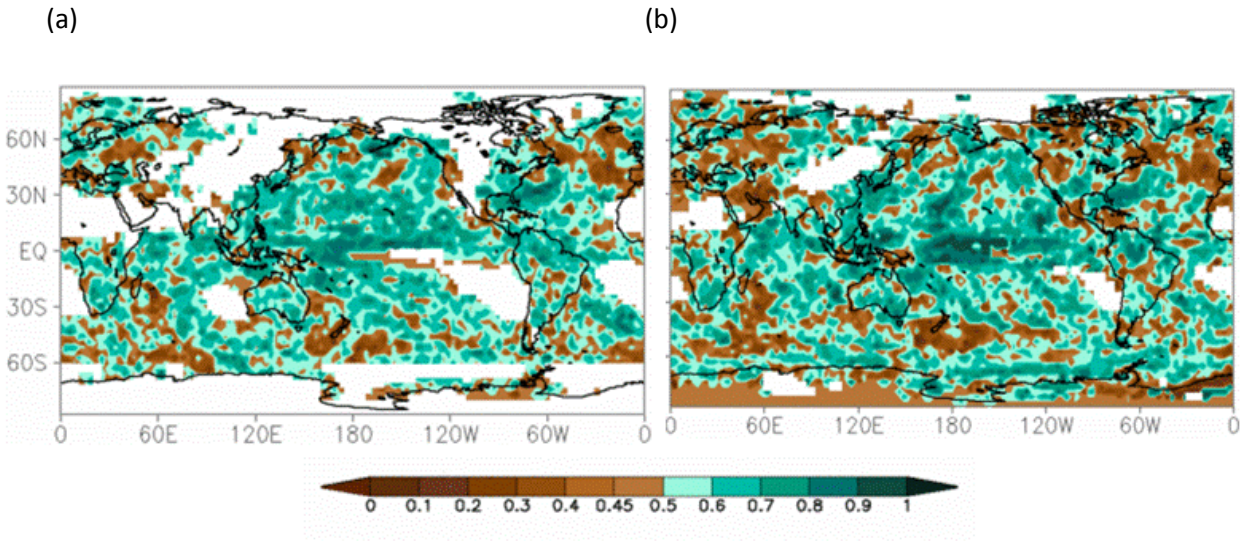

Figure 7.4: Skill of the ECHAM4.5 AGCM in predicting total precipitation probabilistically; ROC area **(a)** below-normal and **(b)** above-normal computed using model hindcasts against CMAP-CPC. Each forecast case were to be issued on the 4th of November each year (1981- 2009).

In contrast to the medium- and extended-range timescales, the model skill for the seasonal time-scale is robust. The skill of the model in predicting seasonal rainfall during the austral summer season is shown in Figure 7.4. This skill is based on the model integrations that truly mimic a set of operational forecasts as if it were routinely issued on the 4th of November starting from 1982 to December, 2009. The model shows comparable skill over the SADC window for both below- (a) and above-normal (b) categories as measured by the relative operating characteristic (ROC) area. The model simulations were conducted on the Centre for High Performance Computing (CHPC) computer clusters. The ROC is a highly flexible method for representing the quality of dichotomous, categorical and probabilistic forecasts (Mason & Graham, 1999) and is one of the skill scores recommended by the Commission for Basic Systems (CBS) of the World Meteorological Organization (WMO) for long-range forecasts. Skillful forecasts are found globally albeit small patches of forecasts not better than chance are also visible. The model forecast shows consistent spatial skill patterns over the southern Africa region.

SAWS's seamless forecasting system is based on the ECHAM4.5 AGCM. Even though the AGCM is more suitable for climate simulations notably for seasonal forecasts as highlighted earlier, the introduction of a semi-data assimilation interface at the SAWS renders the model to be suitably utilized for unified weather and climate

advisories. The model is evaluated for different times-scales. For most of the time-scales considered, the model yields promising results. The strength of the model in predicting surface temperature and rainfall is more pronounced in the seasonal timescale. Similarly it is also skilful over the South Africa segment for the medium- and extended-range forecasts. Notwithstanding, the model is poor in predicting the noted weather elements for the latter time-scales for most part of the SADC region suggesting that there is still room for further improvements and optimization. We suggest that increasing the resolution of the model particularly for shorter timescales may potentially minimize this drawback. Notwithstanding, this goal is only achievable with the availability of more dedicated computational resources.

7.4 Operational ECHAM4.5 seamless forecasts

Numerical Weather Prediction (NWP) can be categorized into different types based on the physical basis they rely on and the timescale they pertain to. Broadly speaking, they might fall in the range from weather forecasting to climate change. Long-range forecasting (LRF) deals with the mean state of the atmosphere beyond medium-range time-scale. When we break it down further, the long-range forecasting may include extended-range forecast (ERF), seasonal and inter-annual forecasts, decadal prediction and multi-decadal (climate change) projections.

7.4.1 Seasonal forecasts

When the ECHAM AGCM was introduced at SAWS in 2007, the main goal was to use the model for seasonal forecasts. The model is more suitable for climate forecasts and it has been extensively used for operational seasonal time-scale advisories. Since then the model configuration has undergone major changes and is continuously optimized. According to the official World Meteorological Organization (WMO) definition seasonal forecasts refer to the description of averaged weather parameters expressed as a departure from climate values for 3-month seasons at any lead-time.

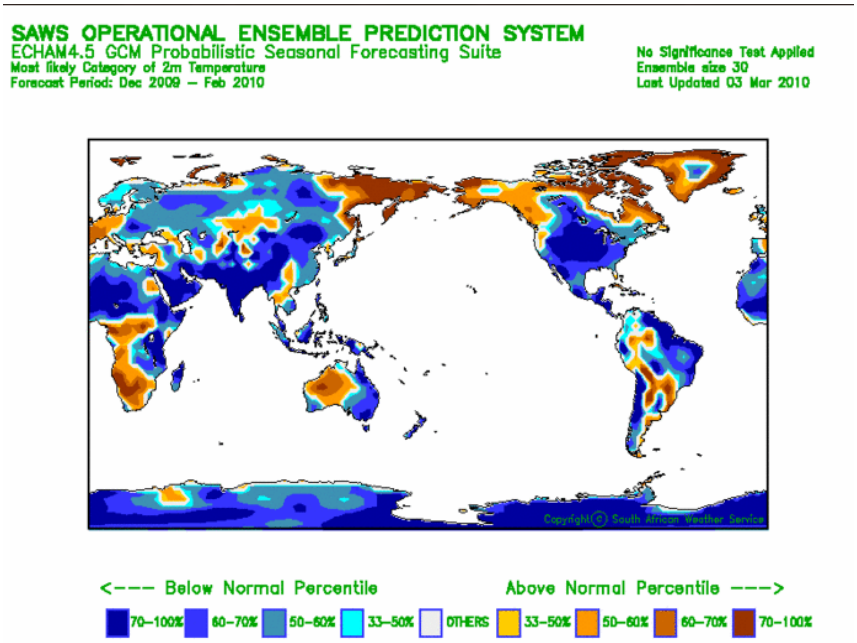

Figure 7.5: ECHAM4.5 AGCM operational probabilistic seasonal forecast for surface air temperature for December to February 2010 issued on 4 November 2010.

Figure 7.5 depicts an example of dynamical global seasonal outlook of the AGCM that was issued on the 4th of November 2010. This 1-month lead-time DJF (December-January-February) season probabilistic seasonal forecast for surface air temperature is based on 30 ensemble members and the probabilities are computed according to the pre-identified threshold values from the model history that uses the same model configuration.

7.4.2 Extended-range forecasts

Extended-range forecasting (ERF) deals with the mean state of the atmosphere beyond the time when predicting the day-to-day fluctuation of the atmosphere becomes scientifically impossible. The extended-range timescale bridges the gap between medium-range and seasonal forecasting. According to official World Meteorological Organization (WMO) definition it is beyond 10 days' and up to 30 days' description of weather parameters and usually averaged and expressed as a departure from climate values for that period. At SAWS, ERF is provided similar to the seasonal forecast probabilistically in order to convey forecast uncertainties (Figure 7.6).

The state-of-the-art operational ERF system of SAWS (Beraki and Olivier, 2009) relies on the 24 ensemble integrations of the ECHAM4.5 AGCM. The ERF is assumed to be the interplay between weather forecast and seasonal predictions. It is also the most complex part of NWP. This is largely attributed to the fact that the physical basis for this time-scale is not as clear as for medium-range and seasonal forecasts. Theoretically, the underlying logic to exercise this type of prediction resides on the assumption that the time range 11 to 30 days is still short enough that the atmosphere retains some memory of its initial state and it is presumably long enough that the slowly evolving boundary conditions have an impact on the atmospheric circulation. Nevertheless, experience at SAWS shows that this modeling guidance holds some potential and may provide useful climate guidance (such as onset of the rain season) to relevant stakeholders. In order to maximize the usability of the ERF climate advisory, statistical recalibration of raw model output may be required in order to generate high resolution forecasts and to recalibrate the forecast biases. In addition the need for high resolution observed long-term daily data is critically important for the recalibration process.

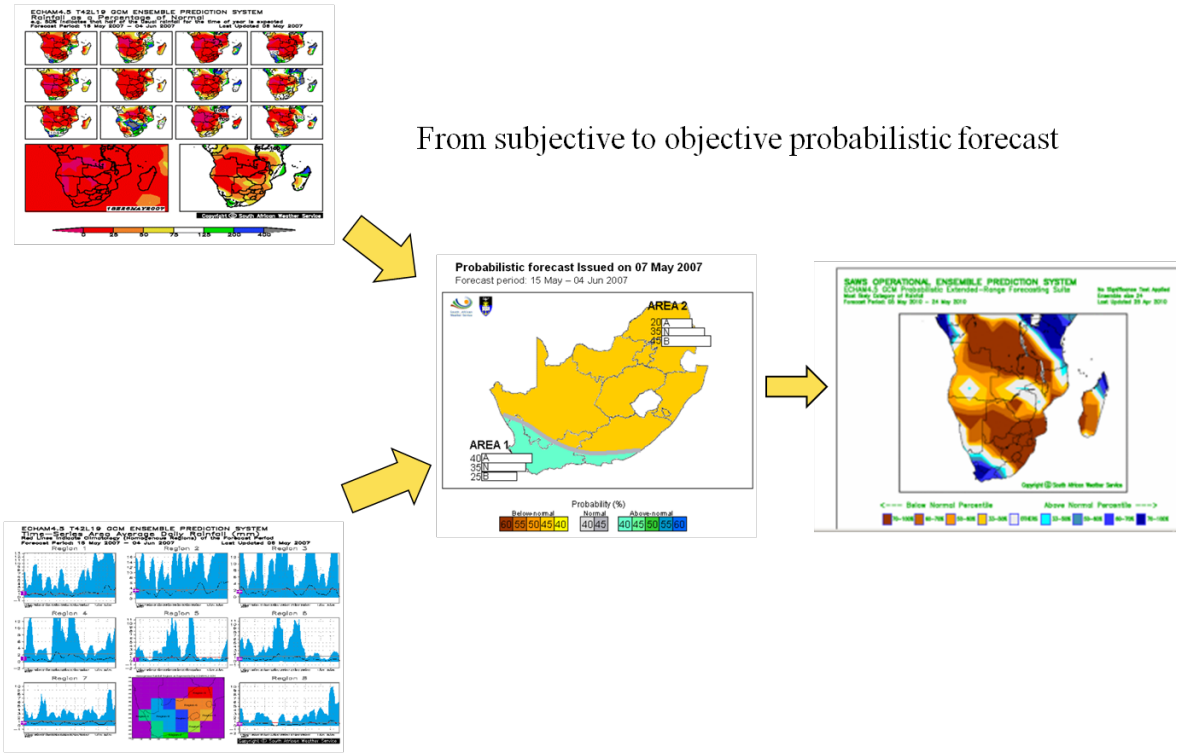

Figure 7.6: The evolution of ERF from subjective to object probabilistic forecast. The subjective consensus forecast (middle) is the outcome of the AGCM forecasts blended with the conveners' opinion in one of the LRF forum conducted at that time.

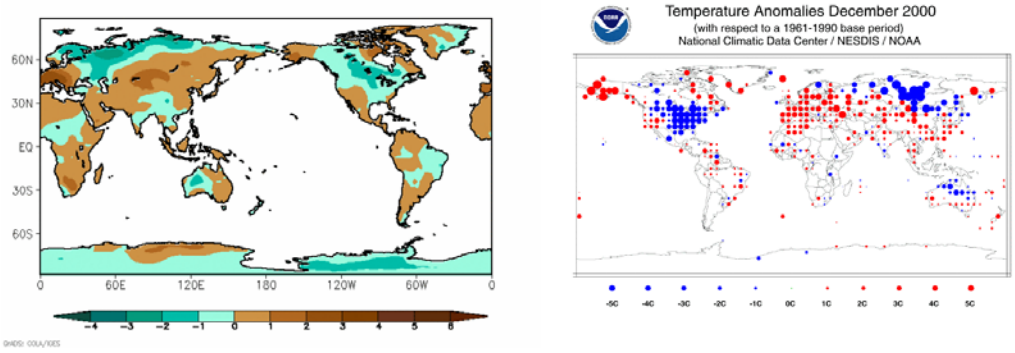

Figure 7.7: Operational surface air temperate forecast issued on 6 of December 2000 for the forecast period spanning 17 Dec 2000 to 6 Jan 2001, (a) ECHAM4.5 AGCM and (b) the corresponding observation (obtained from NOAA as indicated in map) but for December. The forecast shows good harmony with observation albeit the slight mismatch in terms of forecast period.

7.4.3 Medium-range forecasts

Weather refers to the day-to-day state of the atmosphere (e.g. the position of fronts and individual storms, daily precipitation and temperature, as well as humidity, winds, and sea level pressure). Meteorologists have long had the goal of extending accurate predictions of day to day weather to several days and perhaps even weeks, months, and seasons in advance. Notwithstanding, the chaotic nature of the atmosphere imposed a finite limit of about two weeks to weather predictability (Lorenz, 1963). While great progress has been made on forecasts for extended time-scale, the chaotic behaviour of the atmosphere hinders the predictability of day-to-day weather fluctuation beyond Lorenz's limit and it is exclusively asserted (AMS, 2001) that there is no scientific basis for the deterministic forecast of day-to-day weather fluctuation beyond this limit. In fact what has been attained up to now may even be far less than this theoretical limit.

Medium-range forecast (MRF) is more or less similar to short-range weather forecasts in principle. The methods used to produce short-range weather forecast is still applicable for MRF as the time range still falls within the Lorenz limit except that this timescale may be as important for decision makers. As officially defined by WMO, MRF is weather forecast beyond 72 hours' and up to 240 hours' description of weather parameters. The official medium-range (days 3 to 10) timescale forecasts of

SAWS are still based on the National Centers for Environmental Prediction (NCEP) Ensample Prediction System (EPS; Tennant et al. 2007). However, Beraki and Olivier (2009) has shown that the ECHAM4.5 MRF is skilful for the southern Africa region based on the analysis conducted on 1344 surface temperature hindcast cases (Figure 7.1). This notion implies that the model has the potential to replace and/or complement the current system based on the NCEP EPS.

7.4.4 Short-range weather forecasts

Short-range weather forecasts (0-48hrs) issued by SAWS are based primarily on the United Kingdom (UK) Unified Model (UM). The use of the ECHAM4.5 AGCM for short-range weather forecast may potentially provide useful information and complement the official UM forecasts more specifically when severe weather events start outside the UM regional domain (e.g. cut-off low or tropical cyclone). For this reason we explored the ability of the model within the context of severe weather events. Figure 7.9 shows a storm surge along the east coast of South Africa on 18 March 2007 as shown by the Meteosat-8 image (RGB Composite (Airmass RGB) at 18:00 UCT. It is indeed visible from the mean seal-level pressure (MSLP) forecasts (Figure 7.9 c,d) that the AGCM managed to capture the development of this semi-stationary cut-off low pressure system although the model vortex attained its maturity 12 hours later when compared to the NCEP R2 MSLP field and satellite observations. It was reported (Hunter and De Coning, 2007 published in http://oiswww.eumetsat.org/WEBOPS/iotm/iotm/20070318_storm/20070318_storm.html) that this severe weather event caused extensive damage to coastal infrastructure, with initial repair costs estimated at roughly half-a-billion Rand. The total cost of the storm event – including loss of tourist revenue – is likely to be close to 1 billion Rand. Beach houses were partially destroyed. Damage to an outfall pipe resulted in raw sewerage flowing into the surfing zone. Thousands of tons of sand have been removed from the beaches. The whole economy of the area is based heavily on tourism.

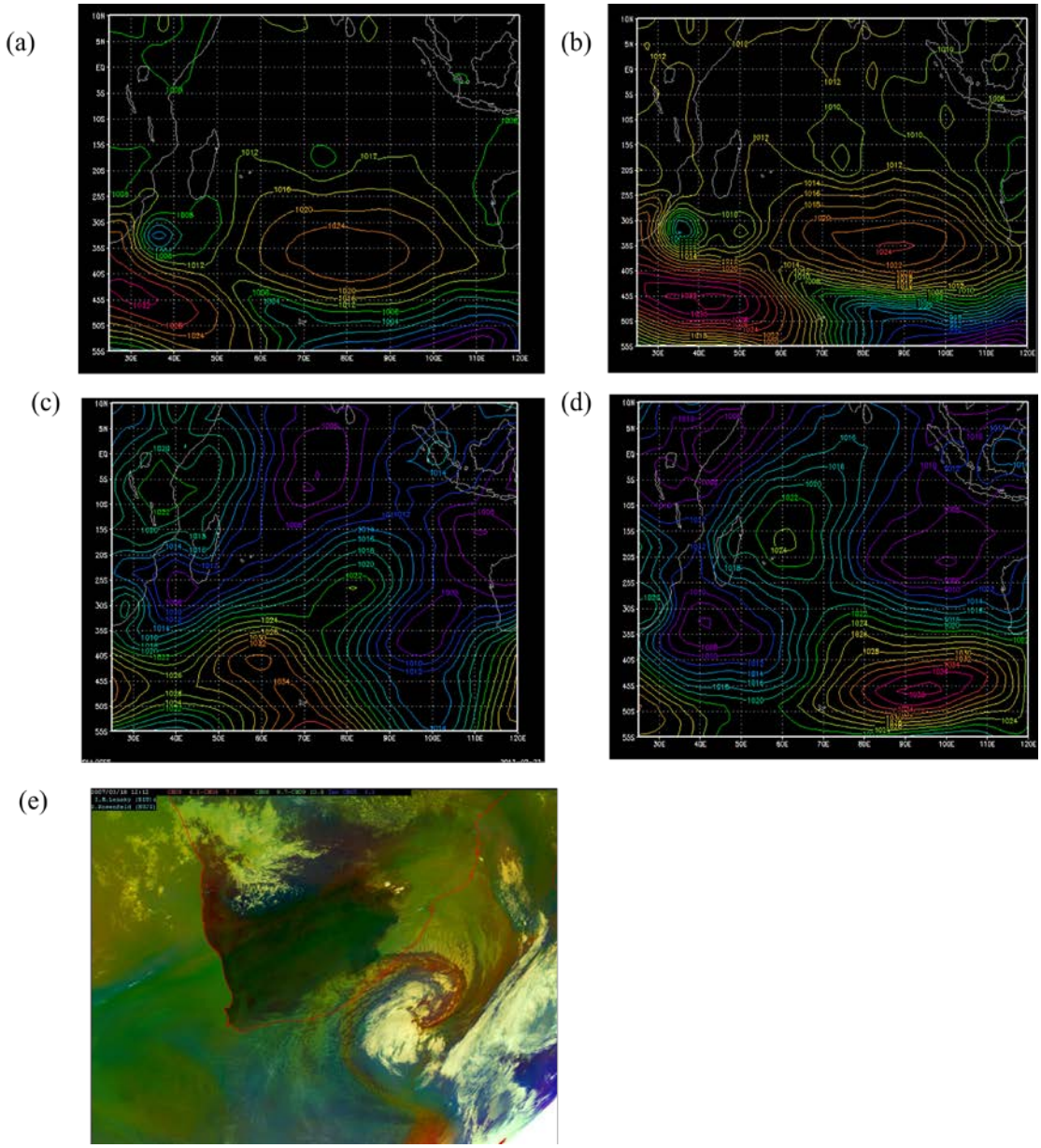

Figure 7.8: The ECHAM4.5 AGCM MSLP forecast (if it were) issued on March 18, 2007. The model indicates the development of trough adjacent south-eastern coast of South Africa on the evening at 18:00 UCT 18 March (c) and it gains its maturity midnight 12hrs later (06:00 UCT 19 March; d). The respective NCEP/R2 field are shown in (a) and (b). The satellite (Meteosat-8) image (RGB Composite (Airmass RGB; 18:00 UCT 18 March) is also shown. The cut-off low incident reportedly caused a massive damage in the coastal infrastructure and tourism industry.

Chapter 8

Summary and conclusions

8.1 Introduction

The main objective of this modelling study was to develop and assess so-called seamless forecasting systems. Such a system is called seamless if a common forecast system is used to predict for multiple time scales. The time scales considered include short-range weather prediction through multi-decadal climate projections. For the shorter time scales up to seasonal climate, a range of re-forecasts or hindcasts were generated and verified. Multi-decadal regional climate simulations were also performed and evaluated.

8.2 Main conclusions

- The atmospheric model CCAM was applied in this research to produce short-range weather predictions, seasonal climate predictions and downscaled projections of future climate change. That is, the model code was used successfully as a seamless forecasting system.
- An ensemble of high-resolution downscalings of future climate change over Africa has been generated and analysed. The downscaled climates represent multiple CGCMs and three different emission scenarios (SRES A2, RCP4.5, and RCP8.5). The projections span the period 1961-2100.
- Temperatures are projected to rise rapidly over Africa, compared to the global rate of temperature increase. Over tropical Africa, temperatures are projected to rise at about 1.5 times the global rate of temperature increase, whilst over subtropical southern and North Africa temperatures are projected to rise at almost twice the global rate.
- Under low mitigation (high emission) scenarios, the temperature climatology of subtropical southern Africa and North Africa is projected to be 4 to 7°C warmer than the present-day climatology.
- Even if the UNFCC is successful in establishing a new binding treaty that limits the global temperature increase to 2°C, temperature increases over southern and North Africa may still be as high as 4°C.

- The frequency of occurrence of heat waves, high fire-danger days and very hot days are likely to increase over most of southern Africa, West Africa and North Africa, including the vulnerable Sahel region. Skilful short-range and seasonal predictions of such events are likely to become increasingly important for these regions under climate change.
- It is plausible that East Africa will become generally wetter with a reduced frequency in the occurrence of years with below-normal rainfall.
- The projections indicate that it is plausible for southern Africa, the Sahel, North Africa and Mediterranean to experience an increase in the frequency of occurrence of years with below-normal rainfall. Skilful seasonal forecasts of anomalous rainfall over these regions may well become increasingly important under climate change.
- Over West Africa, the projections are of a mixed signal with respect to future rainfall changes, indicating greater uncertainty with respect to the evolution of the regional climate system.
- The downscalings exhibit a robust message of increases in the frequency of occurrence of extreme precipitation events over tropical and East Africa. Such increases are also plausible over southern Africa, despite this region being projected to become generally drier in most projections.
- The fact that the CCAM predictions at short-range and seasonal time scales have been shown to be skilful, enhances the confidence in the model projections of future climate change.
- Verification of ensemble numerical weather prediction by the CCAM up to 7 days ahead shows that the largest ensemble (8 members) run at the highest resolution (15 km) outscore smaller ensemble and lower resolution runs in both discrimination and reliability.
- In order for ensemble weather predictions to improve the forecast ensemble may need to be of a size much larger than the eight members considered here, and resolution should be further improved.
- Seasonal forecast modellers using atmospheric general circulation models (AGCMs) may need to consider various options on how to prescribe the lower boundary forcing since it was shown here that the selection of how to prescribe the SST to be used during the model integration period may have a

significant impact on the performance of operational seasonal forecast production.

- The best AGCM forecast for South African mid-summer rainfall was found to be from a single best SST forecast field (the ensemble mean is a more skilful representation than each of the individual members). Such predicted SSTs should be obtained from simulations or predictions produced by fully coupled ocean-atmosphere models.
- In a three-category description of seasonal forecast output (i.e. below-, near- and above-normal), the notion of low predictability of the middle category was again demonstrated in this project.
- The CCAM was shown to be able to skilfully simulate the seasonal-to-interannual variability across South Africa, particularly during mid-summer.
- Seasonal forecast skill is a function of both location and time of the year. The north-eastern parts of South Africa and adjacent regions are often associated with the highest levels of skill for both rainfall and maximum temperatures. Skill is generally the lowest during Spring, improves towards mid-summer and then declines towards Autumn.
- Maximum temperatures are associated with higher levels of skill than rainfall totals. Droughts are often simulated with over-confidence, while wet seasons are more likely to be simulated with high levels of reliability.
- Similar skill levels between seasonal climate simulations and re-forecasts are found at the short lead-time of one month presented here – not much skill is lost as a result of forcing the CCAM with predicted SSTs over the model's integration period.
- Forecast output can be displayed on a variety of ways and may optimise forecast uptake on condition that the users of such forecasts help guide product development.
- Seasonal streamflows can be predicted by the CCAM by downscaling the predicted low-level circulation to catchment level with empirical downscaling equations.
- The fairly course resolution currently being used for CCAM's seasonal climate forecasts provides sufficient information in order to predict tropical cyclone-like vortices over the south-western Indian Ocean.

- A similar seamless approach has been conducted at SAWS and is a consequence of the close collaboration between CSIR and SAWS modellers. Such collaborations should be further encouraged at Executive level.

References

Alexander, M. E., 1990. Computer calculation of the Keetch-Byram Drought Index – programmers beware!. *Fire Management Notes,* Volume 51, pp. 23-25.

Atger, F., 1999. The skill of ensemble prediction systems. *Monthlly Weather Review,* Volume 127, pp. 1941-1953.

Barnett, T. P. & Preisendorfer, 1987. Origins and levels of monthly and seasonal forecast skill for United States air temperature determined by canonical correlation analysis. *Monthly Weather Review,* Volume 115, pp. 1825-1850.

Barnston, A. G. et al., 2010. Verification of the first 11 years or IRI's seasonal climate forecasts. *Journal of Applied Meteorology and Climatology,* Volume 49, pp. 493-520.

Barnston, A. G. & Ropelewski, C. F., 1992. Prediction of ENSO using canonical correlation analysis. *Journal of Climate,* Volume 5, pp. 1316-1245.

Beraki, A., Dewitt, D., Landman, W. A. & Olivier, C., 2014. Dynamical seasonal climate prediction using an ocean-atmosphere coupled climate model developed in partnership between South Africa and the IRI. *Journal of Climate,* p. In Press.

Beraki, A. et al., 2013. Modelled sea surface temperature scenario considerations and southern African seasonal rainfall and temperature predictability. *Water Research Report No. 1913/1/12,* p. 127.

Bowler, N. E. et al., 2008. The MOGREPS short-range ensemble prediction system. *Quaterly Journal of the Royal Meteorological Society,* Volume 134, pp. 703-722.

Brinkop, S. & Roeckner, E., 1995. Sensitivity of a general circulation model toparameterizations of cloud-turbulance interaction in the atmospheric boundary layer. *Tellus,* 47(A), pp. 197-220.

Brinkop, S. & Roeckner, E., 1995. Sensitivity of a general circulation model to parameterizations of cloud-turbulence interactions in the atmospheric boundary layer. *Tellus,* 47(A), pp. 197-220.

Buizza, R., 1997. Potential forecast skill of ensemble prediction, and spread and skill distributions of the ECMWF ensemble prediction system. *Monthly Weather Review,* Volume 125, p. 99-119.

Buizza, R., 2008. Comparison of a 51-Member Low-Resolution (TL399L62) Ensemble with a 6-Member High-Resolution (TL799L91) Lagged-Forecast Ensemble. *American Meteorological Society,* Volume 136, pp. 3343-3362.

Buizza, R. & Palmer, T. N., 1997. Impact of Ensemble Size on Ensemble Prediction. *American Meteorological Society,,* Volume 126, pp. 2503-2518.

Christensen, J. H. et al., 2007. *The Physical Science Basis. Contribution of Working Group I to the forth Assessment Report of the Intergovernmental Panel on Climate Change..* Cambridge: University Press.

Cook, C., Reason, C. J. C. & Hewitson, B. C., 2004. Wet and dry spells within particularly wet and dry summers in the South African summer rainfall region. *Climate Research,* Volume 26, pp. 17-31.

Cook, K. H., 2001. A Southern Hemisphere wave response to ENSO with implications fro Southern African precipitation. *Journal of the Atmospheric Sciences,* Volume 58, pp. 2146-2162.

Dewitt, D. G., 2005. Retrospective forecasts of interannual sea surface temperature anomalies from 1982 to present using a directly coupled atmosphere-ocean general circulation model. *Monthly Weather Review,* Volume 133, pp. 2972-2995.

Dowdy, A. J., Mills, G. A., Finkele, K. & De Groot, W., 2010. Index sensitivity analysis applied to the Canadian Forest Fire Weather Index and the McArthur Forest Fire Danger Index. *Meteorological Applications,* Volume 17, pp. 298-312.

Du, J. & Mullen, S. L., 1997. Short-range ensemble forecasting of quantitative precipitation. *American Meteorological Society,* Volume 125, pp. 2427-2459.

Dumenil, L. & Todini, E., 1992. A rainfall-runoff scheme fro use in the Hamburg climate model. In: J. P. O'Kane, ed. *Advances in Hydrology:A contribute to James Dooge(European Geophysical Society Series on Hydrological Sciences).* Amsterdam: Elsevier Press, pp. 129-157.

Engelbrecht, C. J., Engelbrecht, F. A. & Dyson, L. L., 2012. High resolution model-projected changes in mid-tropospheric closed-lows and extreme rainfall events over southern Africa.. *International Journal of Climatology,* p. DOI: 10/1002/joc.3420.

Engelbrecht, F. A., 2005. Climate change and Water Resources in Southern Africa: Studies on Scenarios, Impacts, Vulnerabilities and Adaptation.WRC Report 1430/1/05. In: R. E. Schulze, ed. *Simulations of climate and climate change over Southern and tropical Africa with the conformal-cubic atmospheric model.* Pretoria: Water Research Commision.

Engelbrecht, F. A., 2010. The physical basis of climate change over southern Africa.in: Climate Change and Trade over Southern Africa. South African Institute for International Affairs.. *In press.*

Engelbrecht, F. A. & Bopape, M. M., 2011. *High-resolution projected climate futures for southern Africa..* Pretoria, South Africa, SASAS conference.

Engelbrecht, F. A. et al., 2011. Multi-scale climate modelling over southern Africa using a variable-resolution global model. *Water SA,* Volume 37, pp. 647-658.

Engelbrecht, F. A., McGregor, J. L. & Engelbrecht, C. J., 2009. Dynamics of the Confromal-Cubic Atmospheric Model projected climate change signal over southern Africa.. *International Journal of Climatology,* Volume 29, pp. 1013-1033.

Engelbrecht, F. A., Naidoo, M. & Bopape, M. M., 2013a. Meteorological climate scenarios for Africa and specific case study of the Nile and Niger river. *DEWFORA,* Volume D3.4.

Engelbrecht, F. et al., 2013b. Impact of cliamte change on drought hazards over Africa. *DEWFORA,* Volume D3.5.

Fouquart, Y. & Bonnel, B., 1980. Computations of solar heating of the Earth's atmosphere: A new parameterization.. *Contributions to Atmospheric Physics,* Volume 53, pp. 35-62.

Fox-Rabinovitz, M. et al., 2008. Stretched-grid Model Intercomparison Project: decadal regional climate simulations with enhanced variable and uniform-resolution GCMs. *Meteorology and Atmospheric Physics,* Volume 100, pp. 159-177.

Gates, W. L., 1992. AMIP: The Atmospheric Model Intercomparison Project. *Bulletin of the American Meteorological Society,* Volume 73, pp. 1962-1970.

Glahn, H. & Lowry, D., 1972. The use of model output statistics (MOS) in objective weather forecasting.. *Journal of Applied Meteorology,* Volume 11, pp. 1203-1211.

Goddard, L. & Mason, S. J., 2002. Sensitivity of seasonal climate forecast to persisted SST anomalies.. *Climate Dynamics,* Volume 19, pp. 619-631.

Graham, R. J. et al., 2002. As assessment of seasonal predictability using atmospheric general circulation models.. *Quarterly Journal of the Royal Meteorological Society,* Volume 126, pp. 2211-2240.

Graham, R. J. et al., 2005. Performance comparison of coupled and uncoupled versions of the Met Office seasonal prediction general circulation model. *Tellus,* 57(A), pp. 320-339.

Graham, R. J. et al., 2011. Long-range forecasting and the Global Framework for Climate Services. *Climate Research,* Volume 47, pp. 47-55.

Grimit, E. P. & Mass, C. F., 2001. Initial Results of a Mesoscale Short-Range Ensemble Forecasting System over the Pacific Northwest. *American Meteorological Society,* Volume 17, pp. 192-205.

Hamill, T. M., 1997. Reliability diagrams for multicategory probabilistic forecasts. *Weather and Forecasting,* Volume 12, pp. 736-741.

Hamill, T. M. & Colucci, S. J., 1997. Verification of eta-RSM short-range ensemble forecasts. *Monthly Weather Review,* Volume 125, p. 1312-1327.

Hardiker, V., 1997. A Global Numerical Weather Prediction Model with Variable Resolution. *American Meteorological Society,* Volume 125, pp. 59-73.

Hewitson, B. C. & Crane, R. G., 2006. Consensus between GCM climate change projections with empirical downscaling.. *International Journal of Climatology,* Volume 26, pp. 1315-1337.

Hoffman, R. N. & Kalnay, E., 1982. Lagged average forecasting, an alternative to Monte Carlo forecasting. *Tellus,* 32(A), pp. 100-118.

Holton, J. R., 2004. *Introduction to Dynamic Meteorology.* 4th ed. California: Academic Press.

Holtslag, A. A. M. & Bonville, B. A., 1993. Local versus non-local boundary layer diffusion in a global climate model. *Journal of climate,* Volume 6, pp. 1825-1842.

Hulme, M., Doherty, R. & Ngara, T., 2001. African climate change: 1900-2100. *Climate Research,* Volume 17, pp. 145-168.

Jolliffe, I. T. & Stephenson, D. B., 2011. Forecast Verification. In: *A Practitioner's Guide in Atmospheric Science.* s.l.:Wiley, p. 274.

Joubert, A. M., Mason, S. J. & Galpin, J. S., 1996. Droughts over southern Africa in a doubled CO2 climate.. *International Journal of Cliamtology,* Volume 16, pp. 1149-1156.

Kalnay, E., 2003. *Atmospheric modeling, data assimilation and predictability.* s.l.:Cambridge University Press.

Katzfey, J. J., McGregor, J. L., Nguyen, K. C. & Thatcher, M., 2009. *Modelling and Simulation Society of Australia and New Zealan Inc.(MSSANZ).* [Online] Available at: http://www.mssanz.org.au/modsim09/dfwww.mssanz.org.au/modsim09/I13/katzfey_I13.pdfwww.mssanz.org.au/modsim09/I13/katzfey_I13.pdf www.mssanz.org.au/modsim09/I13/katzfey_I13.pdf www.mssanz.org.au/modsim09/I13/katzfey_I13.pdf_2377-2383

Keetch, J. J. & Byram, G. M., 1988. A drought Index for Forest Fire control. *U.S. Department of Agriculture- Forest Service Research Paper SE-38,* Volume (Revised November 1988), p. 32.

Knapp, K. R. et al., 2010. The international best track archive for climate stewardship: Unifying tropical cyclone best track data. *Bulletin of the American Meteorological Society,* Volume 91, pp. 363-376.

Kowalczyk, E. A., Garratt, J. R. & Krummel, P. B., 1994. Implementation of a soil-canopy scheme into the CSIRO GCM – regional aspects of the model response. *CSIRO Division of Atmospheric Research Technical Paper,* Volume 32, p. 59.

Kowalczyk, E. A. et al., 2006. CSIRO Atmosphere Biosphere Land Exchange(CABLE) model for use in cliamte models and as an offline model. *CSIRO Marine and Atmospheric Research Paper,* Volume 13, p. 37.

Krishnamurti, T. N. et al., 2000. Multimodel ensemble forecasts for weather and seasonal climate. *Journal of Climate,* Volume 13, pp. 4196-4216.

Lal, M., McGregor, J. L. & Nguyen, K. C., 2008. Very high resolution climate simulation over Fiji using a global variable-resolution model.. *Climate Dynamics,* Volume 30, pp. 293-305.

Landman, S., Engelbrecht, F. A. & Engelbrecht, C. J., 2009. *Development of a new multi-model short-range EPS at the South African Weather Service. 4th Short-range numerical weather prediction Workshop on ensemble prediction systems 23-25 June.* Exeter, s.n.

Landman, W. A. & Beraki, A., 2012. Multi-model forecast skill for mid-summer rainfall over southern Africa. *International Journal of Climatology,* Volume 32, pp. 303-314.

Landman, W. A., Botes, S., Goddard, L. & Shongwe, M., 2005. Assessing the predictability of extreme rainfall seasons over southern Africa. *Geophysical Research Letters,* Volume 32, p. L23818. DOI:10.1029/2005GL023965.

Landman, W. A. et al., 2012. Seasonal rainfall prediction skill over South Africa: 1- vs. 2-tiered forecasting systems. *Weather and Forecasting,* Volume 27, pp. 489-501.

Landman, W. A. et al., 2001. Model output statistics applied to multi-model ensemble long-range forecasts over South Africa. *WRC Report,* Volume No. 1492/1/08, p. 56.

Landman, W. A. & Goddard, L., 2002. Statistical recalibration of GCM forecast over southern Africa using model output statistics. *Journal of Climate,* Volume 15, pp. 2038-2055.

Landman, W. A. et al., 2009. erformance comparison of some dynamical and empirical downscaling methods for South Africa from a seasonal climate modelling perspective. *International Journal of Climatology,* Volume 29, pp. 1535-1549.

Landman, W. A. & Mason, S. J., 1999. Operational long-lead prediction of South African rainfall using canonical correlation analysis. *International Journal of climatololgy,* Volume 19, pp. 1073-1090.

Landman, W. A. & Mason, S. J., 2001. Forecasts of near-global sea surface temperatures using canonical correlation analysis. *Journal of Climate,* Volume 14, pp. 3819-3833.

Landman, W. A., Mason, S. J., Tyson, P. D. & Tennant, W. J., 2001. Retro- Active skill of multi-tiered forecasts of summer rainfall over southern Africa. *International Journal of Climatology,* Volume 21, pp. 1-19.

Landman, W. A., Mason, S. J., Tyson, P. D. & Tennant, W. J., 2001. Statistical downscaling of GCM simulations to streamflow. *Journal of Hydrology,* Volume 252, pp. 221-236.

Laursen, L. & Eliasen, E., 1989. On the effects of the damping mechanisms in an atmospheric general circulation model. *Tellus,* 41(A), pp. 385-400.

Li, S., Goddard, L. & Dewitt, D. G., 2008. Predictive skill of AGCM seasonal climate forecasts subject to different SST prediction methodologies. *Journal of Climate,* Volume 21, pp. 2169-2186.

Louis, J. F., 1979. A parametric model of vertical eddy fluxes in the atmosphere. *Boundary-Layer Meteorology,* Volume 17, pp. 187-202.

Lu, C., Yuan, H., Schwartz, B. E. & Benjamin, S. G., 2007. Short-Range Numerical Weather Prediction Using Time-Lagged Ensembles. *American Meteorological Society,* Volume 22, pp. 580-595.

Malherbe, J., Engelbrecht, F. A. & Landman, W. A., 2013. Projected change in tropical cyclone tracks over the southwestern Indian Ocean under enhaced anthropogenic forcing. *Climate Dynamics,* pp. DOI 10.1007/s00382-012-1635-2.

Malherbe, J., Engelbrecht, F. A., Landman, W. A. & Engelbrecht, C. J., 2011. Tropical systems from the southwest Indian Ocean making landfall over the Limpopo River Basin,souther Africa: A historical perspective. *International Journal of Climatology,* p. DOI:10.1002/joc.2320.

Mason, S. J. & Graham, N. E., 2002. Areas beneath the relative operating characteristics (ROC) and levels (ROL) curves: Statistical significance and interpretation. *Quarterly Journal of the Royal Meteorological Society,* Volume 128, pp. 2145-2166.

Mason, S. J. & Joubert, A. M., 1997. Simulated changes in extreme rainfall over southern Africa. *International Journal of Climatology,* Volume 17, pp. 291-301.

Mason, S. J., Joubert, A. M., Cosijn, C. & Crimp, S. J., 1996. Review of seasonal forecast techniques and their applicability to southern Africa. *Water SA,* Volume 22, pp. 203-209.

Mavume, A. F., Rydberg, L., Rouault, M. & Lutjeharms, J. R. E., 2009. Climatology and landfall of the tropical cyclones in the southwest Indian Ocean. *Western Indian Ocean Journal of Marine Science,* 8(1), pp. 15-36.

McGregor, J. L., 1996. Semi-Lagrangian advection on conformal-cubic grids. *Monthly Weather Review,* Volume 124, pp. 1311-1322.

McGregor, J. L., 2003. A new convection scheme using a simple closure. In 'current issues in the parameterization of convection'. *BMRC Report,* Volume 93, pp. 33-36.

McGregor, J. L., 2005a. Geostophic adjustment for reversibly staggered grids. *Monthly weather Review,* Volume 113, pp. 1119-1128.

McGregor, J. L., 2005b. C-CAM: Geometric aspects and dynamical formulation.. *CSIRO Atmospheric Research Technical Paper,* Volume 70, p. 43.

McGregor, J. L. & Dix, M., 2005. The Conformal-Cubic Atmospheric Model: progress and plans. *CSIRO Marine and Atmospheric Research.*

McGregor, J. L. & Dix, M. R., 2001. The CSIRO conformal-cubic atmospheric GCM. In: P. F. Hodnett, ed. *IUTAM Symposium on Advances in Mathematical Modelling of the Atmosphere and Ocean Dynamics.* Dordrecht: Kluwer Academic Publishers, pp. 197-202.

McGregor, J. L. & Dix, M. R., 2008. An Updated description of the Confromal-cubic Atmospheric Model. In: K. Hamilton & W. Ohfuchi, eds. *In High resolution Simulations of the Atmosphere and Ocean.* s.l.:Spinger, pp. 51-76.

McGregor, J. L. et al., 1993. The CSIRO 9-level atmospheric general circulation model. *CSIRO Atmospheric Research Technical Paper,* Volume 20, p. 89.

McGregor, J. L., Katzfey, J. J., Nguyen, K. C. & Thatcher, M. J., 2011. *Some recent developments for downscalling of climate. Proc. 27th Annual Conference of the Society for Atmospheric Sciences..* Hartebeesboek, s.n.

McGregor, J. L., Nguyen, K. & Katzfey, J. J., 2008. A variety of tropical climate simulations using CCAM. Centre for Weather and Climate Research Aspendale. *2nd CAWCR Modelling Workshop.*

Meadows, M. E., 2006. Global Change and southern Africa. *Geographical Research,* Volume 44, pp. 135-145.

Metzger, S., Latif, M. & Fraedrich, K., 2004. Combining ENSO forecasts: A feasibility study. *Monthly Weather Review,* Volume 132, pp. 456-472.

Michaelsen, J., 1987. Cross-validation in statistical climate forecast models. *Journal of Climate and Applied Meteorology,* Volume 26, p. 589-1600.

Miller, M. J., Palmer, T. N. & Swinbank, R., 1989. Parameterization and influence of sub-grid scale orography in general circulation and numerical weather prediction models. *Meteorology and Atmospheric Physics,* Volume 40, pp. 84-109.

Mitchell, T. D. & Jones, P. D., 2005. An improved method of constructing a database of monthly climate observations and associated high resolution grids. *International Journal of Climatology,* Volume 25, pp. 673-712.

Morcrette, J. -J. & Fouquart, Y., 1985. On systematic errors in parametrized calculations of longwave radiation transfer. *Quaterly Journal of the Royal Meteorological Society,* Volume 111, pp. 691-708.

Nordeng, T. E., 1996. Extended versions of the convective parameterization scheme at ECMWF and their impact on the mean and transient activity of the model in the tropics. *Quaterly Journal of the Royal Meterogical Society,* p. (submitted).

Nunez, N. & McGregor, J. L., 2007. Modelling future water environments of Tasmania, Australia. *Climate Research,* Volume 34, pp. 25-37.

Oouchi, K. et al., 2006. Tropical cyclone climatology in a global-warming climate as simulated in a 20 km-mesh global atmospheric model: Frequency and wind intensity analysis. *Journal of the meteorological Society of Japan,* Volume 84, pp. 259-276.

Palmer, T. et al., 2004. Development of a European multimodel ensemble system for seasonal-to-interannual prediction (DEMETER). *Bulletin of the American Meteorological Society,* pp. DOI: 10.1175/BAMS-85-6-853..

Palmer, T. N. & Anderson, D. L., 1994. The prospects of seasonal forecasting – A review paper. *Quaterly Journal of the Royal Meteorological Society,* Volume 120, pp. 755-793.

Potgieter, C. J., 2007. *Short-range weather forecasting over southern Africa with the conformal-cubic atmospheric model,* University of Pretoria: Unpublished MSc dessertation.

Reason, C. J. C. & Keibel, A., 2004. Tropical Cyclone Eline and Its Unusual Penetration and Impacts over the Southern African Mainland. *Weather and Focasting,* Volume 19, pp. 789-805.

Reynolds, R. W. & Smith, T. M., 1994. Improved global sea surface temperature analyses using optimum interpolation. *Journal of Climate,* Volume 7, pp. 929-948.

Roeckner, E. et al., 1996. *Simulation of present-day climate with the ECHAM4 model: Impact of model physics and resolution. Report No. 93, Max-Planck-Institut fur Meteorologie.* Hamburg, Germany, s.n.

Rotstayn, L. D., 1997. A physically based scheme for the treatment of stratiform clouds and precipitation in large-scale models. I: Description and evaluation of the microphysical processes. *Quaterly Journal of the Royal Meteorological Society,* Volume 123, pp. 1227-1282.

Ruosteenoja, K., Carter, T. R., Jylha, K. & Toumenvirta, H., 2003. *Future cliamte in world regions: An intercomparison of model-based projections for the new IPCC emission scenarios,* Helsinki: Finnish Environment Institude.

Schulze, R. E., Warburton, M., Lumsden, T. G. & Horan, M. J. C., 2005. Chapter 8. In: W. R. 1430/1/05, ed. *The Southern African Quaternary Catchments Database: Refinements to, and Links with, the ACRU System as a Framework for Modelling Impacts of Climate Change on Southern Africa: Studies on Scenarios, Impacts, Vulnerabilities and Adaptation.* Pretoria: Water Research Comission, pp. 111-139.

Seidel, D. J., Fu, Q., Randel, W. J. & Reichler, T. J., 2008. Widening of the tropical belt in a changing climate. *Nature Geoscience,* Volume 1, pp. 21-24.

Shongwe, M. E. L. W. A. & Mason, S. J., 2006. Performance of recalibration systems for GCM forecasts for southern Africa. *International Journal of Climatology,* Volume 26, pp. 1567-1585.

Simmons, A. J. & Burridge, D. M., 1981. An energy and angular- momentum conserving vertical finite difference scheme and hybrid vertical coordinates. *Monthly Weather Review,* Volume 109, pp. 758-766.

Simmons, A. J., Burridge, D. M., Girard, C. & Wergen, W., 1989. The ECMWF medium-range prediction models: Development of the numerical formulations and the impact of increased resolution. *Meteorology and Atmospheric Physics,* Volume 40, pp. 28-60.

Singleton, A. T. & Reason, C. J. C., 2007. Variability in the characteristics of cut-off low pressure systems over southern Africa. *International Journal of Climatology,* Volume 27, pp. 295-310.

Stockdale, T. N., Anderson, D. L. T., lves, J. O. S. & Balmaseda, M. A., 1998. Global seasonal rainfall forecasts using a coupled ocean-atmosphere model. *Nature,* Volume 392, pp. 370-373.

Tadross, M. A., Hewitson, B. C. & Usman, M. T., 2005. The interannual variability of the onset of the maize growing season over South Africa and Zimbabwe. *Journnal of Climate,* Volume 18, pp. 3356-3372.

Tadross, M. A., Jack, C. & Hewitson, B. C., 2006. On RCM-based projections of change in southern African summer climate. *Geophysical Research Letters,* pp. L23713, DOI:10.1029/2005GL024460..

Tangang, F. T., Tang, B., Monahan, A. H. & Hsieh, W. W., 1998. Forecasting ENSO events: A neural network-extended EOF approach. *Journal of Climate,* Volume 11, pp. 29-41.

Tennant, W. J., Toth, Z. & Rae, K. J., 2007. Application of the NCEP ensemble prediction system to medium-range forecasting in South Africa: New products,benefits, and challenges. *Weather and Forecasting,* Volume 22, pp. 18-35.

Thatcher, M. & McGregor, J. L., 2009. Using a scale-selective filter for dynamical downscaling with the conformal cubic atmospheric model. *Monthly Weather Review,* Volume 137, pp. 1742-1752.

Thatcher, M. & McGregor, J. L., 2010. A technique for dynamically downscaling daily-averaged GCM datasets over Australia using the confromal cubic atmospheric model. *Monthly Weather Review,* Volume 139, pp. 79-95.

Thornton, P. K., Jones, P. G., Ericksen, P. J. & Challinor, A. J., 2011. Agriculture and food systems in sud-Saharan Africa in a 4 C+ world. *Philosophical Transactions of the Royal Society of London,* Volume 396, pp. 117-136.

Tiedke, M., 1989. A comprehensive mass flux scheme for cumulus parameterization in largescale models. *Monthly Weather Review,* Volume 117, pp. 1779-1800.

Tippett, M. K., Barnston, A. G. & Dewitt, D., 2005. Statistical correction of tropical Pacific sea surface temperature forecasts. *Journal of Climate,* Volume 18, pp. 5141-5162.

Todd, M., Washington, R. & Palmer, P. I., 2004. Water vapor transport associated with tropical-temperate trough systems over southern Africa and the southwest Indian Ocean. *International Journal of Climatology,* 24(5), pp. 555-568.

Troccoli, A., Harrison, M., Anderson, D. L. T. & Mason, S. J., 2008. Seasonal Climate: Forecasting and managing risk. In: *NATO Science Series.Earth and Environmental Sciences Vol 82.* Dordrecht: Springer, p. 467.

Tyson, P. D. & Preston-Whyte, R. A., 2000. *The Weather and Climate of Southern Africa.* 2nd ed. Cape Town: Oxford University Press.

Van Den Dool, H. M., 1994. Searching for analogues, how long must we wait?. *Tellus,* 46(A), pp. 314-324.

Van Den Dool, H. M. & Toth, Z., 1991. Why do forecasts for near normal often fail?. *Weather and Forecasting,* Volume 6, pp. 76-85.

Van Der Linden, P. & Mitchell, J. F. B., 2009. *ENSEMBLES: Climate Change and its Impacts: Summary of research and results from the ENSEMBLES project.* Exeter: Met Office Hadley Centre.

Van Rooy, M. P., 1972. *District rainfall for South Africa and the annual march ofrainfall over southern Africa, Climate of South Africa,* Pretoria: SA Weather Bureau.

Van Wilgen, B. W. et al., 2010. Fire management in Mediterranean-cliamte shrublands: A case study from the Cape fynbos, South Africa. *Jpurnal of Applied Ecology,* Volume 47, pp. 631-638.

Vitart, F., Anderson, J. L. & Stern, W. F., 1997. Simulation of inter-annual variability of tropical storm frequency in an ensemble of GCM integrations. *Journal of Climate,* Volume 10, pp. 745-760.

Vitart, F. et al., 2008. The new VarEPS-monthly forecasting system: A first step towards seamless prediction. *Quarterly Journal of the Royal Meteorological Society,* Volume 134, pp. 1789-1799.

Walsh, K. J. E., Fiorino, M., Landsea, C. W. & McInnes, K. L., 2007. Objectively determined resolution-dependent threshold criteria for the detection of tropical cyclones in climate models and reanalysis.. *Journal of Climate,* 20(10), pp. 2307-2314.

Wilks, D., 2011. Statistical Methods in the Atmospheric Sciences. In: 3rd ed. Amsterdam: Academic Press, p. 676.

Wilks, D. S., 2006. *Statistical Methods in the Atmospheric Sciences.* 2nd ed. San Diego: Academic Press.

Williamson, D. L. & Rasch, P. J., 1994. Water vapour transport in the NCAR CCM2. *Tellus,* 46(A), pp. 34-51.

Winsemius, H. C. et al., 2014. The potential value of seasonal forecast in a changing climate. *Hydrology and Earth System Sciences,* p. In Press.

Zebiak, S. E. & Cane, M. A., 1987. A model El Niño-Southern Oscillation. *Monthly Weather Review,* Volume 115, pp. 2262-2278.